

**A GEOCHEMICAL AND FLUID INCLUSION
STUDY OF THE ARSENOPYRITE-STIBNITE-
GOLD MINERALIZATION, MORETON'S
HARBOUR, NOTRE DAME BAY, NEWFOUNDLAND**

CENTRE FOR NEWFOUNDLAND STUDIES

**TOTAL OF 10 PAGES ONLY
MAY BE XEROXED**

(Without Author's Permission)

ELIZABETH ALEXANDRA KAY

126499



A GEOCHEMICAL AND FLUID INCLUSION STUDY OF
THE ARSENOPYRITE-STIBNITE-GOLD MINERALIZATION,
MORETON'S HARBOUR, NOTRE DAME BAY, NEWFOUNDLAND

by



E. Alexandra Kay, B.Sc. (Hons.)

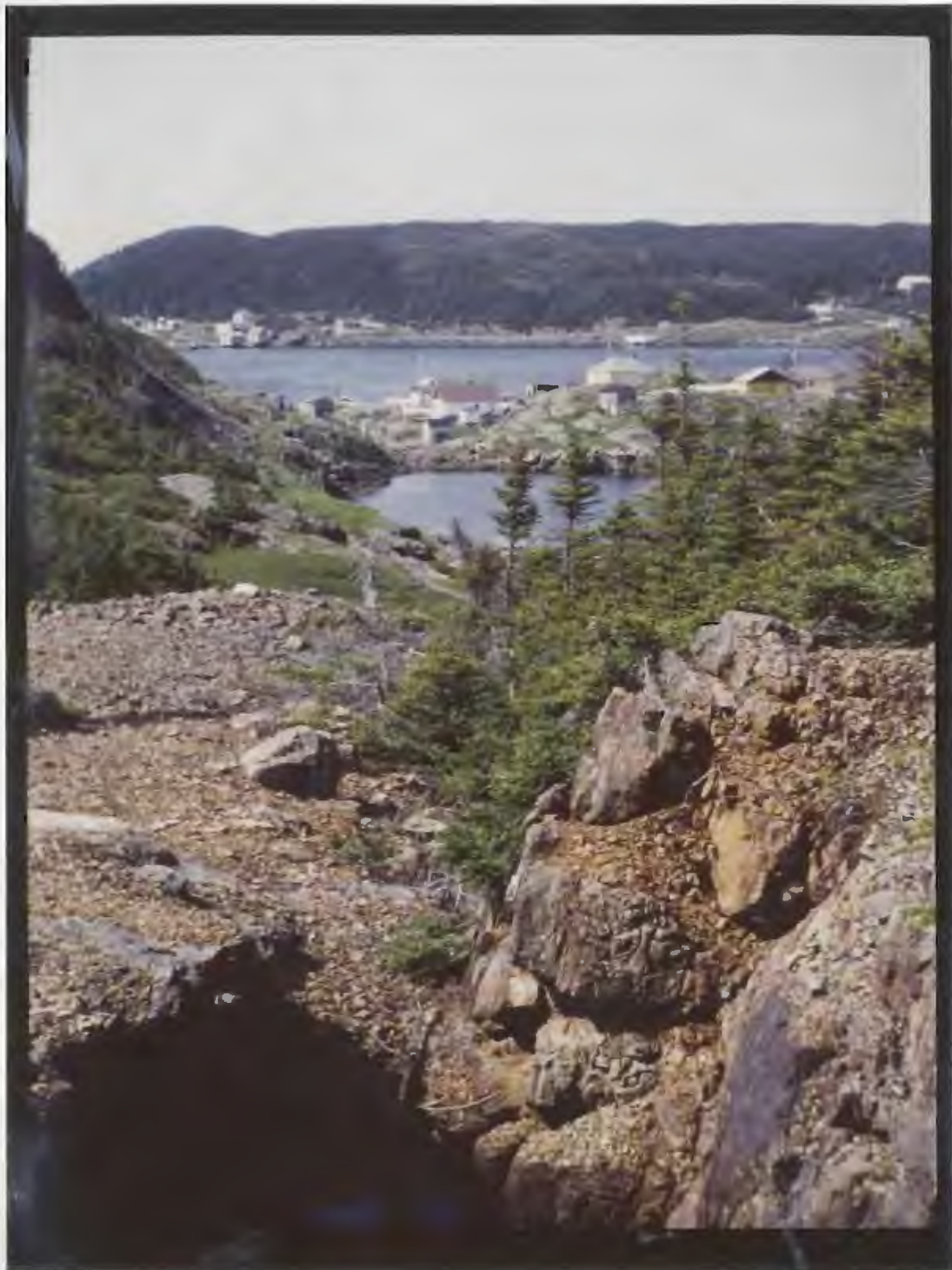
November 1981

A Thesis submitted in partial fulfillment
of the requirements for the degree of
Master of Science

Department of Geology
Memorial University of Newfoundland

St. John's

Newfoundland



FRONTISPIECE: Looking southwestwards from Stewart's Mine across Little Harbour to Moreton's Harbour.

ABSTRACT

Mineralized hydrothermal veins of the Moreton's Harbour area, occurring within a thick sequence of dominantly basaltic pillow lavas and pyroclastic rocks, are concentrated within a central volcanoclastic unit and intimately associated with felsic dykes. There are about fifty veins, up to 30 cm thick, occupying fractures perpendicular to the bedding. They can be broadly classified into three types, viz. I arsenopyrite-dominated, II stibnite-dominated, and III base metal + arsenopyrite-dominated, all with quartz and calcite as the major gangue minerals.

Type I veins are Au-rich, type III are Au + Ag-rich, and type II are Au-poor but slightly enriched in Pd. Fluid inclusion data indicate deposition of Au-rich type I veins from CO₂-rich low salinity fluids above 300°C, whereas the type II Au-poor veins were deposited from relatively saline low-CO₂ fluids at temperatures below 220°C. Both fluid inclusion and arsenopyrite composition data suggest pressures of 900 to 1500 bars, in agreement with lithostatic pressure indicated by the overlying volcanic pile.

The Au mineralization is considered to have resulted from temperature decrease through 300°C, below which the stability of Au-complexes declines abruptly. Carbon dioxide abundance suggests the involvement of carbonate complexes, with retrograde boiling

resulting in loss of CO_2 and drop in carbonate activity, brecciation of arsenopyrite and deposition of calcite. A range of criteria suggest that the fluid was derived from felsic magma which produced the dykes and pyroclastic rocks, and hence was penecontemporaneous with the felsic volcanic activity. Concentration of veins within the central pyroclastic unit results from the fact that it occurs at a depth within the volcanic pile with suitable P-T-X conditions for deposition.

#

TABLE OF CONTENTS

	<u>PAGE NO.</u>
FRONTISPIECE	2
ABSTRACT	3
LIST OF TABLES	8
LIST OF FIGURES	10
LIST OF PLATES	14
ACKNOWLEDGEMENTS	17
CHAPTER 1: INTRODUCTION	
1.1. Introduction	18
1.2. Regional Geological Setting	20
1.3. Previous Geological Work	22
1.4. Economic Geology History	26
1.5. Aims and Approach of Study	26
CHAPTER 2: THE LOCAL GEOLOGY	
2.1. Introduction	28
2.2. Wild Cove Formation	31
2.3. Little Harbour Formation	32
2.3.1. The Little Harbour Section (A-A')	33
a. Massive flow lithofacies	33
b. Pillow lava lithofacies	37
c. Volcaniclastic sedimentary lithofacies	40
d. Coarse tuff-breccia lithofacies	43
2.3.2. Taylor's Room Section (B-B')	46
2.3.3. Pearce Harbour Section (C-C' and D-D')	48
2.4. Western Head Formation	48
2.5. Hayward's Cove Formation	50
2.5.1. Chimney Cove tuff-facies	50
2.5.2. Felsic pyroclastic lithofacies	50
2.6. Intrusive Rocks	53
2.6.1. Mafic dykes	53
2.6.2. Other mafic intrusions	53
2.6.3. Felsic intrusive rocks	54
2.6.4. Lamprophyre	56
2.7. Structural Geology	56
2.8. Metamorphism and Alteration	56
2.9. A summary of the Geologic History of the Moreton's Harbour Area	57

CHAPTER 3: PETROGRAPHY AND GEOCHEMISTRY OF THE EXTRUSIVE AND
INTRUSIVE ROCKS OF THE MORETON'S HARBOUR AREA

	PAGE NO.
3.1. Introduction	58
3.2. Mafic Dykes	58
3.3. Mafic Extrusive Rocks	67
3.4. Mafic Volcaniclastic and Associated Sedimentary Rocks	69
3.5. Moreton's Harbour Head Breccia	70
3.6. Felsic Dykes	70
3.7. Felsic Pyroclastic Rocks of the Hayward's Cove Formation	71
3.8. Geochemistry of the Felsic Rocks: Hayward's Cove Breccia, Tuffs and Felsic Dykes	73
3.9. Other Mafic Intrusive Rocks	79
3.9.1. Gerald Dearing's diorite stock	79
3.9.2. Dick's Head microgabbro	82
3.9.3. Lamprophyre	82
3.10. Alteration and Metamorphism	82
3.11. Silicate Mineral Chemistry	83

CHAPTER 4: ORE PETROGRAPHY

4.1. Mining History	87
4.1.1. Stewart's Mine, Little Harbour	87
4.1.2. Stuckless' Mine, Frost Cove	87
4.1.3. Other prospects	89
4.2. Vein Description	89
4.2.1. Stewart's Mine: Vein Type I	91
4.2.1a. Moreton's Harbour Head: Vein Type I	95
4.2.2. Stuckless' Mine: Vein Type II	97
4.2.3. Taylor's Room: Vein Type III	99
4.3. Summary	101

CHAPTER 5: VEIN CHEMISTRY

5.1. Introduction	106
5.2. Data	106
5.3. Mineral Chemistry	118
5.3.1. Major elements	118
5.3.2. Trace elements	121
5.4. Constraints on Depositional Conditions from Mineralogical Data	125
5.4.1. Sulphur fugacity	125
5.4.2. Temperature and pressure	127
5.5. Summary	130

CHAPTER 6: FLUID INCLUSIONS

	<u>PAGE NO.</u>
6.1. Introduction	132
6.2. Compositional Types of Fluid Inclusions in Moreton's Harbour Veins	136
6.3. Inclusions in Gangue Quartz	136
6.3.1. Vein type I	136
6.3.2. Vein type II	139
6.3.3. Vein type III	142
6.4. The Significance of Solid Mineral Inclusions	142
6.5. Microthermometric Measurements	144
6.5.1. Salinity	144
6.6. Homogenization Temperatures	148
6.7. Density and Composition of CO ₂ -bearing Inclusions	151
6.7.1. Purity of CO ₂	154
6.7.2. Density	154
6.7.3. Composition	154
6.8. Geobarometry	160
6.8.1. Pressure correction	163
6.9. Fluid Inclusions in Other Minerals	164
6.10. Fluid Inclusions in Rhyolite Phenocrysts	164
6.11. Summary	167

CHAPTER 7: DISCUSSION, SUMMARY AND CONCLUSIONS

7.1. The Genesis of the Moreton's Harbour Mineralization	170
7.1.1. Introduction	170
7.1.2. Ore deposition	170
7.1.3. The source of the fluid	173
7.1.4. Metal source and transport with specific reference to gold	174
7.1.5. Other controls on mineralization	178
7.1.6. The summary of ore genesis	178
7.2. Summary and Conclusions	180

REFERENCES	182
------------------	-----

APPENDIX 1: Geochemical Techniques	193
--	-----

APPENDIX 2: Fluid Inclusion Techniques	202
--	-----

LIST OF TABLES

	<u>PAGE NO.</u>
TABLE 2.1: Summary of the Geological Subdivisions of the Moreton's Harbour Area	30
TABLE 3.1: Summary of the Mineral Assemblages of Volcaniclastic, Volcanic and Intrusive Rocks of the Moreton's Harbour Area	59
TABLE 3.2: Electron Microprobe Analyses of Some of the Major Silicate Minerals	61
TABLE 3.3: Chemical Analyses of the Selection of Mafic Dykes	64
TABLE 3.4: Chemical Analyses of a Selection of Mafic Rocks of the Western Head and Little Harbour Formation	66
TABLE 3.5a: Major Element Abundances of Selected Felsic Dykes and Pyroclastic Rocks	74
TABLE 3.5b: Trace Element Abundances in Selected Felsic Rocks	75
TABLE 4.1: Summary of Mineral Assemblages of the Mineralized Veins.	102
TABLE 4.2: Summary of the Properties of the Mineralized Veins, Moreton's Harbour Area	103
TABLE 5.1a: Chemical Analyses of Selected Mineralized Samples	107
TABLE 5.1b: Chemical Analyses of Selected Unmineralized Samples	108
TABLE 5.1c: Analyses of Wall Rock Samples, Stewart's Mine (see Figs. 5.5 and 4.1)	109
TABLE 5.2: Correlation Coefficient Matrix for the Analyses Presented in Table 5.1a,b	110
TABLE 5.3: Examples of Major Element Compositions of Arsenopyrite from Electron Microprobe Point Analyses (giving weight %, formula proportions and standard deviations)	118
TABLE 5.4: Examples of Major Element Compositions of Other Sulphide Minerals, from Electron Microprobe Point Analyses (giving weight % and formulae)	121
TABLE 5.5: Examples of Electron Microprobe Point Analyses for Trace Elements in Sulphide Minerals	122
TABLE 6.1: Terms and Abbreviations Relevant to Fluid Inclusion Microthermometric Data	133

	<u>PAGE NO.</u>
TABLE 6.2: Compositions of Examples of P- and PS-fluid Inclusions from Vein Type I	138
TABLE 6.3: Compositions of Examples of S-fluid Inclusions from all Vein Types	140
TABLE 6.4: Compositions of Examples of P- and PS-fluid Inclusions from Vein Type II	143

LIST OF FIGURES

	<u>PAGE NO.</u>
FIGURE 1.1: Map of the Island of Newfoundland showing the Location of Moreton's Harbour with Respect to the Cambro-Ordovician Rocks and the Tectonostratigraphic Zones	19
FIGURE 1.2: The Geology of Eastern Notre Dame Bay (coloured)	21
FIGURE 2.1: Geology of the Moreton's Harbour Area, Simplified from Map 1 (coloured)	29
FIGURE 2.2: Schematic Sections of the Little Harbour Formation ..	33
FIGURE 2.3: A Detailed 200 m section, x-y from the Little Harbour Volcaniclastic Lithofacies	41
FIGURE 2.4: Schematic section of Felsic Pyroclastic Rocks, Hayward's Cove Formation	51
FIGURE 3.1: The Ca-Fe-Mg Compositional Plot for Electron Microprobe Analyses of Clinopyroxene from Various Samples of Mafic Dykes, Moreton's Harbour, Compared with the Skaergaard and Alkaline Trends	62
FIGURE 3.2: Compositional Triangular Plots of Electron Microprobe Analyses of Other Mafic Minerals (a) Ca-Mg-Fe for amphibole analyses and (b) Mg-Fe-Al for epidote and chlorite analyses	63
FIGURE 3.3: Selected Geochemical Discriminatory Diagrams for Mafic Rocks from the Moreton's Harbour Area	65
FIGURE 3.4: Silica-total Alkalies Harker Diagram for Felsic Rocks, Hayward's Cove Formation	76
FIGURE 3.5: AFM Diagram for Selected Felsic Rocks, Hayward's Cove Formation	76
FIGURE 3.6: Silica Plotted against the Zr/TiO ₂ Ratio for Selected Mafic to Felsic Rock Samples from the Moreton's Harbour Area, Showing the Rock Type Discrimination and Subalkaline Trend	77
FIGURE 3.7: K ₂ O-Na ₂ O Diagram for Selected Felsic Rocks, Hayward's Cove Formation	80
FIGURE 3.8: Rb-K ₂ O Diagram for Selected Felsic Rocks, Hayward's Cove Formation	80

FIGURE 3.9:	Zr-SiO ₂ Diagram for Selected Felsic Rocks Showing a Fairly Linear Trend for the Dyke Rocks and Two of the Breccia Samples, with a Separate Group of High Zr Concentration for Other Felsic Pyroclastic Samples	81
FIGURE 3.10:	TiO ₂ -Zr Diagram for Selected Felsic Rock Samples, Dykes and Pyroclastics	81
FIGURE 4.1:	Sketch Map of the Stewart's Mine Area	88
FIGURE 4.2:	Sketch Map of the Pit, Little Harbour	88
FIGURE 4.3:	A Sketch Map showing the Broad Distribution of the Main Mineralized Veins in the Moreton's Harbour Area	90
FIGURE 4.4:	Paragenetic Sequence of Vein Type I	96
FIGURE 4.5:	Paragenetic Sequence of Vein Type II	100
FIGURE 4.6:	Paragenetic Sequence of Vein Type III	100
FIGURE 5.1:	A Sketch Map showing the Approximate Locations of Samples (ore veins and host rock) which have been Analysed for Gold and Other Elements	106
FIGURE 5.2:	Enrichment and Depletion Factors Displayed Graphically for Veins of Types I, II and III	113
FIGURE 5.3:	(a) Au vs Ni for all Samples (open circles are Pd vs Ni); (b) Au vs Ag Plot Showing Discrimination of Vein Types	114
FIGURE 5.4:	Binary Plots of As vs Ag (above) and As vs Au, Pd (below), Showing Discrimination of Vein Types I, II, and III (Stars indicate background values)	115
FIGURE 5.5:	Variation of Concentrations of Au, Ag, As, Ni, Zn and Pd across the Stewart's Mine Zone	116
FIGURE 5.6:	Electron Microprobe Analyses of Arsenopyrite (a) all analyses on a full Fe-As-S triangular plot; (b) vein type I; (c) vein type III; (d) assemblages of arsenopyrite from observed and experimental data	119
FIGURE 5.7:	Temperature-Sulphur Fugacity Diagram showing the Possible Range as Suggested by Mineralogical Assemblages Observed in the Vein Systems	125

	<u>PAGE NO.</u>
FIGURE 5.8: Sulphidation Equilibria for Part of the Fe-Sb-S System	127
FIGURE 5.9: Phase Relations of the System As-Fe-S and the Affect of Pressure and Temperature on the Composition of Arsenopyrite	130
FIGURE 5.10: Mol. % FeS in Sphalerite vs Temperature (isobaric curves of the system)	130
FIGURE 6.1: Summary of Microthermometric Data that can be Obtained from a Single CO ₂ -H ₂ O-bearing Inclusion ...	134
FIGURE 6.2: A Temperature-Composition Phase Diagram for the System NaCl-H ₂ O-CO ₂	146
FIGURE 6.3: T _{mice} Measurements from P- and PS-inclusions in Quartz, for all Vein Types	147
FIGURE 6.4: Freezing Point Depressions of Water (T _{mice}) for Different Solutes	149
FIGURE 6.5: The mol. % CO ₂ of Examples of Fluid Inclusions from Veins of Type I and II, Plotted Against their Homogenization Temperatures Compared with the 1 kb Solvus for CO ₂ and the Solvus at 1 kb and 6 wt. % NaCl	150
FIGURE 6.6: Frequency Diagrams for Homogenization Temperatures (Th) of P- and PS-inclusions of all Vein Types	152
FIGURE 6.7: Frequency Diagram for Homogenization Temperatures (Th) of S-inclusions of all Vein Types	153
FIGURE 6.8: Equilibria in the CO ₂ -H ₂ O-CH ₄ System (a) clathrate-hydrate equilibria in the CO ₂ -H ₂ O system and (b) phase equilibria in the CH ₄ -CO ₂ system at low temperatures	155
FIGURE 6.9: Melting Temperature of CO ₂ (T _{mCO₂})	156
FIGURE 6.10: Homogenization Temperature of CO ₂ (Th _{CO₂})	156
FIGURE 6.11: Relationship between Density (degree of filling) and Homogenization temperature for Pure CO ₂ -vapour-liquid System showing how the Homogenization goes to one Phase or the Other According to the Density of the Fluid	157

FIGURE 6.12: Relationship between the Degree of Filling (F-ratio) at 25°C and the Total Density of Inclusions, for Different NaCl Brines	158
FIGURE 6.13: Geobarometry using CO ₂ -rich Fluid Isochores (a) isochores for a CO ₂ -bearing fluid at low temperatures and (b) extrapolation of the isochores to higher temperatures	161
FIGURE 6.14: The Two Homogenization Method of Pressure Determination	162
FIGURE 6.15: Frequency Diagram for Th and Td Determinations of P- and PS-inclusions for CO ₂ -bearing Inclusions in Quartz Phenocrysts	166
FIGURE 6.16: A Summary of the Fluid Inclusion Data from the Moreton's Harbour Veins, Indicating a Possible Evolution of the Fluid	169
FIGURE 7.1: The Requirements for the Formation of a Hydrothermal Ore Deposit	171
FIGURE 7.2: A Summary of the Genesis of the Moreton's Harbour Hydrothermal Vein System	179

LIST OF PLATES

	<u>PAGE NO.</u>
FRONTISPIECE: Looking Southwestwards from Stewart's Mine across Little Harbour to Moreton's Harbour	1
PLATE 2.1: Banded, Vesicular Margin of a Basaltic Flow on Pillow Breccia, Wild Cove Head	35
PLATE 2.2: Columnar Jointed Surface of a Basaltic Flow with Calcite- and Epidote-Filled Fractures and Vesicles, Wild Cove Head	35
PLATE 2.3: A Pyritic Jasper Bed Overlying Massive Flow Basalt at Wild Cove Head	36
PLATE 2.4: Close-Packed, Small, Vesicular Basaltic Pillows, South of Beachy Cove	38
PLATE 2.5: Concentrically Zoned Vesicular Pillows, Taylor's Room	38
PLATE 2.6: Large Pillow-Basalts, Pearce Harbour	39
PLATE 2.7: Pillowing-Margins of a Banded, Vesicular Basaltic Dyke, North of Taylor's Room	39
PLATE 2.8: Irregular, Branching, Banded Vesicular Dykes, Little Harbour	39
PLATE 2.9: Broken-Pillow Breccia, Little Harbour	42
PLATE 2.10: Coarse Base of a Tuff-Breccia Bed Overlying a Volcaniclastic Sandstone of the Top of the Preceding Bed, Little Harbour	42
PLATE 2.11: Coarse, Volcanic Breccia Containing Isolated Whole and Broken Pillows and Exhibiting Disorganized Grading, Taylor's Room	44
PLATE 2.12: Pale-Weathering, Vesicular, Marginally-Silicified Blocks in Tuff Breccia, Little Harbour	44
PLATE 2.13: Finely Laminated Silicified Tuff and Grey Chert, Little Harbour	45
PLATE 2.14: Finely Laminated Ferruginous Chert and Tuff Breccia, South of Moreton's Harbour Head	45

PLATE 2.15:	Moreton's Harbour Head Breccia has calcite-quartz-sulphide-filled interstices between variably silicic and chloritic, angular fragments	47
PLATE 2.16:	Close-packed "bologna sausage" type outcrop of pillow basalt, Western Head	49
PLATE 2.17:	A chloritic, crystal-lithic-tuff overlying basaltic pillows, Chimney Cove	49
PLATE 2.18:	Basaltic pillow breccia with red chert fragments of the Hayward's Cove Formation	52
PLATE 2.19:	Coarse felsic, volcanic breccia, Hayward's Cove	52
PLATE 2.20:	Amphibolitic xenoliths in the margin of the microgranite at Pomley Cove	55
PLATE 2.21:	Felsic dyke, Sam's Cove	55
PLATE 2.22:	Internal dacitic portion	55
PLATE 3.1:	Photomicrograph showing intense calcitic alteration of pyroxene in a diabase dyke, Little Harbour .	68
PLATE 3.2:	Photomicrograph of calcite and chlorite filled amygdules in spilitic basalt	68
PLATE 3.3:	An accretionary lapillus in tuff-breccia, Little Harbour	72
PLATE 3.4:	Spherulitic texture in groundmass of a rhyodacitic fragment from the felsic breccia, Hayward's Cove ...	72
PLATE 3.5:	Pervasively calcitized diabase adjacent to ore veins, Stewart's Mine (with Alizarin red staining)	84
PLATE 3.6:	Pervasive calcitic alteration and veining adjacent to Stuckless' Mine stibnite-bearing veins (with Alizarin red staining)	85
PLATE 4.1:	A small, banded, quartz-arsenopyrite vein of Type I, cutting a diabase dyke, Little Harbour	93
PLATE 4.2:	Banded quartz-arsenopyrite vein, with carbonate seams, Little Harbour	93

	<u>PAGE NO.</u>
PLATE 4.3: Banded quartz-arsenopyrite vein, with carbonate seams, Little Harbour	93
PLATE 4.4: Massive arsenopyrite, bearing angular vein and wall- rock fragments, Stewart's Mine	94
PLATE 4.5: Photomicrograph of brecciated arsenopyrite cemented by quartz and calcite, Stewart's Mine	94
PLATE 4.6: Massive stibnite vein, Type II, Stuckless' Mine, with altered felsic dyke wall-rock and intergrown, banded quartz	98
PLATE 4.7: Photomicrograph of irregular sphalerite, bearing large blebs of chalcopyrite	98
PLATE 6.1: P- and PS-inclusions containing liquid CO ₂ , CO ₂ gas and an aqueous solution from gangue quartz of vein type I: (a) with solid carbonate and S-fluid inclusions; (b) with leakage "beak"; and (c) with S-inclusions	137
PLATE 6.2: Aqueous vapour + liquid P-inclusion from gangue quartz, vein type I	141
PLATE 6.3: Large, amoeboid aqueous vapour + liquid, P-inclusion from gangue quartz, vein type II	141
PLATE 6.4: Aqueous vapour + liquid (2-phase) inclusions from buff-coloured, growth-banded, gangue quartz of vein type II	165
PLATE 6.5: Solid and fluid inclusions in a quartz phenocryst of a rhyolite dyke	165

ACKNOWLEDGEMENTS

I would like to thank Dr. Dave Strong for his suggestion and subsequent supervision of this project, and for the financial support from his NSERC Operating Grant, number A7975. My gratitude is extended to all the technical staff of the Geology Department, Memorial University, for their assistance and co-operation, notably D. Press, G. Andrews, H. Longerich, F. Thornhill, L. Warford, W. Marsh, and M. McIntyre, and to the professorial staff. Also, sincerest thanks are rendered to Derek Wilton and other graduate students for their aid and discussion, and to Cynthia Pitts for typing. I am indebted to Norm and Ruby Smith who fed and housed me during my field season (summer, 1980) and to my various field assistants. I also thank R. Gibbons and D.F. Strong for use of their samples and data, to supplement this study.

CHAPTER 1

THE GEOLOGY AND MINERALIZATION OF THE MORETON'S HARBOUR AREA

Introduction

Moreton's Harbour is a small fishing community situated on New World Island, Notre Dame Bay of Newfoundland at $49^{\circ}30'N$, $54^{\circ}52'W$ (Fig. 1.1). The rocks underlying this area were mapped and sampled during July/August 1980 and subsequently studied in detail. The study area is covered by the Twillingate Map Sheet Canada NTS No. 2E/10 and measures approximately 16 km^2 in area. The area is reasonably accessible by gravel roads and woods' trails, supplemented by traverses and coastal boat work.

The region has been extensively glaciated (Tucker, 1976) which created the deeply dissected topography between 25 m and 300 m elevation. The scarp-like ridges are separated by U-shaped and rejuvenated valleys and wide areas of bog. The valleys are traced by erratic streams by which the area is drained.

The fjardic coastline is indented producing sheltered natural harbours, notably Moreton's Harbour itself and Whales Gulch. The rugged cliffs display variable profiles from gently inclined to sheer up to 100 m high. These exhibit various geomorphological features including narrow wave-cut platforms, notches and overhangs. Beach deposits are coarse pebble to cobble, best developed at Pomley Cove.

There are twelve ponds, the largest of which is Moreton's Harbour Pond (250 m^2) bounded by marsh and steep cliffs. The ponds occur between 15 m and 50 m elevation.



Fig. 1.1: Map of the island of Newfoundland showing the location of Moreton's Harbour with respect to the Cambro-Ordovician rocks (black) and the tectonostratigraphic zones of Williams (1979). Inset frame shows area of Figure 1.2.

The rocks are impressively exposed around the coast (100% outcrop). However, the dense vegetation cover of spruce woodland and shrub renders inland exposure poor (<1%), further frustrated by bogs, flies and spruce budworm. Overburden of glacial and alluvial deposits attains a maximum thickness of 1 m on high ground and may exceed 3 m in the low lying areas.

1.2 The Regional Geological Setting

The Moreton's Harbour area is underlain by Lower Palaeozoic volcanic and associated pyroclastic rocks within the Dunnage Zone at the Northeastern extremity of the Appalachian Orogenic belt of North America (Figs. 1.1 and 1.2; Williams, 1979). The Dunnage Zone, formerly classified within the Central Mobile or Volcanic Belt of Newfoundland, comprises a sequence of volcanic, sedimentary and intrusive rocks. The Zone is bounded east and west by the more deformed and metamorphosed rocks of the Gander and Humber Zones respectively.

Various plate tectonic models for the evolution of the Appalachian Orogen have been proposed (e.g. Dewey & Bird, 1971) based on the geology of Notre Dame Bay. The recognition of the Dunnage Mélange (Horne, 1969; Kay, 1970) and its interpretation as a trench fill, subduction related deposit (Kay, 1972; Hibbard & Williams, 1979), general geochemical studies by Smitheringale (1972) and Kean & Strong (1975) and specifically of the sheeted dykes (Strong, 1972; 1973) have been used as evidence that the Dunnage represents the vestiges of the Lower Palaeozoic Iapetus Ocean. The volcanic rocks of the region were first compared to island arc assemblages by Heyl (1936). An island arc mode of origin is substantiated by more recent studies (Strong, 1973; 1974; 1977; Payne & Strong, 1973; Williams & Payne, 1975; Swinden & Strong, 1976).

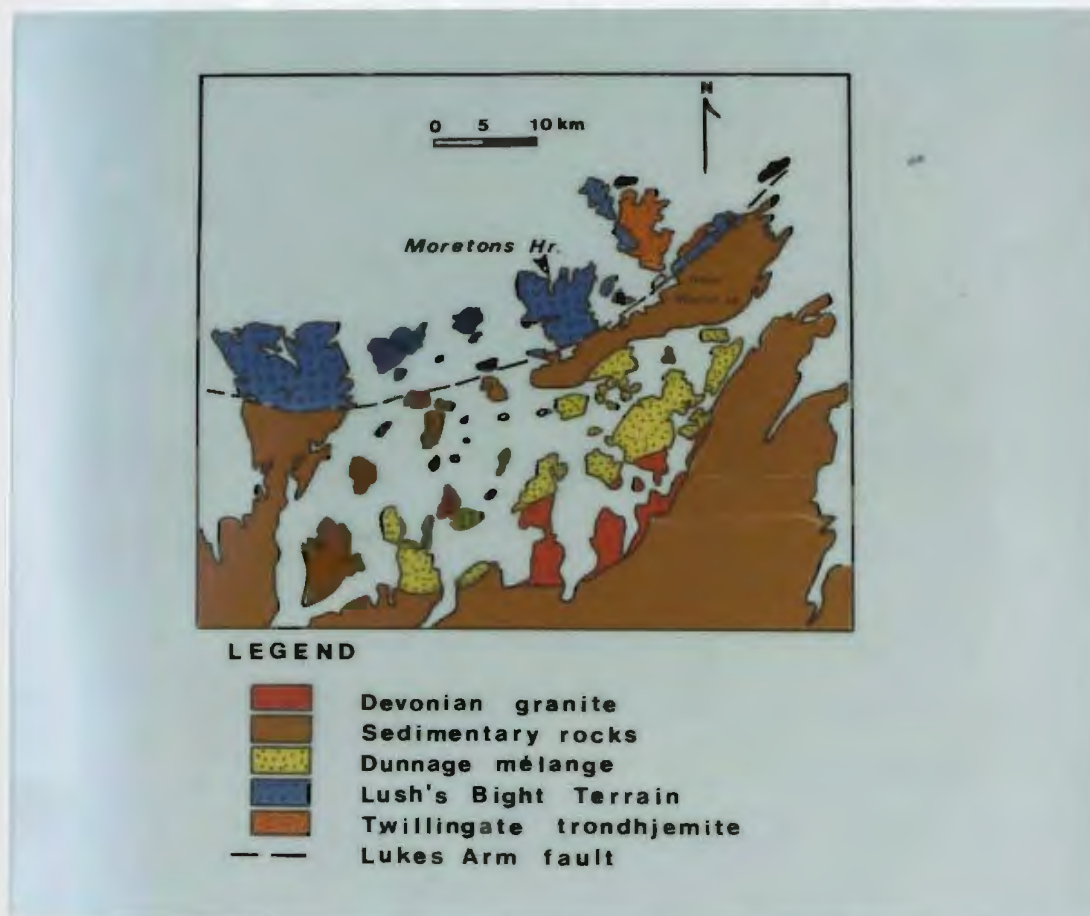


Fig. 1.2: The general geology of eastern Notre Dame Bay.

1.3 Previous geological work

The earliest report pertaining to the study area (J.B. Jukes, 1843) correlated the slates of eastern Notre Dame Bay, the Lower Slate Division, with those of the St. John slates of the Avalon. The "micaceous trap rocks" of Twillingate and Fogo were also noted.

A systematic study of the mineral deposits was made by Alexander Murray in 1864 who later in 1871 mapped the coastline. Murray made a two-fold division of the rock types:

- 1) a Lower Formation of basaltic dykes, lavas and interbedded cherts, correlated with the Quebec Group of the Mainland.

overlain unconformably by

- 2) an Upper Formation fossiliferous sediments, assigned to the Llandovery stage.

He observed that the mineral deposits were confined largely to the Lower Formation (Murray and Howley, 1881).

J.P. Howley (1907) used Murray's data to compile a geological map of the area. Howley kept detailed records of the area's mining activity.

M.E. Wadsworth (1884) studied the volcanic rocks and recognized the subaqueous nature of the pillow basalts, which he described graphically as "writhing... anacondas" and "Bologna sausages".

Buddington, Sampson and Agar from 1915 investigated the stratigraphy, assigning the submarine volcanics a Cambrian age and the overlying sedimentary sequence as Ordovician (Sampson, 1923). Age constraint was enhanced by the recognition of a persistent, black, graptolitic, Llandoilian shale horizon.

Heyl (1936) divided all the stratified rocks of the Bay of Exploits area into nine formations, most of which he considered Middle Ordovician. The volcanic rocks underlying Moreton's Harbour were named the Moreton's Volcanics with a thick pillow lava sequence, the Breakheart Basalt, to the south. The granodiorite batholiths of Loon Bay and Twillingate were considered to be late Silurian to Devonian. Heyl's stratigraphy has been shown to be upside down (Williams, 1963a,b; Helwig, 1967). Despite this, his comparison of the volcanics to island arc rocks and their correlation with the British Ordovician were major contributions.

Extensive fossil collections were obtained from the Ordovician-Silurian sedimentary rocks of the Bay of Exploits by W.H. Twenhofel and R.R. Shrock, from which the following stratigraphy was derived:

Top:	limestone blocks in flow breccia	
	shales and red sandstones	Pikes Arm Fm.
	coarse conglomerate	Goldson Fm.
Base:	thin bedded red sandstones	Botwood Fm.

These units were well defined but their stratigraphy proved erroneous (Williams, 1963a,b).

Reconnaissance mapping of the Fogo-Twillingate-New World Islands was undertaken by Baird (1953). All volcanic rocks were assigned to the Ordovician system due to the presence of Cobbs Arm limestone blocks in some flows. Baird recognized the structural complexity and predicted astutely that the Notre Dame Bay region was the key to understanding of the geology of northeastern America.

Hayes (1951) followed Heyl's (erroneous) stratigraphy and failed to recognize the two-fold basal volcanic and overlying arenaceous and argillaceous sediments.

Between 1956 and 1962, H. Williams undertook several studies around Notre Dame Bay. In 1962 he compiled the Twillingate map sheet and discovered Heyl's errors. He correlated the oldest rocks with the Snooks Arm or Lushs Bight Groups to the north of the Lukes Arm Fault, where he mapped a continuous (erroneously) north facing sequence of Ordovician volcanic rocks (the Headlands Group), middle Ordovician limestones and graptolitic shales overlain by Upper Ordovician to Lower Silurian greywacke. The latter coarsens upwards to become the conglomeratic Goldson Formation. This was the first stratigraphy well established by faunal studies. The structural complications were attributed to folded or steepened thrust faults (Kay & Williams, 1963; Williams, 1963a; Dean & Strong, 1977).

New World Island stratigraphy was correlated with that of Fortune Harbour Peninsula by Horne and Helwig (1969) using earlier work (e.g. Helwig, 1967; Horne, 1969). A two-fold division was established, bisected by the Lukes Arm Fault. The volcanic and volcanoclastic rocks to the North were re-assigned to the Lushs Bight Terrain, whereas to the South were variable Ordo-Silurian sedimentary rocks, including the Dunnage Melange, the Dark Hole Formation (a Caradocian black shale marker horizon), the Sansom and Goldson arenaceous Formations and the Cobbs Arm limestone.

Despite lack of detail, Strong and Payne (1973) showed the subdivision was appropriate and applied the term "Lushs Bight Supergroup" to the rocks North of the Lukes' Arm Fault. The Supergroup encompasses various local groups, for example the Moreton's Harbour Group, pertinent to this study. This group conformably overlies ophiolitic rocks, as do the Western Arm and Snooks Arm Groups (Strong, 1973; Dean, 1978). According

to Strong and Payne (1973) the Moreton's Harbour Group may be subdivided to five formations which are considered a useful framework for the present study (Table 1.1). The Chanceport Group, a north-facing sequence of pillowed-basalts, bedded tuffs and cherts occurs to the south of the Moreton's Harbour Group, juxtaposed along the Chanceport Fault (Fig. 1.2).

Williams and Payne (1975) considered that there was a structural break between their Sleepy Cove Formation, immediately adjacent to the Twillingate Trondjemite and the Moreton's Harbour Group to the west. The Sleepy Cove formation comprises deformed and amphibolitized volcanic rocks intruded by the Twillingate granite. Strong and Payne (1973) discounted any break and proposed a continuous succession from Moreton's Harbour, increasing in metamorphic grade and deformation towards the Twillingate trondjemite contact.

The Twillingate trondjemite is apparently discordant to the country rock and was considered to be Upper Silurian to Devonian (e.g. Heyl, 1936; Williams, 1963a). However, a zircon U-Pb date of 510 ± 17 Ma (Williams et al., 1976) repudiates the Acadian affinity of the intrusion, and implies a Cambrian age for the Sleepy Cove volcanics. The trondjemite has variously been interpreted as a crustal remnant (e.g. Williams and Malpas, 1972) and part of the base of an island arc complex (e.g. Strong and Payne, 1973; Williams and Payne, 1975; Payne and Strong, 1978).

A more detailed review of the work pertaining to the geology of Notre Dame Bay is provided by Dean (1978).

The local geology is described in Chapter 2, and summarized in Table 2.1 and Map 1 (in pocket).

1.4 Economic geology history

There are numerous and variable mineral deposits around Notre Dame Bay, predominantly associated with the "Lower (Volcanic) Formation" as recognized by Murray in 1864. Howley (1907) maintained mining activity records of the area and a compilation of the economic geology of the Central Mineral Belt was provided by Snelgrove (1928). Snelgrove considered the base metal sulphides of Betts Cove and Tilt Cove to be replacements controlled by structure and genetically related to small igneous intrusions; a view supported by several other workers (e.g. Neale, 1958). A volcanogenic origin for these sulphides was proposed by Williams (1963c) and supported by others (e.g. Strong, 1973; Upadhyay, 1973; Swinden and Strong, 1976).

No massive sulphide deposits are encountered within the present study area which is concerned primarily with the precious metal-enriched arsenopyrite, base metal and stibnite lodes, which have previously been described and studied by Heyl (1936) and Gibbons (1969). Prospecting was undertaken by NALCO (Fogwill, 1968).

1.5 Aims and approach of study

The main objective of this project was to examine the vein mineralization in the Moreton's Harbour area, in order to determine the physical and chemical parameters of deposition of the ore minerals, with specific interest in their relation to the precious metal enrichment.

The approach to this study commenced with detailed field work (Map 1) and sampling of the veins and the host volcanic rocks followed by detailed laboratory studies. The petrography of the volcanic and ore samples was studied using transmitted and reflected light (Chapters 3

and 4). Mineralogical compositions were ascertained using the electron microprobe (Chapters 3 and 5). Geochemical data of volcanic and ore samples were obtained using both X-ray fluorescence and atomic absorption spectrophotometry, the latter using both flameless and flame techniques (Chapters 3 and 5). The physicochemical parameters of ore deposition were determined using microthermometric studies of fluid inclusions in gangue quartz (Chapter 5).

Samples collected in the present study were supplemented by those collected by R. Gibbons (1969) and D. Strong (1972) for microprobe and geochemical analyses.

CHAPTER 2

THE LOCAL GEOLOGY

2.1 Introduction

The Moreton's Harbour area is underlain by a thick sequence of Lower Palaeozoic volcanic and volcanoclastic rocks of predominantly spilitized basaltic composition with felsic pyroclastics at the top of sequence. The succession dips steeply and is consistently upward facing to the southwest. The area was intruded by multitudinous dykes and sills which range compositionally from basalt to rhyolite. There are minor intercalated red and grey cherts within the volcanoclastic-sedimentary rocks.

The geology of the area is shown in Map 1 (also in Fig. 2.1) and is summarized in Table 2.1. The following account describes the rock types and field relations, mainly as observed from the spectacular coastal exposure.

The contacts between the formations are gradational and conformable and are based entirely on lithological contrasts. The stratigraphy of volcanic terrains is epitomized by abrupt lithological and facies variations both vertically and horizontally in the section (hence time and space) (e.g. Moore et al., 1973; Dimroth et al., 1978; Ballard et al., 1979; Rust, 1979). Such variation renders correlation difficult, further hampered by repetition of lithofacies and lack of suitable marker horizons. The volcanoclastic terminology is based on that of Wright et



Fig. 2.1: Geology of the Moreton's Harbour area, simplified from Map 1.
 (M.H. - Moreton's Harbour)
 (L.H. - Little Harbour)

TABLE 2.1
Summary of the Geological Subdivisions
of the Moreton's Harbour Area

Lamprophyre	- pyroxene-phyric, analcite-bearing lamprophyre dyke at Taylor's Room (~Jurassic)
Dick's Head Gabbro	- late microgabbro stock
Gerald Dearing's Diorite	- deformed, sheared diorite
Felsic Intrusive Rocks	- rhyolitic to dacitic in composition, pink to buff coloured, <u>+</u> phenocrysts, spherulitic to microgranitic, may be related to the felsic pyroclastic rocks. Abundant throughout the area, generally perpendicular to regional strike; related to mineralization (5 cm to ~150 m)
Hayward's Cove Formation	- (≥ 200 m) characterized by coarse felsic (rhyodacitic) breccia at Hayward's Cove with finer felsic tuffs along strike
Chimney Cove Tuff	- crystal-lithic chloritic tuff within mafic pillow flows and breccias with common jasperoid fragments and interstices
Western Head Formation	- (~2000 m) predominantly mafic pillow basalts with minor breccia horizons (e.g. at Western Head Harbour)
Little Harbour Formation	- (> 2000 m) predominantly volcanoclastic rocks, of mafic composition ranging from chert to coarse boulder-breccia. Massive to pillowed basaltic flows with minor breccias and chert in the lower part of the sequence
Moreton's Harbour Head Breccia	- (? m) pyritic, felsic very coarse breccia of uncertain affinity (possibly related or similar to the felsic breccias of the Hayward's Cove Formation?)
Wild Cove "Formation"	- (> 1000 m) characterized by the preponderance of diabase to microgabbro (<u>+</u> sheeted) dykes with minor pillow screens

a1. (1980) and Wentworth and Williams (1932) as appropriate. Pillow breccia terminology is based on that of Carlisle (1963) who describes the Quadra volcanic succession, Vancouver, which closely resembles the Moreton's Harbour succession.

2.2 Wild Cove Formation

The oldest rocks in the map area are those of the Wild Cove and eastwards towards Webber's Bight and can be traced inland towards Church Hill Pond. This formation is defined by the preponderance of mafic dykes, up to 100% at Wild Cove, where they are seen to be sheeted in places. The dark green-grey dykes are basaltic in composition and range texturally from aphyric and aphanitic to microgabbroic. Diabases, variably plagioclase-phyric are predominant. These dykes exhibit typically chilled margins and some show bands of calcite, chlorite and/or epidote-filled amygdules near and parallel to their margins. The gabbroic dykes are apparently the earliest intrusives as they are cut by the fine grained, dark aphyric dykes. All dykes trend generally east-west.

There are narrow screens of pillow basalts with interstitial dark grey chert, black-green aphanatic basaltic injection with calcite-chlorite-epidote fillings. The pillows are generally less than 50 cm in diameter, ellipsoidal in shape and flattened parallel to their intrusive "walls". They are variably vesicular and commonly contain large central drainaway-cavities.

The Wild Cove Formation is underlain by the mafic volcanic rocks of the Tizzard's Harbour Formation (Strong and Payne, 1975) to the east of this study area. The density of intrusives decreases westwards from Wild Cove giving way to the Little Harbour Formation, which in part was fed by the Wild Cove dyke system.

The Wild Cove Formation must represent an extensional environment but it is well argued (Strong and Payne, 1975) that a mid oceanic ridge-spreading centre is not appropriate. A small back arc or intra-arc basin is a preferable setting.

2.3 Little Harbour Formation

The Little Harbour Formation is dominated by volcanic rocks, ranging from massive flows in the lowermost facies to a succession of impressive volcanoclastic rocks. This Formation is estimated to be ≈ 2 km in thickness, occupying a northwesterly-trending tract from Little Harbour across Moreton's Harbour, Frost Cove and Taylor's Room to Pearce Harbour. It is this Formation that contains the mineralization of the area.

The Little Harbour Formation is here described in three main sections (Fig. 2.2):

A-A' Little Harbour - Wild Cove Head

B-B' Taylors Room - Moreton's Harbour Head

C-C', D-D' Pearce Harbour.

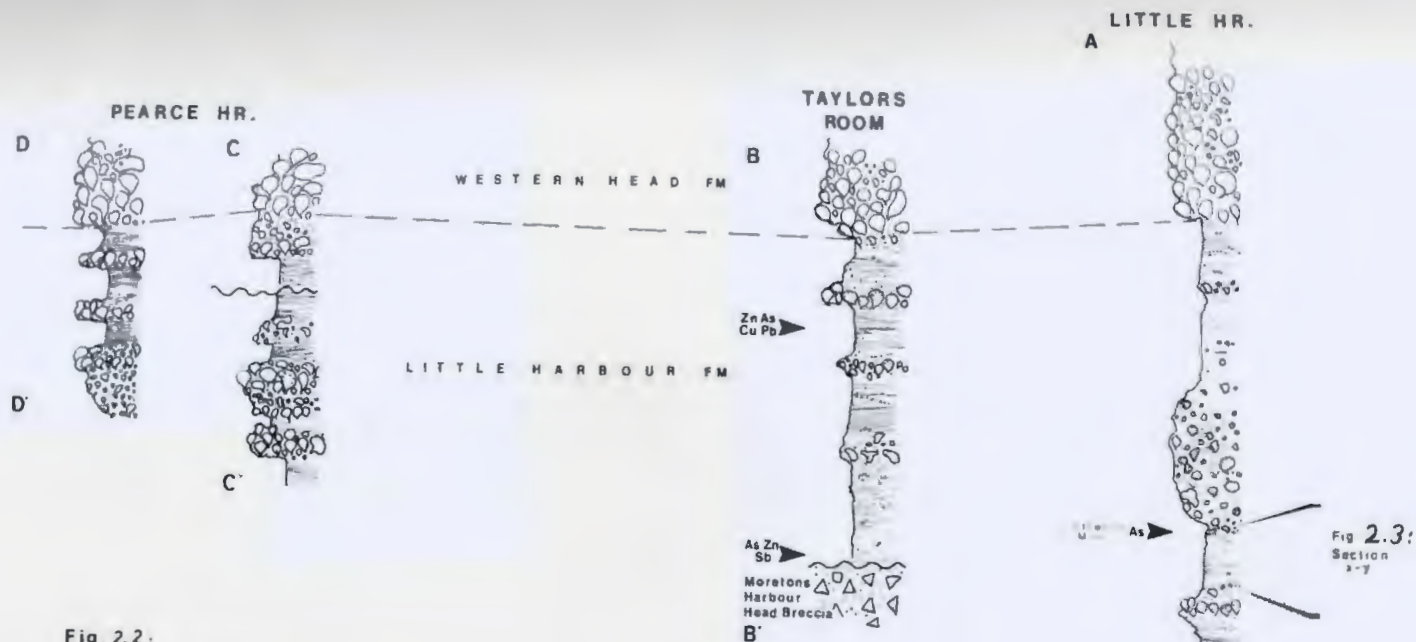


Fig. 2.2:

Schematic sections
of the Little Harbour
Formation.

LEGEND

- Fine grained, laminated tuffa & chert
- Tuff & pillow breccia
- Pillow basalt
- Massive, basaltic flows
- Diabase (sheeted) dykes
- Coarse, felsic breccia

These sections constitute broadly similar sequences of volcanoclastic rocks from coarse boulder breccias, tuff breccias and fine tuffs, with massive and pillowed flows. The tuff breccias are variable in texture from close-packed fragments to matrix-supported. In each section, good sedimentary structures are observed providing facing criteria. The absence of marker horizons with the lithological variation and repetition renders correlations difficult. The top of the Formation is taken where the predominant lithology is pillowed flows of the Western Head Formation, in which volcanoclastic horizons are relatively rare.

2.3.1 The Little Harbour Section (A-A')

2.3.1a Massive flow lithofacies

The lowermost rocks of this section are massive, spilitic flows, up to 3 m in thickness. These flows are fed by mafic dykes traced from the Wild Cove Formation. The flows are black to grey-green in colour and are generally aphyric and aphanitic. Vesiculation at the tops and bases of flows is observed north of Beachy Cove. Vesicles are sparse (<10%) and small (<5 mm in diameter), and delineate a textural margin-parallel banding (Plate 2.1). Flow surfaces rarely exhibit columnar jointing (Plate 2.2).

The flows are interdigitated by flow breccia and pillowed flows. At Wild Cove Head, a pyritic-jasper bed overlies a partly pillowed, columnar-jointed flow (Plate 2.3). This chert is irregular and attains a maximum thickness of 45 cm, and dips at 45° to west-southwest.



PLATE 2.1: Banded, vesicular margin of a basaltic flow (right) overlying pillow breccia (left), Wild Cove Head.



PLATE 2.2: Columnar jointed surface of a variably vesicular basaltic flow, with calcite- and epidote-filled fractures, Wild Cove Head.



PLATE 2.3: A pyritic jasper bed overlying massive flow basalt and breccia at Wild Cove Head. A sample of this jasper (WCH.9) showed primary enrichment of precious metals.

The massive flow lithofacies is cut by abundant diabase dykes of varying orientation. Two main sets are observed:

(1) the earlier set dip gently and trend east-west and are cut by a

(2) more prominent, steeper dipping north-northeast striking set.

The rocks are deformed very locally along shear zones associated with minor faulting through Beachy Cove. The profuse calcite and epidote veins are fault-related.

2.3.1b Pillow lava lithofacies

Southwestwards, there is a gradational increase of pillowed flows with a complementary decrease of massive flows. The pillows are typically close packed, elliptical, vesicular and show way up to the south (Plates 2.4, 5 and 6). The pillows are identical to those classically described from subaqueous volcanic sequences elsewhere (e.g. Jones and Nelson, 1970; Moore, 1970; Moore et al., 1973; Dimroth et al. 1978; Ballard et al., 1979). The pillows are associated with coarse whole- and broken-pillow breccias (Plate 2.9). There is a general increase in size and density of vesiculation of the pillows southwards. This indicates shallowing water depths upwards (e.g. Jones and Nelson, 1970; Moore, 1970; Jones, 1969). Irregular, grey banded "splatter" fragments occur in several breccia horizons. Elongate banded fragments up to 0.5 m long, supported by a dark basaltic matrix occur just north of Little Harbour, reminiscent of the "collapse lava pits" described from Galapagos by Ballard and coworkers (1979).



PLATE 2.4: Close-packed, small, vesicular, basaltic pillows, south of Beachy Cove.



PLATE 2.5: Concentrically-zoned, vesicular pillows, Taylor's Room.



PLATE 2.6: Large
basaltic pillows,
Pearce Harbour.



PLATE 2.7 (above): Pillowing,
vesicular, banded-margin of a
basaltic dyke, north of Taylor's
Room.



PLATE 2.8 (left): Irregular,
branching, banded, vesicular dykes,
Little Harbour.

2.3.1c Volcaniclastic sedimentary lithofacies

This lithofacies comprises a 200 m sequence of well bedded, variably graded volcaniclastic (=epiclastic) sedimentary rocks (Fig. 2.3). Matrix-supported gravel (>2 mm and <64 mm) predominates although grain size varies from boulder to clay.

The coarser, close-packed volcaniclasts at the base of some beds cut into or scour the finer, laminated tuffs of the underlying beds and the coarse, variably rounded fragments may penetrate the underlying tuffs (Plate 2.10). The coarser beds, which may attain several metres in thickness, may exhibit normal, inverse or disorganized gradation. Large banded (pillow) fragments are abundant, with a volcanic crystal-lithic arenite matrix. The clasts weather to a pale buff and show marginal alteration (i.e. hydration, silicification) whereas the matrix is much darker greenish in colour (Plate 2.12).

The finer, volcaniclastic sandstones are distinctively planar laminated, normally graded and rarely exhibit low angle cross-stratification (Plate 2.10).

Fine silicified tuff and grey cherts (Plate 2.13) occur on the coast at Little Harbour and are seen to grade laterally into coarser aquagene tuffs and tuff breccias.

Reworking of the volcanic debris is evident from the fragment roundness and sedimentary features. The sedimentary structures are analogous to those described by Walker (1979) in coarse alluvial fan deposits.



- 41 -

Fig. 2.3: A detailed 200 m section, x-y, from the Little Harbour volcanoclastic lithofacies.

Cherty tuffs overlain by coarse, chaotic breccia (+ whole or broken pillows). Along strike from Stewart's Mine.

Thickly bedded, coarse, graded tuff breccias.

Finely laminated, discontinuous grey tuffaceous cherts overlying coarser volcanic sediments.

Intrusive breccia at the margins of a strongly discordant diabase dyke.
Abundant diabase intrusives.

Mafic intrusions with irregular pillowing margins cutting well bedded, normally graded volcanoclastics. Common scoured tops of the fine grained rocks.

Coarse breccia lenses in discontinuously bedded, graded tuffs and tuff breccias.

Thick porphyritic diabase dyke with chilled margins.

Pillow lavas and "collapse-pit" remnants.



PLATE 2.9: Broken-pillow breccia, Little Harbour.



PLATE 2.10: Coarse base of tuff-breccia bed overlying a volcaniclastic sandstone of the top of preceding bed, Little Harbour.

Pillowed flows are not encountered in this unit although irregular pillow-like intrusions are common (Plates 2.7 and 2.8). These banded dykes and sills with pillowing terminations are considered the result of intrusion into a low density, unconsolidated tuffaceous pile. It is argued by McBirney (1963) that in such sedimentary piles, dykes and sills are more likely to form than extrusive flows due to their density contrast.

The thickness of beds increases upwards although no overall fining sequence is noticeable.

2.3.1d Coarse tuff breccia lithofacies

The upper part of the Little Harbour section of this Formation is exemplified by coarse tuff breccias. These breccias are predominantly fragment-supported framework with dark coarse sand-size lithic, tuffaceous matrix. The fragments are basaltic, angular to subrounded blocks, generally poorly vesicular and are dark grey, sometimes orange iron-stained in colour. Blocks range to greater than 1 m in size (Plate 2.11). Isolated whole- and broken-pillows are also observed.

Bedding of these coarse, proximal deposits is poorly defined and disorganized. The coarsest beds of the Little Harbour Peninsula are along strike from finely laminated tuff-chert beds (Plate 2.13) below Stewart's Mine. Near Osmond's store, Moreton's Harbour, there is an outcrop of matrix-supported lapilli tuff.



PLATE 2.11: Coarse volcanic breccia containing isolated whole- and broken-pillows and exhibiting disorganized grading, Taylor's Room.



PLATE 2.12: Pale-weathering, vesicular, marginally-silicified bombs in tuff breccia, Little Harbour.



PLATE 2.13: Finely-laminated, silicified tuff and grey chert, Little Harbour.



PLATE 2.14: Finely-laminated, ferruginous chert and tuff breccia, south of Moreton's Harbour Head.

The top of the Little Harbour Formation of this section is marked by an increase of pillow lava flows of the Western Head Formation.

2.3.2 Taylor's Room Section

The section of the Little Harbour Formation through the west side of Moreton's Harbour is shown as B-B' (Fig. 2.2). This section is dominated by the volcanoclastic lithofacies with minor pillow horizons. No massive flows are present. The northern part of the section is occupied by the Moreton's Harbour Head Breccia, which is faulted against the mafic volcanoclastic rocks of the Little Harbour Formation. The Breccia comprises coarse, angular felsic blocks with mafic fragments and isolated pillows. Its true affinity is not clearly understood. The Breccia is cut by thin buff to pink felsic dykes and numerous quartz and carbonate veins, many of which contain traces of sulphides (pyrite, arsenopyrite, stibnite, sphalerite) (Plate 2.15).

To the south of the iron-stained fault zone through the "neck" of Moreton's Harbour Head, there occurs a sequence of lithic to vitric tuffs and tuff breccias with red and green, finely laminated cherts (Plate 2.14). The tuffs and cherts are closely intermixed and large green, poorly vesicular irregular mafic clasts up to 10 cm in size are dispersed through a chert matrix. The fragments are leached and silicified. The fine tuffaceous sediments are laminated and normally graded. A general increase in the abundance of pillows occurs up the sequence. Examples of very shallow water, densely vesicular, concentrically banded,



PLATE 2.15: Moreton's Harbour Head Breccia has calcite, quartz, sulphide-filled interstices between variably silicic and chloritic, angular fragments.

spheroidal pillows are observed on the coast just below the road at Taylor's Room (Plate 2.5). These greatly resemble those of the upper part of the Little Harbour section.

This section is similarly cut by abundant mafic intrusives which exhibit distinctive banding and pillowing margins (Plate 2.7). There are also many felsic intrusions.

2.3.3 Pearce Harbour Section

The section of the Little Harbour Formation through Pearce Harbour resembles the sections previously described but contains more large, close-packed pillow lavas (Plate 2.6). These pillows characteristically contain few vesicles and do not exhibit the marked concentric texture; these pillows are considered to be the products of extrusion into relatively deep water. Volcaniclastic rocks are like those to the east.

2.4 Western Head Formation

The Western Head Formation comprises a thick (~2 km) succession dominated by close-packed spilitic pillow basalts with minor intermittent, discontinuous horizons of coarse, broken and isolated whole-pillow breccias (Plate 2.16). The pillows are variably vesicular and are generally of deeper water type. These pillows compare well with those described from modern oceanic, basaltic volcanic fields (e.g. Jones and Nelson, 1970; Moore, 1970; Moore et al., 1973; Ballard and Moore, 1977; Ballard et al., 1979) and no further elaboration is necessary here.



PLATE 2.16: Close packed "bologna sausage" type outcrop of pillow basalt, Western Head.



PLATE 2.17: A chloritic, crystal-lithic tuff overlying pillow basalts, Chimney Cove.

2.5 Hayward Cove Formation

The Hayward Cove Formation overlies the pillow lavas of the Western Head Formation conformably and consists largely of felsic pyroclastic rocks.

2.5.1 Chimney Cove tuff facies

At Chimney Cove, the pillow lavas of the Western Head Formation are overlain by a finely laminated grey chert (≤ 50 cm thick) which is overlain by a chloritic, rubbly-weathering crystal lithic tuff traced along strike to the Old House Cove (Plate 2.17). The chloritic tuff is less than 1 m thick and dips relatively shallowly towards the southwest. Overlying this tuff there are more dark pillow lavas and breccias which contain interstitial red and grey chert and coarse chert-bearing pillow breccias (Plate 2.18).

2.5.2 Felsic pyroclastic lithofacies

At Hayward's Cove, a coarse, polymict breccia outcrops, composed predominantly of pink angular dacitic to rhyolitic blocks (Plate 2.19) with laminated chert and silicified, mafic tuff fragments. This breccia is iron-stained and in places white oxidation is seen, suggesting zinc mineralization (which was not supported by chemical data).

Southwards, the felsic breccia contains variable fragments, and fines along strike to Moreton's Cove, where the Hayward's Cove Formation is juxtaposed against pillow basalts akin to those of the Western Head Formation along a northeasterly-trending fault zone.

NW

SE

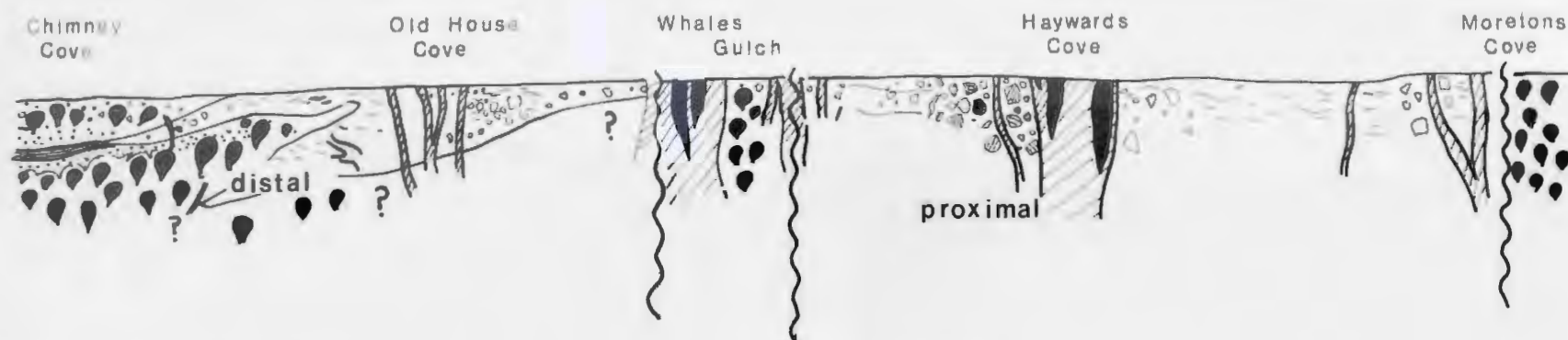


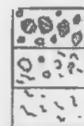
Fig. 2.4 :
Schematic section of
felsic pyroclastics,
Haywards Cove Formation.

0 500m
 scale

LEGEND



Felsic dykes



coarse breccia

fine, ignimbritic

} FELSIC PYROCLASTICS



pillows with jasper fragments



grey, laminated chert & tuff



WESTERN HEAD FM. pillow basalts



fault



amphibolite



PLATE 2.18: Basaltic pillow breccia with red chert fragments, of the Hayward's Cove Formation.



PLATE 2.19: Coarse felsic, volcanic breccia, Hayward's Cove.

Northwards, the felsic breccia is finer grained and more siliceous. These distal pyroclastic (felsic tuffs) are pale buff and contain dark pink glassy "shards" and crystal fragments. There is a primary flattening foliation approximately parallel to the regional strike (i.e. northwest-southeast).

The lateral facies variation of the Hayward's Cove Formation is presented diagrammatically in Fig. 2.4.

The felsic pyroclastic rocks are cut by numerous pink rhyolitic-rhyodacitic dykes which appear to be related to the volcanic rocks.

2.6 Intrusive Rocks

2.6.1 Mafic dykes

There are multitudinous mafic intrusions cutting the volcanic and volcanoclastic sequence, notably in the Wild Cove Formation. Diabase is predominant and may be aphyric to plagioclase and/or clinopyroxene-phyric. The syndepositional feeder dykes through the Little Harbour Formation are characteristically vesicular and banded with pillowing margins (Plates 2.7 and 2.8). Later dykes trend predominantly north-northeast and attain thicknesses up to 10 m, such as the diabase dyke that hosts the Stewart's Mine mineralization. At Little Harbour, a very coarsely pyroxene-phyric, rubbly weathering dyke occurs.

2.6.2 Other mafic intrusions

Dick's Head is underlain by a fine grained gabbro with subophitic texture. The small intrusion has clearly intrusive contacts and is not cut by any other felsic or mafic dykes.

South of Moreton's Harbour Pond a pervasively sheared, calcite-veined metagabbro or diorite is exposed along the new road cutting. This diorite is variably coarse to fine grained and contains phenocrysts of hornblende. This intrusion is referred to as Gerald Dearing's diorite (Map 1).

2.6.3 Felsic intrusive rocks

The map area is cut by abundant rhyolitic to andesitic dykes which post-date (i.e. cut) the mafic dykes. These felsic intrusions predominantly trend northeast and range in width up to 100 m (e.g. Pomley Cove; Hayward's Cove). The finer grained felsic dykes are pale buff to bright pink and vary from glassy to saccharoidal in texture. Phenocrysts of quartz and/or plagioclase are variably present. The microgranitic intrusion through Pomley Cove has caused silicification and amphibolitization of the mafic host rocks which occur as abundant xenoliths in the dyke's margins (Plate 2.20).

The felsic dykes invariably show chilled margins and generally fine southwards. The rhyolite dyke at Sam's Cove shows impressive columnar jointing (Plate 2.21) in the glassy margin and the centre is less silicic, and is saccharoidal (Plate 2.22).

The rhyolite and rhyodacite intrusions may be related to and feed, the Hayward's Cove felsic pyroclastic rocks. The felsic dykes are spatially closely associated with the mineralization within the Little Harbour Formation.



PLATE 2.20:
Amphibolitic
xenoliths in the
margin of the
microgranite
Pomley Cove.



PLATE 2.21: Columnar jointing
in the Sam's Cove rhyolite dyke.

PLATE 2.22 (left): Detail
of coarser, internal dacitic
phase.

2.6.4 Lamprophyre

There is one late (Jurassic) thin lamprophyre dyke seen north of Taylor's Room. It attains a thickness of up to 30 cm and is porphyritic and black in colour (see Chapter 3).

2.7 Structural Geology

The extrusive rocks underlying the map area all dip steeply and face upward to the southwest. No major fold closures or parasitic folds are discerned within this area. The rocks are uncleaved and have no lineation developed. Hence, the rocks lie on part of a larger structure, presumably the western limb of an antiform to the North. The rocks are faulted along the Chanceport fault, against the Chanceport Group, with subsidiary faulting throughout the area (Bridgeport, Wild Cove Head, Moreton's Harbour Head, Pearce Harbour, Moreton's Cove, etc.). Deformation occurred locally along these faults and related shear zones.

2.8 Metamorphism and Alteration

The mafic volcanic rocks have a typical low greenschist facies mineralogy (see Chapter 3) which is partly due to spilitization. The rocks adjacent to the margins of the felsic dykes are baked, i.e. amphibolitized. Mineralizing fluids responsible for the ore deposition caused silicification, calcitization and sericitization of the country rocks.

2.9 A summary of the geologic history of the Moreton's Harbour area

The following is a simplified geological history of the Moreton's Harbour area:

1. Emplacement of semi-sheeted, mafic dykes in a tensional, back arc(?) basinal tectonic environment - WILD COVE FORMATION
2. Extrusion of subalkaline basaltic flows which are variably massive or pillowed and vesicular, with minor volcanoclastic and cherty horizons intercalated, under moderate water depths - LITTLE HARBOUR FORMATION (early)
3. Continuation of mafic volcanism but in decreasing water depths to very shallow, explosive phreatomagmatic volcanism, which produced copious volcanoclastic rocks, variably reworked - LITTLE HARBOUR FORMATION
4. The onset of deep water, basaltic extrusion resulting in a thick sequence of pillow lavas with minor breccia lenses - WESTERN HEAD FORMATION
5. Intrusion of vertical felsic dykes feeding(?) felsic breccias and tuffs at the top of the exposed volcanic pile - HAYWARD'S COVE FORMATION
6. Mineralization
7. Intrusion of gabbro and diorite
8. Faulting and folding, resulting in the present steeply dipping disposition of the rocks
9. Uplift and erosion, including extensive glaciation

CHAPTER 3

PETROGRAPHY AND GEOCHEMISTRY OF THE EXTRUSIVE AND INTRUSIVE ROCKS OF THE MORETON'S HARBOUR AREA

3.1 Introduction

The predominant rock types of the map area (Map 1; Fig. 2.1) are pillowed, mafic lava flows and volcanoclastic rocks, which are difficult to classify petrographically due to pervasive spilitic alteration (cf. Hughes, 1973). The mineral assemblages of ~100 thin sections examined with the petrographic microscope are summarized in Table 3.1. The following is a synopsis of the mineral assemblages and textures observed.

3.2. Mafic dykes

Most of the mafic dykes in the area are diabase, comprising greater than 90% of the Wild Cove Formation in places, and occurring throughout the map area. There are five main types of dyke encountered:

- (1) aphyric (diabase);
- (2) aphanitic-aphyric (basalt);
- (3) phaneritic (gabbro);
- (4) feldspar-phyric;
- (5) clinopyroxene-phyric.

The mineralogy of all these dyke rocks is similar, consisting of variably saussuritized, albitized plagioclase (originally $An_{>50}$) as phenocrysts or flow-aligned laths, interstitial chlorite with marked

TABLE 3.1

Summary of Mineral Assemblages of Volcaniclastic,
Volcanic and Intrusive Rocks of the Moreton's Harbour Area

	Quartz	Plagioclase	K-feldspar	Pyroxene	Hornblende	Tremolite- Actinolite	Biotite	Muscovite	Sericite	Chlorite	Calcite	Epidote	Sphene	Fe-Ti-oxide	Apatite	
MAFIC ROCKS																
Massive basalt flow (Wild Cove Head)	x	X		x		x	x			X	X	x	a	a	a	Banded, spilitized, vesicular
Pillow basalt (Beachy Cove)		X				x				X	X	x	a	a	a	vesicular
Diabase dyke (Wild Cove)		X		X		x				X	x	x	a	a	a	Pyrite disseminated pyroxene phenocrysts
Pillow basalt (Western Head)	x	X				x	x			X	X	x	a	a	a	vesicular, quartz in vesicles
Tuff, tuff breccia (Little Harbour)	x	X					x			X	X	x	a	a	a	pyritic
Pillow breccia (Chimney Cove)	x	X			x	x	x			X	X	x	a	a	a	jasper fragments
Amphibolitic xenolith (Pomley Cove)	x	X			X	x	x			x			a	a	a	
Gerald Dearing's Diorite	x	X			X	x	x			X			a	a	a	very sheared, adjacent to a fault
Dick's Head gabbro		X		X		x		x		x			a	a	a	subophitic
FELSIC ROCKS																
Moreton's Hr. Hd. breccia	X	X	x		x	x	x	x		X	X		a	a	a	highly variable commonly contains pyrite and other sulphides
Hayward's Cove breccia	X	X	x		(x)	x	x	x	x	X	X	x	a	a	a	coarse, polymict spheru- litic fragments includes pyrite
Felsic tuff (Old House Cove)	X	X	x					x	x	x			a	a	a	whole crystal fragments
Felsic dykes a. (Sam's Cove)	X	X	X				x	x	x				a	a	a	rhyolitic spherulitic
(Hayward's Cove) b.	X	X	x		x		x	x	x	x	x		a	a	a	dacitic, porphyritic, saccharoidal
(Pomley Cove) c.	X	X	X		x		x	x	x	x			a	a	a	K-metasomatized microgranite

X - major phase (primary or secondary)
x - minor and/or secondary phase
a - accessory phase

anomalous blue-mauve interference colours and more rarely fresh to intensely uralitized or chloritized salic to diopsidic clinopyroxene. Neither orthopyroxene nor olivine were observed. Accessory minerals include abundant titanomagnetite octahedra, sphene, leucoxene and apatite. Calcite, epidote and pyrite are commonly occurring secondary phases and as amygdale fillings. At Little Harbour, a coarsely pyroxene-phyric diabase dyke occurs which contains interesting, zoned, crenulated alteration patches (Plate 3.1) composed of sphene, apatite, albite, quartz, calcite and opaque oxide. These alteration patches are related to the intense calcitic alteration of pyroxene, possibly associated with the vein mineralization (Chapter 4).

Microprobe analyses of some of the major phases are presented in Table 3.2 and in Figures 3.1 and 3.2. The Ca-Mg-Fe plot for clinopyroxene from diabase dyke samples (phenocrysts and groundmass) displays its salic-diopsidic character with a subalkaline trend.

Chemical analyses of a selection of mafic dykes are given in Table 3.3 and show low SiO_2 (<50%), high TiO_2 (>1%) with high Na_2O (>3%) reflecting their spilitic nature. Furthermore, the Al_2O_3 , alkali and SiO_2 values indicate a subalkaline, high alumina affinity (Kuno, 1960). Trace element concentrations for the Moreton's Harbour mafic rocks are displayed graphically in Figure 3.3, and are interpreted as exhibiting a subalkaline, island arc affinity (Strong and Payne, 1973). The true affinity of the rocks is masked by their strong alteration trends notably in the more mobile elements.

TABLE 3.2

Electron Microprobe Analyses of Some Silicate Minerals
(giving element weight % and cationic proportions, Fm)

Mineral	Sample Number	Element											Total		
		Na	Mg	Al	Si	K	Ca	Ti	Cr	Mn	Fe	Ni			
Clinopyroxene (Ca,Mg,Fe) ₂ (Si,Al) ₂ O ₆	LH-61	wt.%	0.24	15.40	3.84	52.6	0.01	22.46	0.30	0.39	0.19	5.59	0.04	101.13	
		Fm.	0.017	0.833	0.164	1.914	-	0.874	0.007	0.010	0.005	0.169	-	3.992	
		wt.%	0.25	16.95	3.98	51.35	0.01	22.10	0.32	0.67	0.09	5.10	0.00	100.82	
		Fm.	0.17	0.92	0.17	1.872	-	0.863	0.008	0.019	0.002	0.155	-	4.026	
	SM-61	wt.%	0.27	16.29	2.41	52.20	0.00	21.23	0.45	0.00	0.14	8.43	0.09	101.51	
		Fm.	0.018	0.888	0.102	1.918	-	0.832	0.012	-	0.004	0.257	0.002	4.026	
		wt.%	0.27	14.51	1.81	53.41	0.01	20.14	0.52	0.00	0.28	10.95	0.00	101.90	
		Fm.	0.018	0.792	0.077	1.957	-	0.790	0.014	-	0.008	0.335	-	3.992	
	WCH-1	wt.%	0.18	16.20	1.85	52.34	0.02	20.19	0.57	0.02	0.23	9.12	0.00	101.43	
		Fm.	0.013	0.887	0.080	1.922	-	0.822	0.015	-	0.006	0.279	-	4.023	
	CC-11	wt.%	0.27	16.85	3.02	52.21	0.01	19.40	0.45	0.38	0.19	9.09	0.00	101.87	
		Fm.	0.019	0.914	0.129	1.899	-	0.755	0.012	0.010	0.005	0.276	-	4.019	
Hornblende (Na,K) ₁ Ca ₁₋₂ (Mg,Fe,Al,Ti,Mn) ₆ (Si,Al) ₈ O ₂₂ (OH) ₂	WCH-1	wt.%	0.27	13.52	3.04	53.18	0.12	12.21	0.50	0.10	0.31	15.23	0.06	98.52	
		Fm.	0.019	0.759	0.134	2.004	0.005	0.492	0.013	0.002	0.010	0.480	0.001	3.919x4	
		wt.%	1.44	12.05	5.57	54.27	0.13	11.08	0.36	0.09	0.25	13.46	0.01	98.70	
		Fm.	0.102	0.666	0.242	2.011	0.005	0.439	0.010	0.002	0.007	0.417	-	3.900x4	
	PC-1	wt.%	2.18	14.77	9.09	46.60	0.21	11.16	2.14	0.04	0.25	12.46	0.00	98.89	
		Fm.	0.636	3.313	1.612	7.016	0.040	1.798	0.238	-	0.031	1.568	-	16.252	
		wt.%	2.27	14.68	9.06	46.13	0.22	11.33	2.13	0.00	0.25	12.25	0.05	98.38	
		Fm.	0.662	3.312	1.618	6.989	0.040	1.836	0.240	-	0.031	1.551	0.004	16.283	
	PC-1	wt.%	0.18	8.66	13.28	44.11	0.01	23.07	0.00	0.05	0.25	7.05	0.00	96.67	
		Fm.	0.049	1.985	2.410	6.795	-	3.807	-	0.004	0.031	0.904	0.000	15.985	
		TR-35	wt.%	1.06	9.93	6.22	48.34	0.18	12.14	0.05	0.03	0.38	20.33	0.00	98.66
			Fm.	0.320	2.303	1.138	7.526	0.032	2.024	0.004	-	0.045	2.646	-	16.037
Chlorite (Mg,Fe,Al,etc.) ₁₂ (Si,Al) ₈ O ₂₀ (OH) ₁₆	TR-35	wt.%	0.04	15.01	18.62	26.46	0.00	0.01	0.07	0.02	0.22	26.13	0.00	86.57	
		Fm.	0.012	4.802	4.714	5.678	-	-	0.006	-	0.038	4.688	-	19.938	
		wt.%	0.09	17.27	18.22	28.48	0.01	0.11	0.13	0.02	0.30	24.93	0.01	89.48	
		Fm.	0.036	5.286	4.406	5.829	-	0.018	0.018	-	0.048	4.280	-	19.921	
Epidote Ca ₂ (Fe,Al,etc.) ₁ Al ₂ (SiO ₄) (Si ₂ O ₇) ₁ O (OH)	PH-23	wt.%	0.00	0.04	21.26	47.29	0.01	26.39	0.05	0.00	0.03	4.13	0.00	99.18	
		Fm.	-	0.002	1.830	3.456	-	2.066	0.002	-	-	0.251	-	7.607	
	SM-60	wt.%	0.00	0.01	23.84	38.42	0.00	23.32	0.11	0.35	0.20	9.36	0.00	95.61	
		Fm.	-	-	2.208	3.020	-	1.962	0.004	0.020	0.010	0.614	-	7.840	
Muscovite	PC-2	wt.%	0.13	1.12	31.71	51.54	7.02	0.00	0.06	0.00	0.00	1.25	0.02	92.84	
		Fm.	0.013	0.217	4.934	6.806	1.108	-	0.003	-	-	0.135	-	13.309	

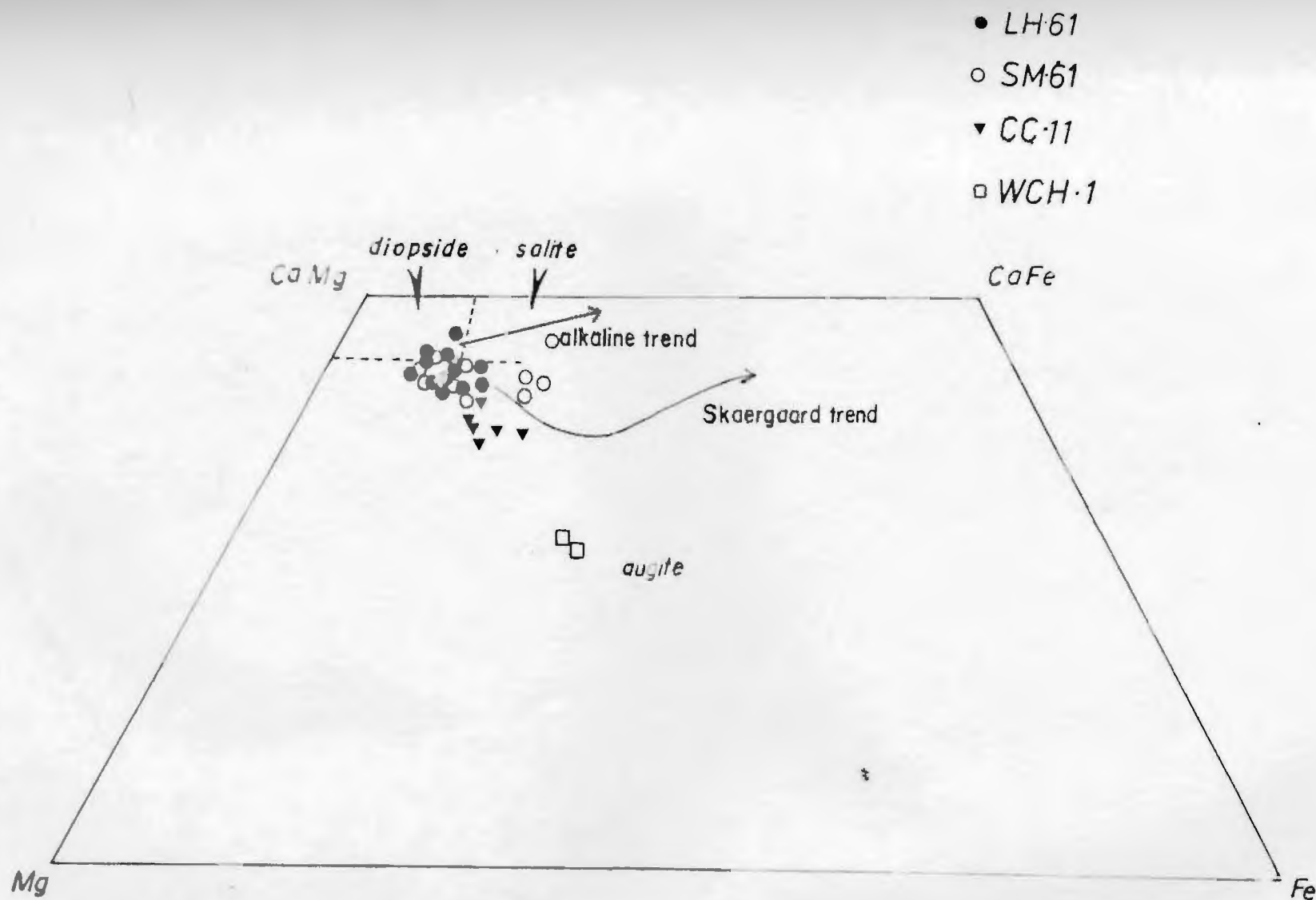


Fig. 3.1: The Ca-Mg-Fe (cationic %) compositions of clinopyroxene electron microprobe analyses from mafic dykes, Moreton's Harbour, compared with the alkaline and Skaergaard (tholeiitic) trends (from Carmichael *et al.*, 1974).

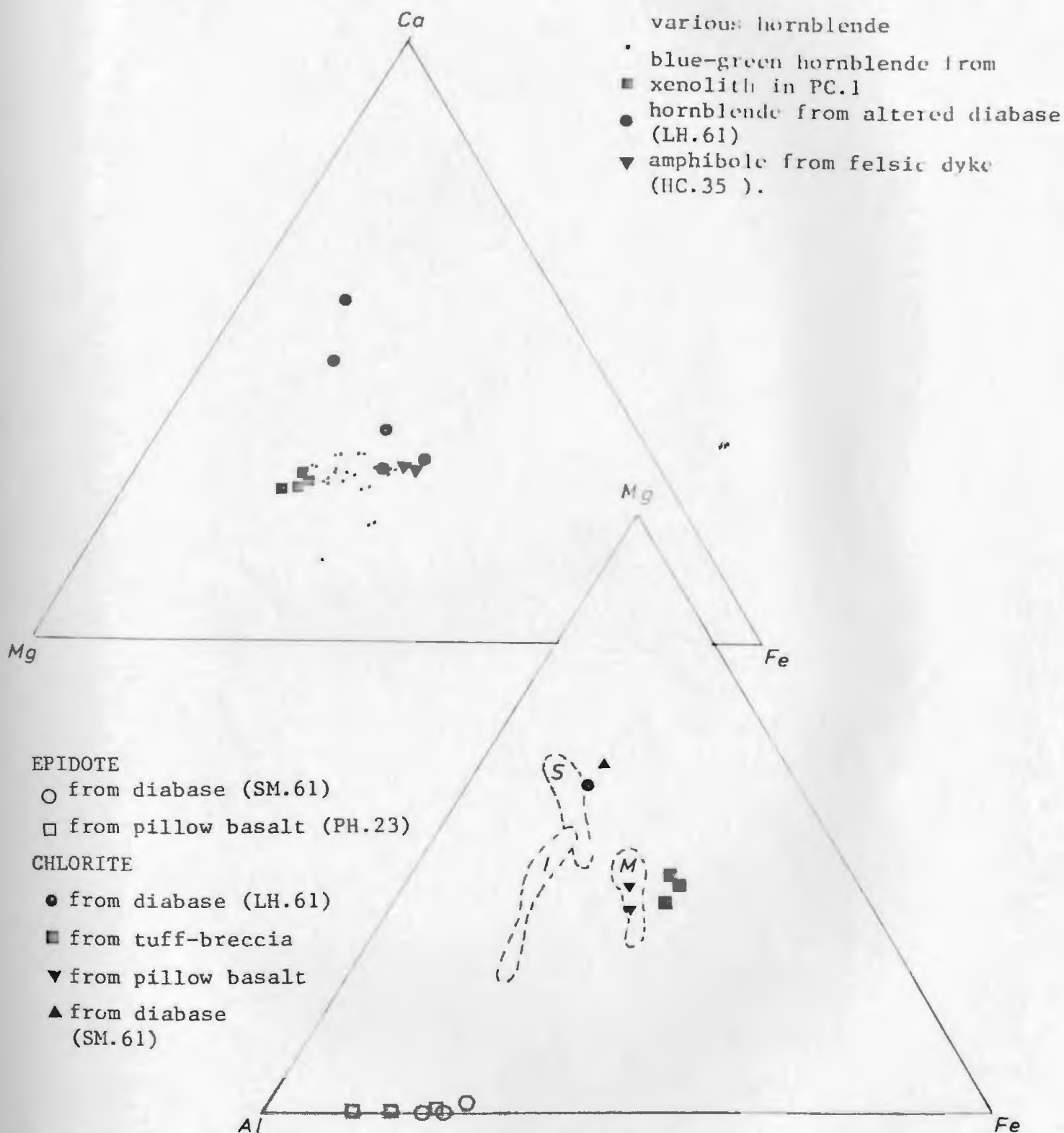


Fig. 3.2: Compositional (cationic %) plots for electron-microprobe analyses of secondary mafic minerals: a) Ca-Mg-Fe for various amphiboles; and b) Mg-Fe-Al for epidote and chlorite, compared with fields of chlorite in hydrothermally altered mafic (M), footwall intermediate (I) and felsic stockwork (S) rocks from the Buchan's mine area (Henley and Thornley, 1981).

TABLE 3.3

Geochemical Analyses of Mafic Dykes

	i Wild Cove Formation						ii Little Harbour Formation					
wt. %	DFS-72 93	DFS-72 100	DFS-72 MH-1	DFS-72 MH-6	DFS-72 91	DFS-72 94	DFS-72 709	DFS-72 88	DFS-72 87	DFS-72 86	DFS-72 208	DFS-72 191
SiO ₂	47.02	46.53	49	49.10	46.59	41.91	49.56	46.18	47.82	45.50	47.71	49.67
TiO ₂	1.18	1.30	2.3	1.47	0.65	0.34	1.32	1.64	2.13	1.82	1.43	0.91
Al ₂ O ₃	16.04	15.69	16.00	18.30	18.46	9.28	15.06	14.69	14.23	16.18	15.06	20.04
Fe ₂ O ₃	10.20	11.26	1.30	0.67	7.47	10.50	12.21	9.22	10.50	11.17	12.19	6.45
FeO	-	-	7.53	6.57	-	-	-	-	-	-	-	-
MnO	0.18	0.18	0.13	0.10	0.11	0.17	0.19	0.17	0.16	0.16	0.29	0.13
MgO	6.61	6.08	6.08	4.98	8.27	21.40	6.09	6.00	4.46	7.13	5.07	4.58
CaO	10.41	8.76	11.25	9.97	11.46	8.55	5.91	8.81	10.61	8.29	9.14	8.74
Na ₂ O	2.87	3.50	3.08	3.68	2.11	0.80	5.54	4.12	3.95	3.38	3.81	4.28
K ₂ O	0.47	0.89	0.75	0.99	0.94	0.08	0.26	0.45	0.04	0.43	0.15	0.81
P ₂ O ₅	0.13	0.16	0.82	0.48	-	0.21	0.33	0.06	0.25	0.27	0.15	0.03
H ₂ O	2.89	-	2.57	3.41	-	3.18	-	4.01	-	4.01	2.48	-
Total	98.0	94.35	101.44	99.72	96.06	96.42	96.47	95.35	94.15	98.34	97.48	95.64
ppm												
Rb			21	26								
Ba			223	271								
Sr			350	438								
Cu			69	61								
Zn			60	52								
Cr			43	52								
Ni			39	22								
Zr			162	125								

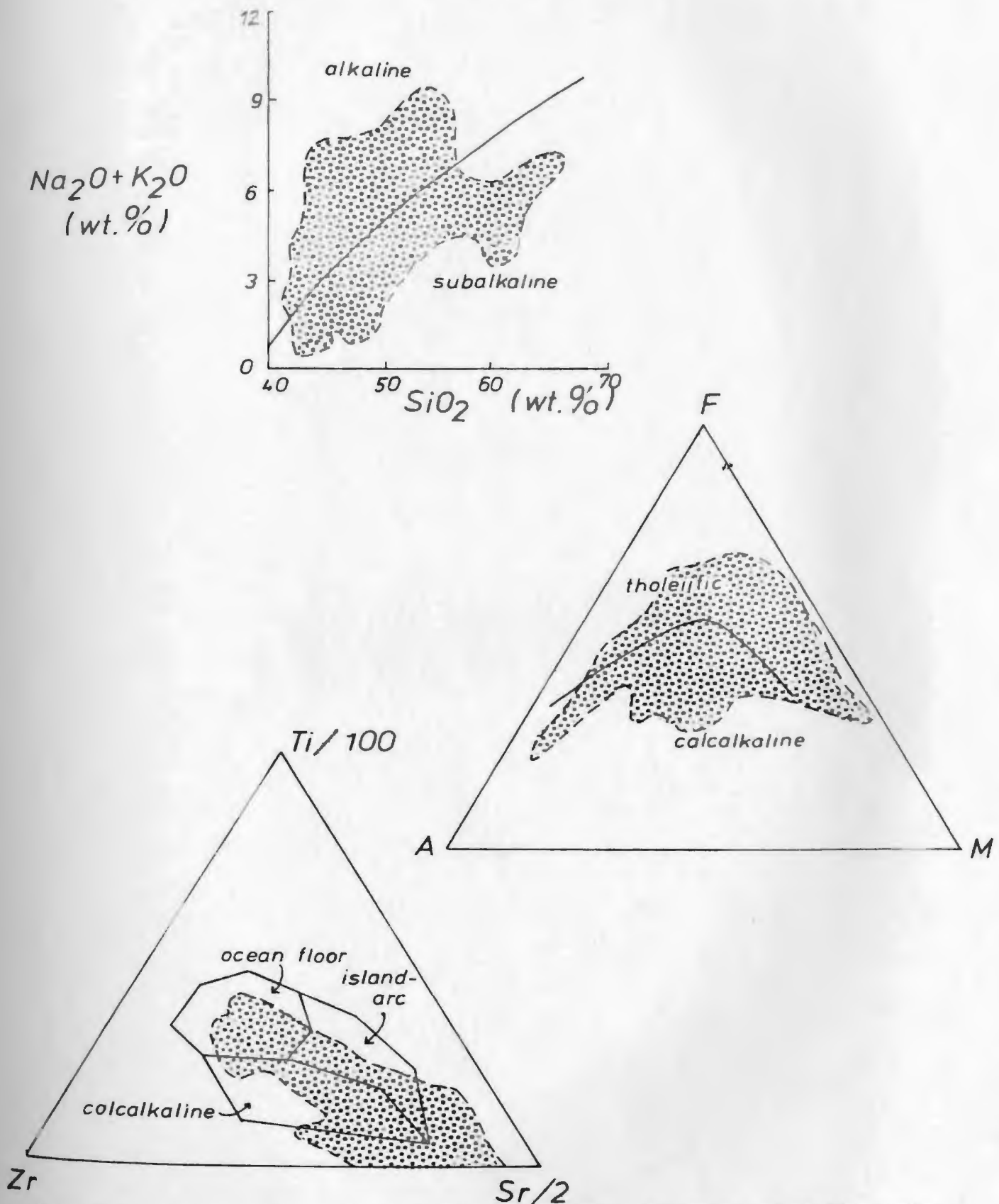


Fig. 3.3: Selected geochemical discrimination diagrams of mafic rock analyses from the Moreton's Harbour area (from Strong, 1972).

TABLE 3.4

Chemical Analyses of Selected Mafic Rocks from the Moreton's
Harbour Area (unpublished data of D. Strong, 1972)

Sample	oxide %											Total	Au ppb
	SiO ₂	TiO ₂	Al ₂ O ₃	Fe ₂ O ₃ *	MnO	MgO	CaO	Na ₂ O	K ₂ O	P ₂ O ₅	H ₂ O		
DS-72-729	63.50	0.70	12.63	5.18	0.16	1.50	2.69	7.15	0.66	0.32	2.66	97.78	15
DS-72-207	52.86	1.45	14.02	7.18	0.16	5.30	8.01	4.89	0.24	0.24	-	94.35	-
DS-72-195	48.90	1.42	14.40	8.11	0.13	5.69	8.32	3.37	0.76	0.05	6.93	98.08	4
DS-72-215	49.76	1.53	15.70	9.01	0.15	6.55	7.05	4.83	0.76	0.46	3.20	99.00	-
DS-72-192	48.40	0.96	17.24	9.85	0.18	5.39	8.44	3.60	1.07	0.09	-	95.22	5

*Fe total as Fe₂O₃

DS-72-729 - sediment

DS-72-207,195,215,192 - pillowed, flows

3.3 Mafic Extrusive Rocks

The mafic extrusive rocks of the Little Harbour and Western Head Formations all possess a typical spilite-greenschist facies mineral assemblage of albite, chlorite, epidote, calcite, quartz with accessory titanomagnetite, sphene and apatite. Only very rarely are primary salic clinopyroxene microphenocrysts observed. Both pillowed and massive flows have basaltic textures, commonly aphyric, with flow-aligned plagioclase laths and are variably vesicular (Plate 3.2). Amygdule fillings are quartz, actinolite, epidote, chlorite and/or calcite. „Calcite staining (Dickson, 1966) shows that the carbonate in vesicles varies from pure iron-free calcite to extremely iron-rich calcite. There is a general trend of increased Fe towards the vesicle margins. Calcite occurring interstitially in the rocks is shown to be ferroan ($>2\%$ Fe), whereas calcite in veins varies in composition, with later cross-veins composed generally of pure calcite, and the earlier veins iron-rich.

Pillows commonly have a concentric zonation delineated by bands of vesicles. Pillow selvages are of sideromelane.

Chemical analyses of pillows and flows from the Western Head and Little Harbour Formations are shown in Table 3.4. Silica concentrations tend to be higher than for basalt classification ($>45\%$ SiO_2) (Carmichael et al., 1974) due to alteration and late vesicle filling. Despite this, the extrusive mafic rocks are considered to have been subalkaline basalts because of their structures, textures and trace element abundances (Figs. 3.3 and 3.6).

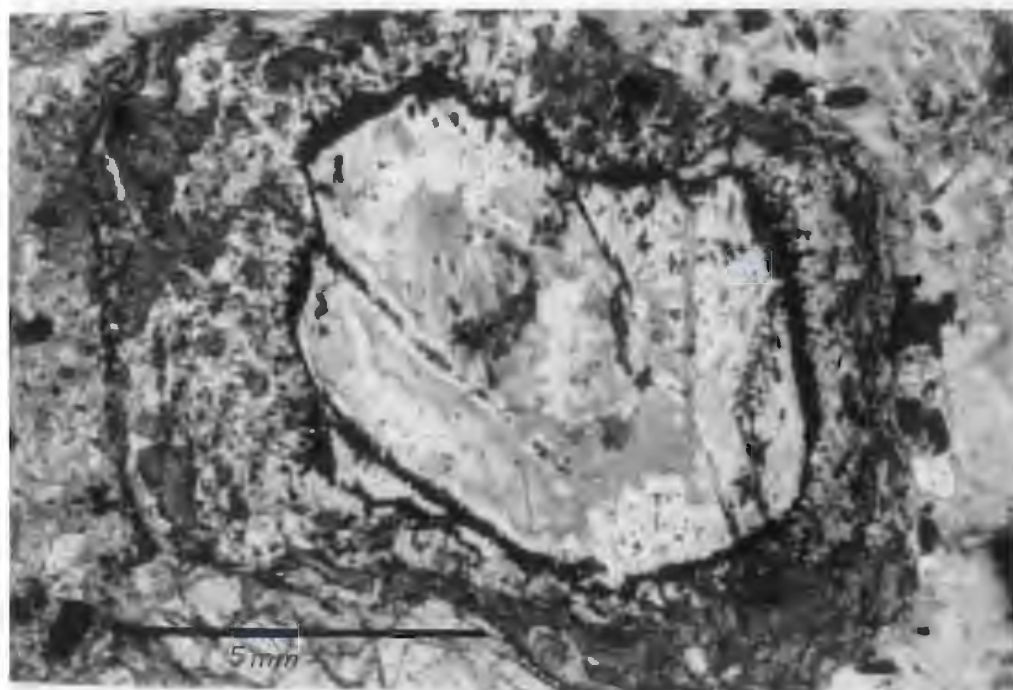


PLATE 3.1: Photomicrograph showing intense calcic alteration of (?pyroxene in a diabase dyke, Little Harbour (plane polarized light).

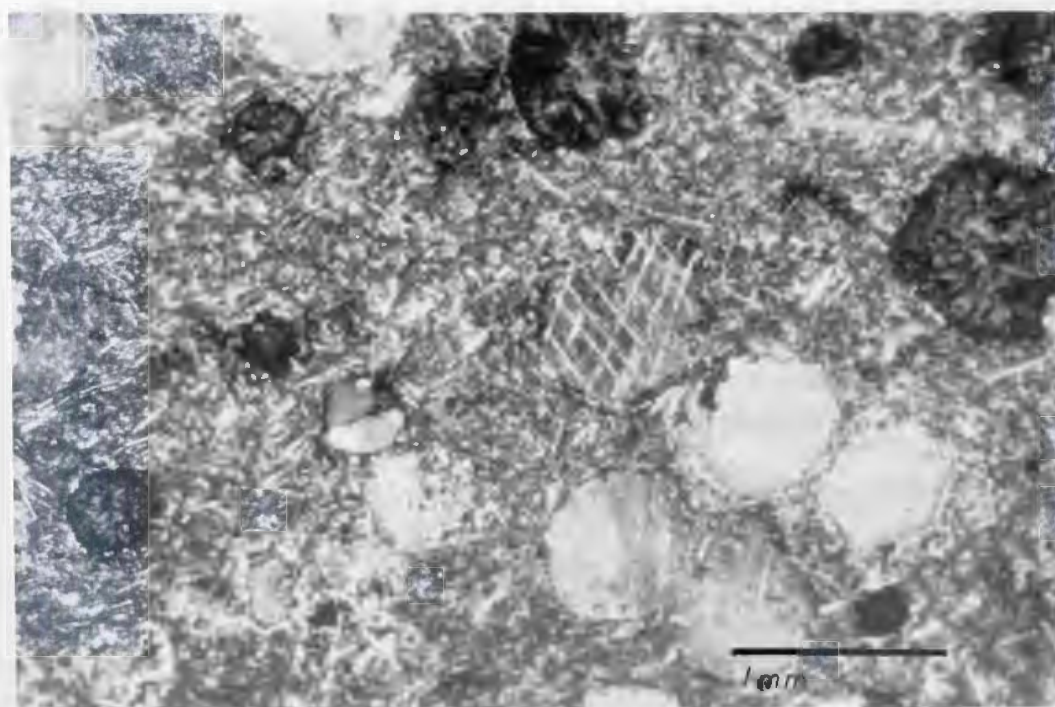


PLATE 3.2: Photomicrograph of calcite-filled amygdules in spilitic basalt (BC-9).

3.4 Mafic Volcaniclastic and Associated Sedimentary Rocks

The volcaniclastic rocks of the Little Harbour Formation are composed largely of altered, silicified, mafic fragments consisting of sodic-plagioclase, quartz and chlorite with abundant calcite, epidote, opaque Fe-Ti oxide, actinolite and apatite. Secondary sulphides are locally abundant, with pyrite most widespread. Matrix mineralogy is dominated by calcite, quartz after chert, epidote and chlorite. Textures like accretionary lapilli are observed in one tuff breccia sample (Plate 3.3). These are considered to be the product of material accreted from the air around volcanic ash nuclei, and as such are good evidence of very shallow water, explosive volcanism (Moore and Peck, 1962).

Chemical analyses of selected volcaniclastic rocks are included in Tables 3.5 and 5.1a. Values of SiO_2 , Fe_2O_3 (total) and Na_2O are higher than those of the mafic flows, whereas Al_2O_3 , MgO and CaO are relatively depleted, as would be expected with silicified and reworked, sedimented mafic components. All the sediments have lower values of Ni, Y, U and Rb, but are variably enriched in Zr, Zn, As, Au and Ag. These patterns may reflect hydrothermal remobilization through the relatively porous volcaniclastic beds, as discussed in Chapter 5.

Grey and red cherts are composed of crypto- to micro-crystalline quartz which may contain various euhedral, opaque minerals notably, hematite and pyrite. The jasper bed from Western Head has slightly enriched precious and base metal concentrations due to primary exhalative processes (Chapter 5).

3.6 Moreton's Harbour Head Breccia

The Moreton's Harbour Head Breccia is a coarse breccia which contains large, angular, felsic blocks with a minor mafic (amphibolitic, pillowed) component. The felsic blocks are composed of fine grained quartz, albite, sericite, biotite and ilmenite with abundant secondary calcite, pyrite and leucoxene, and resemble the felsic dykes intruding the area. Mafic rocks from the Breccia are altered and commonly contain brown-green amphibole and exhibit primary spilitic textures. The rocks are cut by abundant quartz and calcite veins, variably containing sulphides. The calcite is ferroan and the rocks, especially adjacent to the fault contact, are rich in siderite and goethite.

3.7 Felsic Dykes

The volcanic-sedimentary sequence is cut by abundant felsite dykes which vary in composition from rhyolite to dacite and are quartz, albite and/or perthite phenocryst-bearing intrusions. Phenocrysts of quartz are rounded, embayed and commonly show β -quartz forms. These phenocrysts contain abundant solid mineral inclusions (apatite, zircon, rutile) and trapped fluids (see Chapter 6). Plagioclase phenocrysts are ubiquitously euhedral, sodic and may exhibit weak normal zonation with twinning on both albite and pericline laws. Cobaltinitrite staining reveals the presence of abundant groundmass K-feldspar. Only rarely are fingerprint and patch microperthitic phenocrysts observed, which are generally albitized and sericitized.

The Pomley Cove microgranite is composed of holocrystalline quartz and Na-plagioclase with brown-red buff pleochroic biotite and secondary muscovite (sericite), cuniform ilmenite, rare sphene, apatite and zircon. Fine grained, remobilized K-feldspar is detected in the groundmass at the slightly sheared intrusive margins. Southwards from Pomley Cove, the grainsize of the felsic intrusive rocks decreases. At Hayward's Cove, the rhyolitic dykes have spherulitic devitrification textures and are strongly sericitized. A felsitic texture is developed in the coarser, holocrystalline centres of some dykes. Plagioclase-phyric felsites are abundant throughout the area, of which the mafic phases are chloritized. These are less silicic than the quartz-phyric dykes and are classified as rhyodacites and dacites. The dacitic dykes commonly post-date the rhyolite, but are intimately related, as shown at Sam's Cove where the plagioclase-phyric dacite is a more slowly cooled central portion of the spherulitic, columnar jointed quartz-phyric rhyolite dyke.

3.8 Felsic Pyroclastic Rocks of the Hayward's Cove Formation

The coarse felsic breccia at Hayward's Cove is polymictic including rhyodacite bombs and fragments composed largely of spherulitic albite and quartz (Plate 3.4) silicified mafic blocks and bedded chert clasts. The mafic phase in all fragment types is chlorite. Calcite, apatite, pyrite and opaque oxides are abundant. K-feldspar is notably absent. The matrix of the coarse breccia is dark in colour and composed

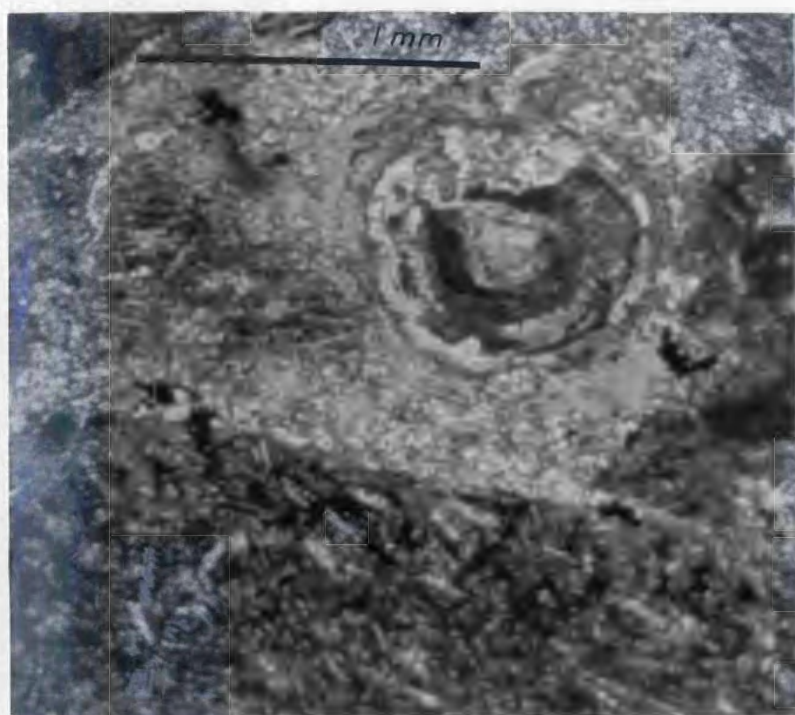


PLATE 3.3: An accretionary lapillus in tuff breccia, Little Harbour (cross polarized light).

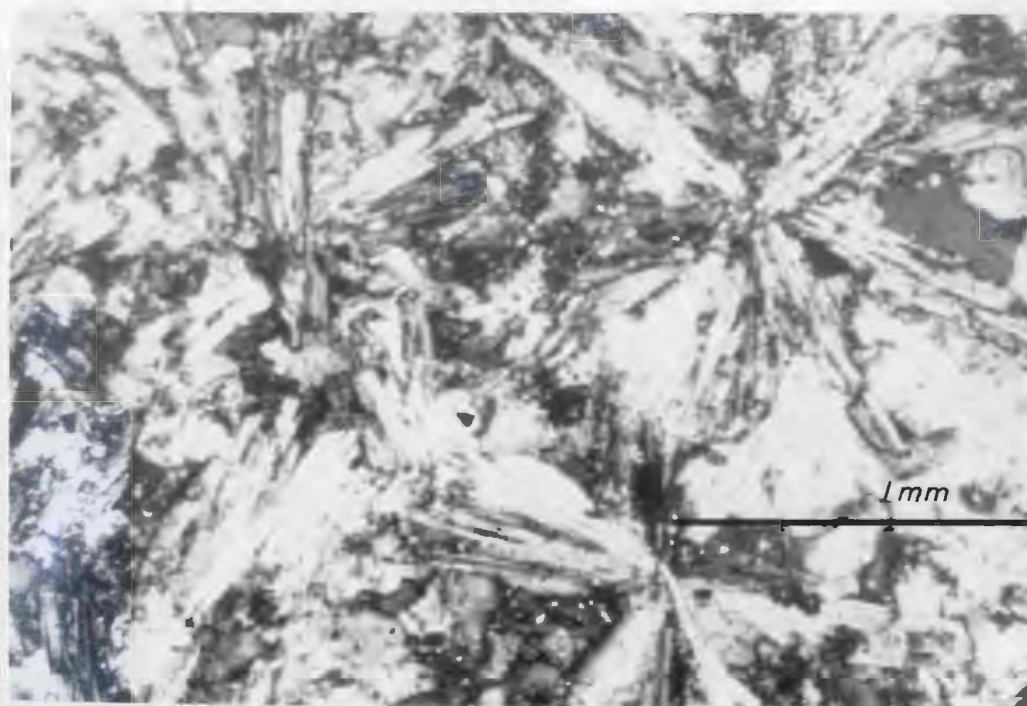


PLATE 3.4: Spherulitic texture in groundmass of rhyodacite fragment from the felsic breccia, Hayward's Cove.

mainly of quartz, calcite, chlorite and rare feldspar. Pyrite is locally abundant. The breccia is more chloritic at Moreton's Cove.

The distal, fine grained, silicic facies is composed of quartz and feldspar, the latter is partly K-feldspar. Crystal fragments of quartz and plagioclase occur sparsely and are rotated, flattened, fragmented and variably recrystallized. Lenses of fine grained calcite and quartz may represent relict flattened, elongate vesicles. In several sections, perlitic devitrification is observed, implying an originally glassy nature of these deposits.

3.8 Geochemistry of the Felsic Rocks: Hayward's Cove Breccia, Tuffs and Felsic dykes

Major and trace element analyses of the felsic rocks from the Moreton's Harbour area are presented in Table 3.6 using data from this study supplemented with unpublished data by D.F. Strong. The dykes range between 60 and 80 wt. % SiO_2 and have high concentrations of Na_2O and K_2O . In the SiO_2 vs total alkalies ($\text{Na}_2\text{O} + \text{K}_2\text{O}$) Harker diagram (Fig. 3.4), the dykes plot in a linear trend, whereas the breccia and tuff samples deviate above and below this line. An alkali-enrichment, iron-depletion trend is apparent from the AFM diagram (Fig. 3.5). Concentrations of Fe_2O_3 (total), MgO and CaO are highly variable. Alumina values are consistently between 12 and 14 wt. %. Concentrations of TiO_2 , MnO and P_2O_5 are ubiquitously low.

The major element chemistry of the dykes substantiate their classification as rhyolitic to rhyodacitic in composition, as does the Winchester and Floyd (1977) discrimination diagram of SiO_2 vs Zr/TiO_2

TABLE 3.5a

Major Element Abundances of Selected Felsic Dykes and Pyroclastic Rocks

Sample #	Weight % of Element Oxide										
Dykes	SiO ₂	TiO ₂	Al ₂ O ₃	Fe ₂ O ₃ *	MnO	MgO	CaO	Na ₂ O	K ₂ O	LOI	Total
BL·3	69.3	.022	14.5	2.26	.02	.95	3.09	3.88	2.6	3.82	100.82
HC·34	73.7	.13	12.7	1.13	.03	.4	1.0	3.88	2.9	2.4	98.27
HC·51	60.7	.65	14.2	3.61	.08	2.27	4.23	3.04	2.67	7.89	99.20
OHC·2	76.8	tr.	13.1	.44	.02	.05	.63	3.36	4.19	1.51	100.10
SM·16	68.3	.28	14.5	1.78	.03	.63	3.16	3.73	2.59	4.40	99.40
WG·4	76.0	tr.	12.2	1.10	.04	.30	.71	4.30	2.45	1.76	98.86
<u>Pyroclastic rocks</u>											
HC·Brla	69.8	.30	13.8	3.49	.04	1.34	.81	3.86	1.78	3.56	98.76
HC·Brlb	64.5	.32	14.2	8.54	.07	3.12	.68	4.11	.64	2.98	99.06
HC·33	58.6	.91	14.2	7.03	.20	2.12	3.88	5.71	1.44	4.65	98.04
HC·38	68.6	.29	14.8	4.58	.06	1.45	.78	5.45	.84	2.04	98.89
HC·41	72.6	.33	10.5	7.14	.06	1.18	.28	3.13	.42	2.27	98.54
HC·46	70.1	.33	13.8	3.88	.07	1.69	.63	4.30	1.23	2.33	98.36
MC·1	69.9	.26	12.2	3.73	.11	1.11	2.26	3.86	2.89	2.88	99.20
WG·10	74.8	.43	10.7	1.97	.08	.85	1.73	2.54	3.29	2.70	99.09
WG·16	73.6	.40	12.7	2.24	.05	.83	.68	3.89	3.34	1.84	99.57
WG·17	70.2	.31	12.6	2.50	.09	1.20	1.63	2.77	4.75	3.62	99.67

*Total Fe-oxide as Fe₂O₃

L.O.I. = Loss on ignition

TABLE 3.5b
Trace Element Abundances in Selected Felsic rocks

Sample #	Element ppm											ppb	
<u>Dykes</u>	Zr	Y	Sr	U	Rb	Th	Pb	Ga	Zn	Ni	As	Au	Ag
BL·3	98	10	194	2	67	5	4	19	26	0	10	30	400
HC·34	74	16	86	5	72	13	16	19	19	1	22	6	800
HC·51	159	19	273	4	67	4	5	21	61	7	44	-	-
OHC·2	51	41	29	8	87	3	22	22	36	0	34	13	100
SM·16	91	5	335	0	34	1	7	21	57	0	7	20	130
WG·4	66	17	74	5	56	10	6	17	14	0	-	-	-
<u>Pyroclastic rocks</u>													
HCBrla	203	50	101	0	31	5	0	18	8	0	-	-	-
HC·33	237	48	152	0	13	4	3	23	145	0	-	-	-
HC·38	353	48	140	0	8	9	0	11	15	0	-	-	-
HC·41	363	47	57	6	10	17	6	12	15	0	50	7	400
HC·42	470	61	63	2	6	23	4	16	19	0	18	4	800
HC·46	360	50	121	5	17	19	0	13	16	0	8	4	tr.
MC·1	321	54	52	5	31	10	1	20	77	0	8	9	800
WG·10	315	45	77	2	64	13	7	13	24	0	-	-	-
WG·16	347	48	56	8	67	22	7	15	34	0	16	8	200
WG·17	355	52	105	3	91	18	11	17	37	0	-	-	-

- not analysed

tr = trace amount, undetermined

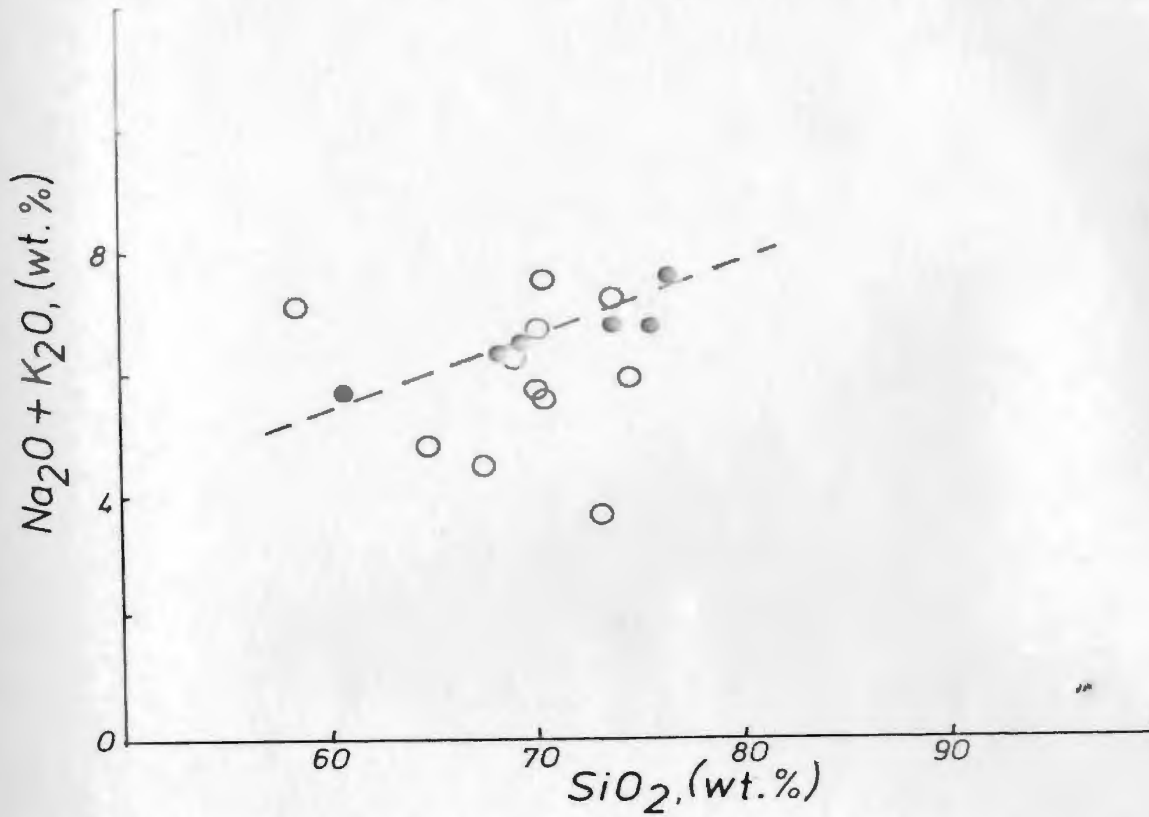


Fig. 3.4: Silica-total alkalis Harker diagram for selected felsic rocks (closed circles, dykes; open circles, pyroclastic rocks).

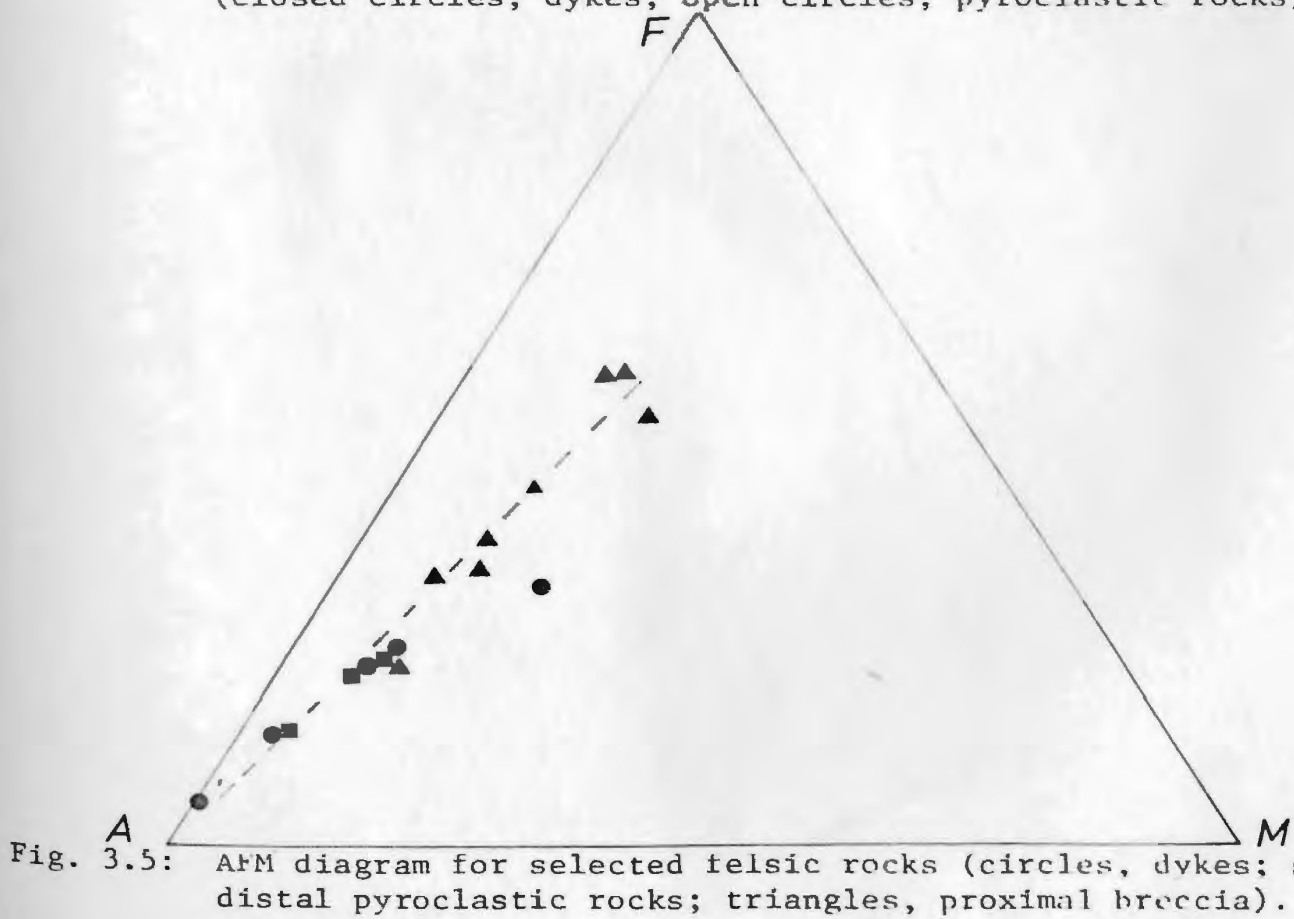


Fig. 3.5: AFM diagram for selected felsic rocks (circles, dykes; squares, distal pyroclastic rocks; triangles, proximal breccia).

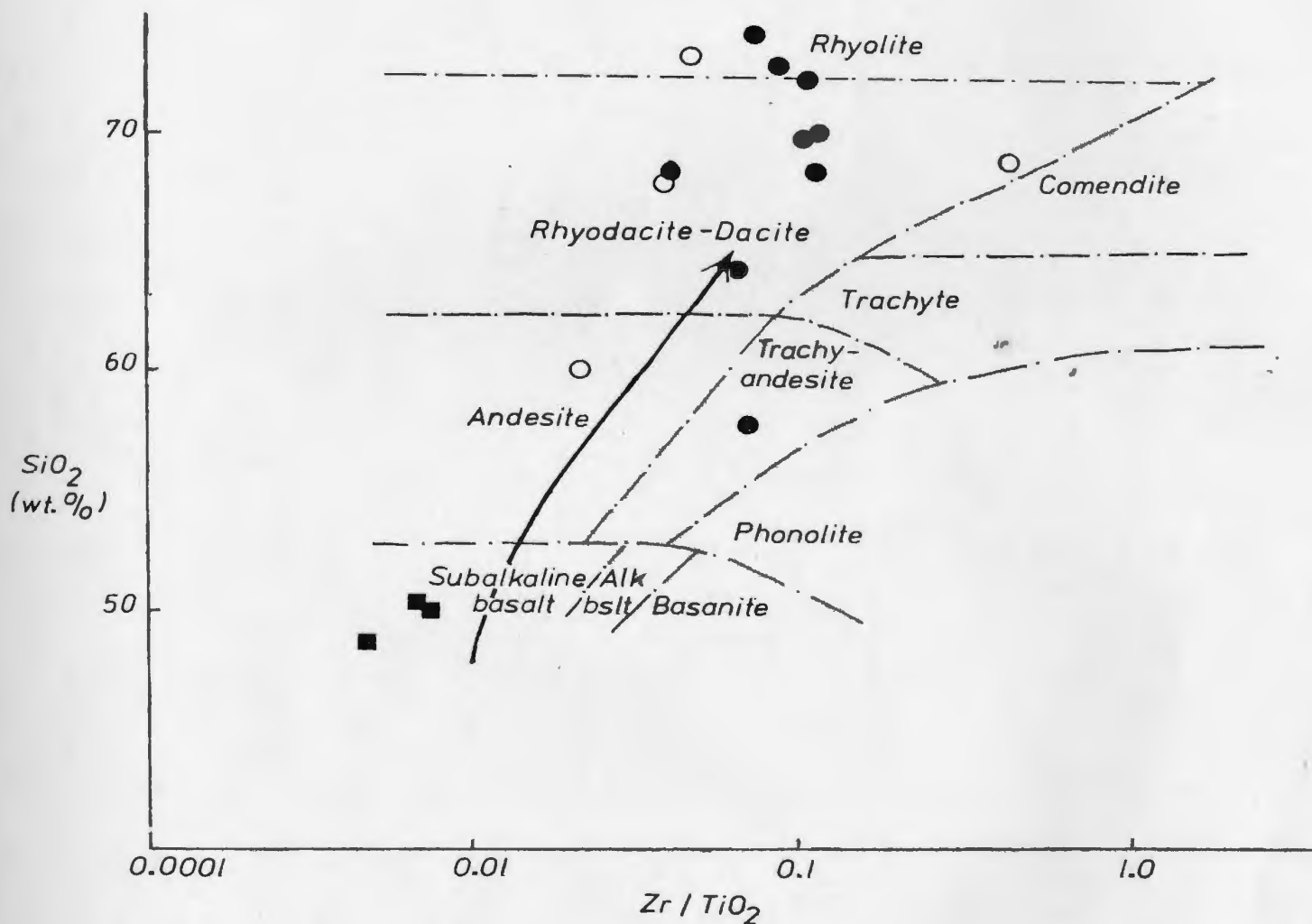


Fig. 3.6: Silica plotted against the Zr / TiO_2 ratio for selected mafic and felsic rocks from Moreton's Harbour, showing rock type discrimination and the sub-alkaline trend of the volcanic rocks (cf. the Mount Misery trend; Floyd and Winchester, 1977).

(Fig. 3.6). The trends observed are largely accounted for by alteration with predominant alkali remobilization. This is recognized in petrographic examination as sericitization and albitization of the feldspars. The margins of most dykes, notably the Pomley Cove intrusive, have clearly been affected by K-metasomatism.

The felsic volcanic rocks are generally less silicic, ranging from 64 to 75 wt % SiO_2 , with lower values for the coarser, proximal breccia than the distal tuff facies. The major and trace element chemistry of the coarse breccia is of little use in determining their magmatic affinity due to their extreme heterogeneity, contamination and alteration. The distal silicic tuffs more closely resemble the felsic dykes with respect to SiO_2 and their high alkali concentrations. The volcanic rocks plot either side of the SiO_2 vs alkalis trend (Fig. 3.4) delineated by the dyke rocks but continue their trend in the AFM diagram (Fig 3.5) which implies that similar processes have controlled the chemistry of all these felsic samples. Concentrations of Fe_2O_3 (Fe-total), MgO and CaO of the volcanic rocks are variable, but Fe_2O_3 and MgO are consistently higher than values from the dykes. The binary plot for Na_2O vs K_2O (Fig. 3.7) shows that $\text{K}_2\text{O}/\text{Na}_2\text{O}$ ratios for the felsic tuffs and dykes are highest, and increasing Na_2O enrichment and contamination for the inhomogenous, coarse breccia samples.

The elements Ti, Zr, Y and Ga, which are considered immobile and incompatible in mafic rocks and can be used to discern differentiation trends and discriminate between magma types (e.g. Pearce and Cann, 1972),

become compatible in the silicic rocks, so that the same discriminant diagrams cannot be used. Rubidium and K_2O give a positive linear relationship (Fig. 3.8), largely due to their implicit chemical similarities. The SiO_2 vs Zr plot shows a linear, negative relationship for the dyke rocks and two of the volcanic samples, but the other volcanic rocks plot in a cluster of high SiO_2 and high Zr concentrations (Fig. 3.9). The difference implies a process of Zr fractionation towards the extrusive rocks. The relationship between $TiO_2/100$ vs Zr is a relatively constant positive trend for all the felsic samples (Fig. 3.10).

The felsic rocks fall into the dacite-rhyolite fields of the Winchester and Floyd (1977) diagram (Fig. 3.6) and show a subalkaline differentiation trend such as that of Mount Misery rocks. Mafic dyke and flow rocks plot similarly in the subalkaline field, continuing the trend downwards and suggesting a subalkaline evolution for all the volcanic and hypabyssal rocks of the area.

The felsic dykes and volcanic rocks are considered to be coeval, from the limited data. Further geochemical work, including rare earth element distribution may substantiate their consanguinity. An isotopic age of the felsic dykes would add a further age constraint on the entire volcanic sequence in this area and possibly on the age of mineralization (see later Chapters).

3.9 Other mafic intrusive rocks

3.9.1 Gerald Dearing's diorite stock

The diorite is composed of coarse, euhedral, twinned, saussuritized plagioclase (An_{50}) and dark brown pleochroic hornblende. The latter is commonly sheared and fragmented along its cleavages.

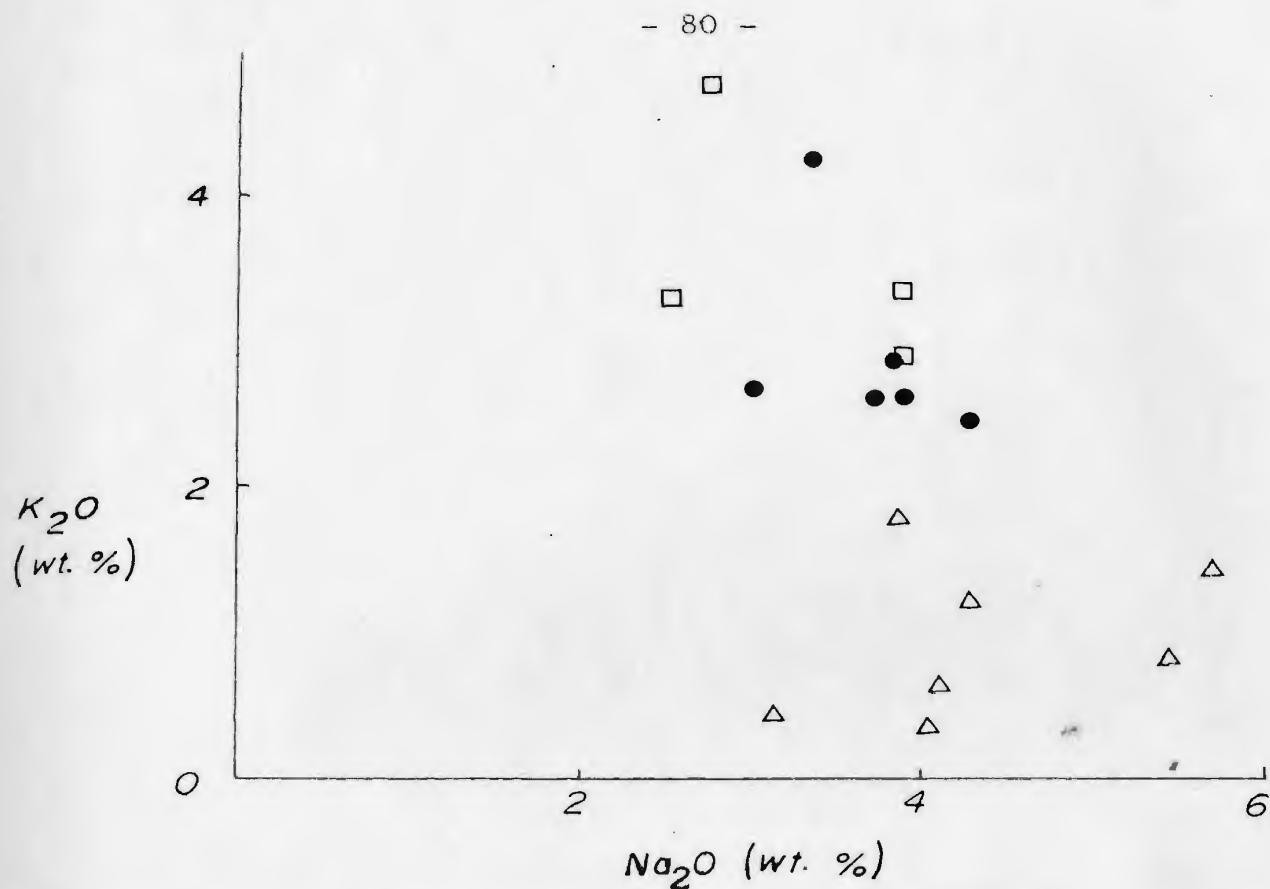


Fig. 3.7: K_2O - Na_2O diagram for selected felsic rocks (circles, dykes; squares; distal pyroclastic rocks; triangles, proximal breccia).

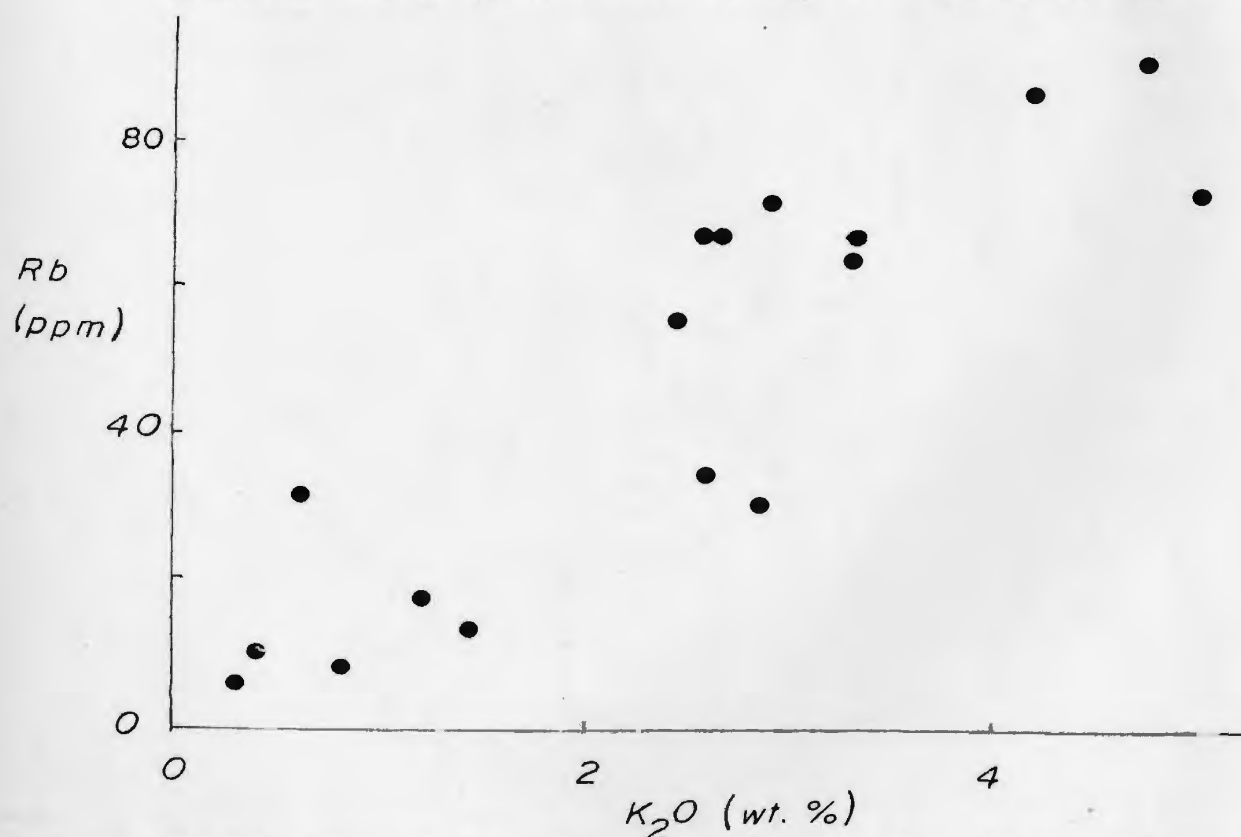


Fig. 3.8: Rb - K_2O diagram for selected felsic rocks, dykes and pyroclastic samples.

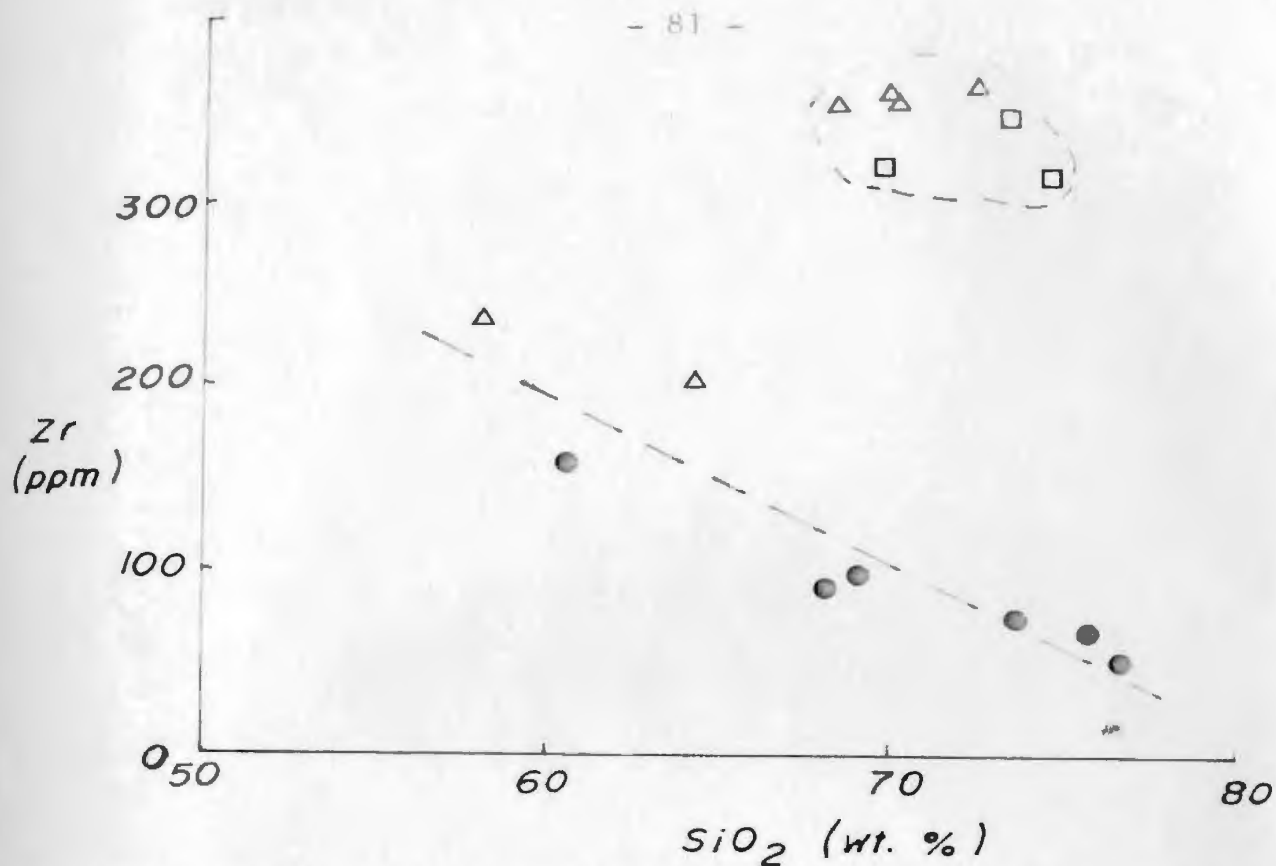


Fig. 3.9: Zr-SiO₂ diagram for selected felsic rocks showing a fairly linear trend for the dyke rocks and two of the breccia samples, but a separate group of high Zr and high SiO₂ for all other felsic pyroclastic rock samples (circles, dykes; squares, distal pyroclastic rocks; triangles, proximal breccia).

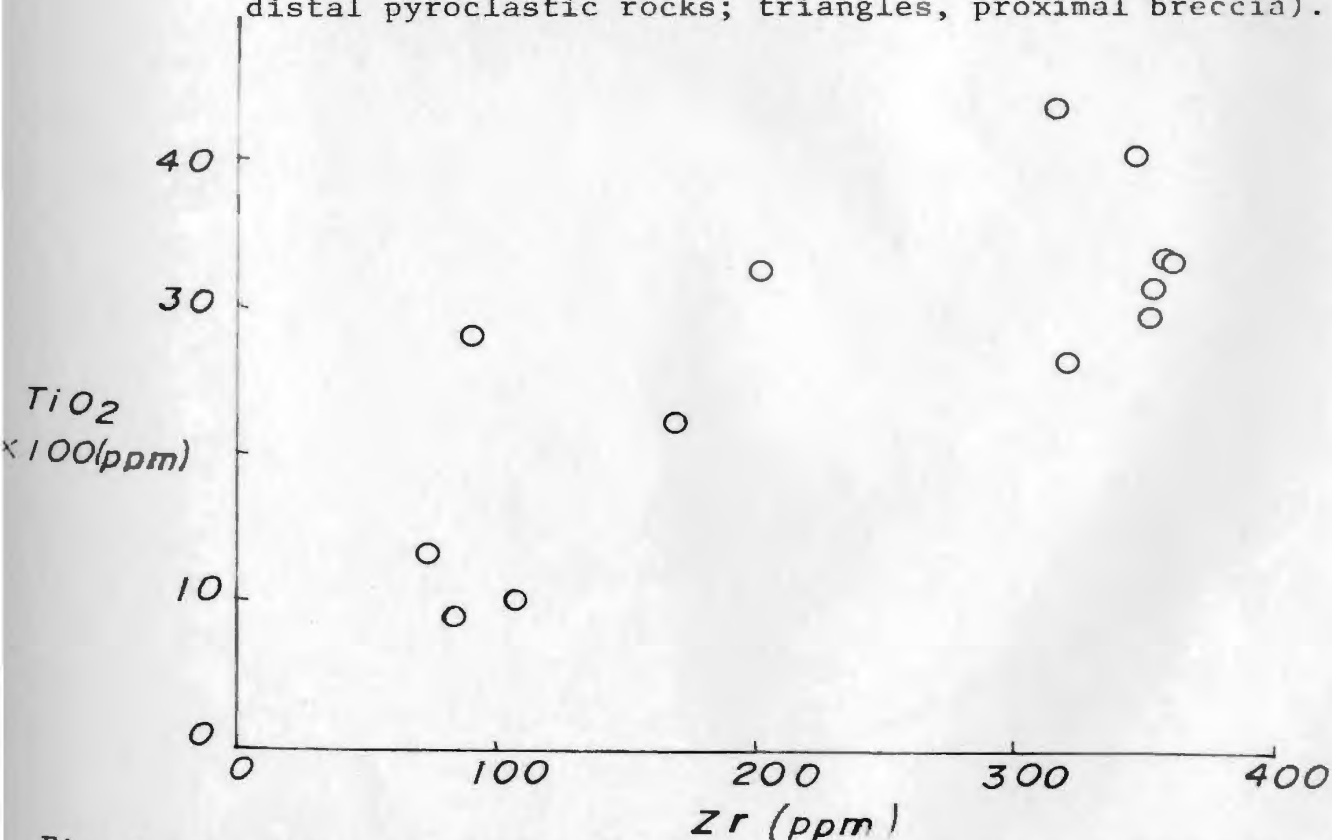


Fig. 3.10: TiO₂-Zr diagram for selected felsic rocks samples (dykes and pyroclastic samples) showing a fairly good, positive, linear trend. See Fig. 3.6.

Other minerals include calcite, sericite and some biotite (after hornblende) with quartz veins. Actinolite, calcite and prehnite occur in veins and are secondary after the primary mafic minerals. The accessory phases are apatite, sphene and ilmenomagnetite.

3.9.2 Dick's Head microgabbro

The microgabbroic stock is composed of salic clinopyroxene and saussuritized plagioclase mostly, with accessory apatite, sphene and opaque Fe-Ti oxide. The gabbro has a maximum grain size of 0.5 cm and exhibits a subophitic texture.

3.9.3 Lamprophyre

The small, black aphanitic lamprophyre dyke is composed of euhedral augite with apatite, pyrite, magnetite, ilmenite and alteration products leucoxene, calcite and chlorite. All phases are contained within a dark glassy material and analcite and so may be classified as monchiquite. Late Jurassic to early Cretaceous lamprophyres are described from elsewhere in the Bay of Exploits (Heyl, 1936; Strong and Harris, 1977) and resemble this occurrence.

3.10 Alteration and Metamorphism

The mafic rocks of the area have a typical lower greenschist facies mineral assemblage, which is partly a result of interaction with seawater. The mineralogy and chemistry of some of the felsic rocks have been modified similarly.

Mafic xenoliths and rocks adjacent to felsic intrusions have been amphibolitized by contact thermal metamorphism. Such aureoles do

not exceed 1 m in width and are typified by the development of brown-green hornblende and tremolite-actinolite and the absence of epidote.

The felsic dykes are sericitized. K-metasomatism is evident in these dykes from the removal of K from relict perthite phenocrysts to the groundmass, and towards the dyke margins. The original feldspars are themselves albitized.

Hydrothermal alteration and elemental redistribution is evident throughout the area with greatest development adjacent to the sulphide-quartz ore veins (Chapters 4 and 5). The slight enrichment of precious and base metals and As in the volcanoclastic-sedimentary strata of the Little Harbour Formation is related to large scale hydrothermal circulation associated with the ore forming processes (see later chapters).

Calcitization of the mafic wall rocks is the predominant alteration adjacent to the ore veins with pure calcite, ferroan calcite and siderite pervading the rocks in irregular veinlets (Plates 3.5, 3.6 and 3.7). Silicification and chloritization is also common, whereas argillic and sericitic alteration is relatively rare, except in unmineralized felsic dykes.

3.11 Silicate mineral chemistry

The chemical compositions of phenocryst and groundmass clinopyroxene are presented in Table 3.2 and diagrammatically in Figure 3.1. The cores of the large clinopyroxene crystals in the coarse, pyroxene-rich diabase dykes from Little Harbour are diopsidic and trend towards salite and calcic augite towards their margins in a subalkaline trend. Small phenocrysts from the diabase hosting the mineralization of Stewart's

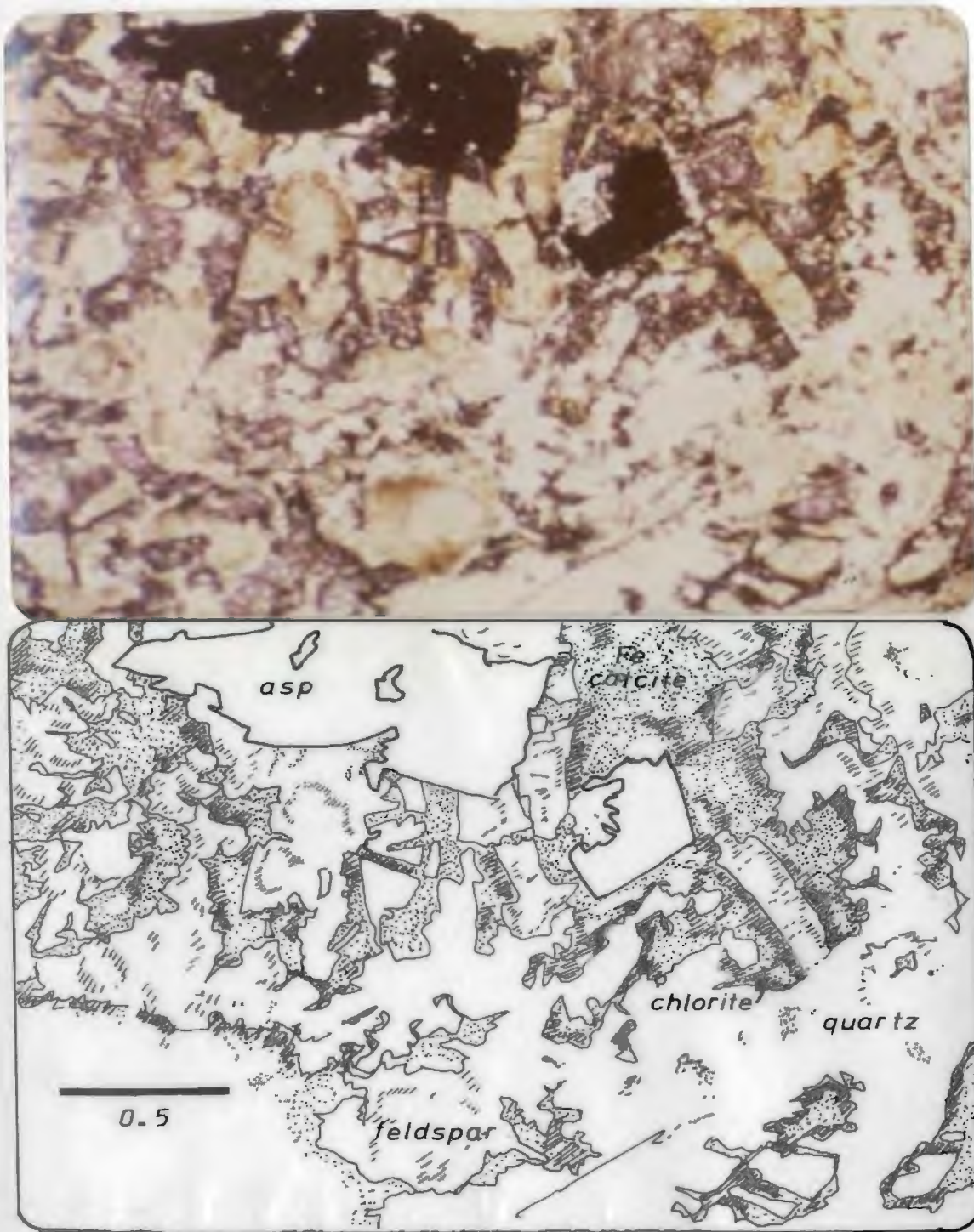


PLATE 3.5: Pervasively calcitized diabase adjacent to ore veins, Stewart's Mine. The feldspars are pseudomorphed by clay minerals and sericite and the groundmass predominantly is ferroan calcite (alizarin red stain, plane polarized light). The opaque rhombic mineral is arsenopyrite with minor pyrite.

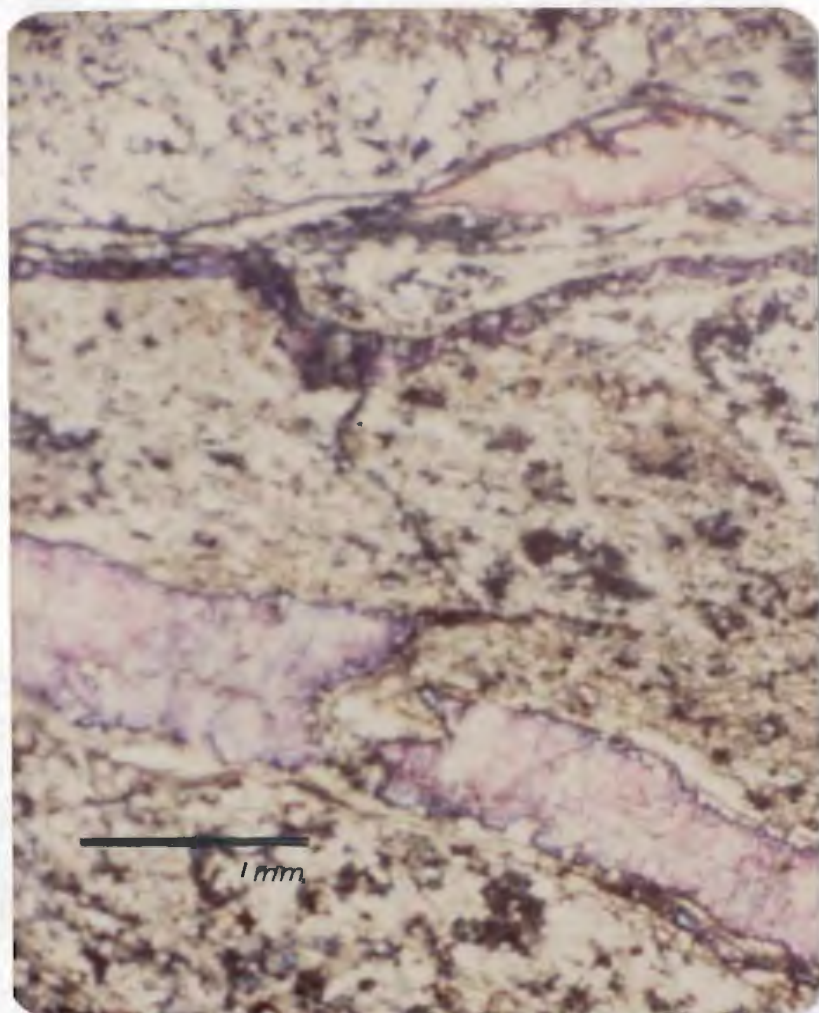


PLATE 3.6: Pervasive calcitic alteration and veining, adjacent to Stuckless' Mine stibnite veins. Alizarin red stain shows upper vein of pure calcite and lower vein zoned from iron-poor to iron-rich.

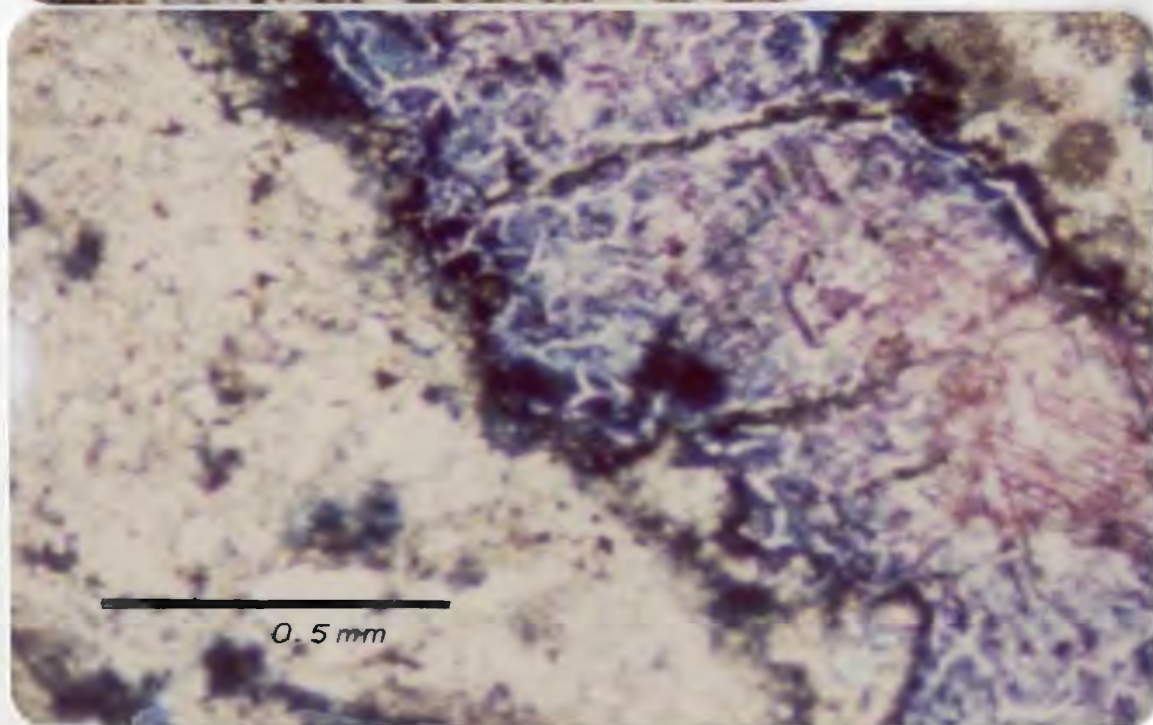


PLATE 3.7: Detail of zoned ferroan calcite vein (from above). The "cracked" blue staining is due to rapid reaction of stain and highly ferroan calcite.

Mine are salic, as are groundmass pyroxenes. Concentrations of Na, Ti and Ni are very low. Cores tend to be slightly enriched in Ni and Cr and depleted in Mn and Ti with respect to the margins. Pyroxene phenocrysts from a diabase at Chimney Cove are calcic augite and show a similar trace element zonation.

Microprobe analyses of secondary mafic minerals (amphiboles, epidote and chlorite) are presented in Table 3.2. Hornblendes from the amphibolitic dykes of Wild Cove Head and from the Pomley Cove microgranite aureole are calcic with variable Na, Mg, Ca, Fe and trace amounts of Mn, Ti, Cr and K. Hornblendes from the Pomley Cove aureole are richer in Na and Ti than those analysed from Wild Cove Head (Fig. 3.2). Plagioclase analyses indicate the predominance of albite which contains traces of K, Ti and Ba. Epidote and chlorite analyses show that both minerals conform to their respective formulae (Fig. 3.2b). Chlorites have a wide range of Mg/Fe ratios.

CHAPTER 4

ORE PETROGRAPHY

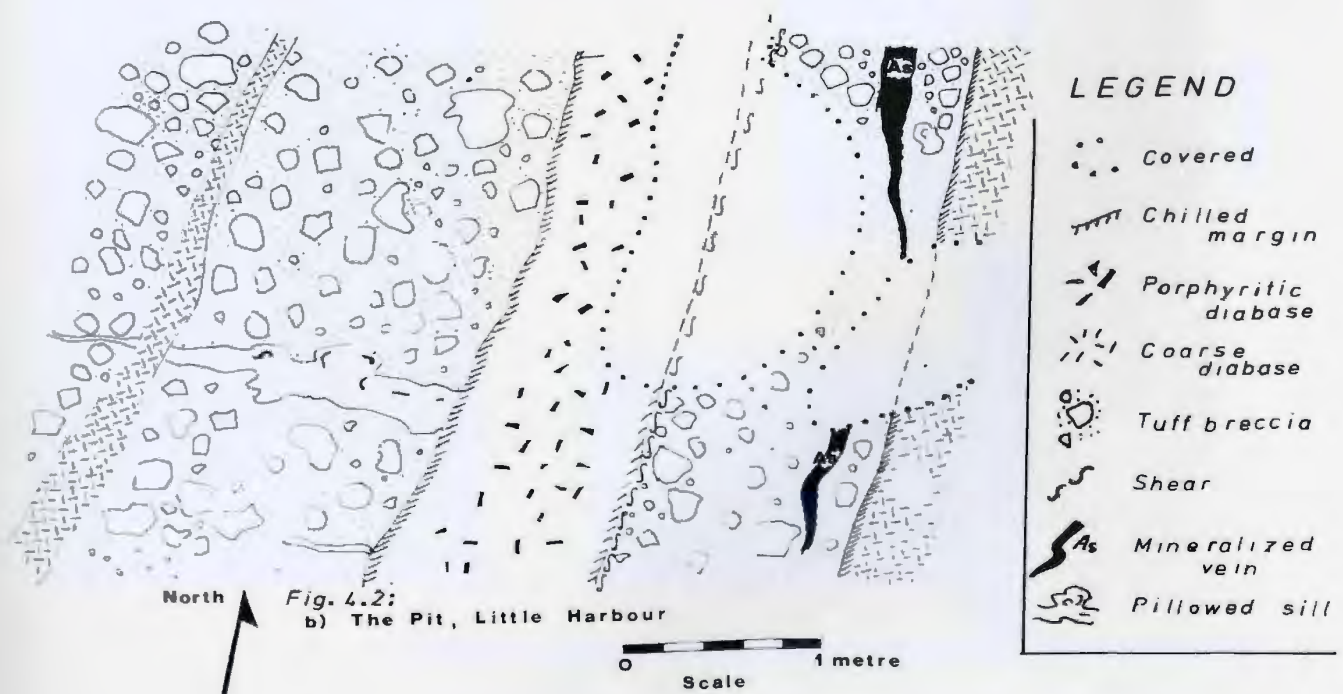
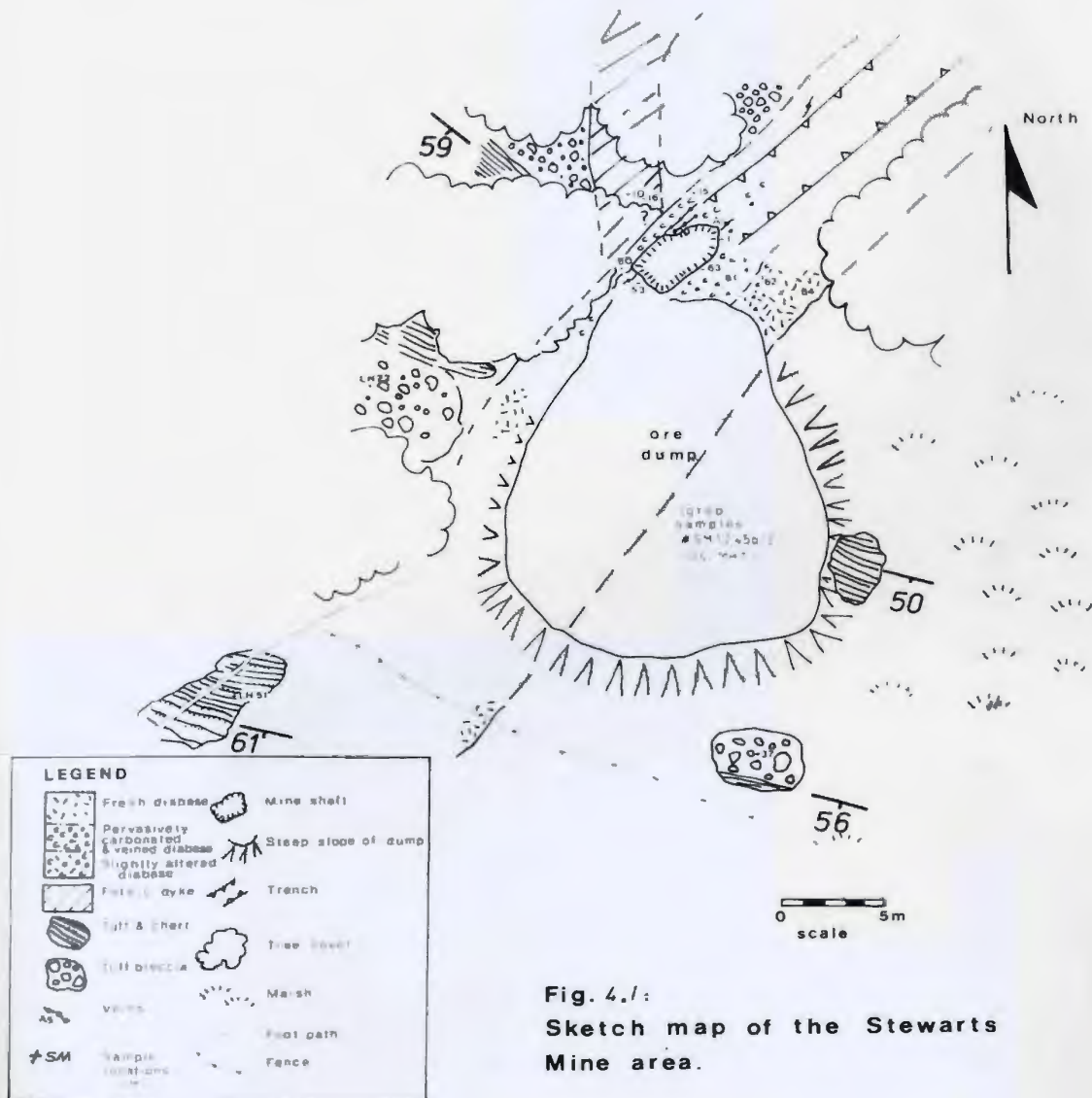
4.1 Mining History

4.1.1 Stewart's Mine, Little Harbour

During 1897, about 125 tons of arsenopyrite were extracted for its gold content from the Stewart's Mine at Little Harbour. By 1900, the main shaft of the mine had reached a depth of 40 m, with several shallow subsidiary pits. Mining activity was apparently discontinued shortly after this (Heyl, 1936). No mining has taken place within the memory of local people and the mine site presently comprises a water-filled shaft measuring $2 \times 4 \text{ m}^2$, associated with a 30 m trench to the north (Fig. 4.1). To the south of the mine is the ore dump from which grab samples were collected for study, as the in situ ore vein is only partly well exposed and severely weathered. The prospect pit at Little Harbour has been covered with debris (Fig. 4.2; frontispiece view southward across Little Harbour).

4.1.2 Stuckless Mine

The Frost Cove antimony mine, currently referred to as Stuckless' Mine was first worked during the 1890's when \$1,200 worth (value at that date) was exported from Newfoundland. Mining activity was sporadic, with peaks during the two World wars. At its zenith the mine consisted of two adits: one 3.5 m below and the other 18.5 m above sea level. The former extended southwards for approximately 80 m. The middle level has



now collapsed. Local residents recall mining of the stibnite, and Mr. C. Stuckless (son of former mine manager, Richard Stuckless) worked there as a boy. He remembers that much of the mine excavation was hand-drilled.

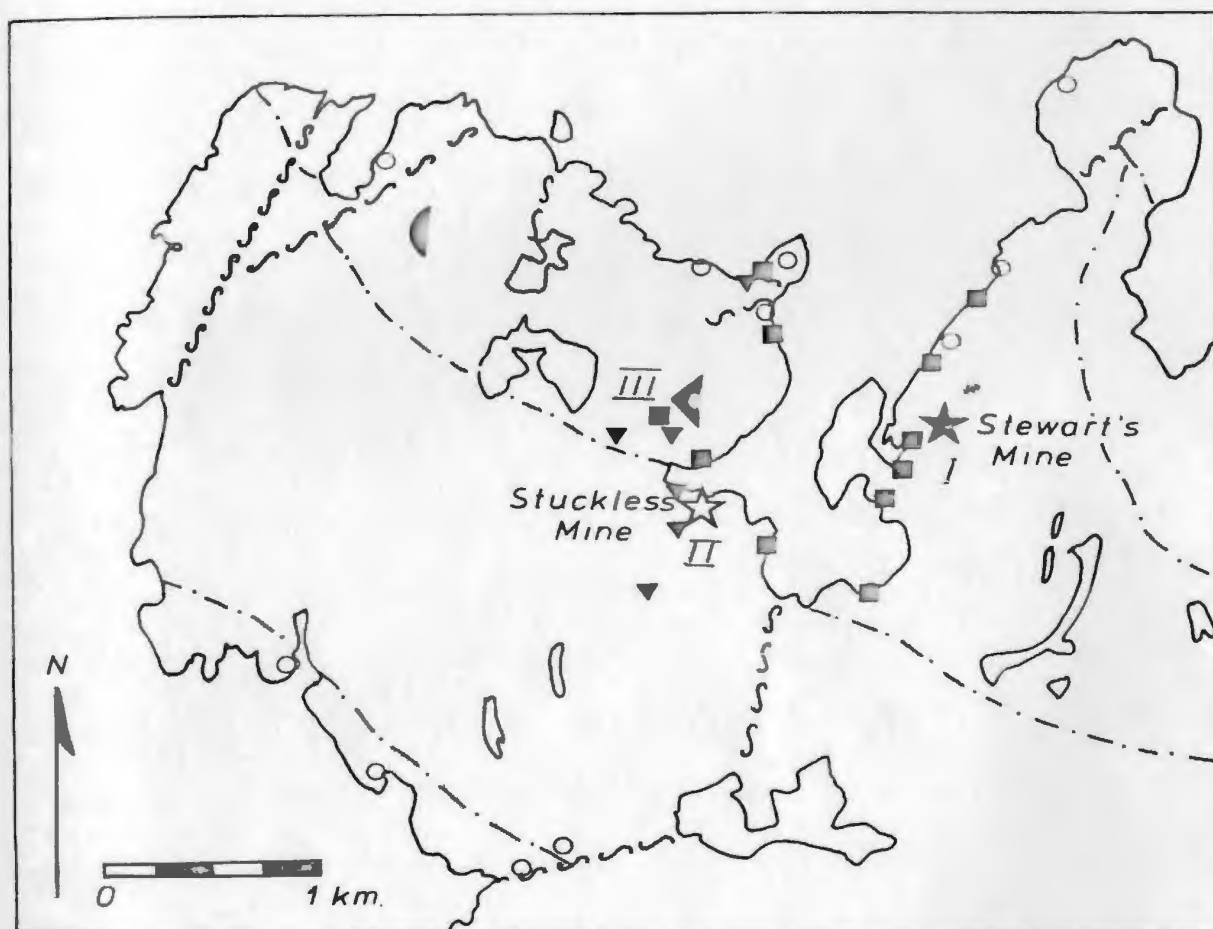
4.1.3 Other prospects

There are no other mine sites within the map area but between 1965 and 1967 the Newfoundland and Labrador Corporation (NALCO) undertook a drilling programme on the Newmont concessions. Four boreholes totalling ~290 m were drilled, notably around the Taylor's Room (gold) prospect, and the Western Head (copper) Prospect (Fogwill, 1968; unpublished and confidential reports). The two mining properties and the Taylor's Room and Western Head Prospects are owned by Nalco and held under the fee simple grants (E.M. Tobin, vol. 1, Folio 156; W.C. Lethbridge et al. (The Moreton's Harbour Mining Company), vol. 1, Folio 65).

4.2 Vein Descriptions

Approximately fifty mineralized veins were seen in the map area (Map 1), the most pertinent of which are shown in the simplified map (Fig. 4.3). The veins are of three main types:

- I. Arsenopyrite + quartz
(+ pyrite + calcite + sphalerite)
- II. Stibnite + quartz
(+ calcite + arsenopyrite)
- III. Sphalerite + arsenopyrite + chalcopyrite + quartz
(+ pyrite + calcite + stibnite).



- Approximate Formation boundaries (see Fig. 2.1)
- ~~~~~ Faults
- I ★ ■ As, Au.
- II ★ ▼ Sb.
- III ★ ▼ Zn, Au, (Cu, Pb), As, Sb.
- Cu, (As).
- pyrite.

Fig. 4.3: A sketch map showing the broad distribution of the main mineralized vein systems in the Moreton's Harbour area.

These veins range in thickness from less than 1 cm up to 50 cm, and can be traced locally for several metres along strike. The veins are perpendicular to the strike and occur almost exclusively through the central part of the map area, essentially within the Little Harbour Formation. The veins are hosted by a variety of rock types including volcanoclastic rocks, pillow lavas and both felsic and mafic dykes. Ore veins are ubiquitously associated spatially to the felsic intrusives. The two mines are based on vein lodes. The Western Head copper mineralization is of sulphide minerals disseminated pervasively through a small ($<0.25 \text{ km}^2$) area with minor irregular quartz veinlets.

4.2.1 Stewart's Mine: Vein Type I

The arsenopyrite-rich veins mined at Little Harbour occur within a thick diabase dyke which is a pyroxene-(salite-diopside) phyric diabase 4.5 m away from the vein (Plate 3.5). The dyke is about 10 m thick, dipping steeply ($\sim 80^\circ$) and striking 035°N . Adjacent to the vein, the diabase is pervasively calcitized, silicified and chloritized and exhibits some brecciation and shearing. Abundant pyritohedra are disseminated through the diabase, with small ($\geq 2 \text{ mm}$) arsenopyrite rhombs adjacent to the mineralized veins. The host dyke is cut by abundant Fe-rich calcite (from carbonate staining technique; Dickson, 1966) and barren quartz veinlets.

The dyke itself intrudes steeply dipping tuffs and tuff breccias, upward facing to the southwest. To the north of the mine shaft, a pink, felsic (quartz-feldspar phyric rhyolite) dyke outcrops striking 025° , dipping 75° to the southeast. This dyke presumably intercepts the diabase dyke near the mineralization, but the actual contact was not observed..

The mineralized vein measures 20 to 30 cm thick and is related to several subsidiary sub-parallel veins. The dominant metallic mineral is arsenopyrite with far lesser amounts of pyrite, pyrrhotite, sphalerite, chalcopyrite and trace stibnite and tetrahedrite. Quartz is the major gangue phase and was deposited in at least four generations:

- (1) euhedral (dog-tooth, comb texture intergrown with arsenopyrite) - cloudy, white to colourless with c-axes approximately perpendicular to vein direction;
- (2) cloudy grey, quartz with clear margins and anhedral, mosaic form filling-in centre of veins;
- (3) iron-stained, cloudy quartz along the margins of veins;
- (4) late, cross-cutting veinlets of cloudy to clear quartz, of commonly euhedral mosaics.

The vein samples commonly exhibit a banded texture of quartz and arsenopyrite (Plates 4.1, 4.2 and 4.3). In some samples, the margins of each band of arsenopyrite is traced by a thin band of iron rich calcite and siderite (Plate 4.3).

The arsenopyrite occurs generally as euhedral rhombs, or is angular, fragmented and brecciated (Plate 4.5) with late quartz veining and carbonate cementing the fragments. There is no evidence of extensive tectonic deformation and so the brecciation is considered to be related to fluid pressure (Chapter 6). Massive arsenopyrite containing angular fragments of altered wall rock, banded vein and gangue minerals occurs in the centre of the thicker veins (Plate 4.4). Pyrite occurs as late



PLATE 4.1: Small, banded quartz-arsenopyrite vein of Type I, cutting a diabase dyke (Little Harbour).

PLATE 4.2: Banded quartz-arsenopyrite vein, with carbonate seams as indicated (Little Harbour).

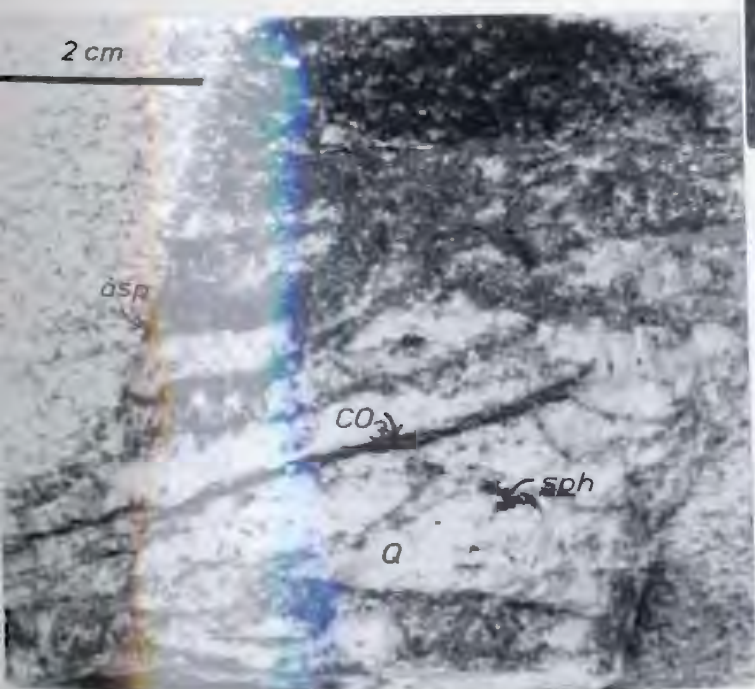
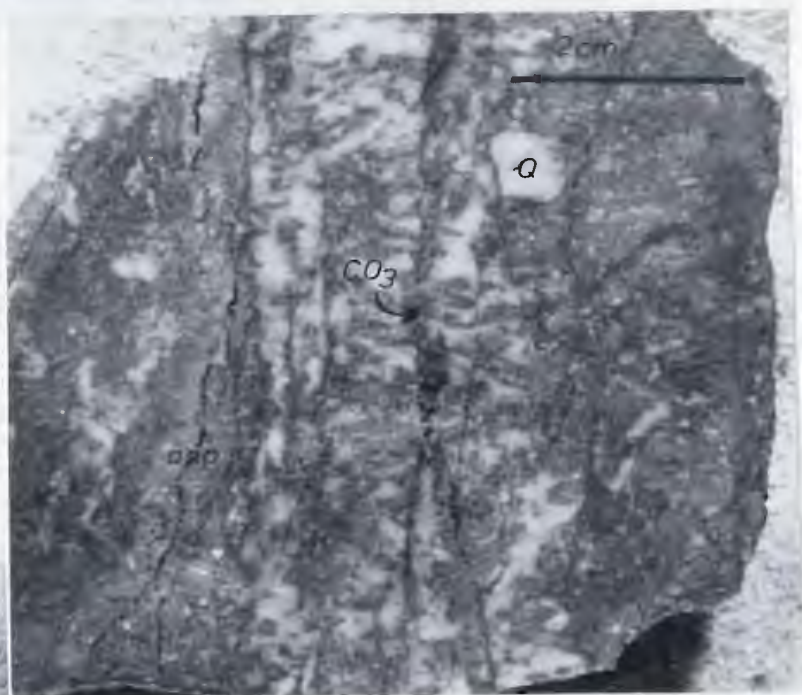


PLATE 4.3: Banded quartz-arsenopyrite-pyrite (+ trace pyrrhotite, sphalerite and chalcoppyrite) vein showing several pulses of deposition. Band margins are cross-cut by ferroan calcite and siderite (Stewart's Mine).

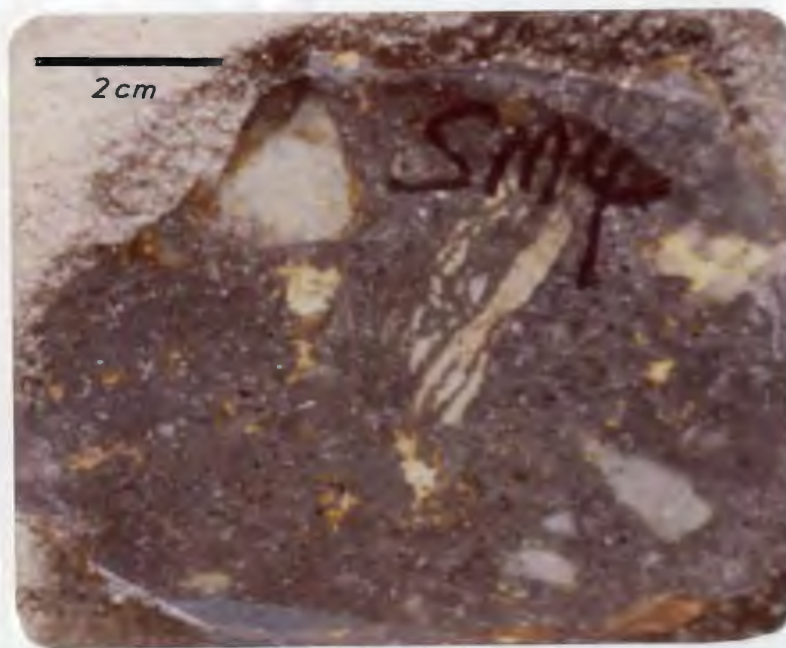


PLATE 4.4: Massive arsenopyrite, bearing angular vein and wall-rock fragments, Stewart's Mine.

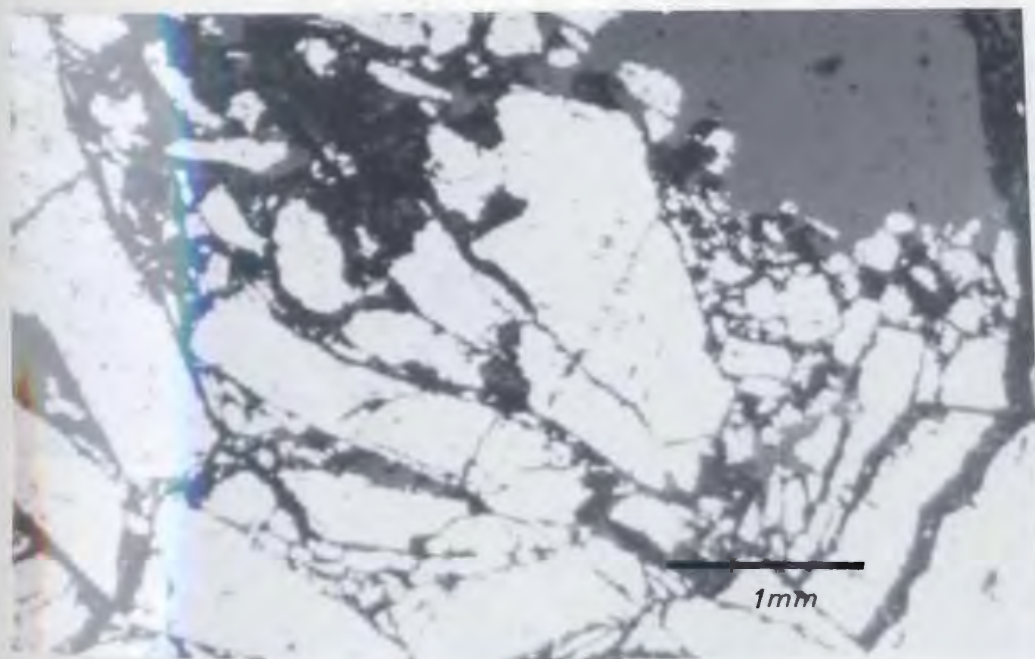


PLATE 4.5: Photomicrograph of brecciated arsenopyrite cemented by quartz and calcite, Stewart's Mine (SM.52).

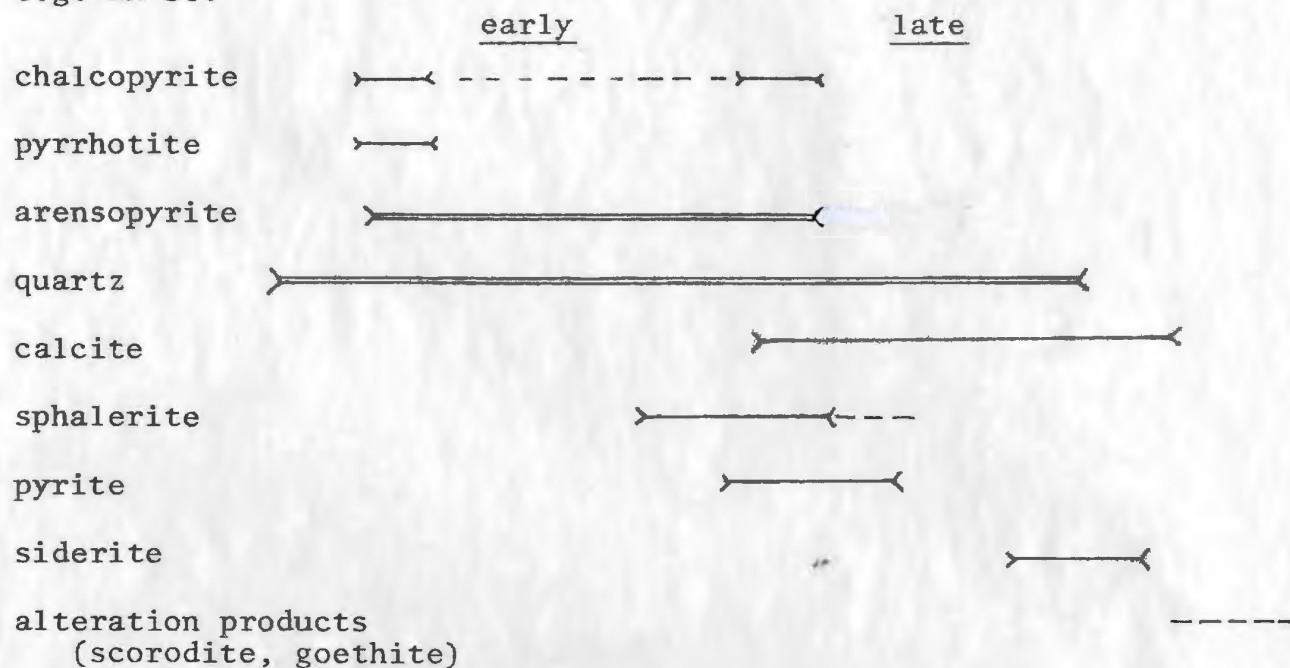
euohedral (cubic) crystals, generally near the vein centres. Sphalerite, ubiquitously bearing chalcopyrite exsolution blebs along the dodecahedral crystallographic planes (Plate 4.7) occupies anhedral, late fillings. Rarely small inclusions of pyrrhotite and chalcopyrite occur in the arsenopyrite masses. Elsewhere arsenopyrite appears to be the earliest sulphide precipitated, intergrown with calcite and quartz succeeded by the base metal sulphides and later gangue deposition (Fig. 4.4). Oxidation products observed include siderite, goethite, and scorodite (Gibbons, 1969).

4.2.1a Moreton's Harbour Head: Vein Type I

Mineralized veins occur at Moreton's Harbour Head, notably adjacent to the fault contact with the Moreton's Harbour Head Breccia and the Little Harbour Formation. Most of these veins are arsenopyrite-dominated (Type I) although more stibnite-rich veins also occur (Type II). The area is pervasively Fe-oxide stained. One example of a vein is about 20 cm thick, dipping steeply to the northwest. The central portion of the vein is silicified, chloritic mafic dyke rock, the margins of which have been overgrown by a comb-intergrowth of quartz and arsenopyrite. Calcite and siderite with pyrite and sphalerite are later phases and are quite abundant sporadically.

4.2.1b Other small veins of Type I occur within the area. These smaller veins do not have the banded texture well developed. One small tetrahedrite grain was identified in one sample.

(a) e.g. SM-56:



(b) Other vein type I:

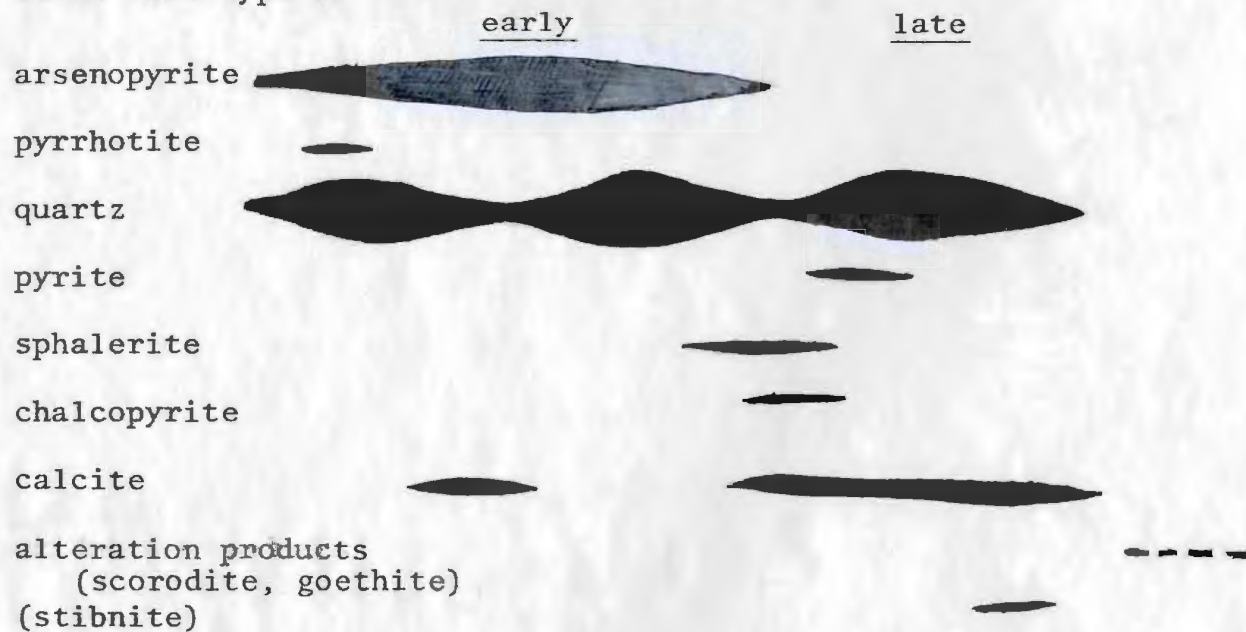


Fig. 4.4: Paragenetic sequence of vein type I.

4.2.2 Stuckless' Mine: Type II

The antimony mine of south Frost Cove is sited on the largest vein within the area. The dominant sulphide is stibnite. The mineralization is hosted by and adjacent to the margins of a pervasively, hydrothermally-altered (silicified-calcitized-chloritised) felsic dyke, which strikes 010° , is steeply dipping and attains a thickness of up to 2.5 m. The dyke intrudes silicified and chloritized pillow basalts which are veined extensively with calcite (± Fe-rich) (Plates 3.6 and 3.7) and siderite and abundant pyrite euhedra. The wall rocks are slightly sheared and brecciated, notably along the margins of the felsic dyke. Southwards along strike of the felsic dyke it is shown to be a pink rhyolite, bearing quartz and feldspar phenocrysts. According to Heyl (1936), the mineralized vein continues southwards along strike for "2600 feet", but this was not confirmed by the present study.

Stibnite is the most abundant mineral, occurring in radiating masses up to 20 cm across (Plate 4.6) and in narrower (~1 cm) veinlets subparallel to the main vein. The stibnite is intergrown with subhedral, dogtooth, clear to buff-coloured-cloudy quartz. Other sulphides occurring in the vein Type II are arsenopyrite, pyrite, galena, sphalerite and chalcopyrite. The paragenetic sequence is presented in Figure 4.5. As alteration products of stibnite, kermesite and cervantite were identified.

Quartz is the predominant gangue mineral with locally abundant carbonate. Fluorite was identified in one galena-rich sample.

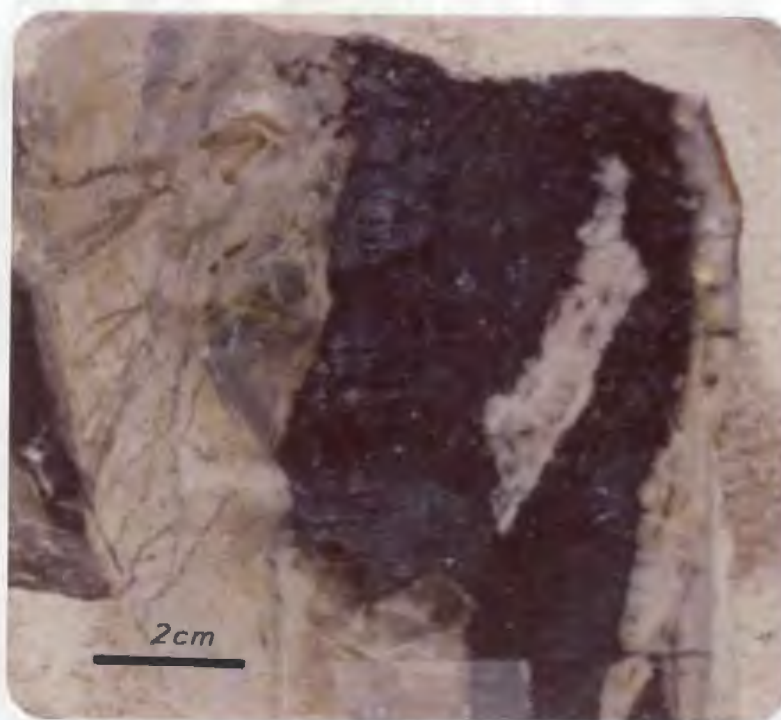


PLATE 4.6: Massive stibnite vein, Type II, Stuckless' Mine, with altered, felsic dyke wall-rock and intergrown, banded quartz (SB.25).

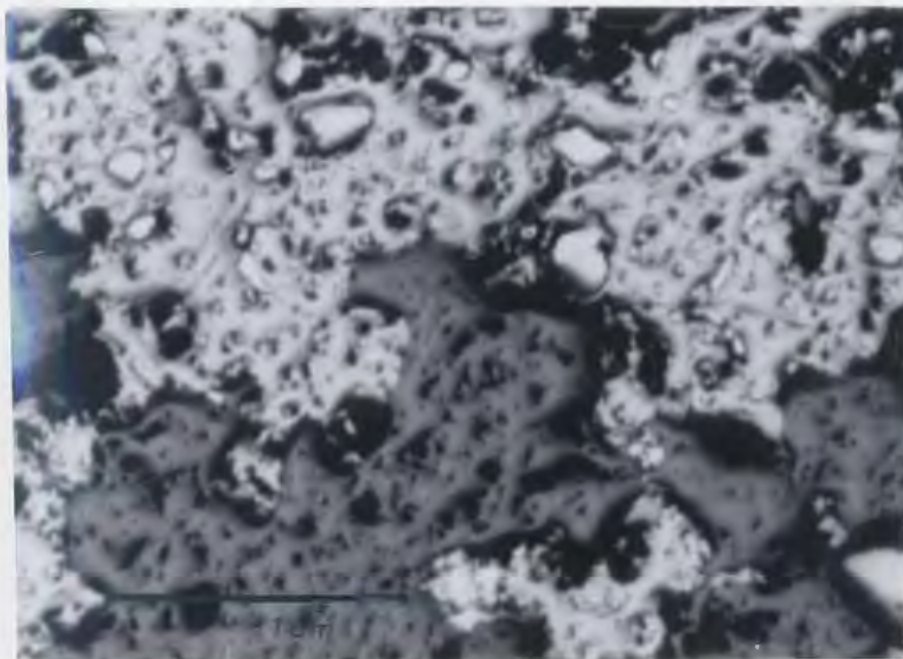


PLATE 4.7: Photomicrograph of irregular sphalerite, bearing large, abundant blebs of chalcopryite (SM.58).

Euhedral quartz, intergrowing in a comb-like texture with the stibnite with c-axes perpendicular to the vein, shows successive growth bands. This quartz is buff, grey to white and cloudy to clear and is considered contemporaneous with the stibnite. Earlier quartz is white and cloudy as similarly are later cross-cutting veinlets.

There is a crude zonation of mineralogy in the Type II veins with the arsenopyrite (earlier) outermost and other (later) minerals towards the centre.

4.2.3 Taylor's Room: Type III Veins

The mineralized veins of the Taylor's Room prospect are not exposed and so field description draws from previous work (Heyl, 1936). There are several veins traced for ~180 m perpendicular to the strike of the host tuffs and tuff breccias, which contain disseminated pyrite and traces of other sulphides. The vein width varied up to 30 cm. The Taylor's Room vein samples are dominated by sphalerite with chalcopyrite and pyrrhotite and lesser galena. Arsenopyrite is also locally abundant. Stibnite is relatively rare. The gangue minerals are quartz and calcite. The paragenesis of the veins of Type III are given in Fig. 4.6. The sphalerite occurs as 1 cm thick, anhedral masses and veinlets with abundant chalcopyrite inclusions.

Arsenopyrite is generally euhedral or fragmented and is found intergrown with pyrrhotite and chalcopyrite with interstitial quartz and calcite. The veins contain altered fragments of wall rock.

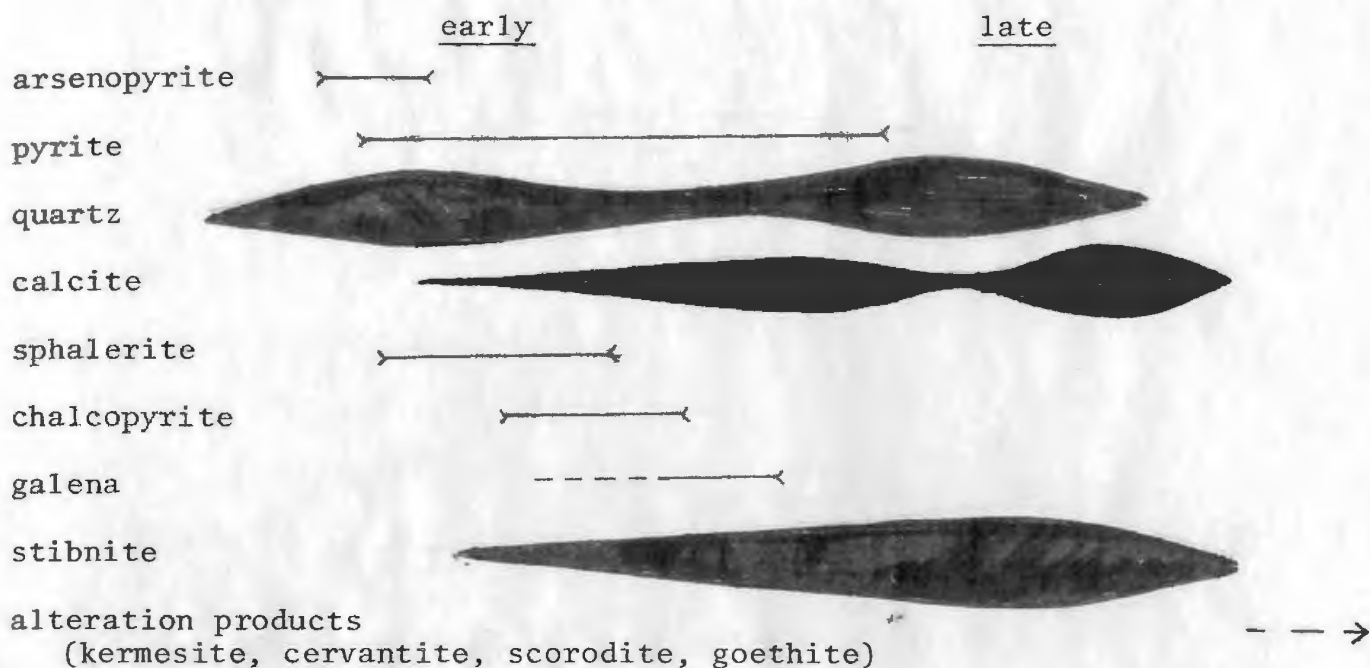


Fig.: 4.5: Paragenetic sequence of vein type II; e.g. Stuckless' Mine.

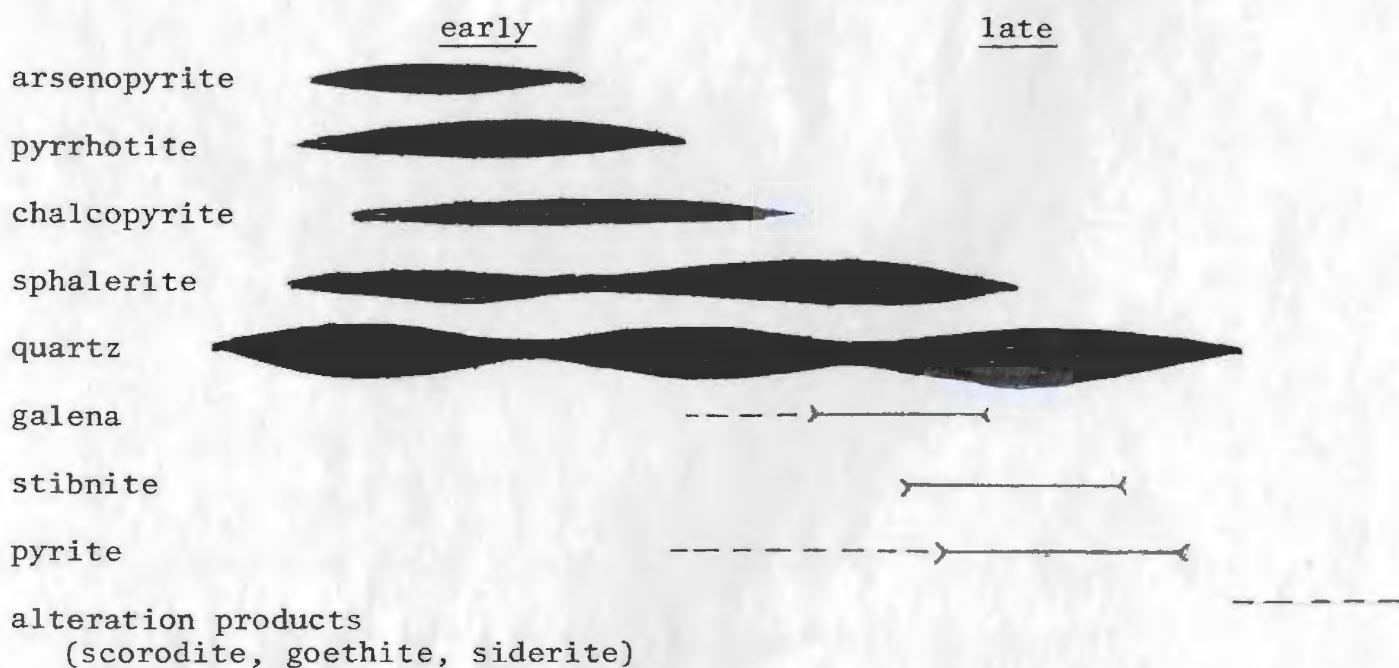


Fig. 4.6: Paragenetic sequence of vein type III, Taylor's Room.

4.2.4 Other Mineralization

Various minor veins of the three vein types occur around Moreton's Harbour, largely within the Little Harbour Formation and uppermost part of the Western Head pillow lava Formation. The Western Head Copper Prospect (Fogwill, 1968) comprises disseminated pyrite with minor chalcopyrite and arsenopyrite and locally in quartz-sulphide filled tension gashes and veinlets, hosted by mafic pillow and tuff breccias, localized adjacent to felsic intrusions (cf. Pomley Cove). Mineralization is presumed to be related to the veins further east, but due to poor exposure and lack of suitably mineralized samples, more detailed discussion of this mineralization is not presented here.

The arsenopyrite or stibnite-bearing veins are not observed far west of Moreton's Harbour Head. Abundant pyritization is observed associated with felsic dykes along the north coast and within the Moreton's Harbour Head Breccia. The felsic volcanic rocks around Hayward's Cove and Moreton's Cove are similarly pyritic in places, but not of economic significance. There are rusty-weathering zones associated with fault and shear zones throughout the area.

4.3 Summary

The properties of the types of mineralized veins encountered in the study area are summarized in Tables 4.1 and 4.2. The chemistry of these veins and the controls of their deposition are discussed in the following chapters.

TABLE 4.1

Summary of Mineral Assemblages of the Mineralized Veins

Mineral	Vein Type		
	I	II	III
Quartz	●	●	●
Calcite*	●	●	●
Arsenopyrite	●	●	○
Stibnite	●	●	●
Sphalerite	○	●	●
Chalcopyrite	●	●	○
Pyrite	○	●	●
Pyrrhotite	●		○
Galena	●	○	○
Tetrahedrite	○		
Scheelite			
Scorodite	■		■
Cervantite		■	
Kermesite		■	
(Fluorite?)		○	
Chlorite	■	■	■
Sericite	■	■	■






-   -Major, locally abundant
 -Minor
 -Trace (and occurrence)
 -Alteration
 * -Fe-free, Fe-rich and siderite

TABLE 4.2
Summary of Properties of the Mineralized Veins,
Moreton's Harbour Area

	Vein Type		
	I	II	III
Vein Thickness	Vein thickness varies from 0.5 to 0.05 m		
Vein Strike	Veins strike perpendicular to bedding		
Associated	Spatially associated with felsic dykes		
Host Rock Types	Wall rock variable; includes diabase (Stewart's Mine), rhyolitic dyke (Stuckless), tuffs and pillows, but generally restricted to the Little Harbour Formation Alteration diminishes within 5 m of the larger veins and 0.25 m others; calcitic.		
Gangue Minerals	Quartz and calcite	Quartz and calcite	Quartz and calcite
Major Sulphide Minerals	Arsenopyrite	Stibnite	Sphalerite, chalcopryrite
Minor Sulphide Minerals	pyrite, chalco-pyrite, sphalerite	galena, arsenopyrite, pyrite	pyrrhotite, arsenopyrite, pyrite, galena, stibnite

CHAPTER 5

VEIN CHEMISTRY

5.1 Introduction

The geochemistry of the ore and its minerals is presented in this Chapter. The elements As, Zn, Pb, Ni, Y, Sr, Ga, Th, U and Rb were analysed by X-ray fluorescence (Appendix I). Determination of Sb using the same technique was unsuccessful. The precious and rare metals Au, Ag and Pd were analysed using the wet chemical-carbon furnace atomic absorption spectrophotometry technique of Fryer and Kerrich (1978) (Appendix I).

Values in excess of 0.1 ppm Au and Ag were checked using the same analyte solutions, with the flame spectrophotometry technique (Appendix I) which showed the results to be consistent. Although no samples were available for determining accuracy, several standard solutions were used for calibration and replicate analyses indicated a precision within the order of magnitude in the ppb range (see Appendix I).

Major elements, S, As, Fe, Cu, Zn, Pb and Sb were determined using the electron microprobe (Appendix I) and similarly spot analyses and scans for Au, Ag, W, Sn, Se, Te, Tl, Bi, Co, Ni and Cd for the sulphide ore minerals. The latter were less reliable analyses owing to their very low concentrations.

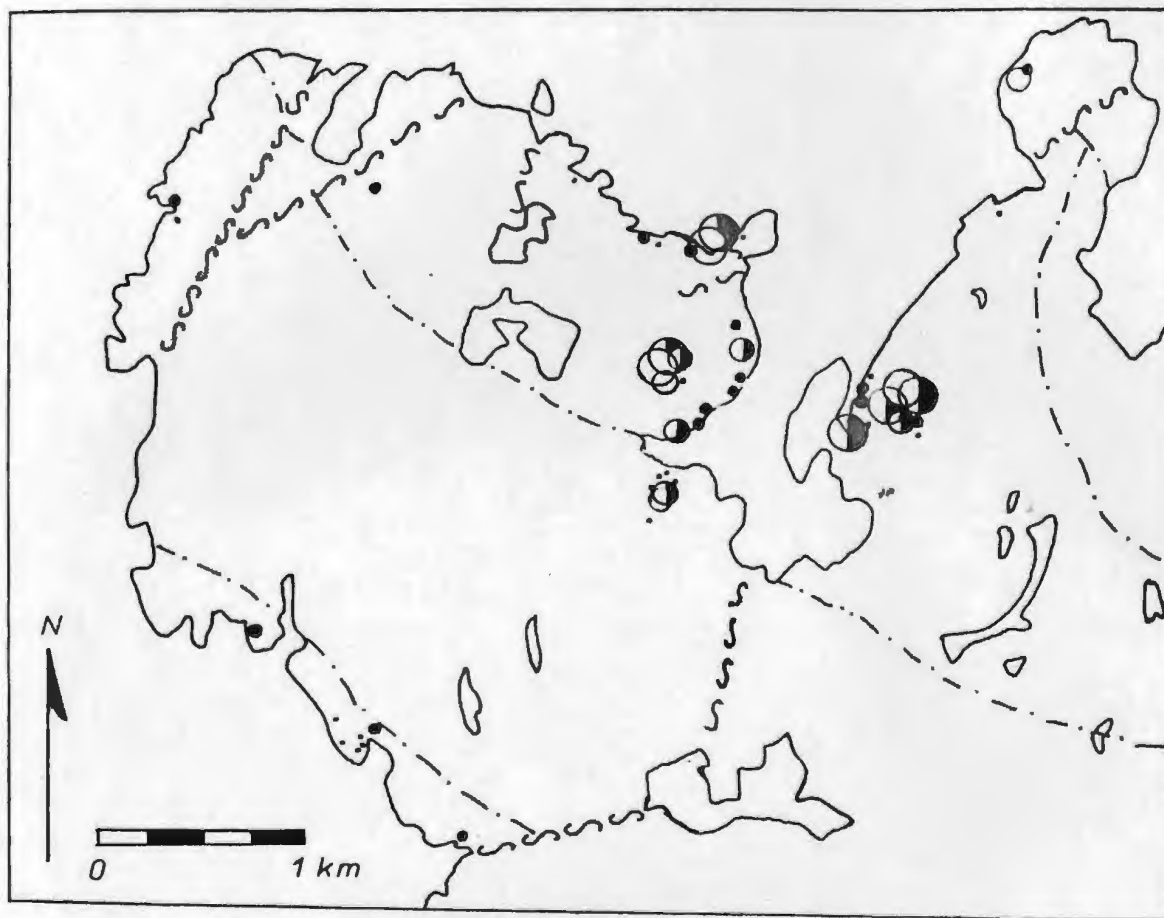
5.2 Data

Fifty-eight samples, from the three vein types and other lithologies from the Moreton's Harbour area were digested and analysed for Au

and Ag and fourteen of these were also analysed for Pd. The concentration of elements As, Zn, Pb, Ni, Zr, Y, Sr, U, Rb, Ga and Th were determined for all but five of these samples, which were too sulphide rich for pellets suitable for analysing. Analyses of the ore vein samples are presented in Table 5.1a and unmineralized samples in Table 5.1b. The mineralogical assemblages are summarized in Tables 3.1 and 4.1. The locations of samples and their relative concentrations are illustrated schematically in Figure 5.1.

The highest concentrations of Au and Ag are from samples of veins of types I and III which also have the lowest values of lithophile trace elements, Y, Sr, U, Rb, Zr and Ni. The wide variation in concentration of any of the elements within one lithological group is due to the heterogeneity of the samples, especially of the ores.

Correlation coefficients are presented in Table 5.2, in the form of a correlation matrix. This shows that Au concentrations strongly correlate with those of Zn and As, and to a lesser extent with Ag and Pb. Moderate negative values between Au and Ni, Zr, Y and Sr are shown suggesting that Au is not hosted by the silicate minerals. Silver is most highly correlated with Pb and Zn. The high coefficient between Ag and Ga is due to the interference peaks emitted by Pb in Pb-rich samples which erroneously enhances the Ga values (from X-ray fluorescence analysis; D. Press, pers. comm., 1981). This explains the perfect correlation of Ga and Pb. The reason for the high correlation between Ag and Th is uncertain. Arsenic and Zn are well correlated, probably due to the common mutual presence of sphalerite and arsenopyrite in ore samples.



--- Formation boundaries (see Fig. 2.1)

~~~~~ Faults

Gold Concentrations

- <5 ppb Au
- 5 - 10 ppb Au
- 10 - 100 ppb Au
- 0.01 - 0.10 ppm Au
- 0.1 - 1.00 ppm Au
- 1.0 - 10.00 ppm Au

Fig. 5.1: A sketch map showing the approximate locations of samples (ore and host rock samples) which have been analysed for gold and other elements. Symbols indicate variation of gold concentrations.

TABLE 5.1a  
Geochemical Analyses of Ore Samples, Moreton's Harbour

| Sample        | Au    | Ag    | Pd    | As%    | Zn%    | Pb    | Ni  | Zr  | Y   | Sr  | U  | Rb | Th  | Ga  |
|---------------|-------|-------|-------|--------|--------|-------|-----|-----|-----|-----|----|----|-----|-----|
| VEIN TYPE I   |       |       |       |        |        |       |     |     |     |     |    |    |     |     |
| SM-2          | 1.00  | 1.00  | 0.01  | 23.0   | 0.40   | 85    | 11  | 14  | 5   | 14  | 5  | 13 | 17  | 0   |
| SM-4*         | 1.70  | 0.80  | -     | (10)   | -      | -     | -   | -   | -   | -   | -  | -  | -   | -   |
| SM-5          | 1.00  | 5.70  | 0.01  | 21.0   | 2.80   | 273   | 0   | 17  | 4   | 15  | 12 | 8  | 38  | 2   |
| SM-52         | 0.40  | 0.40  | -     | 0.14   | 0.02   | 25    | 21  | 8   | 2   | 14  | 2  | 7  | 5   | 2   |
| SM-53         | 0.70  | 1.30  | 0.004 | 19.0   | 2.05   | 143   | 36  | 18  | 5   | 12  | 0  | 11 | 12  | 4   |
| MHH-6         | 9.04  | 10.10 | -     | 12.0   | 2.30   | 6000  | 0   | 32  | 10  | 95  | 4  | 26 | 77  | 170 |
| MHH-4         | 9.28  | 11.14 | -     | 23.5   | 8.50   | 2900  | 0   | 29  | 10  | 71  | 6  | 28 | 61  | 141 |
| LH-2*         | 1.00  | 0.84  | 0.007 | (20)   | -      | -     | -   | -   | -   | -   | -  | -  | -   | -   |
| LH-2a         | 0.08  | 1.96  | -     | 1.84   | 1.06   | 35    | 20  | 122 | 134 | 93  | 0  | 29 | 12  | 5   |
| VEIN TYPE II  |       |       |       |        |        |       |     |     |     |     |    |    |     |     |
| MHH-10        | 0.07  | 0.74  | -     | 1.40   | 0      | 53    | 166 | 12  | 16  | 135 | 8  | 9  | 173 | 0   |
| SB-1*         | 0.02  | 0.014 | 0.20  | -      | -      | -     | -   | -   | -   | -   | -  | -  | -   | -   |
| SB-15         | 0.014 | 0.140 | 0.007 | 0.0014 | 0.0065 | 218   | 12  | 98  | 32  | 462 | 0  | 6  | 1   | 29  |
| SB-17         | 0.009 | 0.68  | -     | 0.75   | 0.037  | 216   | 95  | 23  | 21  | 41  | 4  | 28 | 23  | 1   |
| SB-20         | 0.006 | 2.28  | 0.004 | 0.35   | 0.010  | 228   | 0   | 17  | 18  | 29  | 0  | 11 | 25  | 0   |
| VEIN TYPE III |       |       |       |        |        |       |     |     |     |     |    |    |     |     |
| SB-3          | 0.42  | 50.00 | -     | 1.40   | 1.70   | 22000 | 27  | 120 | 44  | 260 | 0  | 70 | 242 | 569 |
| FC-7          | 0.77  | 16.00 | -     | 9.20   | 0.70   | 7200  | 0   | 72  | 16  | 21  | 6  | 29 | 81  | 220 |
| TR-17         | 0.007 | 1.50  | 0.004 | 0.01   | 0.31   | 20    | 0   | 72  | 27  | 175 | 2  | 4  | 11  | 16  |
| TR-44         | 2.60  | 2.50  | 0.012 | (15)   | -      | -     | -   | -   | -   | -   | -  | -  | -   | -   |
| TR-45         | 0.034 | 1.50  | 0.020 | 0.01   | 0.62   | 457   | 0   | 98  | 33  | 135 | 1  | 29 | 12  | 31  |
| TR-52         | 1.00  | 48.90 | -     | 6.30   | 2.60   | 34    | 0   | 24  | 0   | 1   | 0  | 16 | 327 | 0   |
| TR-53         | 0.80  | 60.20 | 0.020 | 0.06   | 1.20   | 84    | 0   | 6   | 0   | 2   | 0  | 4  | 29  | 14  |

As% in parentheses are estimated from mineralogy

\*XRF analyses not obtained

High Ga values not valid because of Pb-peak interference in Pb-rich samples

-not analysed



TABLE 5.1b

Trace and Precious Metal Analyses of Various Unmineralized  
("background") Samples (also see Table 3.6)

| Sample<br>Number | ppb |     |    | ppm |     |    |    |     |    |     |   |    |    |    | Rock Type      |
|------------------|-----|-----|----|-----|-----|----|----|-----|----|-----|---|----|----|----|----------------|
|                  | Au  | Ag  | Pd | As  | Zn  | Pb | Ni | Zr  | Y  | Sr  | U | Rb | Th | Ga |                |
| WCH•9            | 200 | 420 | -  | 113 | 50  | 22 | 18 | 5   | 4  | 26  | 1 | 0  | 1  | 0  | pyritic jasper |
| LH•10            | 4   | 60  | -  | 120 | 71  | 6  | 1  | 75  | 30 | 179 | 0 | 6  | 1  | 18 | cherty tuff    |
| LH•23            | -   | -   | -  | 10  | 100 | 5  | 49 | 140 | 30 | 192 | 0 | 17 | 1  | 16 | mafic tuff     |
| LH•31            | 2   | 40  | -  | 31  | 103 | 7  | -  | 106 | 46 | 151 | 2 | 1  | 1  | 18 | diabase dyke   |
| LH•52            | 20  | 160 | -  | 32  | 63  | 6  | 6  | 160 | 23 | 96  | 0 | 26 | 1  | 13 | chert          |
| TR•31            | 14  | 260 | -  | 97  | 136 | 5  | 17 | 115 | 28 | 194 | 0 | 15 | 3  | 16 | cherty tuff    |
| TR•37            | 16  | 160 | -  | 18  | 173 | 5  | 11 | 126 | 28 | 205 | 1 | 30 | 3  | 16 | cherty tuff    |
| FC•31            | 45  | 240 | -  | 47  | 122 | 7  | 44 | 108 | 22 | 144 | 0 | 21 | 1  | 13 | mafic tuff     |
| WG•16            | 8   | 60  | -  | 16  | 34  | 7  | 0  | 347 | 48 | 56  | 8 | 67 | 22 | 15 | felsic tuff    |
| HC•42            | 4   | 80  | -  | 18  | 19  | 4  | 0  | 470 | 61 | 63  | 2 | 6  | 23 | 16 | felsic breccia |
| MC•1             | 6   | 80  | -  | 8   | 77  | 1  | 0  | 321 | 54 | 52  | 5 | 31 | 10 | 20 | felsic breccia |
| HC•34            | 9   | 80  | -  | 22  | 19  | 16 | 1  | 74  | 16 | 86  | 5 | 72 | 13 | 19 | rhyolitic dyke |

TABLE 5.1c

Analyses of Wall Rock Samples, Stewart's Mine  
(see Figs. 5.5 and 4.1)

| Sample<br>Number | ppb |     |    |      |     |    |     |     |    | ppm |   |    |    |    |
|------------------|-----|-----|----|------|-----|----|-----|-----|----|-----|---|----|----|----|
|                  | Au  | Ag  | Pd | As   | Zn  | Pb | Ni  | Zr  | Y  | Sr  | U | Rb | Th | Ga |
| SM-15            | 17  | 80  | 7  | 280  | 100 | 0  | 97  | 34  | 24 | 307 | 0 | 5  | 1  | 13 |
| SM-16            | 25  | 120 | 13 | 7    | 57  | 7  | 0   | 91  | 5  | 355 | 0 | 34 | 1  | 21 |
| SM-60            | 23  | 80  | 1  | 14   | 79  | 6  | 76  | 161 | 32 | 178 | 3 | 2  | 1  | 14 |
| SM-61            | 22  | 100 | -  | 156  | 71  | 0  | 204 | 34  | 19 | 201 | 0 | 1  | 0  | 12 |
| SM-62            | 16  | 360 | -  | 1361 | 484 | 21 | 78  | 33  | 23 | 96  | 0 | 26 | 1  | 13 |
| SM-63            | 50  | 540 | -  | 440  | 259 | 50 | 105 | 37  | 22 | 163 | 0 | 21 | 6  | 15 |
| SM-64            | 14  | 100 | -  | 22   | 64  | 0  | 12  | 107 | 28 | 129 | 0 | 3  | 3  | 0  |

SM-16 - quartz-feldspar-phyric rhyolite dyke

SM-60,61,62,63 - variably calcitized diabase  $\pm$  sulphides

SM-64 - relatively fresh salite-phyric diabase (4.5 m from adi)

TABLE 5.2

Correlation Coefficients for Element Pairs  
in Mineralized and Unmineralized Rock Samples  
Total Number of Samples = 50

|    | Au  | Ag  | As  | Zn  | Pb  | Ni  | Zr  | Y   | Sr  | U   | Rb  | Th  | Ga  |
|----|-----|-----|-----|-----|-----|-----|-----|-----|-----|-----|-----|-----|-----|
| Au | 100 | 20  | 62  | 80  | 26  | -15 | -21 | -28 | -18 | 22  | -1  | 22  | 31  |
| Ag | 20  | 100 | 14  | 38  | 54  | -14 | -20 | -24 | -20 | -12 | 3   | 71  | 52  |
| As | 62  | 14  | 100 | 73  | 15  | -13 | -30 | -43 | -36 | 39  | -12 | 22  | 16  |
| Zn | 80  | 38  | 73  | 100 | 28  | -16 | -24 | -31 | -25 | 23  | -2  | 38  | 33  |
| Pb | 26  | 54  | 15  | 28  | 100 | -6  | -5  | 8   | 6   | -1  | 28  | 55  | 99  |
| Ni | -15 | -14 | -13 | -16 | -6  | 100 | -29 | -13 | 10  | -7  | -22 | 4   | -9  |
| Zr | -21 | -20 | -30 | -24 | -5  | -29 | 100 | 77  | 5   | 17  | 18  | -14 | -2  |
| Y  | -28 | -24 | -43 | -31 | 8   | -13 | 77  | 100 | 8   | 11  | 10  | -15 | 11  |
| Sr | -18 | -20 | -36 | -25 | 6   | 10  | 5   | 8   | 100 | -40 | 25  | -18 | 10  |
| U  | 22  | -12 | 39  | 23  | -1  | -7  | 17  | 11  | -40 | 100 | 18  | 9   | 0   |
| Rb | -1  | 3   | -12 | -2  | 28  | -22 | 10  | 10  | 25  | 18  | 100 | 7   | 30  |
| Th | 22  | 71  | 22  | 38  | 55  | 4   | -14 | -15 | -18 | 9   | 7   | 100 | 52  |
| Ga | 31  | 52  | 16  | 33  | 99  | -9  | -2  | 11  | 10  | 0   | 30  | 52  | 100 |

Average concentrations of 2 ppb, 100 ppb and 8 ppb, for Au, Ag and Pd respectively have been determined for a range of rock types not associated with ore bodies (Parthé and Crocket, 1972; Tilling et al., 1973; Frueh and Vincent, 1974). The maximum values obtained for the Moreton's Harbour samples of 9 ppm (Au), 60 ppm (Ag) and 0.2 ppm (Pd) require enrichment factors of  $\sim 4500$ ,  $\sim 600$  and  $\sim 25$  respectively. Compared with values from Archean Au-lodes in Ontario (Kerrick and Fryer, 1979), the Au enrichment is lower. The Pd values are erratic and apparently enriched in the stibnite veins (Type II).

The average concentration of the base metals such as Zn, Pb and Cu, in the Moreton's Harbour ore samples are up to  $\sim 1000$  times their average crustal abundances (Tilling et al., 1973). The Archean deposits are reported to have lower average base metal enrichment factors ( $\sim \times 5$ ). Silver behaved more as a chalcophile base metal, such as Cu and Pb.

Arsenic has an estimated average concentration in basalt of only  $\sim 2$  ppm (Turekian and Wedephol, 1961). Arsenopyrite occurs ubiquitously in the Au-rich samples in which the As concentrations commonly exceed 10%, an enrichment factor of  $\sim 10,000$  times, in vein Type I. Similarly, Sb is enriched by  $\sim 10,000$  times background in vein Type II.

Thorium and Ga are considerably enriched in several ore samples, although values are erratic. Lithophile elements, Zr, Y and Sr as well as Ni, are depleted with respect to background values and average concentrations. This is due to the lack of silicate minerals in the ore samples other than quartz and minor chlorite and sericite. Higher values are seen in samples which have incorporated wall rock, however altered. Such samples show correspondingly low precious metal concentrations.



The enrichment-depletion factors for the different elements are summarized in Figure 5.2, which illustrates the difference between the vein types. The diagrams were derived by dividing ore sample abundances by the average crustal abundances. Values of Cu and Sb were estimated from the proportion of chalcopyrite and stibnite observed in the various samples. The diagrams are schematic. The concentrations of Au, Ag and As are slightly enriched in the sedimentary rocks of the Little Harbour Formation (Table 5.1) with respect to abundances from elsewhere (Western Head, Hayward's Cove). A pyritic jasper sample of Wild Cove Head (WCH-9) has 0.2 ppm Au and 0.42 ppm Ag. Similarly, cherty tuffs of Taylor's Room-Moreton's Harbour Head (samples #MHH-10, TR-37, TR-31, FC-31) are enriched in precious metals. It is apparent, from the Au-Ag binary plot (Fig. 5.3), that most determined abundances plot above the average crustal abundance "star" - even the unmineralized samples.

Histograms of relative abundances of Au, Ag, Ni and Pd are given in Figures 5.3, 5.4 and 5.5 which illustrate the geochemical discrimination of the vein types I, II and III. Gold, Ag and As show moderate positive correlations whereas all three correlate randomly or negatively with Pd and Ni (see Table 5.2).

The variation of the elements across the Stewart's Mine mineralized zone is shown in the Table 5.1c and Figure 5.5. Sample locations are shown in Figure 4.1. It is evident that there is a very sharp increase of Ag, Au, Zn and As at the narrow mineralized zoned and less than 4.5 m away from the mine, the host diabase bears fresh salic-pyroxene phenocrysts and the

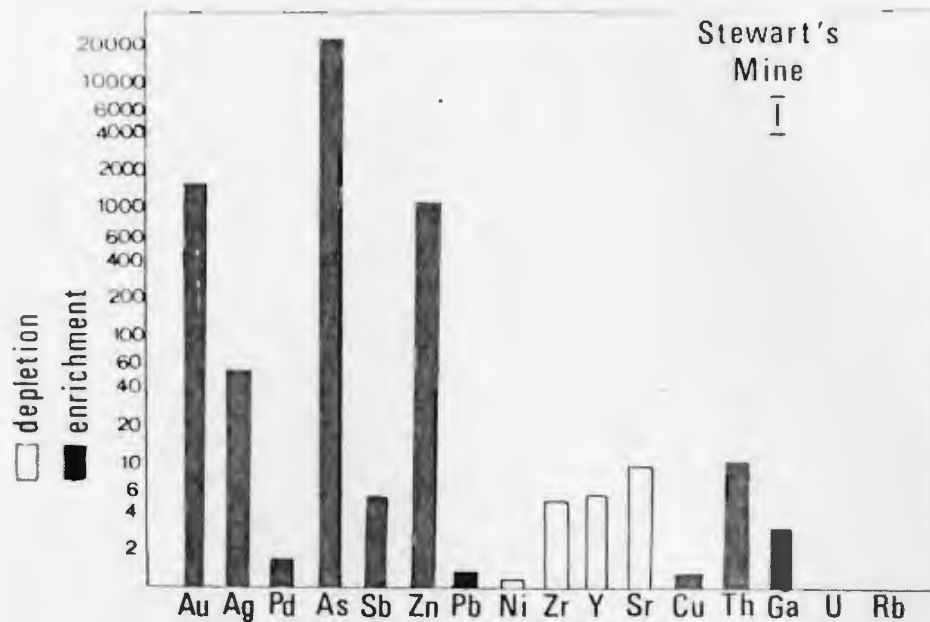
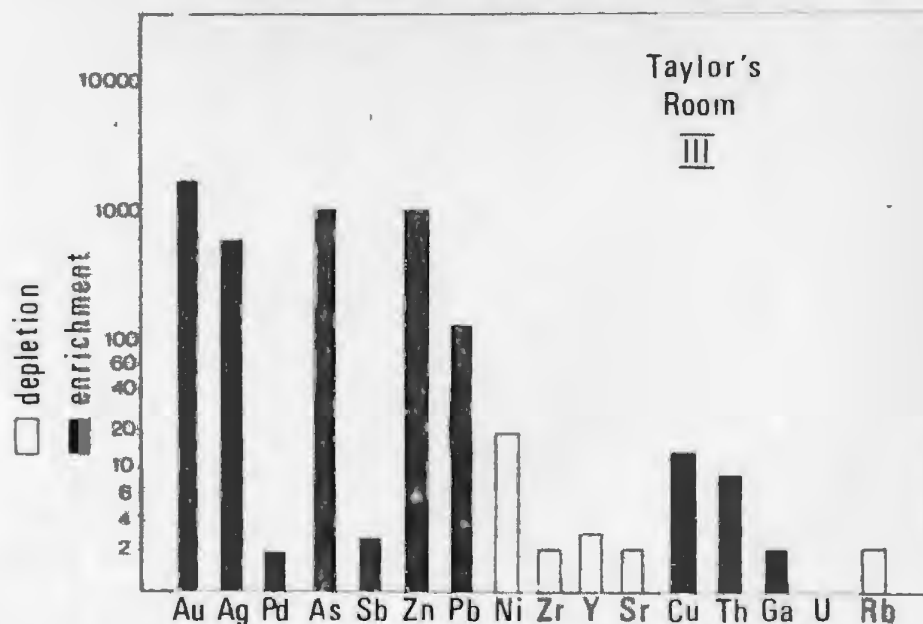
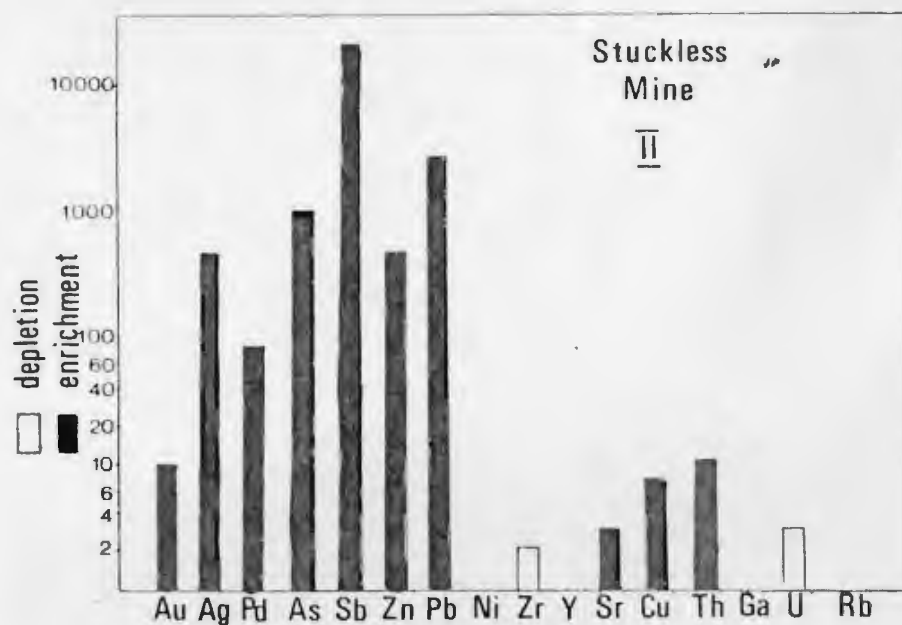


Fig. 5.2:  
Enrichment and  
depletion  
factors dis-  
played graph-  
ically for  
veins of Types  
I, II and III.



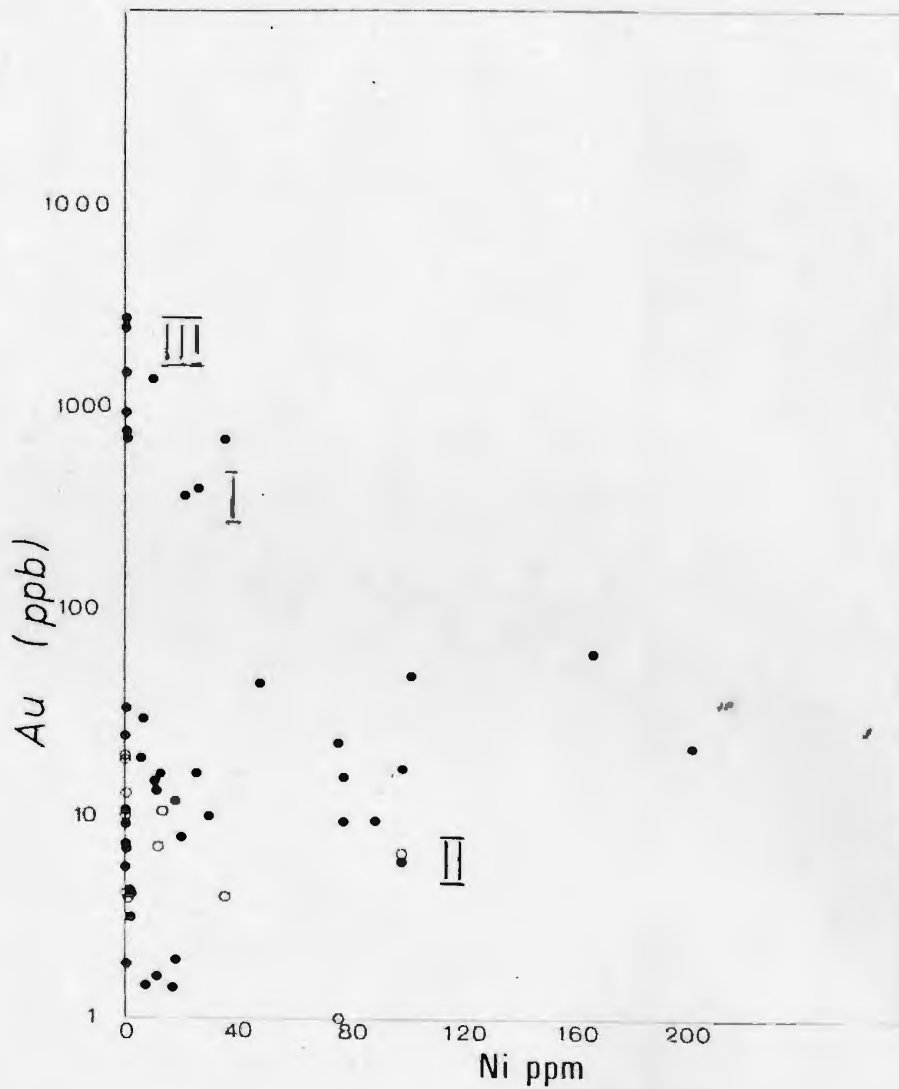


Fig. 5.3a:  
Au vs Ni for  
all samples  
(Open circles  
are Pd vs Ni).

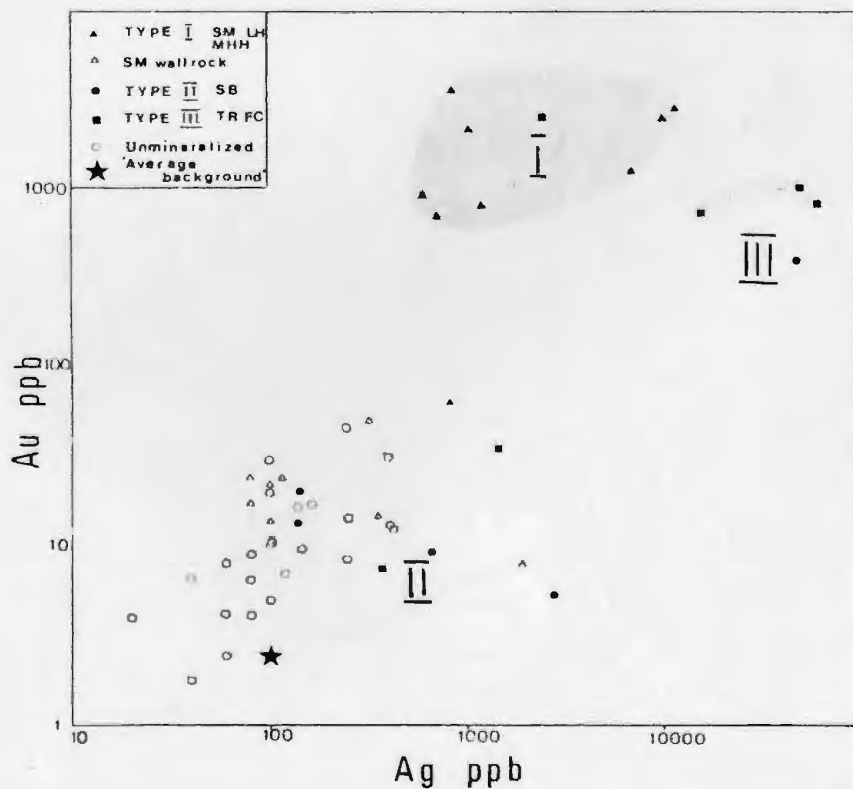


Fig. 5.3b:  
Au vs Ag.  
Plot showing  
discrimina-  
tion of vein  
types.

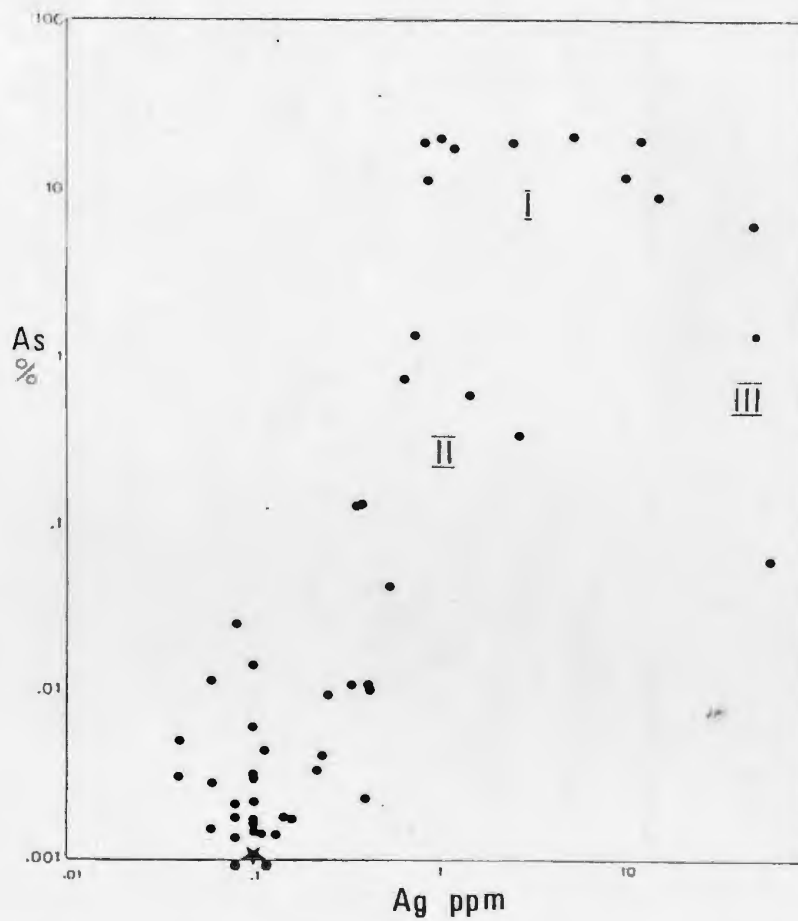
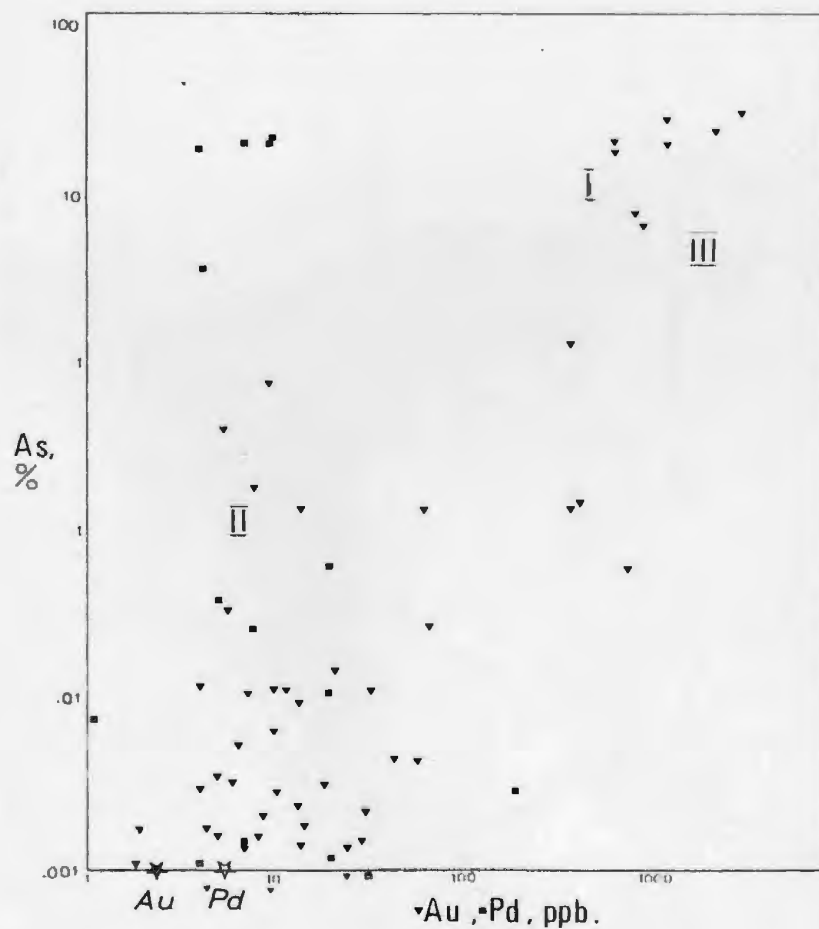


Fig. 5.4 : Binary plots of As vs Ag (above) and As vs Au, Pd (below) showing discrimination of vein types I, II, and III (Stars indicate background values).





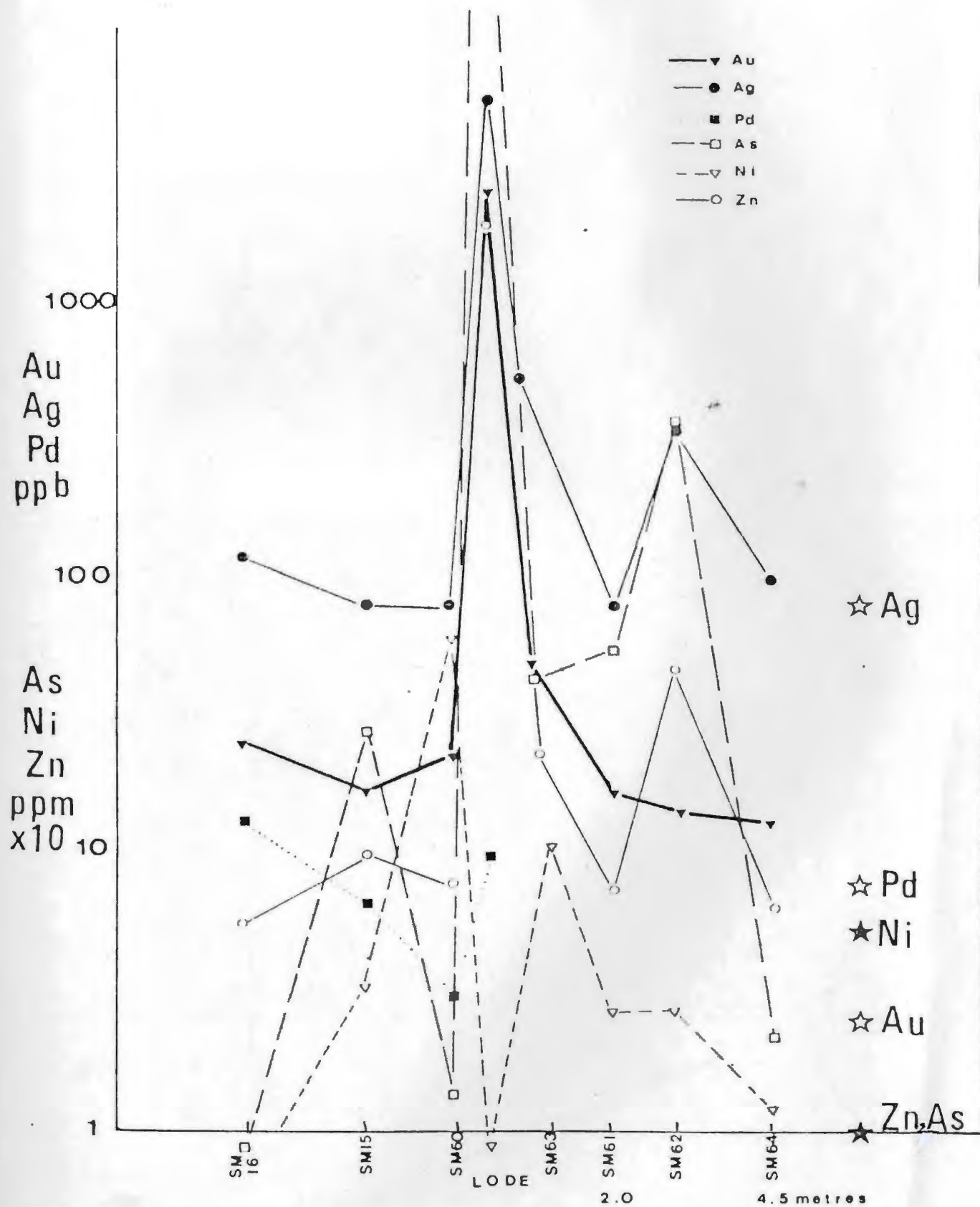


Fig. 5.5: Variation of concentrations of Au, Ag, As, Ni, Zn and Pd across the Stewart's Mine zone (Stars at the right indicate background values, horizontal distances are approximate).

concentrations of Ag, Pd, Ni, Au, As and Zn approach average background values. The concentration of Ni is depleted and erratic across the zone. The four analyses for Pd indicate little variation around background concentration.

### 5.3 Mineral Chemistry

#### 5.3.1 Major elements

The major element compositions of arsenopyrite from some Moreton's Harbour samples are presented in Table 5.3. The analyses show a general homogeneity of arsenopyrite throughout the area with a small range of As/S ratios,  $1.00 \pm 0.2$ . However, a consistent but slight zonation of composition is detected, having relatively As-rich cores and S-rich rims. The variation in composition of arsenopyrite is illustrated in As-Fe-S plots (Fig. 5.6).

Major element analyses of other minerals are presented in Table 5.4. Sphalerite is ubiquitously associated with chalcopyrite. Analyses of both show good stoichiometry. Sphalerite contains between 5 and 13 mol. % Fe, as well as traces of Cu, As, Sb and Pb. Chalcopyrite tends to be less contaminated.

Pyrite analyses tend to have low total values, as the microprobe calibration was made using single bond S (from an arsenopyrite standard), not as the  $S_2$ , combined as in the pyrite lattice; the pyrite S values are consequently too low. However, stoichiometry is shown to be fair and the pyrite is generally pure with rare traces of other metals up to a total 1 wt. %.

TABLE 5.3

Examples of Major Element Compositions of Arsenopyrite from  
Electron Microprobe Point Analyses (giving weight %, formula proportions and standard deviations)

| Sample No.         |          | Element |       |       |       |       |       |       |        |
|--------------------|----------|---------|-------|-------|-------|-------|-------|-------|--------|
|                    |          | S       | Fe    | Cu    | Zn    | As    | Sb    | Pb    | Total  |
| MHH-5              | wt. %    | 20.73   | 35.91 |       | 0.07  | 42.76 | 0.12  | 0.87  | 100.67 |
|                    | form.    | 1.039   | 1.031 | -     | 0.008 | 0.914 |       | .008  | 8.000  |
| D3-13R*            | wt. %    | 18.74   | 25.52 | -     | -     | 47.73 | -     | 0.01  | 101.68 |
|                    | form.    | 0.93    | 1.035 | -     | -     | 1.035 | -     | -     | 3.000  |
|                    | s.d.     | 0.67    | 0.70  | 0.07  | 0.20  | 1.10  | 0.01  | 0.05  |        |
| MHH-23<br>(margin) | wt. %    | 20.49   | 35.39 | -     | -     | 44.54 | 0.07  | 0.56  | 100.94 |
|                    | form.    | 1.027   | 1.016 | -     | -     | 0.953 | -     | 0.004 | 3.000  |
|                    | s.d.     | 0.86    | 0.38  | .06   | 0.11  | 1.79  | 0.06  | 0.22  |        |
| (centre)           | wt. %    | 19.73   | 34.71 | .02   | 0.08  | 45.57 | 0.02  | 1.17  | 101.3  |
|                    | form.    | 0.996   | 1.008 | -     | 0.04  | 0.984 | -     | .008  | 3.000  |
|                    | s.d.     | 0.41    | 1.16  | 0.06  | 0.11  | 0.984 | 0.03  | 0.44  |        |
| MHH-3              | wt. %    | 20.55   | 34.56 | -     | -     | 44.27 | 0.05  | 0.19  | 99.67  |
|                    | form.    | 1.000   | 1.02  | -     | -     | 0.957 | -     | -     | 3.000  |
|                    | s.d.     | 0.48    | 0.41  | 0.18  | 0.11  | 0.67  | 0.05  | 0.26  |        |
| SM-6<br>(centre)   | wt. %    | 19.11   | 35.69 | 0.01  | 0.05  | 45.68 | 0.03* | 0.25  | 100.82 |
|                    | form.    | 0.969   | 1.039 |       |       | 0.992 |       |       | 3.000  |
|                    | s.d.     | 1.29    | 0.85  | 0.05  | 0.02  | 2.16  | 0.05  | 0.09  |        |
| (margin)           | wt. %    | 19.19   | 35.79 |       | 0.07  | 46.68 | 0.05  | 0.37  | 101.96 |
|                    | form.    | 0.965   | 1.031 | -     | -     | 1.000 | -     | .004  | 3.000  |
|                    | s.d.     | 2.24    | 0.49  | .06   | 0.19  | 3.79  | 0.03  | 0.12  |        |
| SM-51<br>(centre)  | wt. %    | 18.71   | 34.27 | 0.07  |       | 45.51 | 0.02  | 0.40  | 98.98  |
|                    | form.    | 0.969   | 1.02  | 0.004 |       | 1.008 |       | .004  | 3.004  |
|                    | (margin) | wt. %   | 20.14 | 35.26 | 0.10  | .09   | 44.47 | 0.04  | 0.72   |
|                    | form.    | 1.012   | 1.02  | 0.004 | 0.004 | 0.957 |       | 0.004 | 3.000  |
| LH-1               | wt. %    | 19.05   | 34.68 |       | .08   | 45.70 | -     | 0.31  | 99.83  |
|                    | form.    | 0.977   | 1.02  |       | .004  | 1.000 | -     | .004  | 3.004  |
| SM-12              | wt. %    | 19.62   | 34.34 | 0.04  | 0.12  | 43.41 | 0.09  | 0.50  | 98.13  |
|                    | form.    | 1.012   | 1.02  |       | 0.004 | 0.961 | -     | 0.004 | 3.000  |
| MHH-11             | wt. %    | 20.54   | 35.96 | 0.09  |       | 42.96 | 0.04  | 0.23  | 100.13 |
|                    | form.    | 1.043   | 1.031 | 0.004 |       | 0.918 | -     | -     | 2.996  |
| JP-1*              | wt. %    | 20.88   | 36.88 | 0.11  | -     | 42.22 | 0.04  | 0.19  | 99.81  |
|                    | form.    | 1.047   | 1.047 | 0.004 | -     | 0.906 | -     | -     | 3.004  |
| D3-12R*            | wt. %    | 18.17   | 35.14 | -     | -     | 46.64 | 0.10  | 0.35  | 100.5  |
|                    | form.    | 0.934   | 1.035 | -     | -     | 1.027 | -     | 0.004 | 3.000  |
| MH-750*            | wt. %    | 20.17   | 36.13 | 0.06  | 0.08  | 43.98 | 0.07  | -     | 100.5  |
|                    | form.    | 1.012   | 1.039 | -     | 0.004 | 0.945 |       | -     | 3.000  |
|                    | s.d.     | 0.69    | 0.53  | 0.18  | 0.13  | 1.14  | 0.02  | 0.09  |        |
| D3-1R*<br>(centre) | wt. %    | 20.01   | 34.10 | 0.02  | -     | 45.25 | 0.06  | 0.20  | 99.64  |
|                    | form.    | 1.016   | 0.996 | -     | -     | 0.984 | -     | -     | 2.996  |
|                    | (margin) | wt. %   | 21.79 | 34.23 | 0.08  | 0.01  | 42.88 | 0.02  | 0.18   |
|                    | form.    | 1.09    | 0.984 | -     |       | 0.918 |       |       | 2.992  |
| MH-741*            | wt. %    | 21.84   | 34.23 | -     | 0.07  | 44.37 | 0.04  | -     | 100.55 |
|                    | form.    | 1.082   | 0.973 | -     | -     | 0.941 | -     | -     | 2.996  |
| MH-875*            | wt. %    | 21.98   | 35.85 | 0.06  | -     | 42.63 | 0.07  | 0.01  | 100.6  |
|                    | form.    | 1.082   | 1.016 | -     | -     | 0.898 |       |       | 2.996  |
| TR-11              | wt. %    | 19.64   | 32.86 | -     | -     | 44.71 | 0.08  | 0.46  | 97.75  |
|                    | form.    | 1.02    | 0.98  |       |       | 0.996 |       |       | 3.000  |
| LHP-3A*            | wt. %    | 20.82   | 34.75 | -     | 0.05  | 44.89 | 0.09  | 0.04  | 100.63 |
|                    | form.    | 1.039   | 0.996 | -     | -     | 0.961 | -     | -     | 2.996  |
| LHP-1*             | wt. %    | 20.09   | 33.95 | -     | 0.02  | 45.52 | -     | -     | 99.71  |
|                    | form.    | 1.02    | 0.988 | -     |       | 0.988 | -     | -     | 2.996  |

\*R. Gibbons' samples, 1969

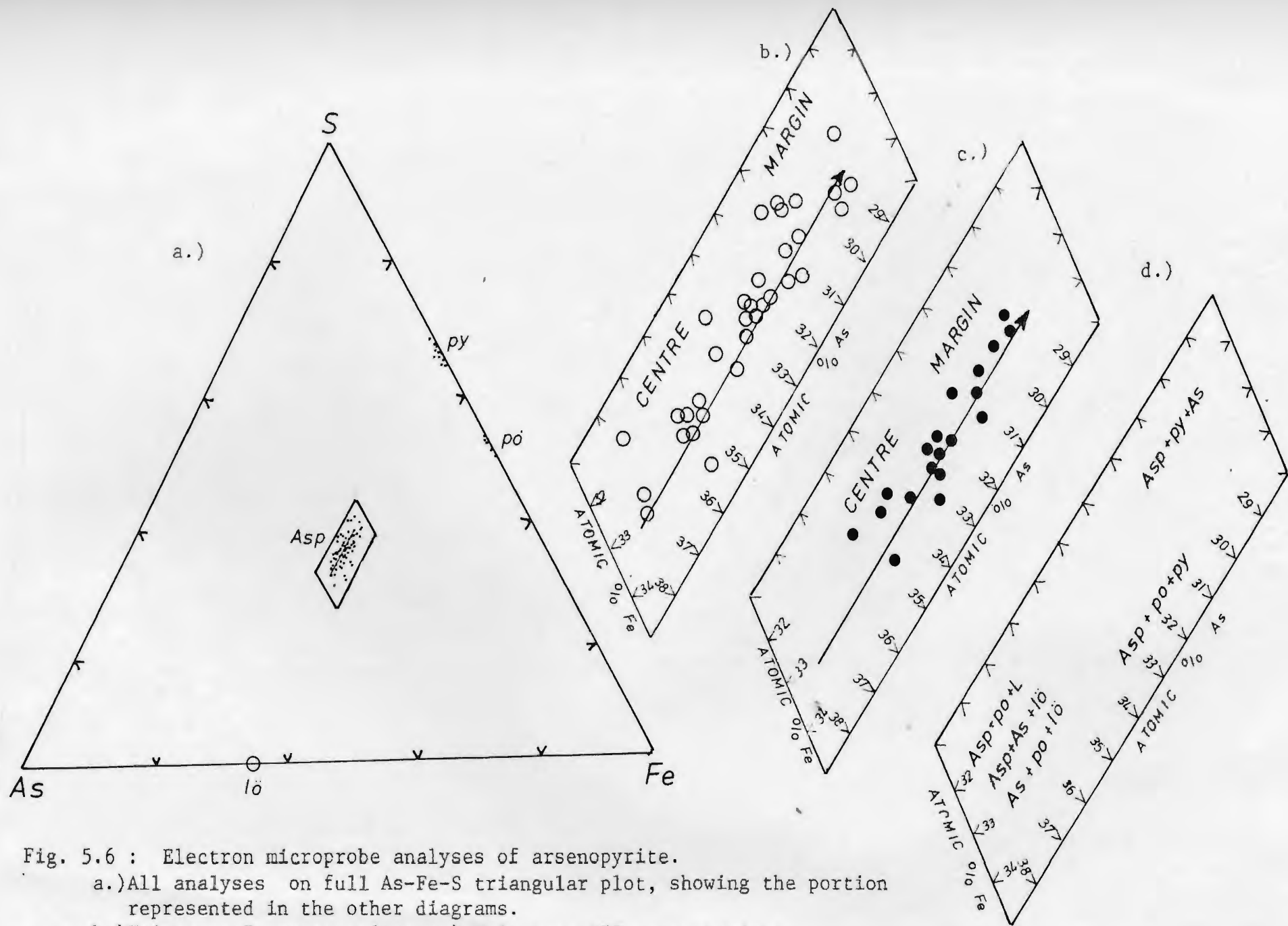


Fig. 5.6 : Electron microprobe analyses of arsenopyrite.

- a.) All analyses on full As-Fe-S triangular plot, showing the portion represented in the other diagrams.
- b.) Vein type I arsenopyrite; c.) Vein type III arsenopyrite;
- d.) Assemblages with arsenopyrite from observed and experimental data, ( from Kretschmar & Scott, 1971 ). ( Arsenopyrite, asp; pyrite, py; pyrrhotite, po; loellingite, lo; arsenic, As; liquid, L ).



Pyrrhotite analyses are of similarly low totals. Determined values of  $x$  in its formula,  $\text{Fe}_{1-x}\text{S}$  are  $0.05 \pm .01$ . No systematic compositional zoning of either pyrite or pyrrhotite was detected.

Stibnite analyses approximate closely to the formula  $\text{Sb}_2\text{S}_3$ , with traces of Fe, Zn, As, Pb and Cu, commonly  $\leq 0.5$  wt.% total, and rarely exceeding 1.0 wt.% total. Oxidation products of the stibnite margins are identified as kermesite and cervantite. The alteration products contain larger concentrations of the other major metallic elements.

### 5.3.2 Trace elements

Having verified that some of the ore has anomalously high concentrations of Au and Ag, it was decided to attempt to locate the site of these metals. Electron microprobe scans and point analyses of ore samples were executed but no significant Au was detected. Results for point analyses for Au, Ag, Se, Te, Tl, Bi, Co, Ni, Cd, Sn, and W were relatively poor, due to the inability of the electron microprobe to detect and determine such low concentrations (Table 5.5). This is especially true for heavy elements such as Au and W, which have high background values and numerous interference peaks (ie. "noise") in their emission spectra. For example, the lowest reliable detection limit for Au would be  $\sim 2\%$  (H. Longerich, pers. comm., 1980). Silver values exceeding 0.1% may be considered probable, as located in galena (MH-733), tetrahedrite (TR-52) and arsenopyrite (SM-53). Traces of Te, Tl, Bi, Cd, Sn were recorded in various minerals. Cobalt and Ni are notably absent from all mineral phases. The Co and Ni concentrations in pyrite and pyrrhotite may be useful indi-

TABLE 5.4

Examples of Major Element Compositions of Other Sulphide Minerals, from Electron Microprobe Point Analyses (giving wt. % and formulae)

| Sample   | Mineral                                                                       |       | Element |       |       |       |       |       |       |       |
|----------|-------------------------------------------------------------------------------|-------|---------|-------|-------|-------|-------|-------|-------|-------|
|          |                                                                               |       | S       | Fe    | Cu    | Zn    | As    | Sb    | Pb    | Total |
| MHH-11*  | PYRITE<br>FeS <sub>2</sub>                                                    | wt. % | 49.28   | 47.89 | 0.15  |       | 0.13  | 0.04  | 0.84  | 98.35 |
|          |                                                                               | form. | 1.918   | 1.07  | 0.004 |       | 0.004 |       | 0.004 | 3.000 |
| D4-2R*   | PYRITE<br>FeS <sub>2</sub>                                                    | wt. % | 50.09   | 47.0  | 0.11  | 0.07  | 0.02  | -     | 0.38  | 97.66 |
|          |                                                                               | form. | 1.945   | 1.047 | 0.004 | -     | -     | -     | 0.004 | 3.000 |
| MH-875*  | PYRITE<br>FeS <sub>2</sub>                                                    | wt. % | 51.64   | 45.93 | 0.05  | 0.02  | 0.61  | -     | -     | 98.5  |
|          |                                                                               | form. | 1.984   | 1.008 | -     | -     | 0.012 | -     | -     | 3.000 |
|          |                                                                               | wt. % | 52.06   | 47.14 | -     | -     | 0.04  | 0.02  | 0.07  | 99.33 |
|          |                                                                               | form. | 1.973   | 1.027 | -     | -     | -     | -     | -     | 3.000 |
| MH-874*  | PYRITE<br>FeS <sub>2</sub>                                                    | wt. % | 51.16   | 46.07 | -     | 0.12  | 0.83  | 0.04  | 0.17  | 98.85 |
|          |                                                                               | form. | 1.973   | 1.012 | -     | 0.004 | 0.012 | -     |       | 3.000 |
| D3-10R*  | PYRRHOTITE                                                                    | wt. % | 35.85   | 59.78 | -     | -     | -     | -     | 0.14  | 95.77 |
|          |                                                                               | form. | 1.000   | 0.956 | -     | -     | -     | -     | -     | 1.956 |
| D3-6R*   | PYRRHOTITE<br>Fe <sub>(1-x)</sub> S                                           | wt. % | 35.47   | 60.3  | 0.27  | -     | -     | 0.12  | 0.09  | 96.5  |
|          |                                                                               | form. | 1.000   | 0.976 |       |       |       |       |       | 1.976 |
| MH-580*  | CHALCOPYRITE<br>CuFeS <sub>2</sub>                                            | wt. % | 32.01   | 28.88 | 34.47 | -     | 0.01  | 0.02  | 0.15  | 95.53 |
|          |                                                                               | form. | 1.453   | 0.754 | 0.789 | -     | -     | -     | -     | 2.996 |
| D3-5R*   | CHALCOPYRITE<br>CuFeS <sub>2</sub>                                            | wt. % | 31.97   | 28.88 | 35.75 | 1.27  | 0.07  | 0.02  | 0.12  | 98.08 |
|          |                                                                               | form. | 1.902   | 0.984 | 1.074 | 0.035 | -     | -     | -     | 4.000 |
| D3-5R*   | SPHALERITE<br>Zn (Fe) S                                                       | wt. % | 29.87   | 3.10  | 0.25  | 63.70 | 0.09  | 0.04  | 0.21  | 97.2  |
|          |                                                                               | form. | 0.945   | 0.55  | 0.004 | 0.992 | -     | -     |       | 1.996 |
| TR-1     | SPHALERITE<br>Zn (Fe) S                                                       | wt. % | 31.29   | 6.97  | 0.06  | 54.82 | 0.01  | 0.07  | 1.21  | 94.42 |
|          |                                                                               | form. | 1.004   | 0.129 | -     | 0.863 | -     | -     | 0.008 | 2.004 |
| MHH-733* | GALENA<br>PbS                                                                 | wt. % | 12.28   | 0.06  | 0.13  | -     | 0.05  | 0.19  | 85.60 | 98.3  |
|          |                                                                               | form. | 0.957   | 0.004 | -     | -     | -     | 0.004 | 1.031 | 2.000 |
| MHH-732* | GALENA<br>PbS                                                                 | wt. % | 12.52   | 0.04  | 0.09  | -     | 0.03  | 0.16  | 85.8  | 98.64 |
|          |                                                                               | form. | 0.965   |       | 0.004 | -     | -     | 0.004 | 1.023 | 1.996 |
| FCE-3*   | STIBNITE<br>Sb <sub>2</sub> S <sub>3</sub>                                    | wt. % | 25.53   | -     | -     | 0.04  | 0.49  | 73.17 | 0.19  | 99.41 |
|          |                                                                               | form. | 2.83    | -     | -     | -     | 0.02  | 2.15  | -     | 5.000 |
| FCE-3*   | STIBNITE<br>Sb <sub>2</sub> S <sub>3</sub>                                    | wt. % | 26.55   | 0.05  | -     | 0.12  | 0.43  | 72.7  | 0.11  | 99.25 |
|          |                                                                               | form. | 28.55   | 0.004 | -     | 0.008 | 0.02  | 2.113 | -     | 5.000 |
| FCE-3A*  | STIBNITE<br>Sb <sub>2</sub> S <sub>3</sub>                                    | wt. % | 26.04   | 0.02  | 0.11  | 0.20  | 0.30  | 73.08 | 0.11  | 99.86 |
|          |                                                                               | form. | 2.855   | -     | 0.008 | 0.012 | 0.016 | 2.109 | -     | 5.000 |
| MH-563*  | TETRAHEDRITE<br>(CuFeZn) <sub>13</sub><br>(SbAs) <sub>4</sub> S <sub>12</sub> | wt. % | 22.5    | 5.61  | 40.03 | 1.82  | 0.32  | 29.48 | 0.05  | 99.87 |

\*R. Gibbons' samples

| Sample    | Mineral      | Element (wt. %) |     |     |     |     |     |    |     |     |     |   |
|-----------|--------------|-----------------|-----|-----|-----|-----|-----|----|-----|-----|-----|---|
|           |              | Se              | Ag  | Te  | Tl  | Au  | Bi  | Co | Ni  | Cd  | Sn  | W |
| MH.733*   | ARSENOPYRITE |                 | .02 | -   | -   | -   | .05 | -  | .03 | -   | .02 | - |
|           |              | .04             | -   | .05 | .3  | -   | .09 | -  | -   | -   | -   | - |
|           |              | -               | -   | .02 | .26 | -   | .09 | -  | -   | -   | -   | - |
|           |              | -               | .05 | -   | .11 | .08 | .07 | -  | -   | -   | -   | - |
| LH.P3*    |              | -               | .06 | .06 | -   | -   | .04 | -  | -   | -   | -   | - |
| MH.732*   | PYRITE       | .01             | .02 | .05 | -   | .12 | -   | -  | -   | -   | -   | - |
| MH.563*   |              | -               | -   | .04 | .07 | -   | .07 | -  | -   | -   | -   | - |
| MH.741*   |              | -               | .02 | -   | -   | .05 | .11 | 0  | .04 | .05 | .05 | 0 |
|           |              |                 |     |     |     |     |     |    |     |     |     |   |
| MH.372*   | PYRITE       | -               | -   | -   | .25 | .03 | .09 | -  | -   | -   | -   | - |
| HC.39     |              | -               | .01 | .01 | -   | -   | .1  | -  | -   | -   | -   | - |
| FCE.3*    |              | .04             | .05 | -   | -   | -   | .01 | -  | .04 | -   | .39 | - |
|           |              |                 |     |     |     |     |     |    |     |     |     |   |
| TR.41     | SPHALERITE   | -               | .03 | .04 | .3  | -   | .07 | -  | -   | -   | -   | - |
| MH.498A*  |              | .02             | -   | .03 | -   | .09 | .05 | -  | -   | -   | -   | - |
|           |              | .01             | -   | .02 | .07 | .07 | .04 |    |     |     |     |   |
| MH.580*   | CHALCOPYRITE | .03             | .06 | -   | .06 | .07 | .25 | -  | -   | -   | -   | - |
| MH.563*   |              | .04             | -   | .05 | .14 | -   | .05 | -  | -   | -   | -   | - |
| MH.732*   | GALENA       | .08             | .09 | .1  | .17 | .1  | -   | -  | -   | -   | -   | - |
|           |              | .07             | .13 | .06 | -   | .2  | .22 | -  | -   | -   | -   | - |
|           |              | -               | .12 | .06 | .19 | .18 | -   | -  | -   | -   | -   | - |
| MH.498A*  |              | .02             | .03 | .09 | .07 | .1  | .06 | -  | -   | -   | -   | - |
| MH.609A   | (MH.733)*    | .02             | .06 | .08 | -   | .02 | -   | -  | -   | -   | -   | - |
| MH.733*   |              | -               | .14 | -   | -   | -   | -   | -  | -   | -   | -   | - |
| (MH.733)* |              | -               | .17 | -   | -   | -   | .25 | -  | -   | -   | .04 | - |
|           |              | -               | .1  | -   | -   | -   | .05 | -  | .07 | .01 | .04 | - |
| FCE.3*    | STIBNITE     | .05             | .07 | -   | .14 | .07 | .06 | -  | -   | -   | -   | - |
|           |              | -               | .02 | -   | -   | -   | .03 | -  | .03 | -   | .04 | - |

\*R. Gibbons' samples, 1969

\*\* Au-analyses not significant

- not detected/not analysed

Table 5.5: Examples of Electron Microprobe Point Analyses of Trace Elements in Sulphide Minerals.

cators of the ore depositional environment and possible metal source (Cambel and Jarovsky, 1967; 1977). The greater preponderance of the so-called "misfit" elements, commonly related to granite hosted deposits (e.g. Sn, W, Bi, Sb) as opposed to Ni and Co, suggest an affinity of the Moreton's Harbour veins with some felsic, differentiated source.

The failure to detect free Au suggests that it is dispersed through the ore minerals. The ubiquitous occurrence of arsenopyrite in Au-rich samples implies that the arsenopyrite is a likely candidate. This is supported by the high correlation coefficient between Au and As ( $r=0.62$ ). There is a higher positive correlation between Au and Zn, which suggests that sphalerite may be an important host mineral. The sphalerite-rich veins of Type III have the highest concentrations of Au and Ag. Both Au and Ag correlate moderately with Pb and may be hosted in Pb-bearing minerals, such as galena. In some samples (e.g. #SB-3, TR-53, TR-52), the Ag concentrations are sufficiently high that Ag minerals may be present, although none were observed.

Several samples from the Taylor's Room veins had traces of pale blue luminescence under a short wave ultraviolet light, suggesting the presence of scheelite. The luminescence apparently emanated from small, interstitial patches of ferroan calcite and no scheelite was identified. Only trace amounts of W were detected in analyses (e.g. TR-52 in sphalerite and pyrite; SM-53 in arsenopyrite).



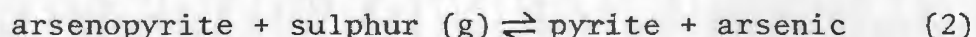
## 5.4 Constraints on depositional conditions from mineralogical data

### 5.4.1 Sulphur fugacity

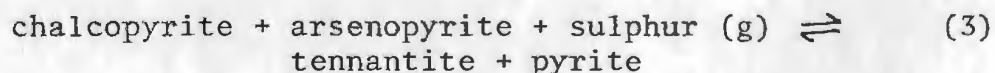
The presence of arsenopyrite and pyrite in most of the vein type I assemblages restricts the  $f_{S_2}$  to a relatively narrow range. The lower limit is established by pyrite and pyrrhotite (Fig. 5.7). Pyrrhotite is a minor and early phase such that the  $f_{S_2}$  was lower at the onset of sulphide deposition and subsequently increased, providing that other factors (pressure, temperature) remained constant. An increase of  $f_{S_2}$  is further reflected by the zonation of outward increasing of S in arsenopyrite. For the most part  $f_{S_2}$  was maintained above or at the equilibrium:



The upper limit must be set by the reaction:



as the assemblage pyrite + arsenic is not observed (Clark, 1960; Kretschmar and Scott, 1976; Barton and Skinner, 1979). Further constraints may be the common occurrence of chalcopyrite and absence of tennantite, such that the equilibrium:



may set the upper  $f_{S_2}$  limit.

In veins of type III, pyrrhotite is quite abundant coexisting with arsenopyrite, chalcopyrite, sphalerite  $\pm$  pyrite. Thus, the maximum  $f_{S_2}$  may be defined by equations 2 and 3 but the lower values may be below reaction 1. The small deficit of Fe in the pyrrhotite lattice (ie.  $x \approx 0.1$ ) implies a relatively high  $f_{S_2}$  within the pyrrhotite field.

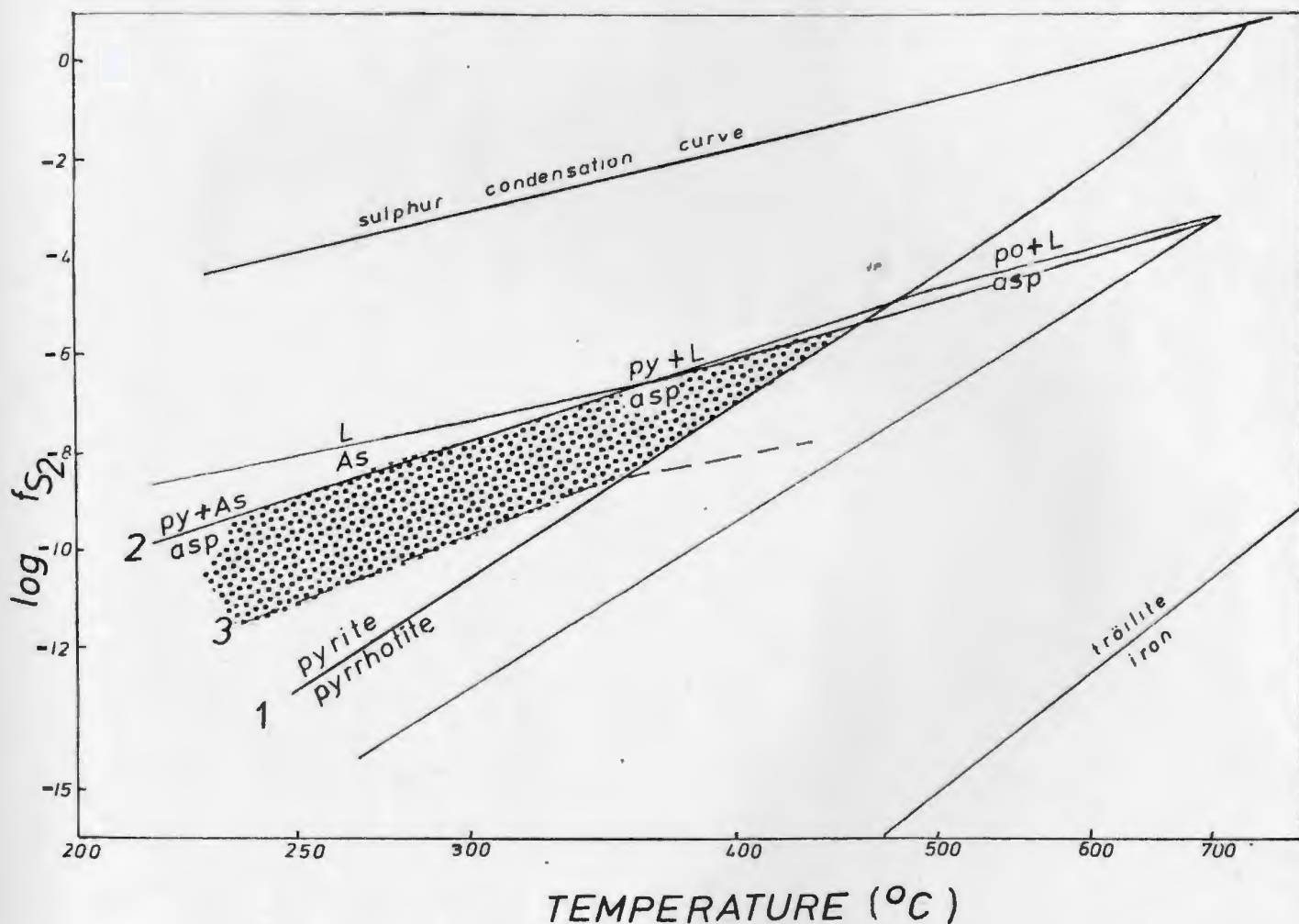
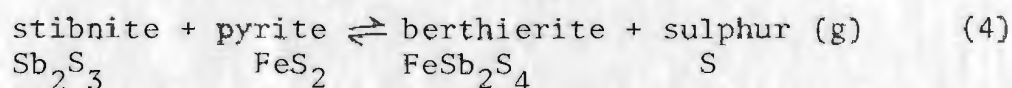


Fig. 5.7: Temperature-sulphur fugacity diagram showing the possible range (shaded area) as suggested by mineralogical assemblages observed in the vein system. Numbers 1 to 3 refer to the reactions (see text). (From Clark, 1960; Barton and Skinner, 1979).

Lastly, the veins of type II are almost wholly monominerallic, of stibnite. Minor early phases of coexisting arsenopyrite and pyrite indicate an initial upper  $f_{S_2}$  limit at equation 2, or at 3 by the common occurrence of chalcopyrite. The absence of pyrrhotite and all Sb-species other than stibnite (and late oxidation products) sets the lower  $f_{S_2}$  limit at the reaction:



(Barton, 1971) and reaction 1 (Fig. 5.8).

To attempt to ascertain the actual values for the  $f_{S_2}$  of the depositional environment, values for other variables, notably temperature, pressure and composition, are required. The above is merely an outline of the constraints on  $f_{S_2}$  made by the mineral assemblages.

#### 5.4.2 Temperature and pressure

Arsenopyrite and sphalerite may be useful P-T indicators according to experimental data (Scott, 1973; Kretschmar and Scott, 1976). If arsenopyrite is buffered with respect to S, then the As/Fe ratio is largely a function of temperature. The mol.% FeS in ZnS may be largely dependent on the confining pressure (but is also sensitive to  $f_{S_2}$  and presence of other metals, notably Cu).

Univariant curves for the Fe-As-S system were calculated from thermochemical data by Barton (1969) and confirmed by Kretschmar and Scott (1976). The As/S ratios for arsenopyrite from Moreton's Harbour were

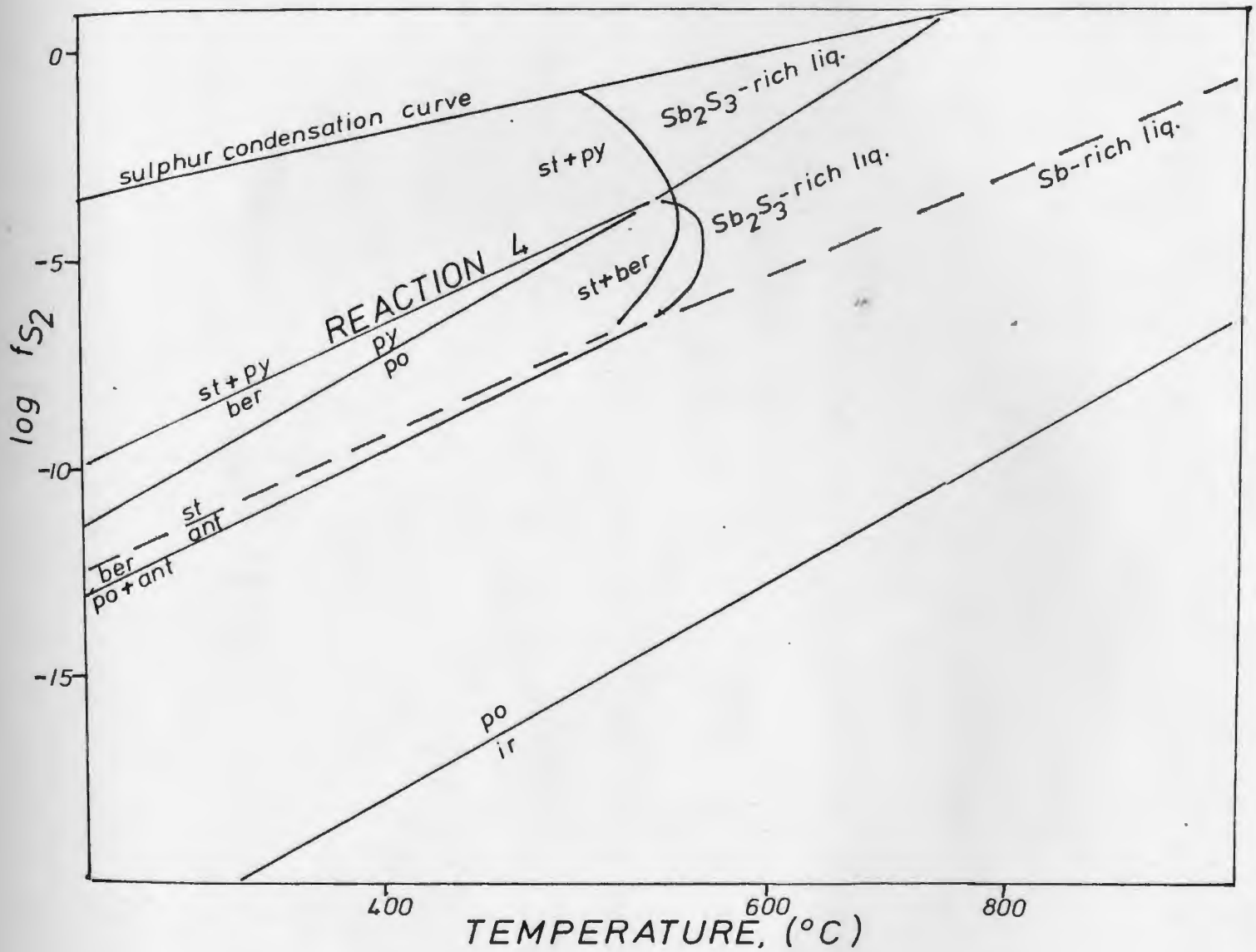


Fig. 5.8: Sulphidation equilibria for part of the Sb-Fe-S system (from Barton, 1971). (Abbreviations used: stibnite, st; pyrite, py; pyrrhotite, po; berthierite, ber; antimony, ant; iron, ir).



determined by Gibbons (1969), who measured the  $d_{131}$  spacings by X-ray diffraction to determine the As/S values. He applied his data to similar curves provided by Clark (1960) and deduced temperatures for the Moreton's Harbour arsenopyrite deposition around  $369^{\circ} \pm 30^{\circ}\text{C}$ , with confining pressures of 1 to 2 kb (Fig. 5.9).

Confining pressure is considered to have negligible affect on the As-Fe-S system and so it may be a sensitive geothermometer and  $f_{\text{S}_2}$  indicator during ore deposition according to Kretschmar and Scott (1976), contrary to Clark (1960). The refractory nature of arsenopyrite further commends its usefulness, in that post-depositional changes of composition are unlikely. Arsenopyrite should be chosen carefully from equilibrium  $f_{\text{S}_2}$ -buffered assemblages. Because arsenopyrite is so abundant and commonly forms monomineralic masses within the veins, it may itself buffer the ore-forming environment, in which case the geothermometric determinations may be affected. The combined minor element concentration in the arsenopyrite must be less than 1 wt. % (Kretschmar and Scott, 1976) as is the case with the Moreton's Harbour samples.

In this study, all arsenopyrite analyses (Table 5.3) were determined by electron microprobe which was calibrated using an arsenopyrite standard. The compositions and As-S ratios compared well with those by Gibbons (1969) and temperature estimates, therefore, are taken as around  $390^{\circ}$ - $400^{\circ}\text{C}$ . The slight zonation of As-rich cores to S-rich rims may reflect a temperature decrease and/or  $f_{\text{S}_2}$  increase with ongoing deposition.

Sphalerite geobarometry could not be applied to the Moreton's Harbour samples due to the high content of contaminants, notably Cu in the ZnS lattice and the lack of suitable coexisting assemblages (Barton and Toulmin, 1966; Scott and Barnes, 1971; Scott, 1973; Czamanske, 1974; Boctor, 1980). The range of 5 to 13 mol.% FeS in sphalerite analyses would give pressure determinations of greater than 3.5 kb, at 400°C (Fig. 5.10) which would seem very unlikely.

The assemblage stibnite + pyrite is a common ore assemblage, shown experimentally to be stable below 545±5°C (Barton, 1971). The Sb-Fe-S system is not very sensitive to physicochemical variation during deposition. However, deposits of As and Sb are commonly associated, and considered to be higher temperature, granite-related deposits, with a zonation from As to Sb (e.g. Cambel and Jarovsky, 1978).

The metamorphic grade of the host volcanic and volcanoclastic rocks at low greenschist facies implies that overall the area has not been subjected to temperatures in excess of 300 to 425°C or pressures >2 kb (Miyashiro, 1973; Winkler, 1976). Metamorphic grade increases adjacent to the felsic intrusives to low amphibolite facies (ie. ≥400°C).

## 5.5 Summary

The chemistry of the ore deposits and sulphide minerals show that:

- (a) the samples of veins of types I and III are enriched in Au and Ag;
- (b) the ore samples have a granitic affinity (ie. rich in elements);

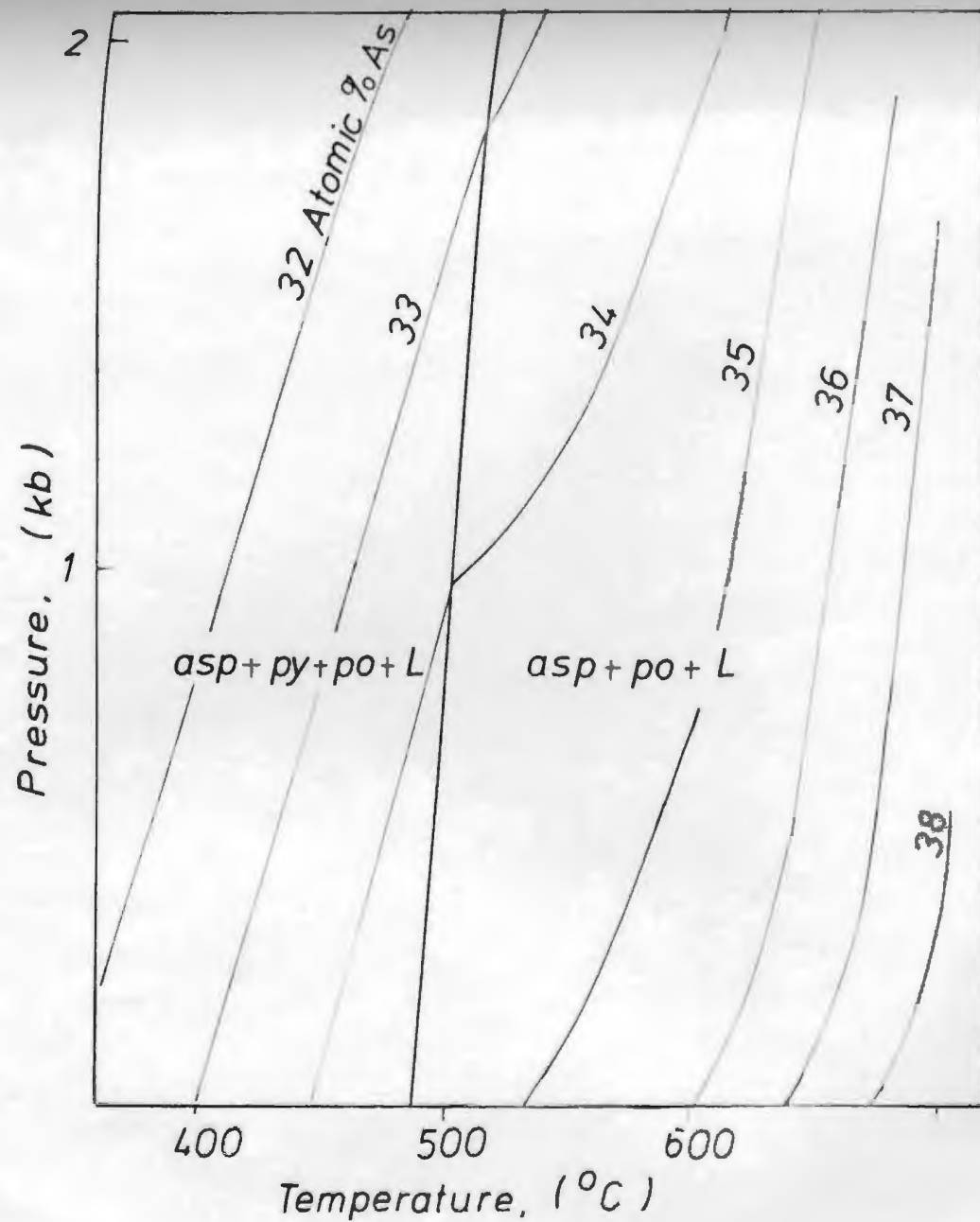


Fig. 5.9: Phase relations of the As-Fe-S system and the affect of pressure and temperature on the composition of arsenopyrite (Clark, 1960; Kretschmar and Scott, 1976).

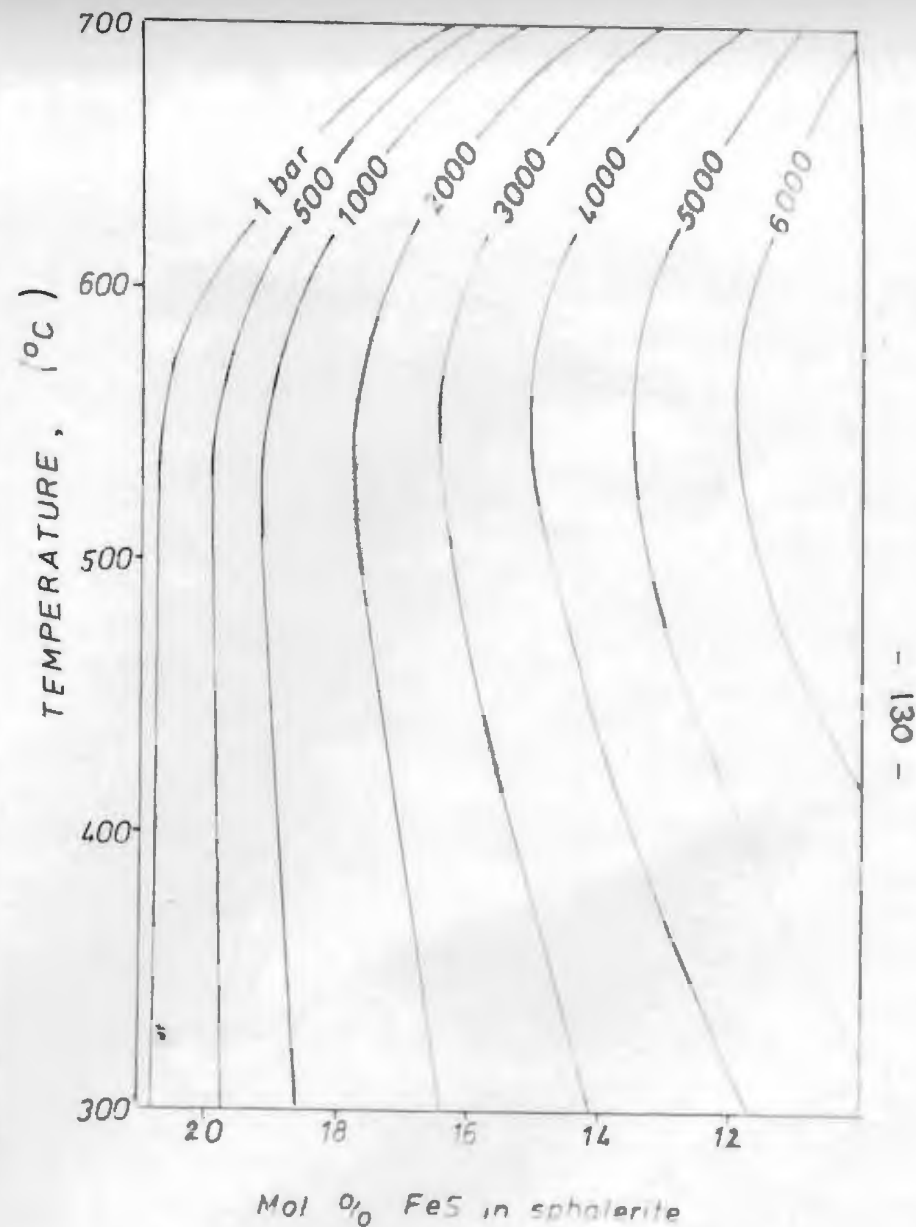


Fig. 5.10: Mol. % FeS in sphalerite vs temperature; isobaric curves for the system (Barton and Toulmin, 1966).

- (c) gold does not appear to occur in isolated, concentrated areas but is dispersed through other minerals, notably arsenopyrite and sphalerite;
- (d) the different vein types may be discriminated geochemically;
- (e) the different metals behaved differently during transport and deposition of the veins;
- (f) precious metals correlate most strongly with the chalcophile base metals and each other, and negatively with the lithophile elements;
- (g) temperature, pressure and  $f_{S_2}$  conditions varied during deposition (see also Chapters 6 and 7);
- (h) the enrichment of the precious metals is confined to very narrow zones across the mineralized veins;
- (i) there is slight enrichment of Au, Ag, As and Zn in many "background" samples, notably the fine grained sediments and tuffs which may be due to primary, volcanogenic enrichment or related to the ore vein-forming fluids.



## CHAPTER 6

### FLUID INCLUSIONS

#### 6.1 Introduction

During crystal growth from a fluid medium, small pockets of the fluid may be trapped in the crystal, resulting from growth irregularities or lattice defects (Roedder, 1976). The fluid inclusions may provide valuable information on the temperature, pressure, composition and density of fluids associated with geological processes such as ore deposition, assuming that the trapped fluids are representative of the depositional fluid and no significant changes take place subsequently (Roedder, 1976). Crystal-fluid interface inhomogeneities are considered negligible so that the first assumption may hold. Post-trapping modifications are commonly observed in well-cleaved minerals such as baryte and fluorite (Roedder, 1972) whereas most inclusions in quartz do not leak under natural conditions (Roedder, 1965). Inclusions which exhibit post-trapping changes (eg. necking-down, when large inclusions pinch-off and segregate into trails of smaller inclusions of inhomogeneous composition) should be excluded from study.

Primary (P), pseudosecondary (PS) and secondary (S) inclusions have been recognized by the criteria given by Roedder (1976). Most inclusions from Moreton's Harbour vein samples are between 5 and 40  $\mu\text{m}$  in size and exhibit wide variation in morphology from regular (ovoid, multifaceted-negative crystal shapes, spherical, tubular) to highly irregular (stellate, amoeboid). Composition may be variable proportions

TABLE 6.1  
Terms and Abbreviations Relevant to Fluid  
Inclusions Microthermometric Data

| <u>Term</u>                    | <u>Abbreviation</u> | <u>Definition</u>                                                                                                                                                                                                                |
|--------------------------------|---------------------|----------------------------------------------------------------------------------------------------------------------------------------------------------------------------------------------------------------------------------|
| Homogenization temperature     | Th                  | Temperature at which two phases become one (disregarding the behaviour of the daughter minerals) either to the vapour phase (Th V) or to the liquid phase (Th L) or showing critical phenomena (Th CP).                          |
| CO <sub>2</sub> homogenization | Th CO <sub>2</sub>  | Temperature at which liquid and vapour CO <sub>2</sub> homogenise (ie. ThCO <sub>2</sub> - L, ThCO <sub>2</sub> - V, ThCO <sub>2</sub> - CP).                                                                                    |
| Trapping temperature           | Tt                  | Th corrected for pressure and salinity.                                                                                                                                                                                          |
| Decrepitation temperature      | Td                  | Temperature at which the inclusion ruptures and the fluid is lost (ie. decrepitates) before homogenization could take place.                                                                                                     |
| Nucleation temperature         | Tn                  | Temperature at which a phase first freezes on cooling; considerable supercooling is usually first required (depending on factors such as availability of nuclei, cooling rate, inclusion size, etc.).                            |
| Melting temperature            | Tm                  | Temperature at which specific solid phases melt and is equivalent to the dissolution temperature. The Tm values are recorded at the disappearance of the last crystal (e.g. Tm <sub>ice</sub> , Tm <sub>clathrate</sub> , etc.). |
| Immiscibility                  |                     | (Roedder and Coombs, 1967)<br>Immiscibility refers to the existence of two or more non-crystalline polycomponent solutions (in this case two fluids) differing in physical properties and generally composition.                 |
| Degree of Filling              | F                   | <u>Volume of liquid in the inclusion</u><br><u>Total volume of the inclusion</u>                                                                                                                                                 |
| Density                        | d                   | Refers to the density of any phase, according to the subscript (e.g. d <sub>CO<sub>2</sub></sub> , d <sub>H<sub>2</sub>O</sub> , d <sub>NaCl</sub> , etc.)                                                                       |

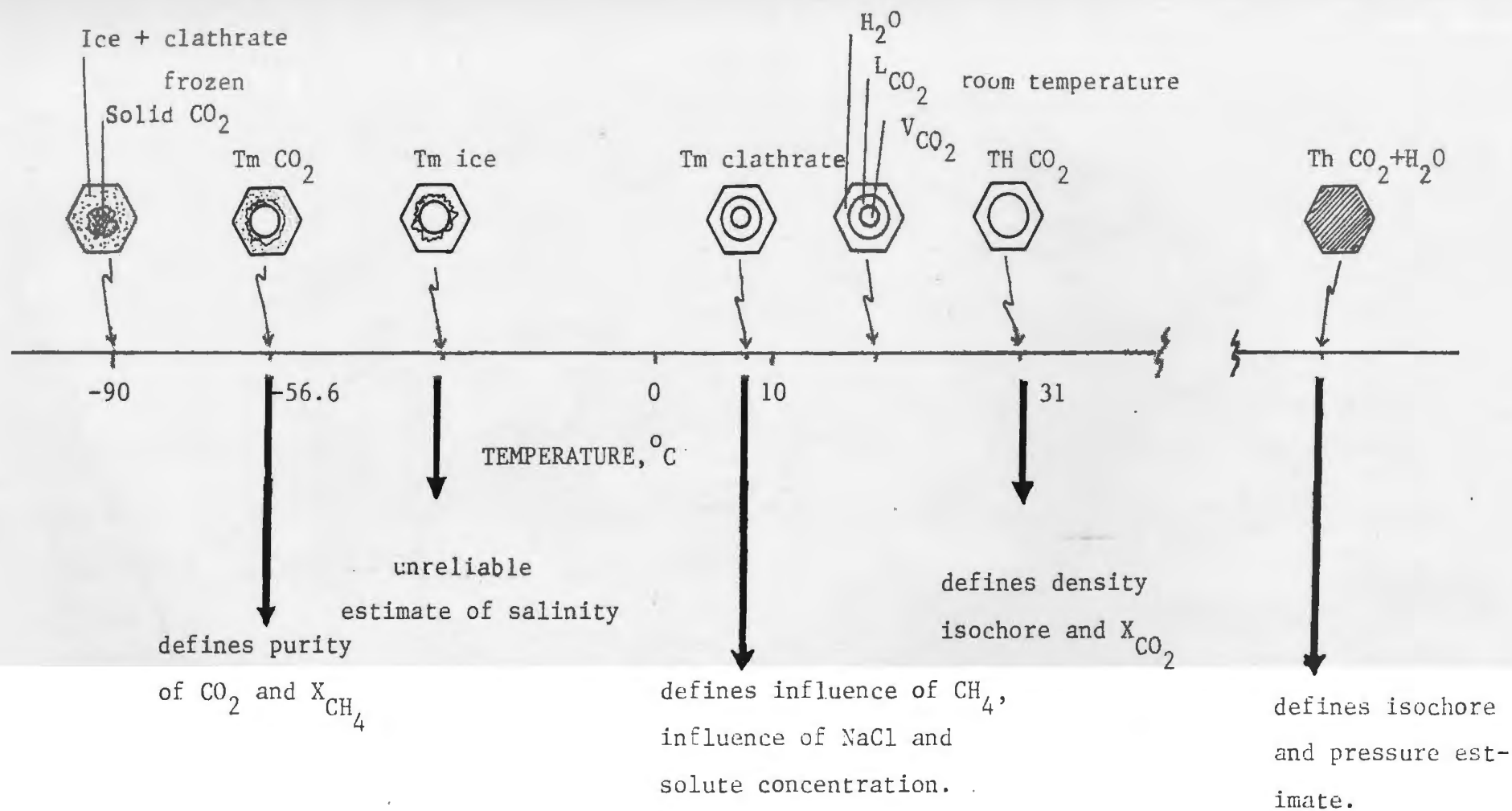


Figure 6.1: Summary of microthermometric data that can be obtained from a single CO<sub>2</sub>-H<sub>2</sub>O bearing inclusion (from Higgins, 1980).

of gas, liquid or solid, with predominant components being  $\text{H}_2\text{O}$ ,  $\text{CO}_2$ ,  $\text{Na}^+$  and  $\text{Cl}^-$  (Roedder, 1972) with minor  $\text{K}^+$ ,  $\text{Mg}^{2+}$ ,  $\text{Ca}^{2+}$ , and  $\text{CH}_4$  in some environments (e.g. Touret, 1977; Konnerup-Madsen, 1981).

The microthermometric terms used in the following account with their abbreviations and definitions are summarized in Table 6.1. The information that may be obtained from observation of the microthermometric phenomena in a  $\text{CO}_2$ - $\text{H}_2\text{O}$  mix (i.e. fluid salinity, density, pressure and temperature) is summarized in Figure 6.1.

Salinity of the inclusion fluids is conventionally expressed in equivalent wt. % NaCl, which is determined using the colligative property of freezing point depression ( $T_{m_{\text{ice}}}$ ), although presence of dissolved species other than NaCl, such as  $\text{CO}_2$  may lower the freezing point. The fluid density ( $d$ ) is partly dependent on its salinity and is determined from the degree of filling of the inclusion cavity ( $F$  = volume of liquid/total inclusion volume), and homogenization data. The temperature and pressure prevailing at the time of trapping of the fluid may be estimated from homogenization temperatures and compositional determinations, as discussed below.

In this study 50 doubly polished plates (Appendix 2.2) of vein and rhyolite samples were examined and where suitable inclusions were identified, data were obtained using the Chaixmeca heating/freezing stage and procedures as outlined in Appendix 2.1. In the following account these data were interpreted using experimentally determined equilibria of the  $\text{CO}_2$ - $\text{H}_2\text{O}$  and  $\text{NaCl}$ - $\text{H}_2\text{O}$  systems (from Cunningham, 1976; Haas, 1971; Hollister & Burruss, 1976; Kennedy & Holser, 1966; Rankin, 1978; Takenouchi & Kennedy, 1965; Todheide & Franck, 1963; Weisbrod & Poty, 1975; Ympa, 1963).



More detailed discussion of the execution and application of fluid inclusion microthermometry is given by Roedder (1976) and Higgins (1979; 1980).

## 6.2 Compositional types of inclusions in Moreton's Harbour veins

Inclusions observed in vein samples from Moreton's Harbour are of a fairly narrow compositional range compared with the contrasting environment of hydrothermal Sn-W veins (e.g. Higgins, 1980) or veins associated with porphyry copper (eg. Bodnar and Beane, 1980).

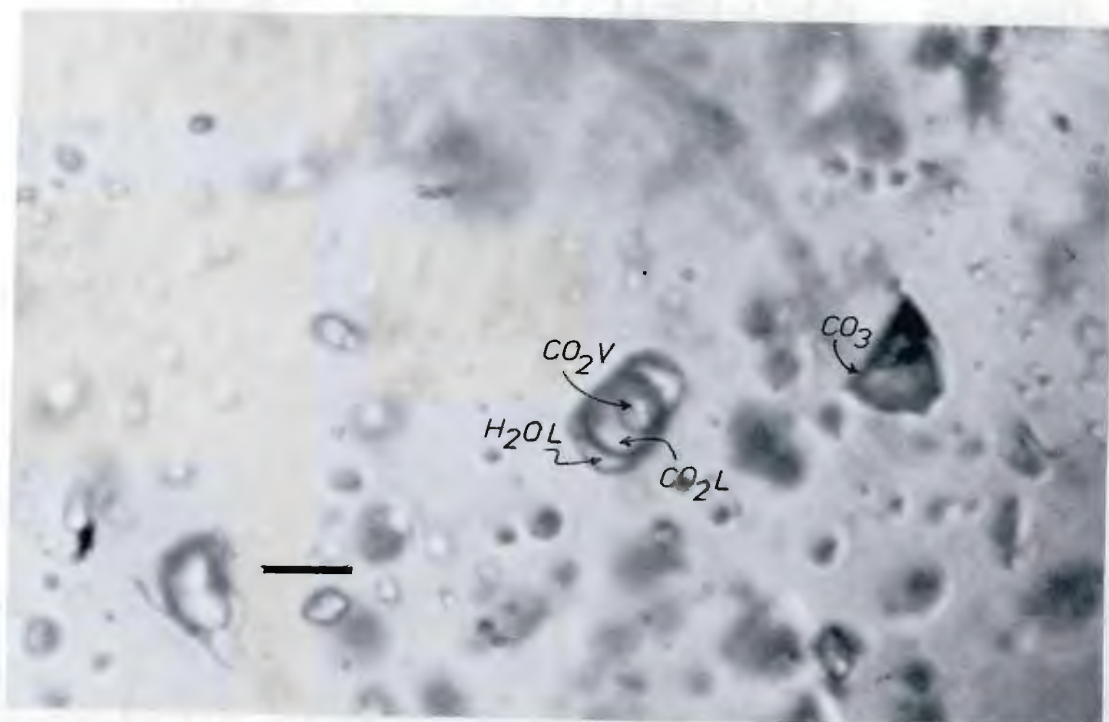
Complex three-phase inclusions consisting of liquid  $\text{CO}_2$ ,  $\text{CO}_2$  gas and an aqueous solution are predominant in the P and PS inclusions of veins of type I, and are observed in types II and III (Plates 6.1a,b,c). Simple two-phase liquid + vapour aqueous but variably  $\text{CO}_2$ -rich inclusions are also abundant as P, PS and S inclusions. Daughter minerals in the inclusions are rare although there are some solid phases observed. Microthermometric measurements were made wherever possible, although many inclusions were too small, especially for  $T_{m_{\text{ice}}}$  or  $T_{m_{\text{clathrate}}}$  determinations.

## 6.3 Inclusions in gangue quartz

### 6.3.1 Vein Type I

The P and P-S inclusions observed in gangue quartz of arsenopyrite-gold rich veins are mostly between 5 and 25  $\mu\text{m}$  in size, with abundant S- inclusions ( $\leq 10 \mu\text{m}$ ) dispersed through, imparting the white cloudiness of the quartz. Morphology is quite variable as represented in Table 6.2, together with the compositional data for the vein type I inclusions.

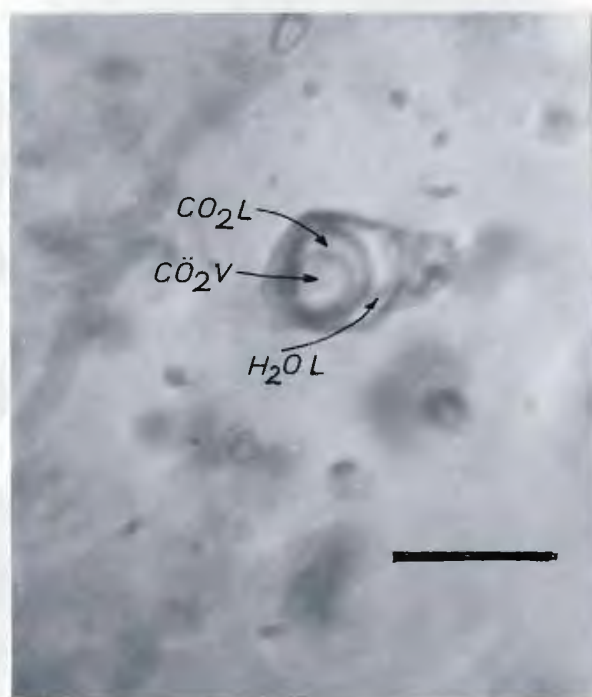
The predominant P- inclusions are complex 3-phase  $\text{CO}_2$  liquid +  $\text{CO}_2$  gas + aqueous liquid (Plates 6.1a,b,c). Daughter



(a)



(b)














(c)

PLATE 6.1: P and PS inclusions containing liquid  $CO_2$ ,  $CO_2$  gas and an aqueous solution (L) from gangue quartz of vein type I. Scale bar = 10  $\mu m$ . Note the solid (carbonate) and secondary (fluid) inclusions crowded around a. and the leakage "beak" of the large inclusion b. (a. SM-52a; b. MHH-1; c. SM-5).

TABLE 6.2

Morphology and Composition for Selected  
Examples of P-/PS-CO<sub>2</sub> Bearing Inclusions of Vein Type I

| Sample  | Inclusion Shape                                                                     | d<br>(g cm <sup>-3</sup> ) | V <sub>1</sub><br>Vol. CO <sub>2</sub> | V <sub>2</sub><br>Vol. H <sub>2</sub> O | X <sub>CO2</sub> * | X <sub>H2O</sub> | X <sub>NaCl</sub> | Th °C |
|---------|-------------------------------------------------------------------------------------|----------------------------|----------------------------------------|-----------------------------------------|--------------------|------------------|-------------------|-------|
| SM-3    |    | 0.64                       | 0.25                                   | 0.75                                    | 9.3                | 88.7             | 2.0               | 280.9 |
| SM-12a  |    | 0.65                       | 0.18                                   | 0.82                                    | 8.4                | 89.8             | 2.4               | 200D* |
| SM-50a  |    | 0.70                       | 0.49                                   | 0.51                                    | 20.0               | 77.5             | 2.5               | 225D* |
| SM-50b  |    | 0.63                       | 0.23                                   | 0.77                                    | 10.0               | 85.4             | 4.6               | 298.9 |
| SM-52a  |   | 0.62                       | 0.18                                   | 0.82                                    | 7.2                | 91.0             | 1.8               | 286.6 |
| SM-52b  |  | 0.65                       | 0.31                                   | 0.69                                    | 11.2               | 87.3             | 1.5               | 274*D |
| SM-56   |  | 0.65                       | 0.27                                   | 0.73                                    | 12.4               | 85               | 2.6               | 251.9 |
| MH-1    |  | 0.68                       | 0.22                                   | 0.78                                    | 8.8                | 89.4             | 1.8               | 322   |
| MHH-1   |  | 0.62                       | 0.29                                   | 0.71                                    | 11.0               | 87.2             | 1.8               | 172*D |
| MHH-22a |  | 0.69                       | 0.38                                   | 0.72                                    | 14.2               | 83.4             | 2.4               | 298.9 |
| MHH-22b |  | 0.65                       | 0.29                                   | 0.31                                    | 11                 | 84.0             | 5.0               | 277.8 |

\*Mol. %

D\*decrepitation temperature

minerals are not observed, indicating salinity of the aqueous solution below 23.6 equivalent wt. % NaCl. Simpler 2-phase aqueous inclusions occur occasionally in the type I veins as P-PS inclusions (Plate 6.2), presumably coexisting with the 3-phase inclusions. The proportions of various phases are variable with F- values of 0.7 for CO<sub>2</sub> gas + liquid + H<sub>2</sub>O inclusions and 0.85 for H<sub>2</sub>O gas + liquid inclusions. The CO<sub>2</sub> gas + liquid bubble occupies approximately 30% by volume of the total cavity, and between 30 to 50% volume of the bubble is occupied by CO<sub>2</sub> gas. All S- inclusions are 2-phase and aqueous with variable F- ratios (Table 6.3). Solid inclusions of sulphide and carbonate are observed, some of which may have precipitated directly from the fluid while others may have been incorporated from pre-existing solid phases caught up in the fluid flow. The solid inclusions are predominantly calcite, siderite, sphalerite and arsenopyrite. These are especially abundant near the quartz-arsenopyrite grain boundaries, where typical fluid (gas + liquid) inclusions tend to be far smaller, so difficult to study.

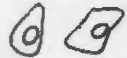


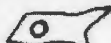



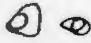
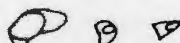
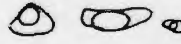

#### 6.3.2 Vein Type II


Inclusions in the buff to clear quartz surrounding the stibnite masses and fibres of veins type II (eg. Plate 4.6) are larger than those of vein type I, ranging up to ~50µm, and are highly variable in morphology. The larger inclusions are randomly distributed and central in the quartz grains with common stellate, amoeboid, irregular outline (eg. Plate 6.3). Smaller inclusions of P-, PS- and S- affinities tend toward greater regularity in shape (Plate 6.4). Trains of inclusions impart a "growth banding" in some of the quartz intergrowths. Inclusions within minor quartz veins



TABLE 6.3

Morphology and Thermometric Data for  
Selected S- Inclusions of all Vein Types

| Vein Type | Sample | Inclusion Shape and Size                                                            | F (average or range) | Th (average or range) <sup>°C</sup> | T <sub>mice</sub> (average or range) <sup>°C</sup> |
|-----------|--------|-------------------------------------------------------------------------------------|----------------------|-------------------------------------|----------------------------------------------------|
| I         | MH.1   |    | 0.86                 | 120-196                             | -                                                  |
|           | MHH.1  |    | 0.82 to 0.90         | 112-141                             | -12                                                |
|           | MHH.22 |    | 0.75 to 0.86         | 159-176                             | -5 - -14                                           |
|           | SM.3   |    | 0.10 to 0.75         | 130                                 | -                                                  |
|           | SM.50  |   | 0.79                 | 89-281                              | -5 - -10                                           |
| II        | SB.1   |  | 0.85                 | 190                                 | -                                                  |
|           | SB.25a |  | 0.83                 | 186                                 | -                                                  |
|           | SB.25b |  | 0.60-0.85            | 45 to 100                           | -5                                                 |
| III       | TR.1   |  | 0.35-0.62            | 112                                 | -                                                  |
|           | TR.12  |  | 0.75 to 0.8          | 172                                 | -                                                  |
|           | TR.40  |  | 0.75 to 0.92         | 150                                 | -9.8                                               |

  
~10  $\mu$ m

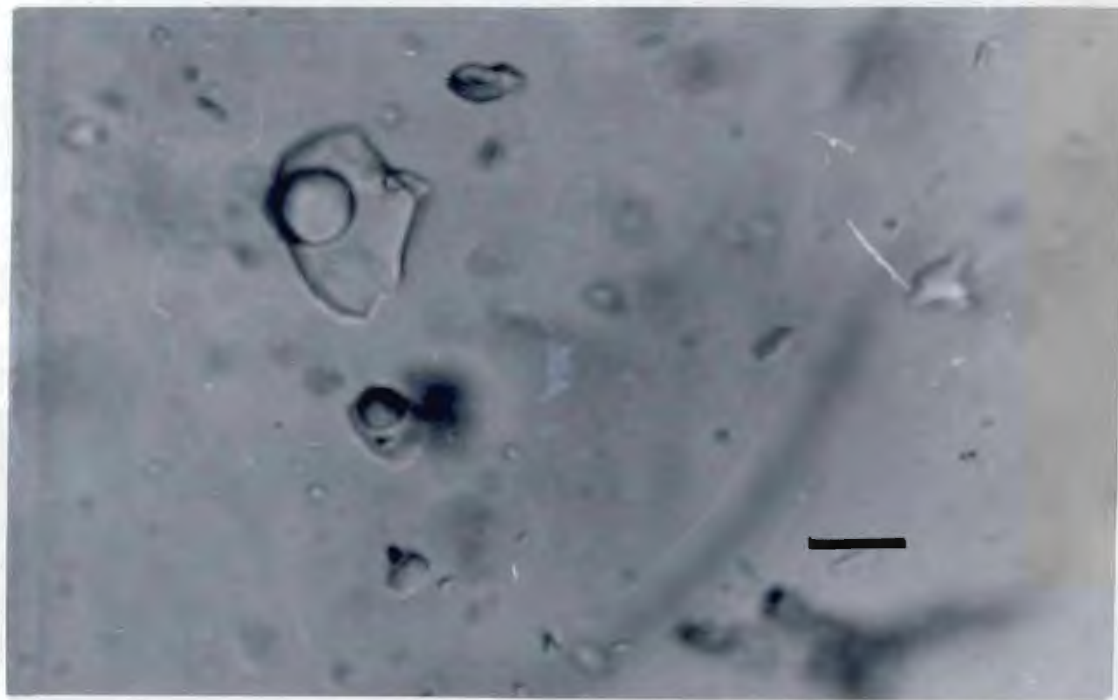


PLATE 6.2: Aqueous vapour + liquid P-inclusion from gangue quartz vein type 1 (SM.2). Scale bar  $10\mu\text{m}$ .

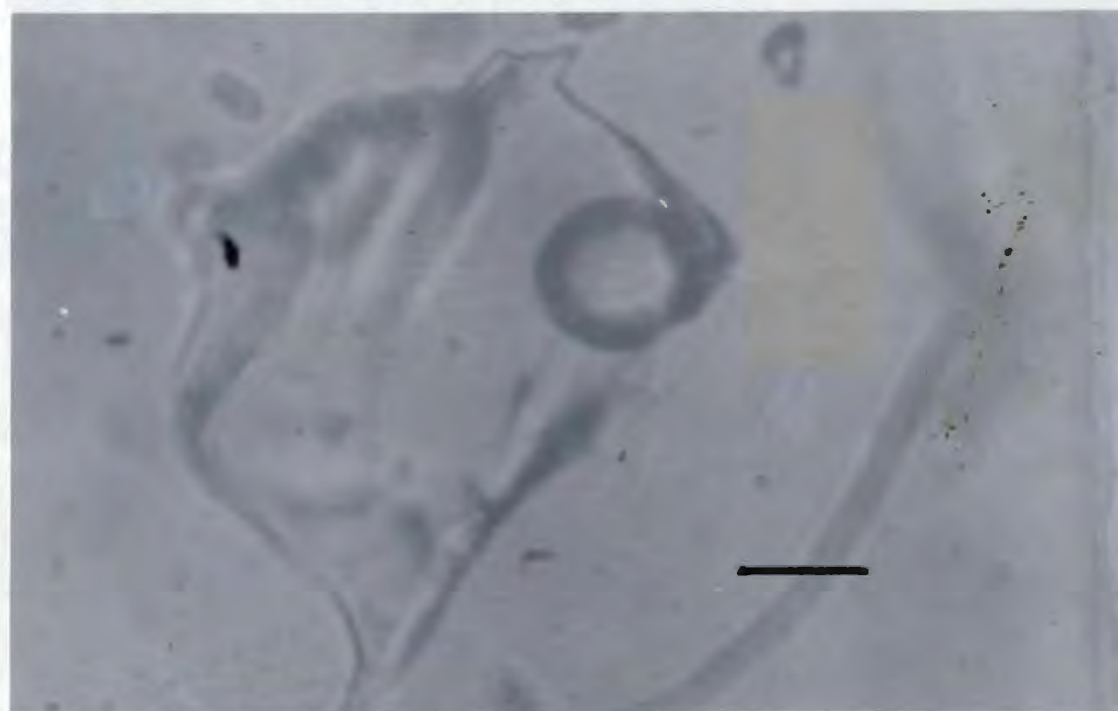


PLATE 6.3: Large amoeboid aqueous vapour + liquid P-inclusion from gangue quartz, vein type II (SB.25). Scale bar  $10\mu\text{m}$ .

adjacent to the major veins at Stuckless' Mine have been leaked, and no p-/PS- inclusions suitable for study were observed.

P- and PS- inclusions are mostly simple two phase aqueous inclusions but occasionally a ring of liquid  $\text{CO}_2$  around the gas bubble is evident. F- values for the  $\text{CO}_2$ - inclusions of veins type II average 0.78 with 40 to 60% volume of the bubble occupied by  $\text{CO}_2$  gas. The aqueous inclusions have F- values between 0.80 to 0.85 (Table 6.4).

Daughter minerals are observed in a few of the inclusions:

(a) a single opaque, acicular crystal, possibly a Sb-S species and/or

(b) fibrous clusters of dawsonite ( $\text{NaAl CO}_3 (\text{OH})_2$ ).

The latter is associated with  $\text{CO}_2$ -rich inclusions.

### 6.3.3 Vein Type III










Very few, large unaltered P-/PS- inclusions were identified from any sections made from type III vein samples due to leakage along microfractures within the quartz.  $\text{CO}_2$ -rich (P) inclusions were seen, but small, 2-phase aqueous inclusions were more common. Very little micro-thermometry was possible.

### 6.4 The significance of solid mineral inclusions

The occurrence of daughter minerals in fluid inclusions indicates saturation of the fluid with respect to that phase at room temperature. The identification of the daughter minerals provides valuable information on the composition of the fluid, although it is difficult to discern

TABLE 6.4

Compositional Data of Selected Fluid Inclusions  
from Quartz of Vein Type II

| Sample<br>Number | Inclusion<br>Shape                                                                  | F<br>(=d) | Vol. % H <sub>2</sub> O<br>Vapour | Liquid | CO <sub>2</sub><br>(mol. %) | Salinity<br>(from T <sub>mice</sub><br>wt. % NaCl) | Th<br>(°C)    |
|------------------|-------------------------------------------------------------------------------------|-----------|-----------------------------------|--------|-----------------------------|----------------------------------------------------|---------------|
| SB.1             |    | 0.93      | 7.0                               | 93.0   | -                           | 8.5                                                | 188.6         |
|                  |    | 0.94      | 6.5                               | 93.5   | -                           | 8.8                                                | 192.6         |
|                  |    | 0.83      | 16.6                              | 83.4   | -                           | 5.5                                                | 218.2         |
|                  |   | 0.77      | 23.4                              | 76.6   | 0.3                         | 4.5                                                | 190.0         |
| SB.25            |  | 0.87      | 13.7                              | 87.3   | 0.5                         | 10.0                                               | 160.0<br>(Td) |
|                  |  | 0.94      | 7.3                               | 93.6   | -                           | 9.2                                                | 174.9         |
|                  |  | 0.73      | 22.1<br>(+CO <sub>2</sub> )       | 78.8   | 0.8                         | 7.0                                                | 159.0         |
|                  |  | 0.76      | 23.7                              | 76.3   | -                           | 5.0                                                | 230.3         |
|                  |  | 0.82      | 18.2                              | 81.8   | -                           | 8.1                                                | 168.0         |



whether the crystals nucleated from cooling of the solution in the inclusion or if they were particles caught up accidentally. The latter is considered the case for the opaque Sb-S needles due to their rarity and the generally low salinities determined (Section 6.5). The occurrence of dawsonite together with the abundance of  $\text{CO}_2$ -rich inclusions and gangue carbonate minerals (siderite-calcite) substantiate the inference that the fluid was  $\text{CO}_2$ -rich. Neither daughter mineral was observed to dissolve on heating to homogenization temperature ( $\sim 400^\circ\text{C}$ ) due to retrograde solubilities of carbonates and sulphides with increasing temperature (Holland, 1967).

Carbonate mineral precipitation depends largely on pH and  $P_{\text{CO}_2}$ . Calcite cannot be precipitated from a cooling hydrothermal brine in most situations but may form on the release of  $\text{CO}_2$  from the system (Holland, 1967), possibly as a result of retrograde boiling off of the  $\text{CO}_2$ -rich phase. This is further inferred by the carbonate solid inclusions adjacent to the arsenopyrite masses, the occurrence of calcite and siderite in veinlets and along the vein margins, the absence of most other fluid inclusions in these areas and the ubiquitous brecciation of the arsenopyrite (Plate 4.5). Furthermore, the unmixing of an initially homogeneous fluid to  $\text{H}_2\text{O}$ - and  $\text{CO}_2$ -rich phases due to boiling immiscibility is apparent from the coexistence of P-/PS-  $\text{H}_2\text{O}$  rich and P-/PS-, 3 phase inclusions.

## 6.5 Microthermometric measurements

### 6.5.1 Salinity

Salinity was determined from  $T_{m, \text{ice}}$  determinations for

inclusions with values shown in Table 6.2. Ideally, measurements are accurate to within  $\pm 0.2^{\circ}\text{C}$ , resulting in a salinity error of  $\pm 0.4$  equivalent wt. % NaCl. However, due to the small size of inclusions and abundance of  $\text{CO}_2$ , the  $T_{m_{\text{ice}}}$  are approximately accurate to  $\pm 2.0$  equivalent wt. % NaCl.

The predominance of  $\text{CO}_2$  in the inclusions and absence of halite indicate that NaCl is not a major constituent of the fluid due to the "salting out effect" (Ellis, 1959). The absence of solid components in most inclusions indicates that the salinity of the fluid is lower than saturation, i.e. 23.6 equivalent wt. % NaCl (Fig. 6.2). Salinity determinations from  $T_{m_{\text{ice}}}$  are presented in Fig. 6.3. Salinity of the fluid is between 2 and 6 equivalent wt. % NaCl with a mean value of 3 wt. %. In freezing runs all inclusions exhibited metastable phenomena (Roedder, 1976) as  $T_{m_{\text{ice}}}$  values were between  $-40$  and  $-50^{\circ}\text{C}$ , indicating considerable super-cooling. This metastability, according to Kerrich et al. (1978) indicates relatively slow rate of flow of the fluid in the vein system, although it is affected also by the cooling rate, density, salinity and availability of nuclei.

In  $\text{CO}_2$ -rich inclusions ( $\pm \text{CO}_2$ -liquid) the clathrate hydrate ( $\text{CO}_2 \cdot 5.75 \text{H}_2\text{O}$ ) forms at low temperatures ( $T_{m_{\text{clathrate}}} \sim -30^{\circ}\text{C}$ ). The formation of clathrate is a sensitive test for the presence of  $\text{CO}_2$  in the inclusion. The clathrate has a great affect on the residual fluid in the inclusion (Collins, 1979) as all components other than  $\text{CO}_2 + \text{H}_2\text{O}$  are excluded from the clathrate structure. Salinities may be increased by up to 50%. The presence of the radial 'feathers' of clathrate nucleate around the vapour bubble and persist metastably up to  $+10^{\circ}\text{C}$ . The presence of clathrate obscures  $T_{m_{\text{ice}}}$  observations. These factors explain the

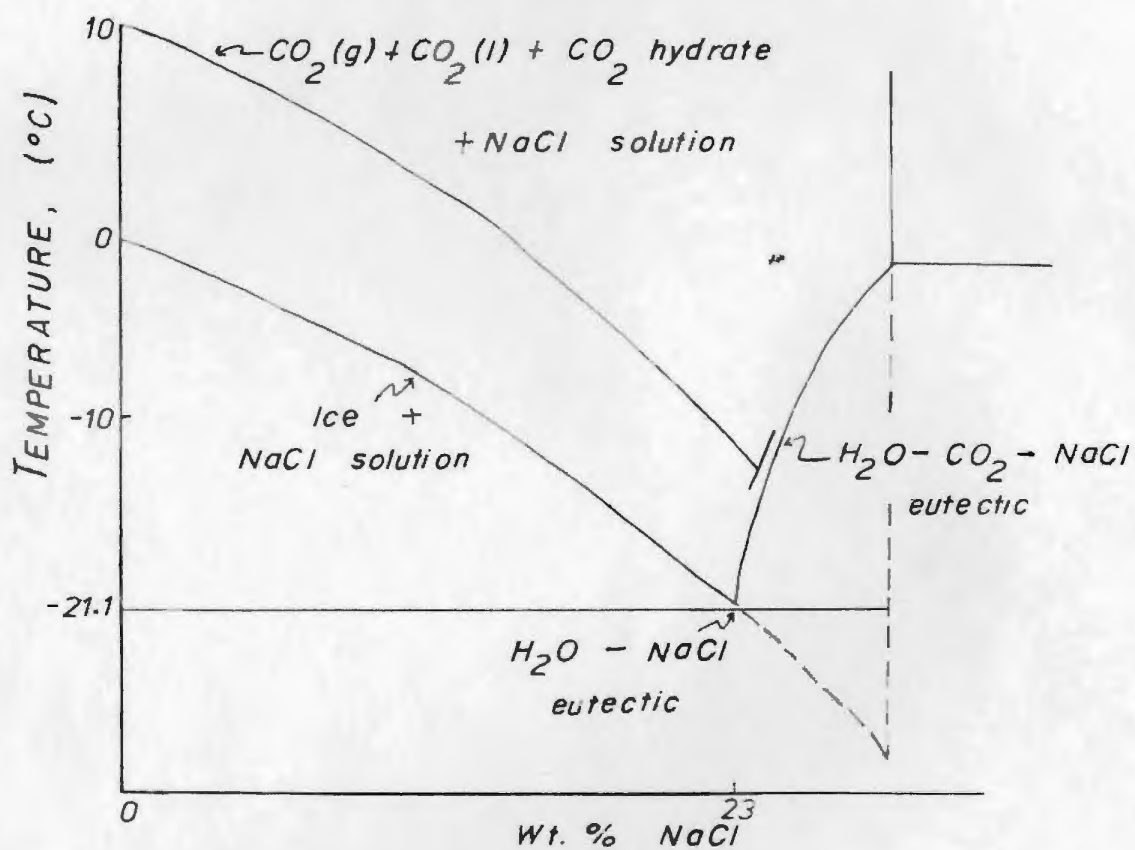


Figure 6.2: A temperature-composition phase diagram for the NaCl- $\text{H}_2\text{O}$ - $\text{CO}_2$  system (from Collins, 1979).

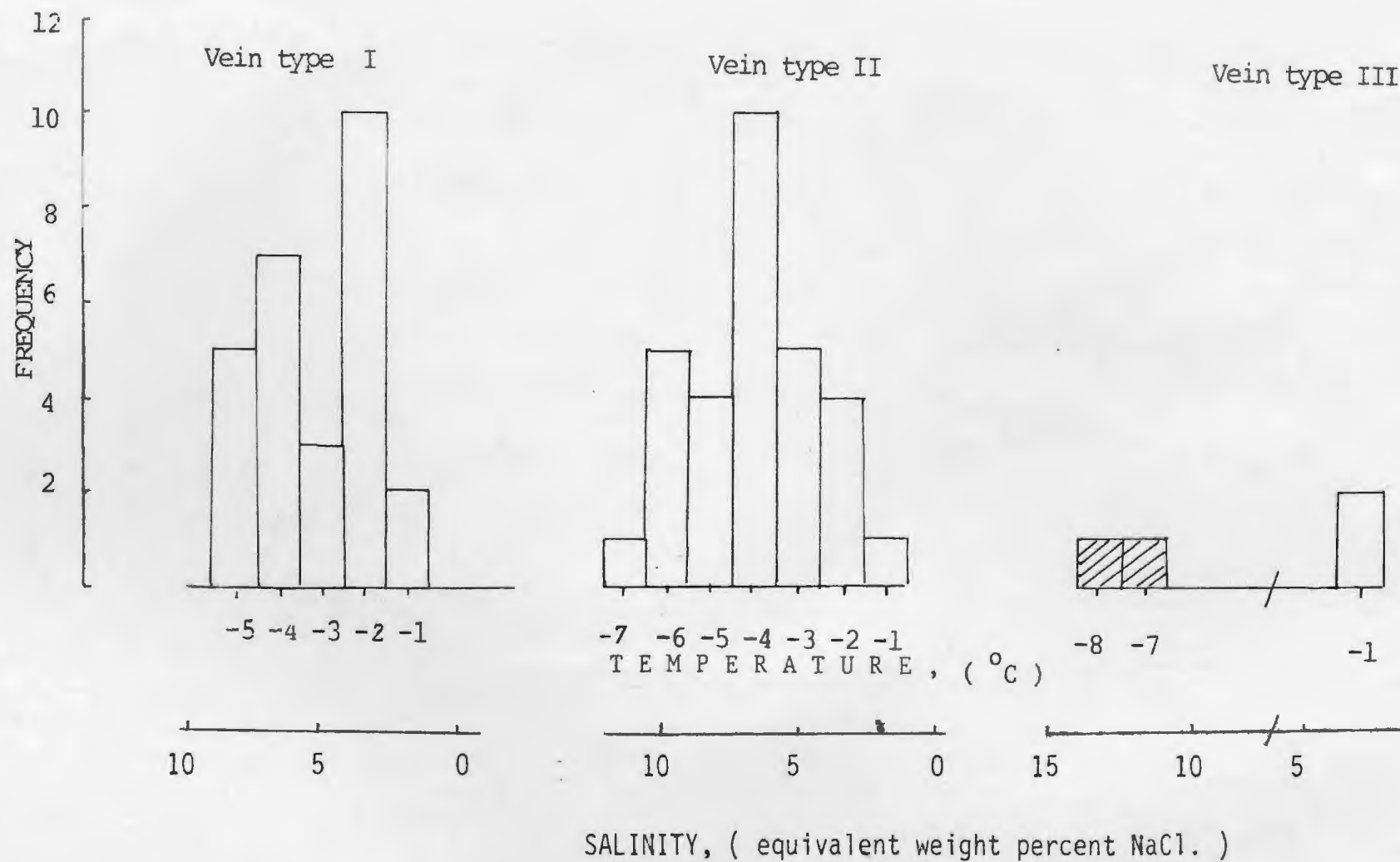


Figure 6.3:  $T_{m_{ice}}$  measurements for P- and PS- inclusions in quartz.



errors on measurement of salinities of inclusions imposed by their high  $\text{CO}_2$  content.

The average  $T_{m_{\text{clathrate}}}$  is  $+8.0^\circ\text{C}$  which is a depression of  $2^\circ\text{C}$  from the pure  $\text{CO}_2\text{-H}_2\text{O}$  system (Fig. 6.8). From this phase diagram (after Hollister & Burruss, 1976) it is evident that with the average  $T_{m_{\text{ice}}}$  of  $-4^\circ\text{C}$  and  $T_{m_{\text{clathrate}}}$  of  $+8^\circ\text{C}$ , the salinity of the fluid of inclusions from veins of Types I and II is between 2.0 and 8.8 equivalent wt. % NaCl.  $T_{m_{\text{ice}}}$  salinity values may be increased by an estimated 25 to 50% by the presence of clathrate (Collins, 1979).

The different species that may be dissolved in the aqueous fluid affect the freezing point depression (ie.  $T_{m_{\text{ice}}}$ ) differently as shown in Fig. 6.4, after Roedder, (1967). The effect of dissolved  $\text{CO}_2$  is quite considerable: 3 mol %  $\text{CO}_2$  (= 7.6wt. %) may depress  $T_{m_{\text{ice}}}$  by  $-3.2^\circ\text{C}$ . About 2 to 3 mol %  $\text{CO}_2$  is soluble in  $\text{H}_2\text{O}$  at room temperature (eg. Roscasco, et al., 1975).

In summary, the presence of  $\text{CO}_2$  has a profound effect on the  $T_{m_{\text{ice}}}$  and hence salinity determinations of the inclusions from hydrothermal vein samples of Moreton's Harbour. There is a  $\text{CO}_2$  depletion matched by decrease in salinity recorded for different inclusions as shown in Fig. 6.5 (cf. Takenouchi & Kennedy, 1965; Higgins, 1980)

## 6.6 Homogenization temperatures

Measurements of homogenization temperatures were made on the heating stage as described in Appendix 2.1. Data were obtained from inclusions in quartz gangue only. All data above  $200^\circ\text{C}$  have an error of  $\sim 0.5\%$  of

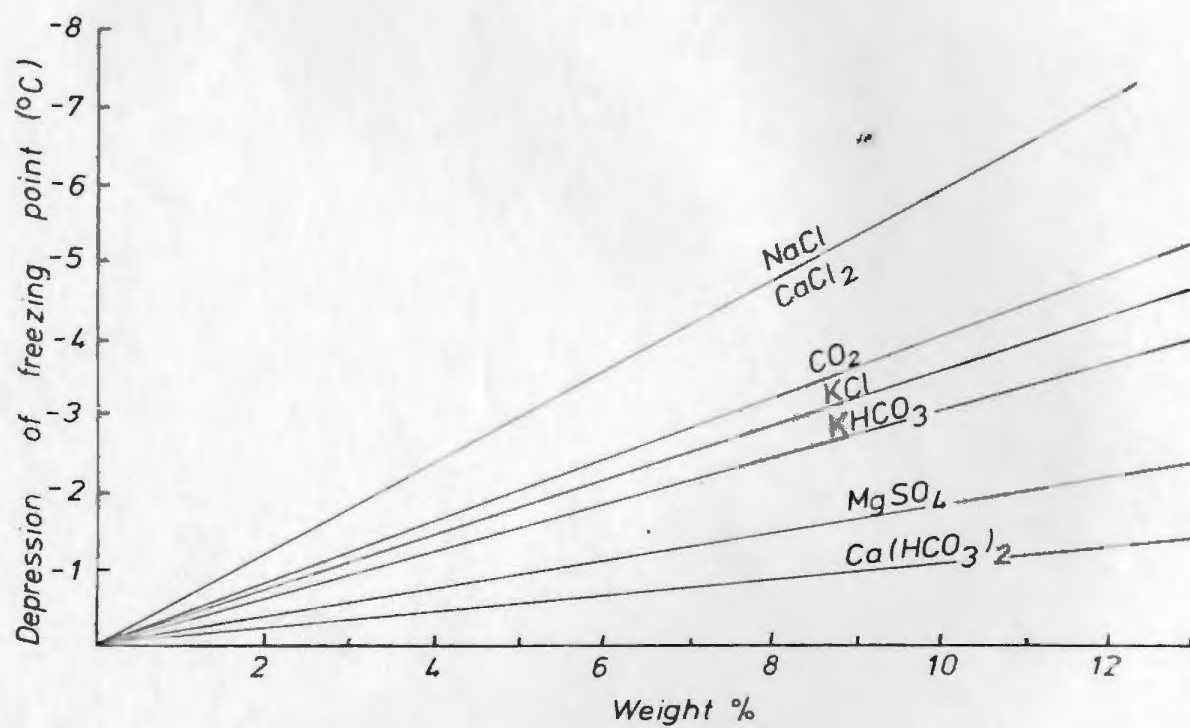


Figure 6.4: Freezing point depressions of water ( $T_{m, \text{ice}}$ ) for different solutes. (From Roedder, 1967).

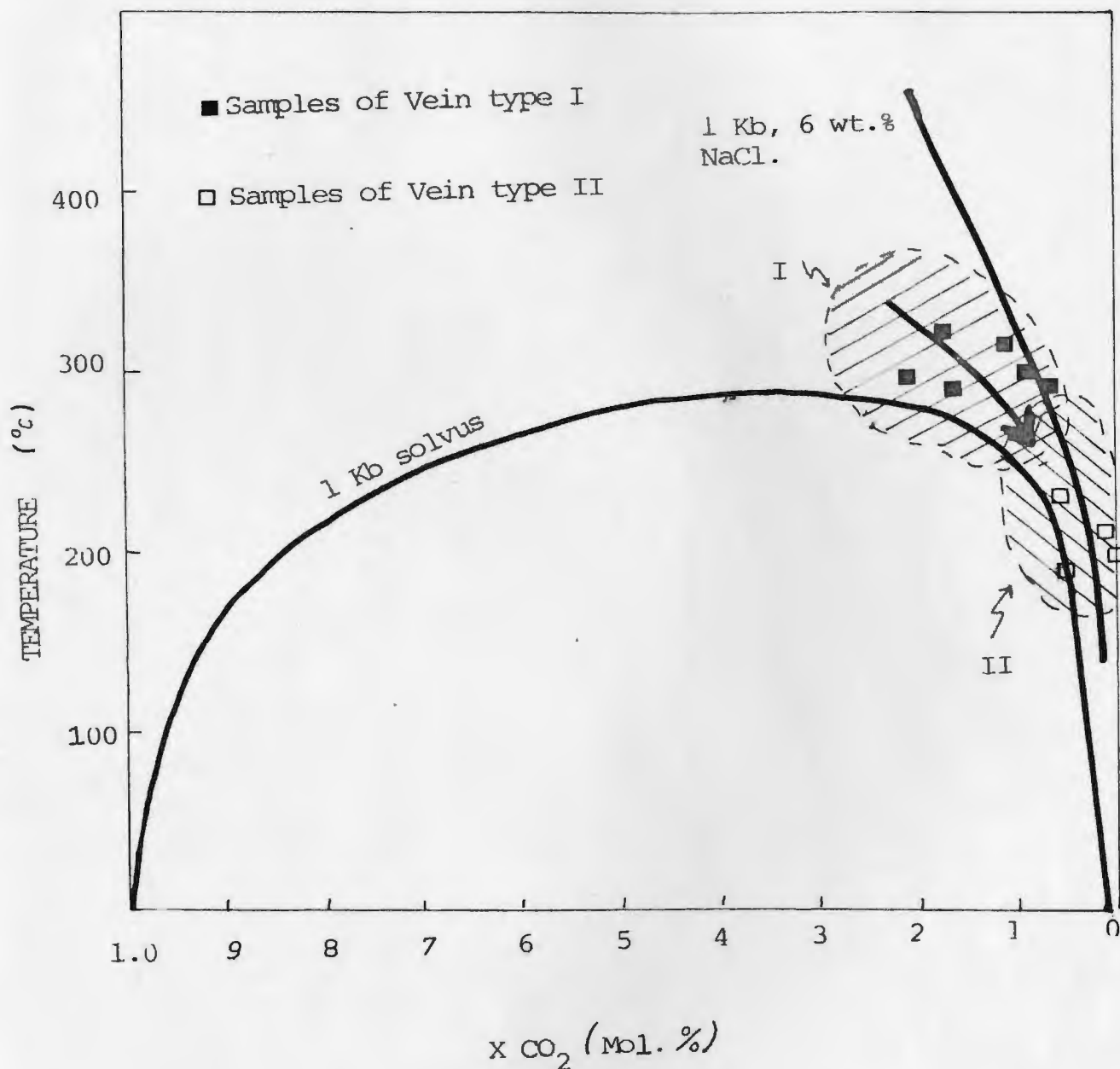


Figure 6.5: The mol. % CO<sub>2</sub> of examples of fluid inclusions from veins of type I and II, plotted against Th values, compared with the 1kb solvus of CO<sub>2</sub> (Todheide & Franck, 1963) and the solvus at 1kb and 6 wt. % NaCl (from Takenouchi & Kennedy, 1965a).

the measurement. Leakage was checked by re-examination of the inclusions after heating, at room temperature. All Th values are presented in Fig. 6.6. Many of the CO<sub>2</sub>-rich inclusions decrepitated before homogenizing, due to high internal pressures. All P-/PS- aqueous inclusions homogenized to the liquid phase and CO<sub>2</sub>-rich inclusions to a liquid aqueous phase (ie. in both cases the bubble decreased in size with increasing temperature until they disappeared).

The distribution of Th and Td values for P-/PS- inclusions for veins of Type I, II and III are presented in the histograms of Fig. 6.6 (a, b and c). 36% of Th values for vein type I inclusions are between 276 and 300°C, with 80% greater than 225°C. The six values obtained from Taylor's Room samples are between 275 and 300°C. Secondary inclusions (Fig. 6.7) gave a wide range of Th values for all vein types from 75° to 300°C.

In summary, the mean Th value ( 275°C) for inclusions of veins type I (ie. arsenopyrite-gold bearing veins) is significantly greater than that (Th=180°C) for veins of type II (ie. stibnite rich-gold poor veins).

#### 6.7 Density and composition of CO<sub>2</sub>-bearing inclusions

Liquid CO<sub>2</sub>-bearing inclusions occur as P-/PS- inclusions in all vein samples of Type I and less commonly in veins of Type II. Regularity of phase ratio (Table 6.2) of inclusions indicates that they developed from an homogeneous CO<sub>2</sub>-H<sub>2</sub>O fluid, although irregularities and coexistence with 2-phase inclusions with similarly constant phase



- 152 -

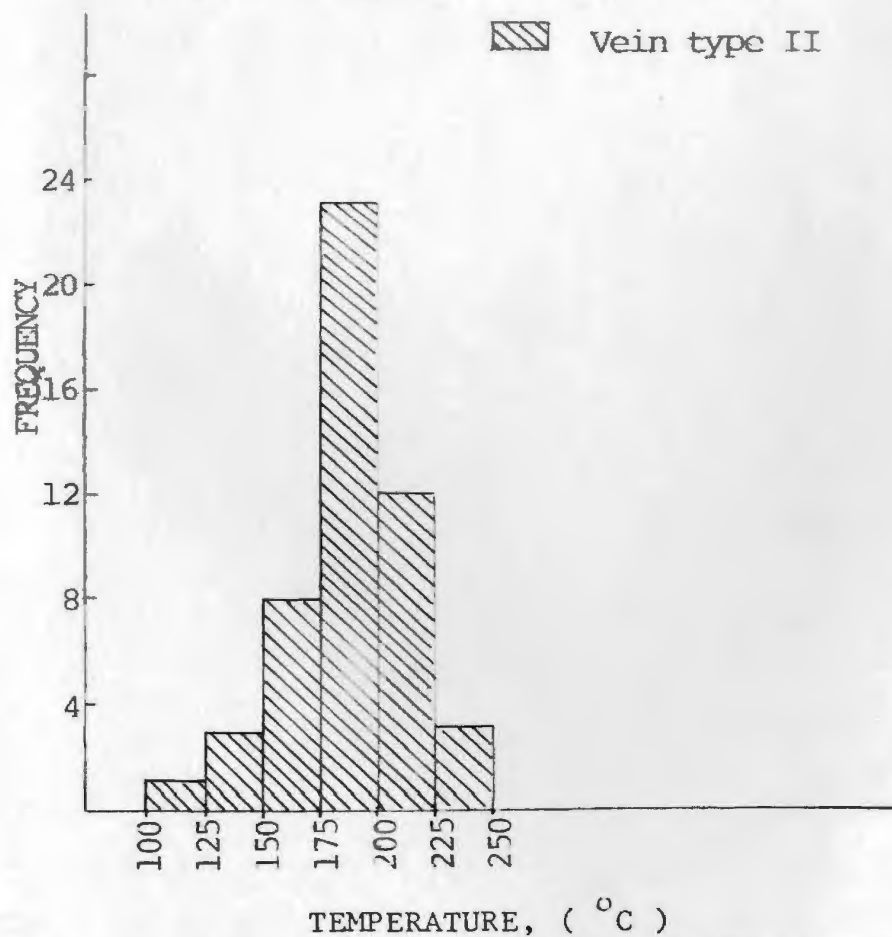
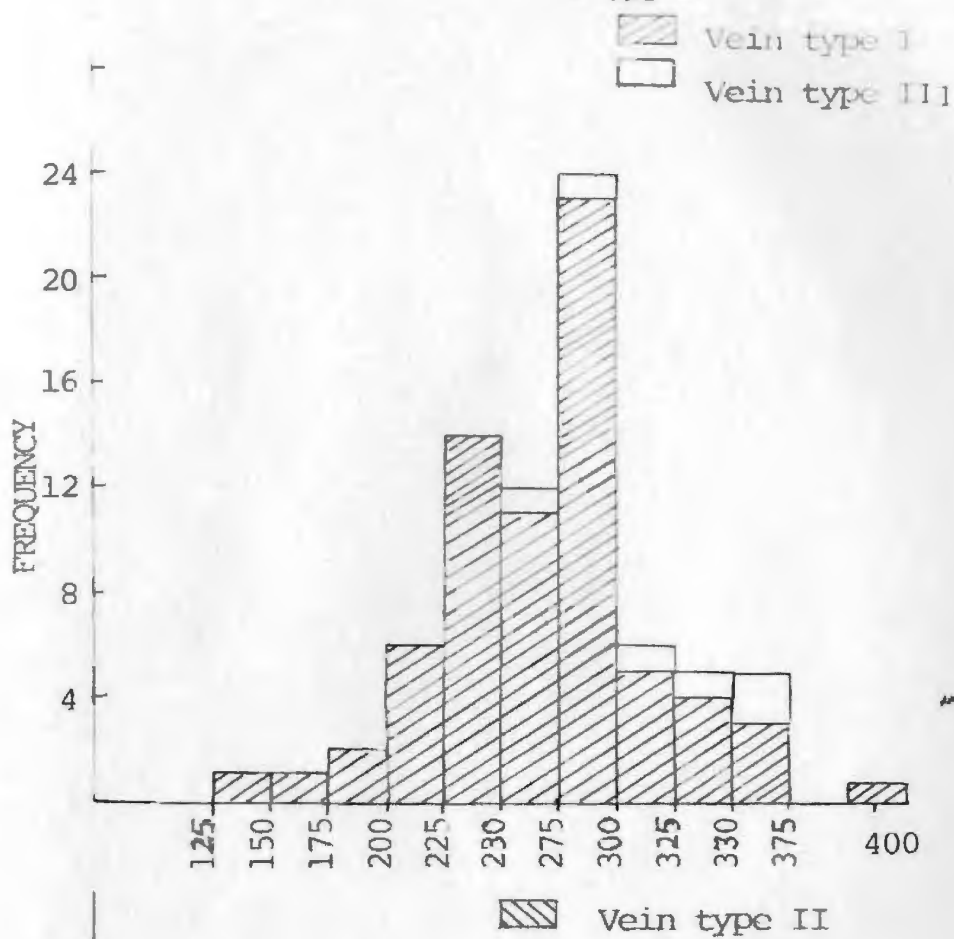


Figure 6.6: Frequency diagrams for Th and Td values for P- and PS- inclusions of all vein types.

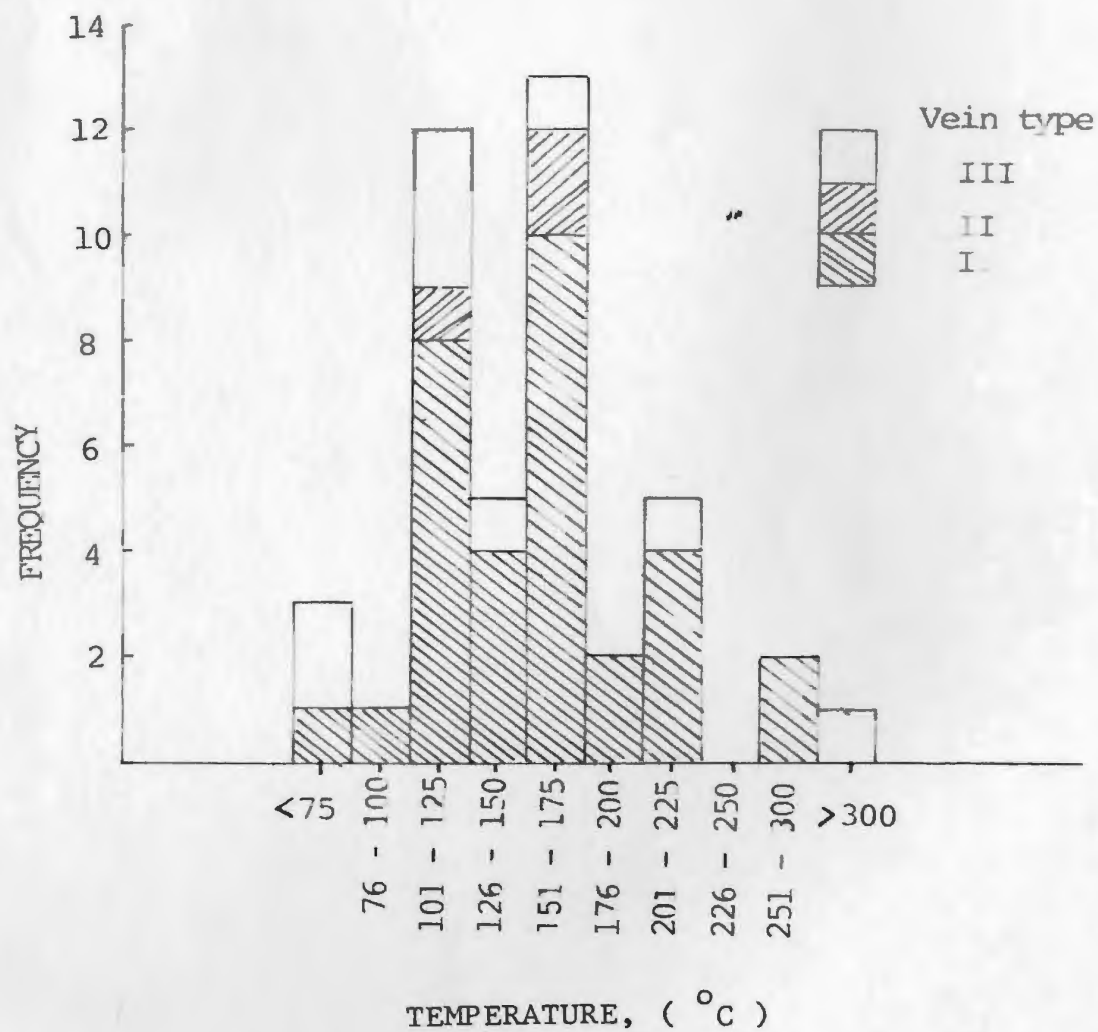


Figure 6.7: Frequency diagram for Th determinations of S- inclusions of all vein types.

ratios and high  $T_h$  values indicate that some unmixing to a  $\text{CO}_2$ -rich and  $\text{H}_2\text{O}$ -rich fluid may have occurred (see Section 6.4).

#### 6.7.1 Purity of $\text{CO}_2$

The purity of  $\text{CO}_2$  can be ascertained from the values  $T_{m\text{CO}_2}$ . Pure  $\text{CO}_2$  freezes at  $-56.6^\circ\text{C}$  and homogenizes to a single phase at  $31.1^\circ\text{C}$  (Fig. 6.8).  $T_{m\text{CO}_2}$  is relatively easy to determine, as the transition  $\text{CO}_2$  solid  $\rightarrow$   $\text{CO}_2$  liquid/gas occurs suddenly, provided that there is no condensation problem. Ice forms on the lens and sample at these low temperatures which obscures observation of  $T_{n\text{CO}_2}$ ,  $T_{m\text{ice}}$ , and  $T_{n\text{clathrate}}$ . Errors in measurements are  $1.5^\circ\text{C}$ .

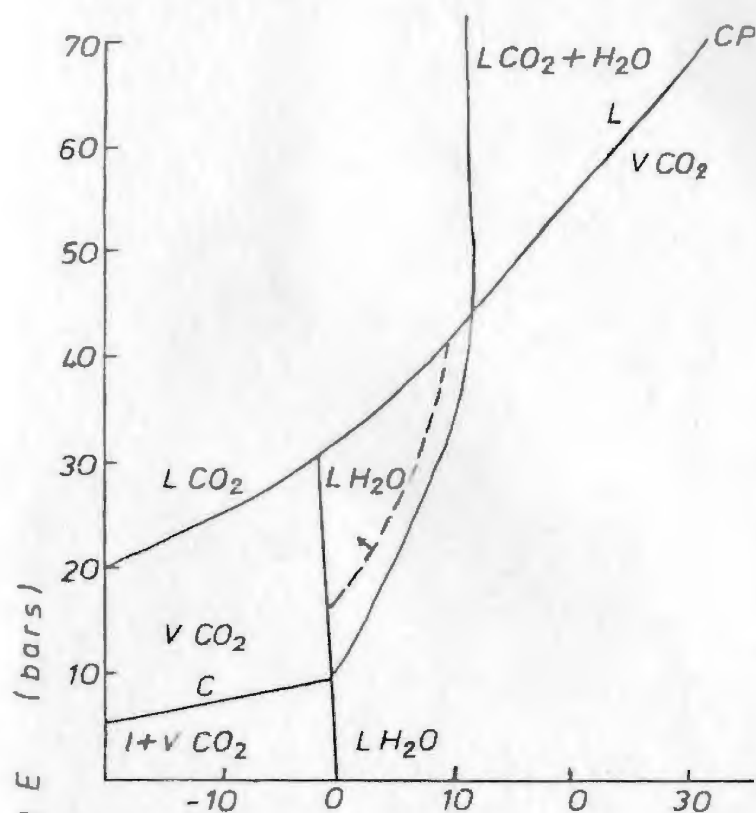
Values of  $T_{m\text{CO}_2}$  and  $T_{h\text{CO}_2}$  (Figs. 6.9 and 6.10) both approximate closely to the values for pure  $\text{CO}_2$  indicating an absence of other components such as  $\text{CH}_4$ .

#### 6.7.2 Density

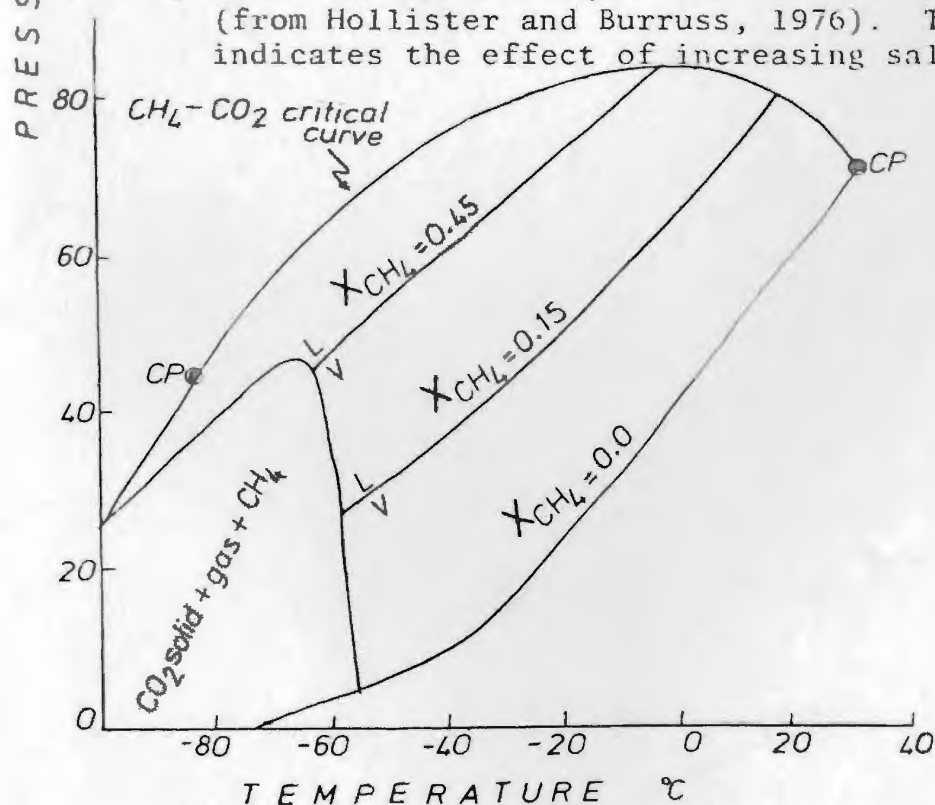
All inclusions partially homogenized to the  $\text{CO}_2$ -liquid phase and hence have a density of greater than  $0.5 \text{ g cm}^{-3}$  (Lowry and Erickson, 1927; Fig. 6.11).  $T_{h\text{CO}_2}$  determinations approximate to  $31^\circ\text{C}$  and are close to the critical point of pure  $\text{CO}_2$ , giving a density value of  $0.65 \text{ g cm}^{-3}$ . Densities of the whole inclusions are derived from their F-ratios which range from 0.6 to 0.85 (Table 6.3; Fig. 6.12).

#### 6.7.3 Composition

The phase ratios of the  $\text{CO}_2$ -bearing inclusions were determined by accurately sketching each inclusion on cards which are then cut out and



a) Clathrate-hydrate equilibria in the  $\text{CO}_2$ - $\text{H}_2\text{O}$  system (from Hollister and Burruss, 1976). The dashed line indicates the effect of increasing salinity.



b) Phase equilibria in the  $\text{CH}_4$  system at low temperatures.

Figure 6.8: Equilibria in the  $\text{CO}_2$ - $\text{H}_2\text{O}$ - $\text{CH}_4$  system, (Abbreviations: ice, I; liquid, L; vapour, V; clathrate, C; critical point, C.P.)



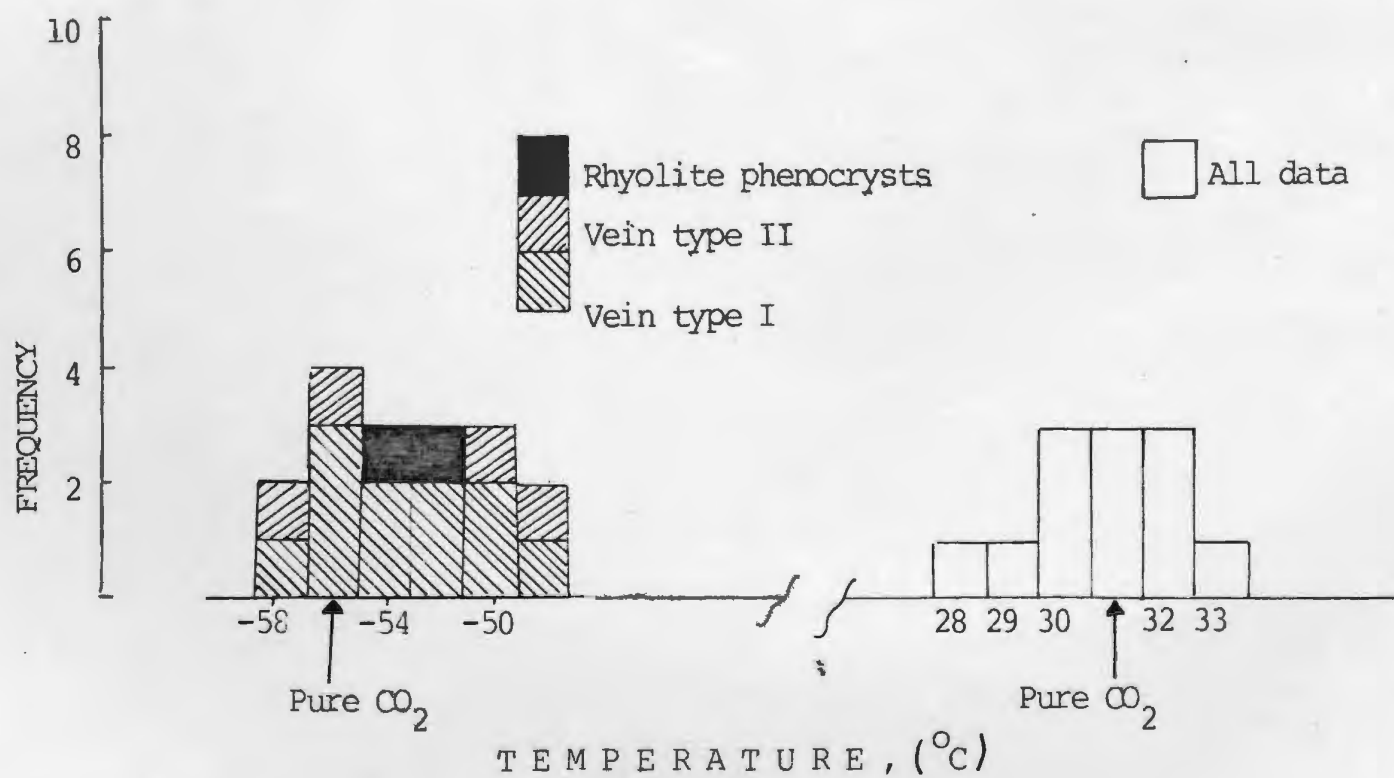


Figure 6.9: Frequency diagram for  $T_{m_{CO_2}}$ ; all samples.

Figure 6.10: Frequency diagram for  $T_{h_{CO_2}}$ ; all samples.

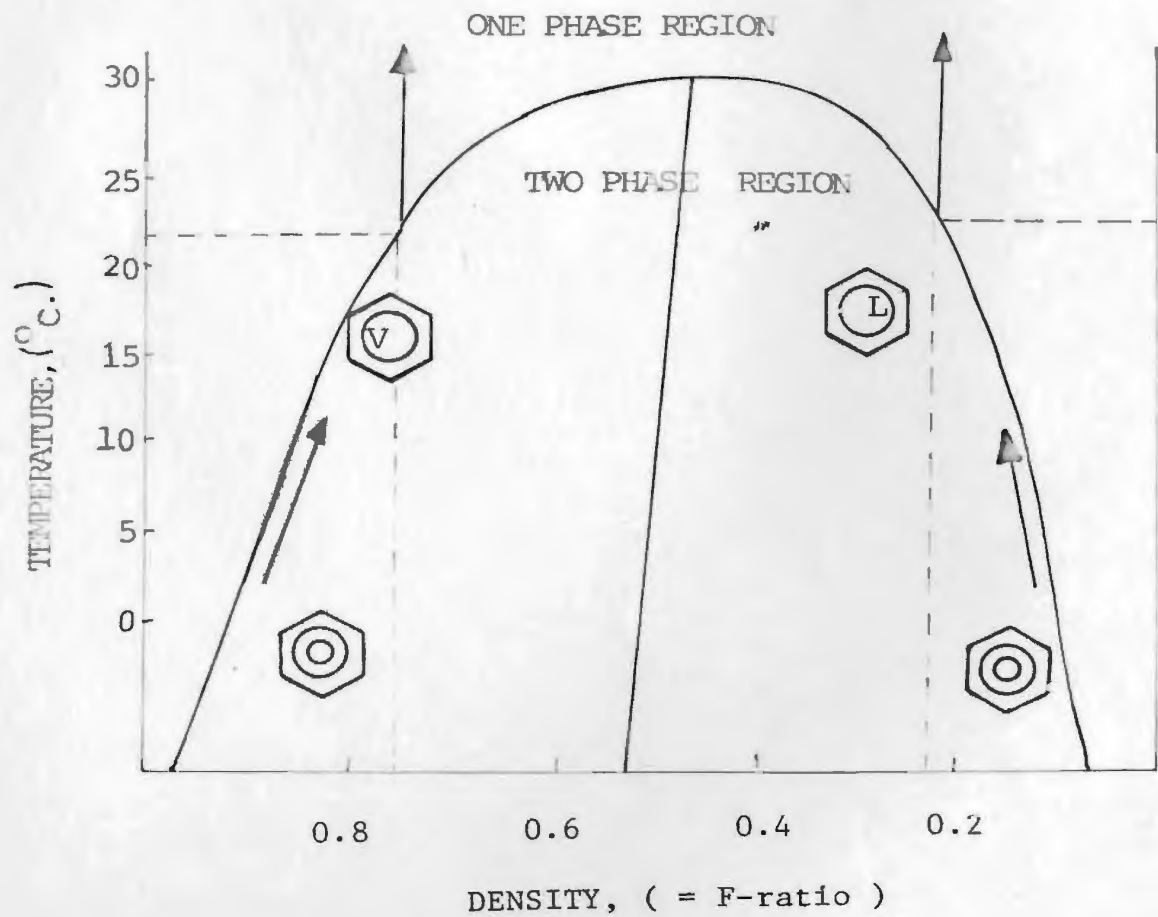


Figure 6.11: Relationship between density and homogenization temperature for pure CO<sub>2</sub> vapour-liquid system, showing how the homogenization goes to one phase or other according to the density (Roedder, 1965).

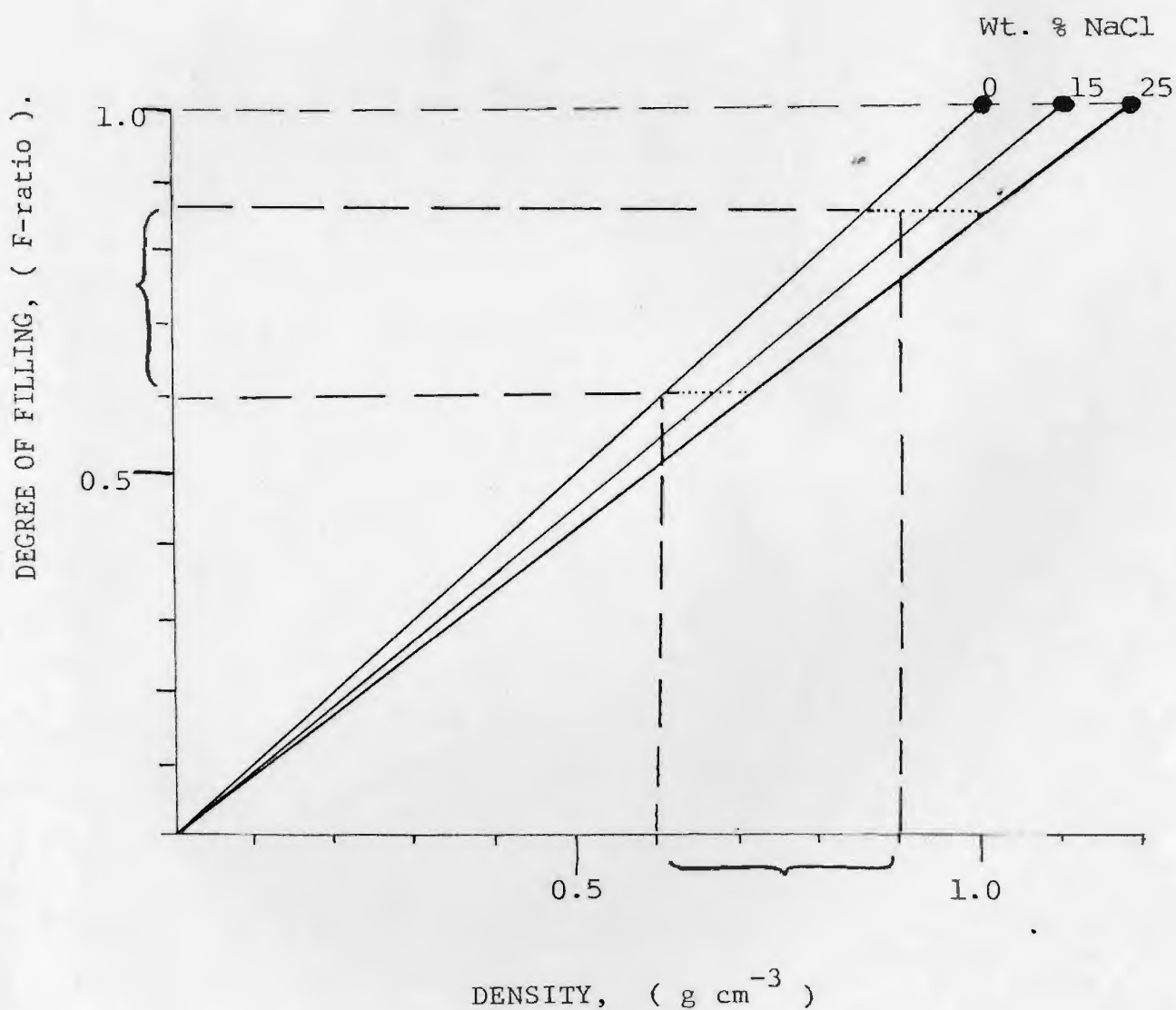


Figure 6.12: Relationship between the degree of filling (F-ratio) at 25°C and the total density (d) of inclusions for different NaCl-brines, (Rankin, 1978). The range of values of F and d for inclusions of this study is indicated.

each "phase" weighed. The composition of the fluid may be determined if the following parameters are known:-

$V_1$  = volume  $\text{CO}_2$  (liquid + gas)

$V_2$  = volume  $\text{H}_2\text{O}$

salinity from microthermometry ( $T_{m_{ice}}$ ).

density, from microthermometry ( $d_{\text{CO}_2}$ ).

If the  $T_{m_{\text{CO}_2}} \approx -56.6^\circ\text{C}$ , then the fluid inclusion approximates to the system  $\text{CO}_2\text{-H}_2\text{O-NaCl}$ . Assuming that the mutual solubilities of  $\text{CO}_2$  and  $\text{H}_2\text{O}$  are low and the  $P_{\text{H}_2\text{O}}$  at room temperature is negligible, then:-

$$X_{\text{CO}_2} = \frac{N_1}{N_1 + N_2 + N_3},$$

where  $N_1$  is the number of moles  $\text{CO}_2$ ,  $N_2$ , of  $\text{H}_2\text{O}$  and  $N_3$ , of  $\text{NaCl}$ ,

$$\text{and } N_1 = \frac{V_1 d_{\text{CO}_2}}{MW_{\text{CO}_2}} + \frac{2.3 V_2 d_{\text{H}_2\text{O}}}{100. MW_{\text{H}_2\text{O}}}$$

$$N_2 = \frac{V_2 d_{\text{H}_2\text{O}}}{MW_{\text{H}_2\text{O}}}$$

$$N_3 = N_2 \cdot x$$

where MW refers to the molecular weights, x is the equivalent mol. %  $\text{NaCl}$  derived from  $T_{m_{ice}}$  (molarity = concentration/molecular weight) and d is the density of the subscripted phase (i.e.  $d_{\text{CO}_2}$ ,  $d_{\text{H}_2\text{O}}$ ).

The molecular compositions of examples of individual inclusions are given in Tables 6.2 and 4. The P-/PS- inclusions of veins of Type I contain greater than 10 mol. %  $\text{CO}_2$ , whereas values determined for Type II veins are generally lower than 10 mol. %  $\text{CO}_2$ . The mol. %  $\text{CO}_2$  of examples of individual compositions are plotted against temperature in Fig. 6.5,



which shows their distribution above the 1 kb solvus (Todheide & Franck, 1963) and mostly below the 1 kb 6 wt % NaCl solvus (Takenouchi & Kennedy, 1965).

## 6.8 Geobarometry

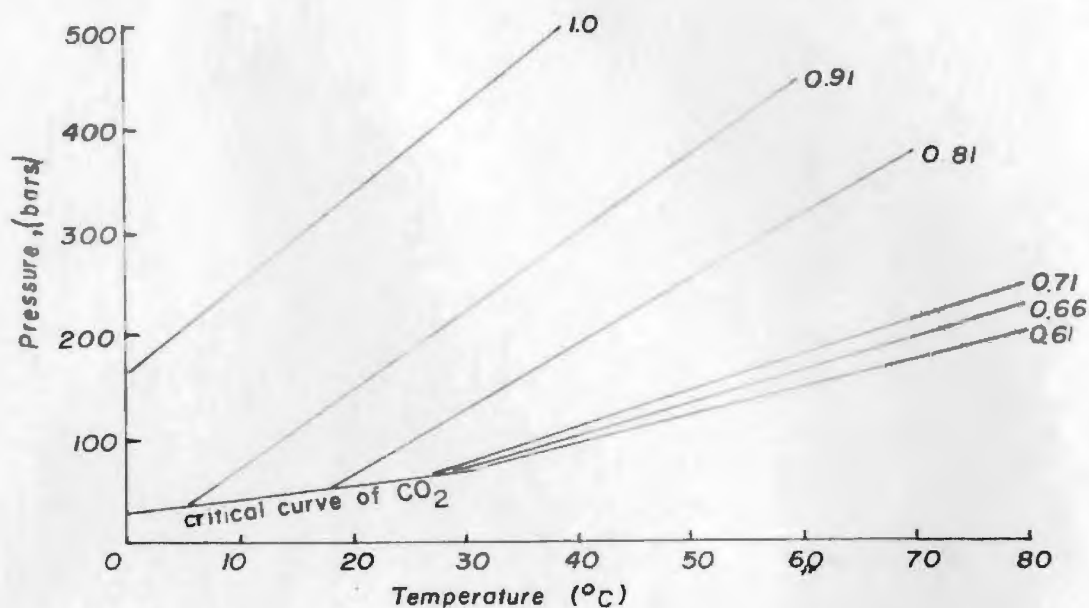
In order to correct the values of  $T_h$  to  $T_t$  (trapping temperature), an independent estimate of pressure is required, either by:-

- a. reconstruction of lithostatic load from geologic evidence
- or b. mineralogical geobarometry (Chapter 5).
- or c. application of appropriate phase equilibria to density-composition determinations of fluid inclusions.

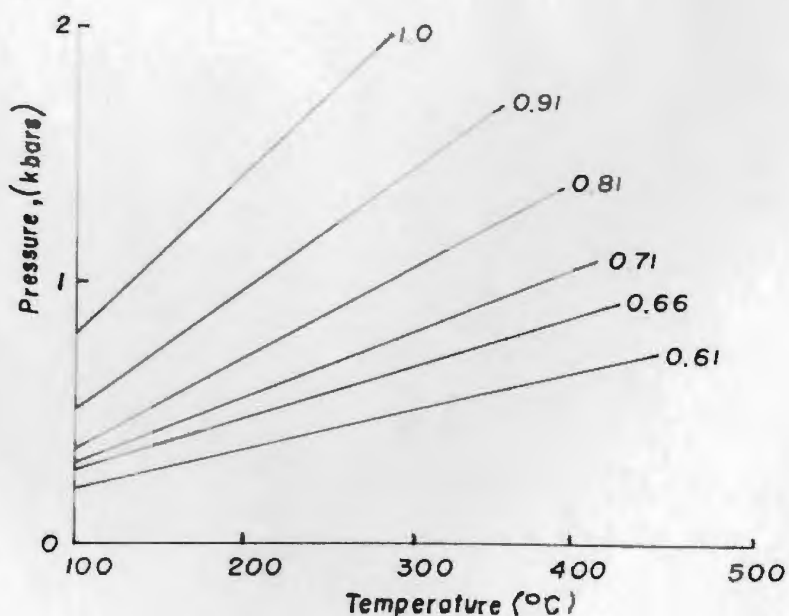
If the vein mineralization was produced by hydrothermal activity associated with the felsic intrusives, and they in turn are related to the felsic volcanic rocks of the Haywards Cove Formation (see Chapters 3, 4 and 7), then the veins at Stewarts Mine formed at a minimum depth of 2-2.5 km (i.e. an approximation of the thickness of rock from Hayward's Cove to Stewarts Mine). This thickness would impart a lithostatic pressure of approximately 1 to 1.5 kb, a pressure which compares well with estimates from arsenopyrite composition (Chapter 5).

Approximations of pressure are possible by construction of isochores from  $\text{CO}_2$ -rich inclusions (Touret, 1977) which may be extrapolated assuming straight lines to appropriate conditions for geological environment, despite the known deviation from the ideal of unmixing of two phases at higher temperatures and pressures (eg. Greenwood, 1973).

The partial pressures of  $\text{CO}_2$  and  $\text{H}_2\text{O}$  in the inclusions may be added together to provide a good estimate of trapping temperatures. The  $P_{\text{CO}_2}$  and  $P_{\text{H}_2\text{O}}$  are determined by assuming that each occupies the entire cavity at room temperature. The average density of the  $\text{CO}_2$ -bearing



a) Isochores for CO<sub>2</sub>-rich fluids at low temperatures (Kennedy & Holser, 1966)



b) Extrapolation of isochores of the isochores shown above, to higher temperatures and pressures.

Figure 6.13: Geobarometry using CO<sub>2</sub>-rich fluid isochores.

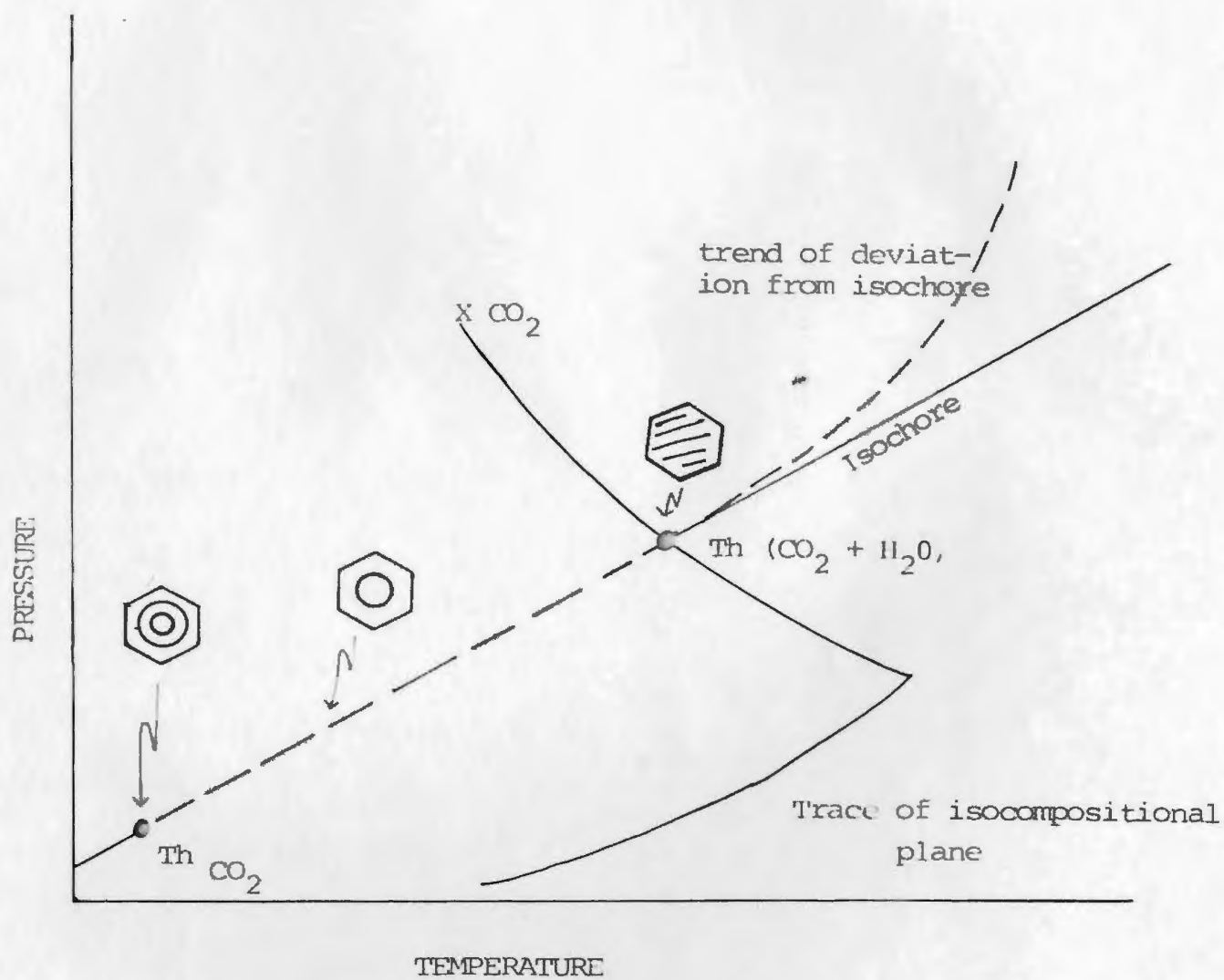


Figure 6.14: The two-homogenization method of pressure determination (Ympa, 1965).

inclusions from Moreton's Harbour samples is  $0.7 \text{ g cm}^{-3}$  and a visual estimate of the  $V_{\text{CO}_2}$  (liquid + gas):  $V_{\text{H}_2\text{O}}$  is 0.25:0.75. The apparent densities ( $d^*$ ) for the components then are:

$$d^* \text{ H}_2\text{O} = 1 \times 0.75 = 0.75$$

and  $d^* \text{ CO}_2 = 0.7 \times 0.25 = 0.1875.$

If a typical homogenization temperature for such an inclusion was  $300^\circ\text{C}$ , then the  $P_{\text{H}_2\text{O}}$  and  $P_{\text{CO}_2}$  are 350 bars and 250 bars respectively (from Kennedy and Holser, 1966; Burnham et al., 1969). Therefore the minimum pressure prevalent during deposition would have been 600 bars.

A second estimate of 1000 bars is obtained by assuming that the  $\text{H}_2\text{O}-\text{CO}_2$  isochores are straight lines and extrapolating upwards from  $\text{Th}_{\text{CO}_2}$  values to  $\text{Th}_{\text{total}}$  (Fig. 6.13).

If the  $\text{CO}_2$ -rich inclusions were trapped simultaneously with the 2-phase aqueous inclusions, then the intersection of isochores for such coexisting pairs may provide a further pressure determination. In this case values in excess of 1 kb are deduced (following arguments from Higgins, 1980 and data from Kennedy and Holser, 1966; Burnham et al., 1969; Fig. 6.14).

In summary, the pressure prevailing during vein deposition was apparently greater than 1000 bars. The pressure determinations from fluid inclusion data are hydrostatic rather than lithostatic pressure (Roedder and Bodnar, 1980). Local, marked pressure variation may result from fracturing, boiling and vein choking.

#### 6.8.1. Pressure correction

Homogenization temperatures ( $\text{Th}$ ) do not represent trapping temperatures ( $\text{Tt}$ ) in non-boiling hydrothermal fluids because the vapour



bubble only nucleates when the internal pressure of the inclusion falls below the total vapour pressure. Although pressure probably fluctuated during lode deposition, for a fluid of salinity  $\sim 5$  equivalent wt. % NaCl, a pressure correction of  $+90$  to  $+140^{\circ}\text{C}$  would be required. Therefore the  $T_t$  of vein type I is  $390$  to  $440^{\circ}\text{C}$  and for vein type II,  $290$  to  $340^{\circ}\text{C}$ . (Potter, 1977).

#### 6.9 Fluid inclusions in other minerals

Small (S-) fluid inclusions were observed in sphalerite and calcite. The inclusions in calcite showed signs of severe leakage and decrepitated readily ( $\sim 50^{\circ}\text{C}$ ) due to the well-cleaved nature of the calcite. Very small inclusions were observed in sphalerite, but could not be studied due to low transmission of light by sphalerite. Opaque sulphide and other minerals may contain fluid inclusions but to determine composition and  $T_h$ ,  $T_t$ ,  $T_d$  etc., the decrepitating stage would be required.

#### 6.10 Fluid inclusions in rhyolite phenocrysts

Quartz phenocrysts from a spherulitic, rhyolitic dyke (OHC-2) and a buff, saccharoidal - rhyodacite dyke (HC-39) were examined and found to contain a few, small P-/PS- 3-phase ( $\text{CO}_2$  gas +  $\text{CO}_2$  liquid +  $\text{H}_2\text{O}$  liquid) inclusions (Plate 6.5). The properties of these inclusions are presented in Figure 6.15.

These inclusions were shown to be similar in density and composition to the 3-phase  $\text{CO}_2$ -bearing inclusions of vein samples of veins type I. The  $T_{h\text{CO}_2}$  and  $T_{m\text{CO}_2}$  indicated the  $\text{CO}_2$  to be pure. The  $T_h$  of

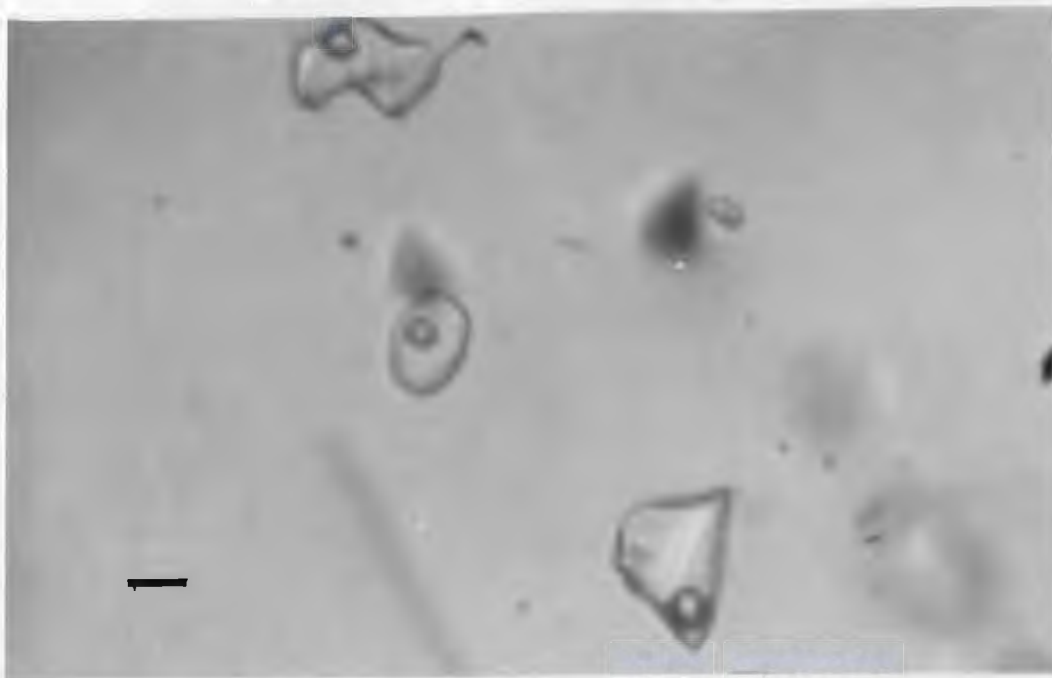


PLATE 6.4: Aqueous vapour + liquid (2 phase) inclusions from buff coloured, growth-banded gangue quartz of vein type II (SB.1a). Scale bar 10  $\mu$ m.

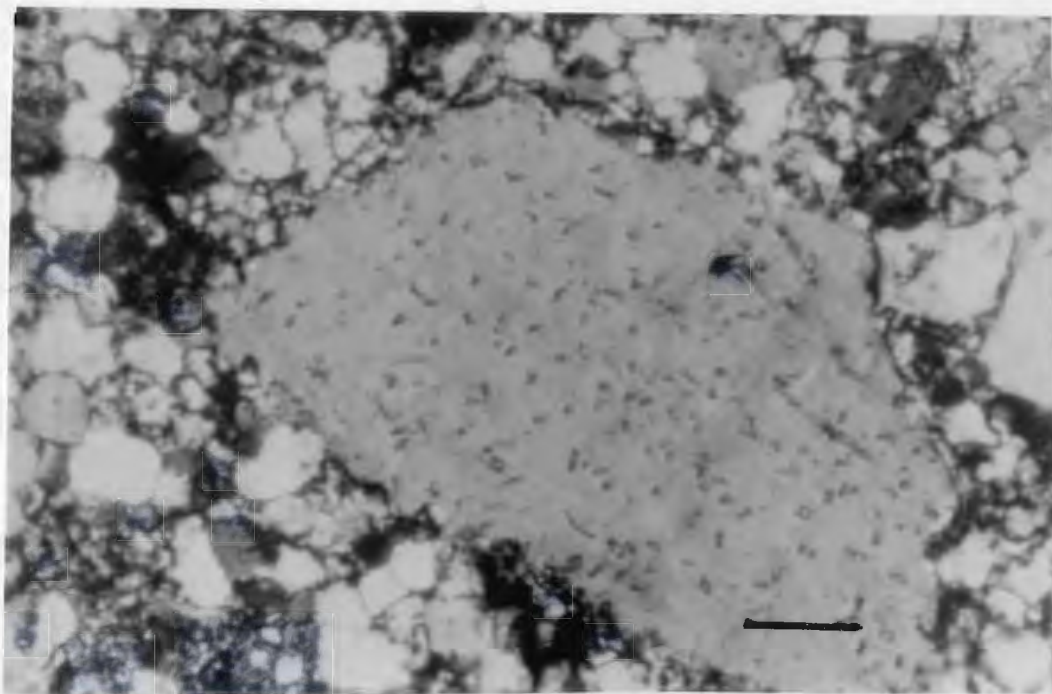


PLATE 6.5: Solid and fluid inclusions in a quartz phenocryst of a rhyolitic dyke (HC.49); the P-fluid inclusions are found to be CO<sub>2</sub>-bearing (cross-polarized light). Scale bar 1 mm.

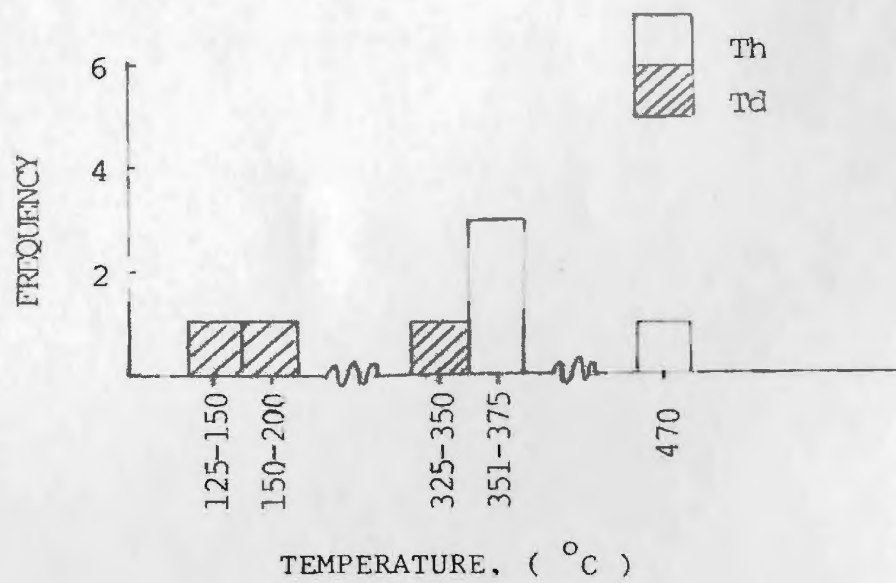


Figure 6.15: Frequency diagram for Th and Td values for P- and PS-, CO<sub>2</sub>-bearing fluid inclusions in quartz phenocrysts in felsic dyke samples.

the inclusions is greater than  $\sim 350^{\circ}\text{C}$ , although generally the inclusions decrepitated at lower temperatures before homogenizing. After correction,  $T_t$  values are in the order of  $>500^{\circ}\text{C}$  approaching the range of magmatic temperatures\* for felsic rocks.

This provides evidence that fluids emanating from the felsic magma were:

1. high temperature;
2. low salinity;
3. high density;

and 4. rich in (pure)  $\text{CO}_2$

Such  $\text{CO}_2$ -rich inclusions have been reported from granitic intrusives elsewhere (eg. Holloway, 1976; Konnerup-Madsen, 1981) and observed by the author in peralkaline granite samples from Davis Inlet, Labrador.

Two-phase aqueous (gas + liquid) secondary inclusions of variable size, morphology and composition are present along microfractures and grain boundaries of quartz phenocrysts. These exhibit a range of lower  $T_h$  values.

#### 6.11 Summary

The fluid inclusion data for the vein types and the rhyolite phenocrysts are summarized in Fig. 6.16. These data indicate a fairly simple sequence of decreasing  $T_t$  and  $X_{\text{CO}_2}$  from the rhyolite dykes to vein type I and then vein type II. The banded nature of the ore veins (eg. Plate 4.2) implies a pulsatory process of deposition, but it is considered that ore deposition was short-lived and the fluid did not

---

The  $T_t$  determined for the phenocrysts is too low for probable magmatic temperature of the felsic dykes, which may be explained by applying greater pressure corrections, if the phenocrysts formed at a deeper level. Some post-trapping (post-crystallization) modification is also likely.



vary radically during vein evolution. The ore forming fluid was initially of high density and rich in  $\text{CO}_2$ , with low salinity, from which the higher temperature assemblage was deposited (vein type I: quartz-arsenopyrite-gold). Some retrograde boiling of the fluid produced two immiscible fluids and the escape of  $\text{CO}_2$  gas and the precipitation of carbonate minerals and arsenopyrite brecciation. This also resulted in the depletion of  $\text{CO}_2$  in the fluids passing through the early vein stage. The later assemblage of stibnite + quartz were deposited at a higher level in the system from a lower temperature, relatively  $\text{CO}_2$ -poor and higher salinity fluid. Besides  $\text{CO}_2$ , the fluids precipitating the vein type II assemblage were relatively depleted in As, Au and Ag.

The following factors suggest that the ore forming fluid emanated from the silicic magmatism of the area (ie.. felsic dykes-volcanism) which also provided the heat energy to drive the convective hydrothermal system:-

1. Similar  $\text{CO}_2$ -rich, high density, low salinity inclusions in the rhyolite dykes' phenocrysts and the vein samples.
2. High temperature vein deposition.
3. The ore mineral chemistry having a felsic affinity (ie. Bi-Sb-As rich; Co-Ni poor).
4. Proximity of ore veins to the felsic dykes.
5. The comparison of hydrothermal As-Sb veins with zonation around granitic intrusives in other areas (see Chapter 7).

More detailed analysis of the fluids contained within the fluid inclusions of these samples, notably the use of stable isotope data, would verify the affinity of the mineralizing fluids.

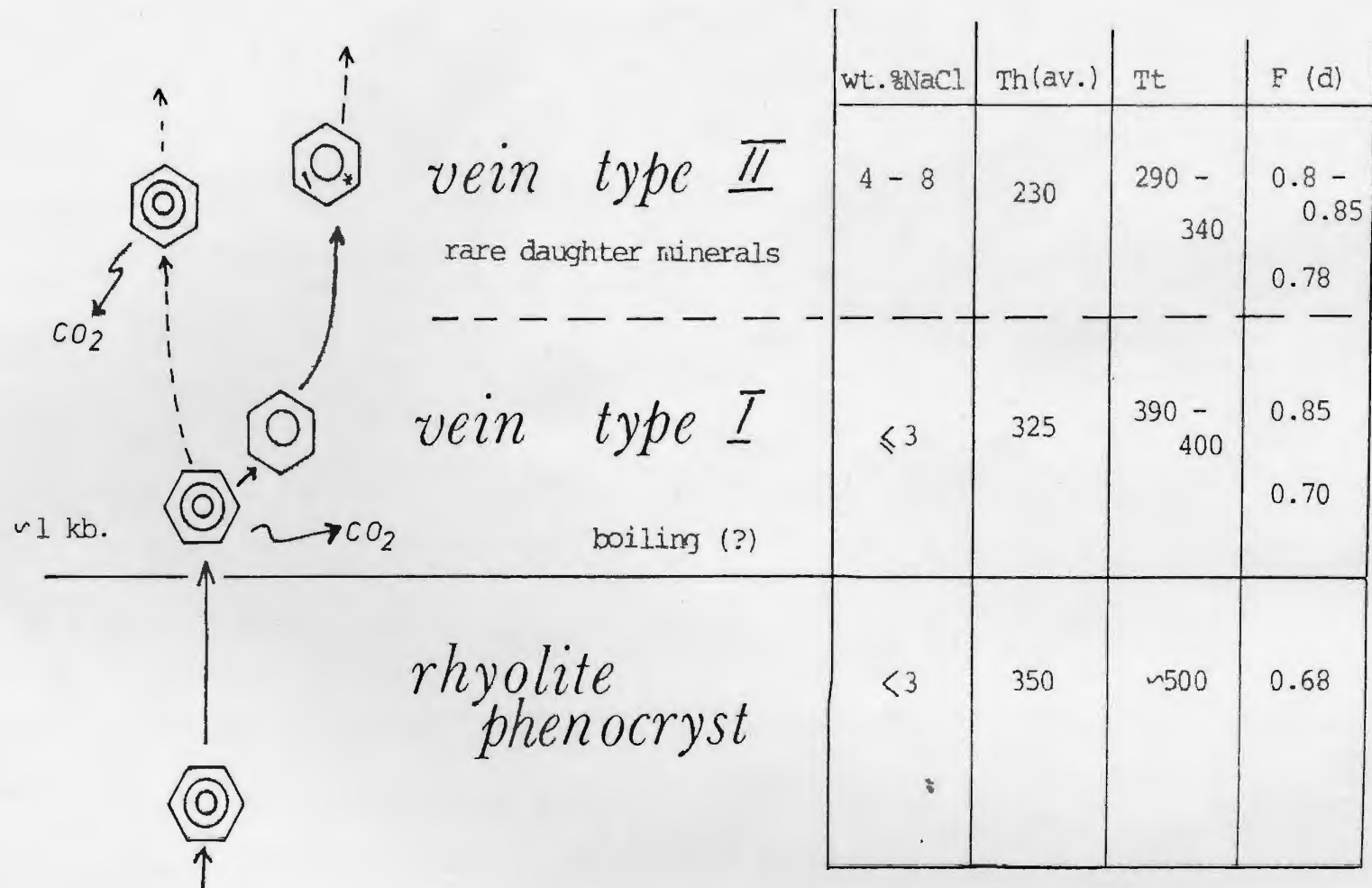


Figure 6.16: A summary of the fluid inclusion data from the Moreton's Harbour veins, indicating a possible evolution of the fluid.

## CHAPTER 7

### DISCUSSION, SUMMARY AND CONCLUSIONS

#### 7.1 The Genesis of the Moreton's Harbour Mineralization

##### 7.1.1 Introduction

The mineralization in the Moreton's Harbour area is contained largely within a hydrothermal vein system. Requirements for the formation of such an ore deposit are discussed by Fyfe and Henley (1973) and summarized in Figure 7.1. A hydrothermal system depends on a suitable fluid capable of transporting the economic element(s) from a dispersed, large source region to a focussed site, where deposition and concentration of the element(s) may take place from the fluid.

By studying the ore deposit itself, the physico-chemical conditions prevalent during the ultimate depositional stage may be ascertained (cf. Tugarinov and Naumov, 1972). Postulating the source of the ore components and the fluid and the parameters responsible for focussing and concentrating the ore is far more difficult, and eminently more tenuous. The following is a review of the evolution and genesis of the Moreton's Harbour mineralization, based on the field, petrographic, geochemical and fluid inclusion data (presented above) and by comparison with other ore deposits.

##### 7.1.2 Ore deposition

The main characteristics of the ore veins are as follows:

- (a) thin (<50 cm), discontinuous, sulphide-quartz-carbonate veins, perpendicular to the regional strike;

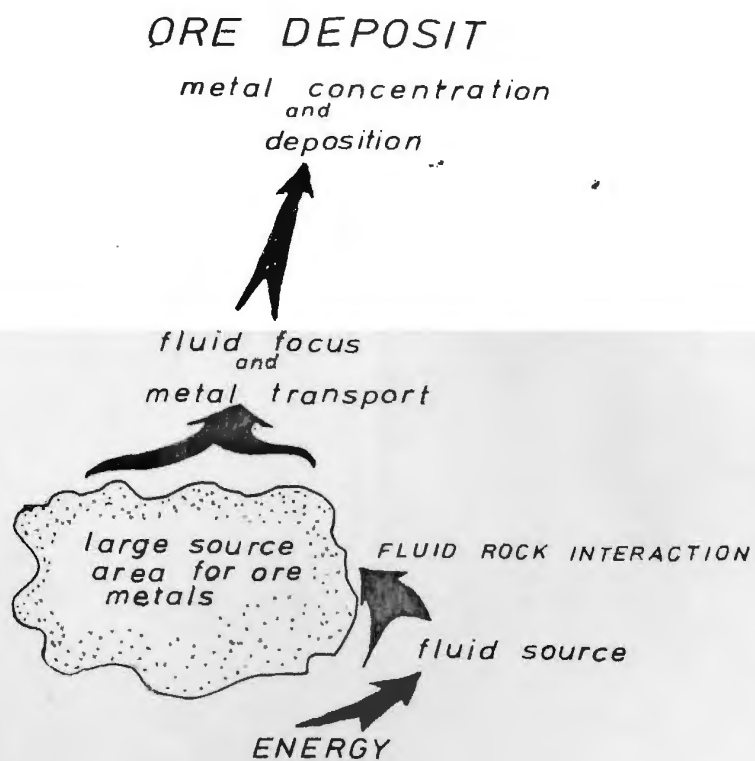


Fig. 7.1 : The requirements for the formation of a hydrothermal ore deposit ( after Fyfe & Henl y, 1973 ).



- (b) hosted largely by the mafic volcanic and volcanoclastic rocks of the Little Harbour Formation, which has precious metal concentrations elevated above average background;
- (c) spatially associated with felsic dykes;
- (d) associated with pervasive calcitization.

The vein samples are classified loosely according to their sulphide mineralogy:

Type I - arsenopyrite-dominated

Type II - stibnite-dominated

Type III - polymetallic, including sphalerite-chalcopyrite-pyrrhotite-arsenopyrite and galena.

From mineralogical and fluid inclusion observations the veins of Type I are shown to be high temperature ( $>300^{\circ}\text{C}$ ) whereas those of Type II are low temperature ( $<220^{\circ}\text{C}$ ). General confining pressure is considered to be 1.0 to 1.5 kb. The fluids trapped in inclusions of quartz from Type I were typically low salinity and high  $\text{CO}_2$  whereas the converse was true for Type II. Furthermore, the Au concentrations were only appreciably elevated in arsenopyrite- and sphalerite-bearing veins, and Ag in galena-rich samples. Therefore the high temperature, low salinity,  $\text{CO}_2$ , As, Zn, Pb-rich environment was most favourable for concentration and deposition of Au and Ag, and least favourable for stibnite crystallization.

The  $\log f_{\text{S}_2}$  value may be estimated from the mineral assemblages (Fig. 5.7) using P-T conditions derived from fluid inclusion data, as near -10. The  $f_{\text{S}_2}$  increased slightly during the precipitation of the ore veins, evident from the As-S zonation of arsenopyrite samples.

The conditions ( $\text{CO}_2$ , Au, Ag,  $f_{\text{S}_2}$ , etc.) of the fluids depositing the ore lodes varied both temporally and spatially. Variations in the composition, pressure and temperature were interdependent.

Precipitation of the ore minerals occurred as a response to a change in one or more of these physicochemical parameters. It is not possible to ascertain which factor was most critical to the ore deposition. Retrograde boiling of the fluids causing evolution of  $\text{CO}_2$  and precipitation of calcite may have been a major factor, as this process would have caused a change in the hydrostatic pressure, pH, temperature and solubility of other elements carried in the fluid (cf. Weissberg, 1969; Phillips, 1974; Krupka et al., 1977; Higgins, 1980).

### 7.1.3 The source of the fluid

Hydrothermal aqueous fluids may be derived from such diverse sources as mantle degassing, metamorphic dehydration and pore water elimination (White, 1974; Fyfe et al., 1978) and segregation from silicate melts (Burnham, 1967, 1979). The fluids which were responsible for the Moreton's Harbour vein mineralization are considered to be derived from the magmatic source of the felsic dykes for the following reasons:

- (a) the similarity of trapped fluids observed in quartz phenocrysts of felsic dykes and high temperature vein quartz;
- (b) high temperature of deposition;
- (c) the granitic affinity of the geochemistry of the sulphide mineral;
- (c) the ubiquitous proximity of the veins to the felsic dykes and their adjacent fracture systems;

- (e) similarity to vein systems also genetically related to acid magmatism (cf. Tischendorf, 1977; Burnol, 1978; Cambel and Jarovsky, 1978; Moore, 1979).

Other Au-rich sulphide vein deposits such as various mostly meta-sediment-hosted veins (e.g. Radtke and Scheiner, 1970; Henley et al., 1976; Glasson and Keays, 1978; Piranjo, 1979; Sawkins et al., 1979) have been shown to be related to metamorphically generated fluids. However, the veins at Moreton's Harbour differ by their:

- (a) much higher concentrations of As and Sb;
- (b) calcitic wall rock alteration;
- (c) very low greenschist facies, volcanic host rock;
- (d) close proximity to felsic intrusions; and
- (e) slightly higher temperatures.

A magmatic fluid source would also provide the heat energy source required to drive the hydrothermal system.

#### 7.1.4 Metal source and transport, with specific reference to gold.

It may be assumed that the source region for the metals occurred between the fluid source and sites of deposition. Although the fluids were probably sourced by the felsic intrusives, there is no reason that at least some of the ore metals may not have been derived from other rock types.

According to various workers (Barnes and Czamanske, 1967; Krauskopf, 1971; Tilling et al., 1973), the source of ore metals does not necessarily require any primary enrichment in the source or host rock, provided that the fluid:rock interaction is such that sufficient metal is

leached from a large enough volume of source rock and concentrated to a small enough site to produce the required environment. This is particularly the case for a rare element like Au which has a background concentration of 3 ppb and requires enrichment to ~10 ppm to attain economic grade (Kerrick et al., 1979; Fryer and Kerrich, 1979).

Under normal surface conditions of pressure and temperature, the solubility of Au is low being < 1 ppb in fresh or pure water, and may be slightly greater ( $\leq 46$  ppb) in seawater. At low temperatures ( $\sim 25^{\circ}\text{C}$ ), Au may combine with various anions or anionic complexes such as  $\text{Cl}^-$ ,  $\text{S}^{2-}$ ,  $\text{HS}^-$ ,  $\text{HCO}_3^-$ ,  $\text{CN}^-$ , and this may greatly enhance the solubility of Au and other metals. The solution chemistry of Au and its complexes is dominantly ionic below  $300^{\circ}\text{C}$  but at higher temperatures, the molecular "gaseous" complexes, with Cl for example, predominate (Henley, 1973). Krauskopf (1951) showed that the type of complex formed was dependent on the pH of the solution, such that in acidic, oxidizing conditions, Au dissolves more readily as  $\text{Cl}^-$  complexes (e.g.  $\text{AuCl}_4^-$ ) whereas  $\text{S}^{2-}$  complexes (e.g.  $\text{Au}(\text{HS})_2^-$ ,  $\text{Au}_2(\text{HS})_2\text{S}^{2-}$ ) are more stable in near neutral to alkaline conditions. In non-sulphide, neutral aqueous solutions, the solubility of Au is negligible. Weissberg (1970) demonstrated that higher sulphide concentration enhanced the Au solubility below  $300^{\circ}\text{C}$ , but the affect of NaCl concentration was negligible.

The solubility of Au as complexes is greatly increased by increasing temperature as shown by the thermodynamic and experimental data of Helgeson and Garrels (1968) and later by Seward (1973) and Fyfe and Henley (1973) and Henley (1973). Seward (1973) showed an almost exponential increase in



the solubility of Au- thio complexes, towards 300°C at 1 kb, and also that increasing pressure enhances solubility at low pH and depresses it under conditions of higher pH and of high HS-/H<sub>2</sub>S ratio. He showed that the presence of NaCl (and hence, Cl-) had little affect on the Au-content of the solutions whereas increasing S<sup>2-</sup> content had a positive affect on the Au-solubility. Above 300°C, Henley (1973) and Fyfe and Henley (1973) show a sharp increase of Au-solubility in chloride solutions between 450° and 500°C, which was further enhanced by greater Cl concentration at higher pressures.

Although most work pertains to the chemistry of S<sup>2-</sup> and Cl- species, it is considered that other complexing agents, including organic compounds and CO<sub>3</sub><sup>2-</sup>, HCO<sub>3</sub><sup>2-</sup>, are important (Boyle, 1979; Higgins, 1980).

In the fluids responsible for transporting the metals to the Moreton's Harbour ore-vines it is evident that S<sup>2-</sup> would have been available for complexing, from the sulphide mineral assemblages. From observation of fluid inclusions it is evident that the most prominent component of the fluid, other than water, was CO<sub>2</sub>. Even if CO<sub>2</sub> (as CO<sub>3</sub><sup>2-</sup>, HCO<sub>3</sub><sup>-</sup>) was not directly responsible for carrying Au or other metals, the character of the fluid is greatly influenced by the presence of CO<sub>2</sub>. Carbon dioxide affects the solubility of other components (including NaCl; see Chapter 6) and the viscosity of the fluid, hence the flow rate. It acts as a pH buffer and if retrograde boiling occurred and CO<sub>2</sub> lost from the system, then the HCO<sub>3</sub><sup>-</sup> activity may be decreased. Therefore, the pH/Eh balance may be disturbed, which may be a sufficient stimulus for precipitation of the ore metals.



The temperatures determined for deposition of the Au-rich ore assemblages at Moreton's Harbour approximate to 300°C. The almost exponential decrease of Au-solubility at this temperature (Seward, 1973) suggests that a temperature decrease alone (through 300°C) may be sufficient for the precipitation and chemical changes may have been induced by the temperature decrease. Pressure has much less influence on the affect of the Au-transport and deposition.

In summary the temperature and behaviour of CO<sub>2</sub> are considered to have been the major parameters determining the transport and deposition of Au and other metals in the Moreton's Harbour hydrothermal vein system.

Although primary enrichment of Au in host-source rocks may not be necessary, there are many examples described where the lode-Au deposits result from remobilization and reconcentration from primarily enriched horizons, commonly by some volcanogenic exhalative process (e.g. Radtke and Scheiner, 1970; Worthington, 1970; Glasson and Keays, 1978; Fryer et al., 1979; Karvinen, 1980). There does appear to be a stratigraphic control on the localization of the Moreton's Harbour mineralization, too; that is, within the volcanoclastic Little Harbour Formation (see Chapter 5).

The precious metal analyses of some of the unmineralized volcanic and sedimentary rock show that most have Au and Ag concentrations slightly above average crustal background values. In some examples the elevated Au and Ag concentrations may be due to primary volcanogenic enrichment (e.g. the Wild Cove Head pyritic chert). However, for the most part, the slightly elevated Au concentrations in the volcanoclastic rocks may be due to secondary enrichment, related to widespread circulation and percolation

of the mineralizing fluids. The rocks of the Little Harbour Formation are not considered to have been the major source of metals. The lack of highly enriched host-source rocks in the Moreton's Harbour area may be a factor contributing to the subeconomic nature of the deposits.

#### 7.1.5 Other controls on mineralization

There is a broad stratigraphic localization of the mineralization within the Little Harbour Formation. This could be simply because it occupied a depth in the volcanic pile corresponding to P-T-X conditions suitable for deposition rather than any primary enrichment. This is based on the assumption that:

- (a) the mineralization was dependent on the felsic intrusions, both for fluid and energy source;
- (b) the felsic volcanoclastic rocks of the Hayward's Cove Formation are coeval (hence fed by) the felsic intrusive rocks (Chapter 3);
- (c) if (a) and (b) are true, the mineralization was penecontemporaneous with the felsic volcanism and occurred at a depth approximately equivalent to the distance between Stewart's Mine and Hayward's Cove, which compares well with estimated pressures.

There is some structural control on the mineralization. Veins are more or less perpendicular to bedding and occupy small tensional gashes and larger fractures and shear zones. The mineralizing fluids take advantage of any structural weaknesses for circulation and for deposition.

#### 7.1.6 A summary of the ore genesis

The genesis and evolution of the Moreton's Harbour ore veins are summarized in Figure 7.2.

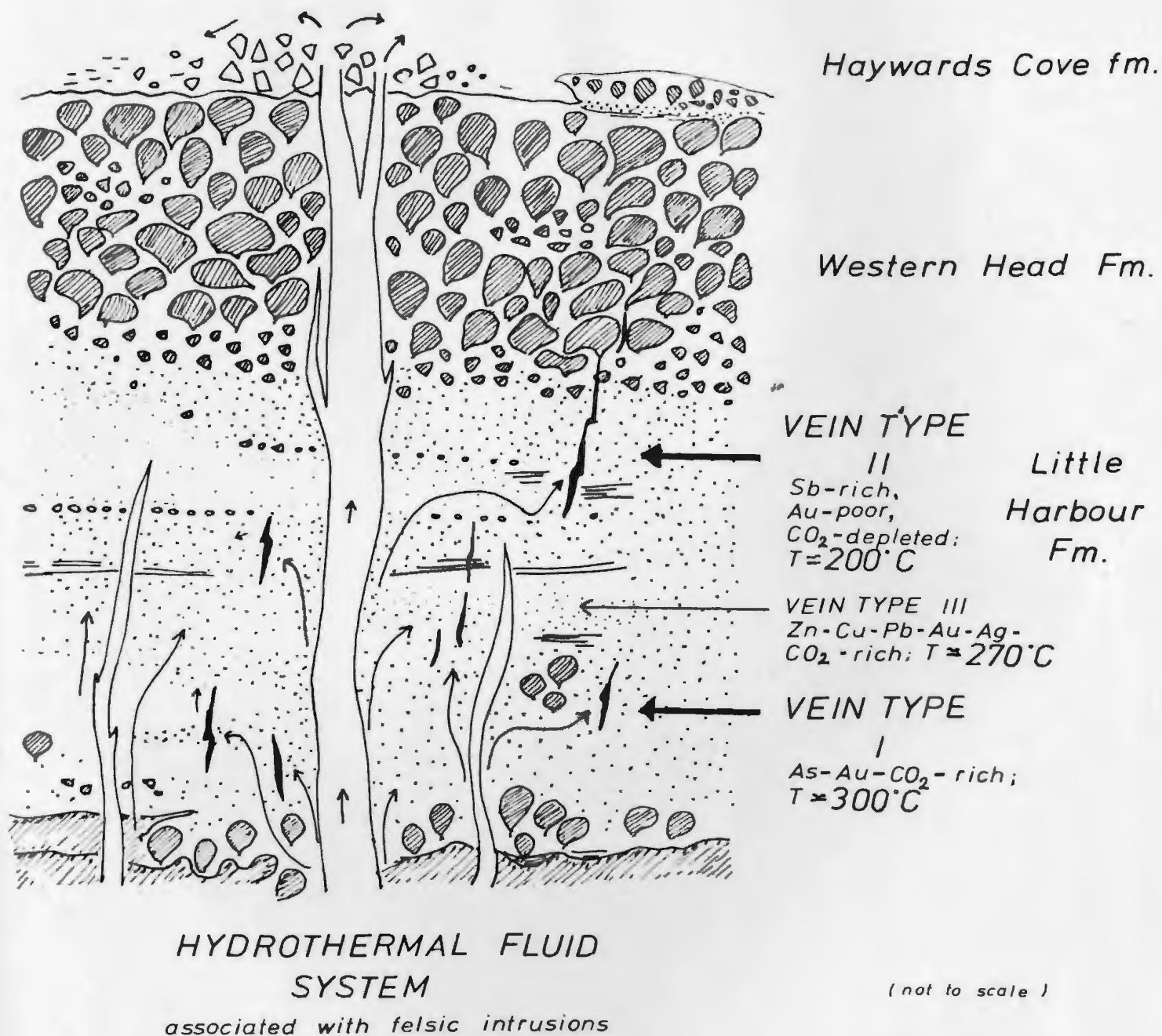


Fig. 7.2: Summary of the evolution of the vein mineralization of the Moreton's Harbour area.

## 7.2 Summary and Conclusions

The following is a summary of the geological and geochemical features of the Moreton's Harbour mineralization:

1. The Moreton's Harbour mineralization comprises a subvolcanic, hydrothermal vein system genetically related to the felsic intrusions.
2. The veins are hosted by the Little Harbour Formation in structures perpendicular to the regional strike.
3. The veins are broadly classified into three main types on the basis of mineralogy. This classification is substantiated by geochemical and thermometric data

Vein Type I - Arsenopyrite dominated, Au-rich, high temperature with CO<sub>2</sub>-bearing fluid inclusions.

Vein Type II - Stibnite dominated, Au-Ag poor, Pd-relatively rich, low temperature, with CO<sub>2</sub>-poor fluid inclusions.

Vein Type III - Base metal sulphide dominated, Au- and Ag-rich, high temperature with CO<sub>2</sub>-bearing fluid inclusions.

4. The higher temperature vein assemblages (I) are preferentially enriched in As and Au and relatively poor in Sb.
5. The Au and Ag are dispersed through arsenopyrite and sphalerite.
6. Fluids responsible for deposition of the ore veins were CO<sub>2</sub>-rich and low salinity in the Au-bearing, higher temperature veins, but with boiling off of CO<sub>2</sub> and increased contamination from the countryrock, the CO<sub>2</sub> concentration decreased and the salinity increased.
7. CO<sub>2</sub> (as CO<sub>3</sub><sup>2-</sup>, HCO<sub>3</sub><sup>-</sup>, etc.) is considered to have been a major control on the ore deposition, and probably an important complexing agent for the ore metals to enable transporation.
8. The energy and fluid required for the hydrothermal system is thought to have been provided by the felsic intrusions of the area.

9. The mineralization is penecontemporaneous with the Hayward's Cove Formation and the coeval(?) felsic intrusions. As no great time hiatus is envisaged between the Western Head Formation and the Hayward Cove Formation, the age of mineralization is probably Lower to Middle Ordovician.
10. The Little Harbour Formation is preferentially mineralized largely due to its location (ie. depth) within the volcanic pile. There is only weak primary volcanogenic enrichment of ore metals and minor secondary enrichment through the volcaniclastic sediments, due to greater permeability than other rock types.



REFERENCES

- BALLARD, R.D., HOLCOMB, R.T. and van ANDEL, T.H., 1979: The Galapagos Rift at 86°W: 3. Sheet flows, collapse pits and lava lakes of the Rift Valley: J. Geophys. Res., v. 85 (B. 10), pp. 5407-5422.
- BAIRD, D.M., 1953: Reconnaissance geology of part of the New World Island - Twillingate area: Geol. Surv. Nfld., Rept. No. 1, 20 p.
- BARNES, H.L. and CZAMANSKE, G.K., 1967: Solubilities and transport of ore minerals: In Geochemistry of Hydrothermal Ore Deposits. Barnes, H.L. (ed.), pp. 334-381. Holt, Rinehart and Winston Inc., N.Y.
- BARTON, P.B., Jr., 1969: Thermochemical study of the system Fe-As-S: Geochim. Cosmochim. Acta, v. 33, pp. 841-858.
- \_\_\_\_\_, 1971: The Fe-Sb-S system: Econ. Géol., v. 66, pp. 121-132.
- \_\_\_\_\_, and SKINNER, B.J., 1979: Sulfide mineral stabilities: In Geochemistry of Hydrothermal Ore Deposits. 2nd Edition. Barnes, H.L. (ed.), pp. 278-403. Wiley Interscience.
- \_\_\_\_\_, and TOULIMIN, P., 1966: Phase relations in the FeZnS system: Econ. Geol., v. 61, pp. 815-849.
- BERGLAND, S. and EKSTRÖM, T.K., 1980: Arsenopyrite and sphalerite as T-P indicators in sulphide ores from Northern Sweden: Mineral. Deposita, v. 15, pp. 175-187.
- BOCTOR, N.Z., 1980: Sphalerite geobarometry in Bodenmais ore, Bavaria: Am. Mineral., v. 65, pp. 1031-1037.
- BODNAR, R.J. and BEANE, R.E., 1980: Temporal and spatial variations in hydrothermal fluid characteristics during vein filling in Preore cover overlying deeply buried porphyry-copper type mineralization at Red Mountain, Arizona: Econ. Geol., v. 75, pp. 875-893.
- BOYLE, R.W., 1979: The geochemistry of gold and its deposits: Geol. Surv. Can., Bull. 280, 584 p.
- BURNHAM, C.W., 1967: Hydrothermal fluids at the magmatic stage: In Geochemistry of Hydrothermal Ore Deposits. Barnes, H.L. (ed.), pp. 34-76. Holt, Rinehart and Winston Inc., N.Y.
- \_\_\_\_\_, 1979: Magmas and hydrothermal fluids: In Geochemistry of Hydrothermal Ore Deposits. 2nd Edition, Barnes, H.L. (ed.), pp. 71-136. Wiley Interscience.

- \_\_\_\_\_, HOLLOWAY, J.R. and DAVIS, N.F., 1969: The specific volume of water in the range 1000 to 8900 bars, 20° to 900°C: Am. J. Sci., v. 267-A, pp. 70-95.
- BURNOL, L., 1978. Different types of leucogranites and classification of types of mineralization associated with acid magmatism in the north-western part of the French Massif Central: In Metall. Assoc. with Acid Magma., v. 3, pp. 191-205. Stempok, M., Burnol, L. and Tischendorf, G. (eds.), Ustr. Ust. Geol., Praha.
- CAMBEL, B. and JAROVSKY, J., 1967: Geochemie der Pyrite einiger Lagerstätten der Tschechoslowakei: Vydavatel'stvo Slovenskej Akademie vied Bratislava, 1967, 493 p.
- \_\_\_\_\_, 1978: Geochemia mikraprvkov v antimonitoch z ceskosloven-skych lozisk: ydavatel'stvo slovenskej Akademie Vied Brataslava, Naka Ozemi: Geologica 13, 226 p.
- \_\_\_\_\_, and KRITIN, J., 1977: Geochemichy vyskum blaunych sulfidichya mineralov zezeza pomocov eletronovej micro-sandy: Veda Vydavalel'stvo, slovenskej Akademie Vied, 316 p.
- CARLISLE, D., 1963: Pillow breccias and their aquagene tuffs, Quadra Island, British Columbia: J. Geol., v. 70, pp. 48-71.
- CARMICHAEL, I.S.E., TURNER, S.J. and VERHOOGEN, J., 1974: Igneous petrology: Int. Series in the Earth and Planetary Sci., McGraw-Hill Inc., 739 p.
- CLARK, L.A., 1960: The Fe-As-S system: phase relations and applications: Econ. Geol., v. 55, pp. 1345-1381, pp. 1631-1652.
- COLLINS, P.L.F., 1979: Gas hydrates in CO<sub>2</sub>-bearing fluid inclusions and the use of freezing data for estimation of salinity: Econ. Geol., v. 75, pp. 1435-1444.
- CUNNINGHAM, C.G., Jr., 1977: Fluid inclusion geothermometry: Geol. Rundsch., v. 66, pp. 1-9.
- CZAMANSKE, G.K., 1974: The FeS content of sphalerite along the chalcopyrite-pyrite-bornite sulfur fugacity buffer: Econ. Geol., v. 69, pp. 1328-1334.
- DEAN, P.L., 1978: The volcanic stratigraphy and metallogeny of Notre Dame Bay, Newfoundland, Memorial University of Newfoundland, Geol. Report 7, 205 p.
- \_\_\_\_\_, and STRONG, D.F., 1977: Folded thrust faults in Notre Dame Bay, Central Newfoundland: Am. J. Sci., v. 277, pp. 97-108.
- DEWEY, J.F. and BIRD, J.M., 1971: Origin and emplacement of the ophiolite suite: Appalachian ophiolites in Newfoundland: J. Geophys. Res., v. 76, pp. 3179-3206.
- DICKSON, J.A.D., 1966: Carbonate identification and genesis as revealed by staining: J. Sed. Pet., v. 36 (2), pp. 491-505.

- DIMROTH, E., COUSINEAU, P., LEDUC, M. and SANSCHAGRIN, Y., 1978: Structure and organization of Archean subaqueous basalt flows Rouyn-Noranda area, Quebec, Canada: Can. J. Earth Sci., v. 15, pp. 902-918.
- ELLIS, A.J., 1959: The solubility of carbon dioxide in water at high temperature: Am. J. Sci., v. 257, pp. 217-234.
- FOGWILL, W.D., 1968: Western Head Copper Prospect, Notre Dame Bay, Newfoundland: Nfld. and Lab. Corp. Ltd., Report.
- FRUEH, A.J. and VINCENT, E.A., 1974: Silver-abundance in common igneous rock types: In Handbook of Geochemistry II/2, Wedepohl, K.H. (ed.), Springer-Verlag, pp. 47·E1-47·E4.
- FRYER, B.J. and KERRICH, R., 1978: Determination of precious metals at ppb levels in rocks by a combined wet chemical and flameless AAS technique: Atom. Abs. Newsletter, v. 17 (1), pp. 406.
- \_\_\_\_\_, HUTCHINSON, R.W., PEIRCE, M.G. and ROGERS, D.S., 1979: Archean precious metal hydrothermal systems, Dome Mine, Abitibi Greenstone Belt - I. Patterns of alteration and metal distribution: Can. J. Earth Sci., v. 16 (3), pp. 421-439.
- FYFE, W.S. and HENLEY, R.W., 1973: Some thoughts on chemical transport processes, with particular reference to gold: Min. Sci. Engng., v. 5, pp. 295-303.
- \_\_\_\_\_, PRICE, N.J. and THOMPSON, A.B., 1978: Fluids in the Earth's Crust (Their significance in metamorphic tectonic and chemical transport processes): Developments in Geochem. I, Fyfe, W.S. (ed.), Elsevier Sci. Publ. Co., Amst., Oxf., N.Y.
- GIBBONS, R.V., 1969: Geology of the Moreton's Harbour area, Newfoundland with emphasis on the environment and mode of formation of the arsenopyrite veins: Unpub. M.Sc. Thesis, Memorial University, Nfld., 165 p.
- \_\_\_\_\_, and PAPEZIK, V.S., 1970: Volcanic rocks and arsenopyrite veins of the Moreton's Harbour Area. Notre Dame Bay, Newfoundland: Geol. Assoc. Can. Proc., v. 22, pp. 1-9.
- GLASSON, M.J. and KEAYS, R.R., 1978: Gold mobilization during cleavage development in sedimentary rocks from the Auriferous Slate Belt of Central Victoria, Australia: some important boundary conditions: Econ. Geol., v. 73, pp. 496-511.
- GREENWOOD, H.F., 1973: Thermodynamic properties of gaseous mixtures of H<sub>2</sub>O and CO<sub>2</sub> between 450°C and 800°C and 0 to 500 bars: Am. J. Sci., v. 273, pp. 561-571.

- HAAAS, J.L., 1971: The effect of salinity on the maximum thermal gradient of a hydrothermal system at hydrostatic pressure: Econ. Geol., pp. 940-946.
- HAYES, J.J., 1951: Geology of the Hodges Hill-Marks Lake area, northern Newfoundland, Unpub. Ph.D. thesis, Univ. Michigan, 163 p.
- HELGESON, H.C. and GARRELS, R.M., 1968: Hydrothermal transport and deposition of gold: Econ. Geol., v. 63, pp. 622-635.
- HELWIG, J.A., 1967: Stratigraphy and structural history of the New Bay area, north central Newfoundland. Ph.D. thesis, Columbia Univ., 211 p.
- HENLEY, R.W., 1973: Solubility of gold in hydrothermal chloride solutions: Chem. Geol., v. 11, pp. 73-87.
- \_\_\_\_\_, NORRIS, R.J. and PATERSON, C.J., 1976: Multistage ore genesis in the New Zealand Geosyncline - a history of post-metamorphic lode emplacement: Mineral. Deposita, v. 11 (2), pp. 180-196.
- HENLEY, R.W. and THORNLEY, P., 1981: Low grade metamorphism and the geothermal environment of massive sulphide ore formation, Buchans, Newfoundland: In The Buchans Orebodies: Fifty years of Mining and Geology; E.W. Swanson, D.F. Strong and F.G. Thurlow, Eds.; Geol. Assoc. Can. Spec. Paper 22, 1981, pp. 205-228.
- HEYL, G.R., 1936: Geology and Mineral deposits of the Bay of Exploits area: Nfld. Dept. Nat. Resources, Bull. 3, 66 p.
- HIBBARD, J. and WILLIAMS, H., 1979: Regional setting of the Dunnage Melange in the Newfoundland Appalachians: Am. J. Sci., v. 297, pp. 993-1121.
- HIGGINS, N.C., 1979: Theory methods and application of fluid inclusion research; short course notes. Geol. Dept., Memorial Univ. of Nfld., 42 p.
- \_\_\_\_\_, 1980: The genesis of Grey River Tungsten Prospect: a fluid inclusion, geochemical and isotopic study: Unpub. Ph.D. thesis, Memorial Univ. of Nfld., 404 p.
- HOLLAND, H.D., 1967: Gangue minerals in hydrothermal deposits: In Geochemistry of Hydrothermal Ore Deposits, Barnes, H.L. (ed.), pp. 382-436. Holt, Rinehart, Winston, Inc., N.Y.
- HOLLISTER, L.S. and BURRUSS, R.C., 1976: Phase equilibria in fluid inclusions from the Khtada Lake Metamorphic Complex: Geochim. Cosmochim. Acta, v. 40, pp. 163-175.
- HOLLOWAY, J.R., 1976: Fluids in the evolution of granitic magmas - consequences of finite CO<sub>2</sub> solubility: Geol. Soc. Am. Bull., v. 87, pp. 1513-1518.



- HORNE, G.S., 1969: Early Ordovician chaotic deposits in the central volcanic belt of northwestern Newfoundland: Geol. Soc. Am. Bull., v. 80, pp. 2451-2464.
- \_\_\_\_\_ and HELWIG, J.A., 1969: Ordovician stratigraphy of Notre Dame Bay, Newfoundland: In North Atlantic - Geology and Continental Drift, Kay, M. (ed.), Am. Assoc. Pet. Geol., Mem. 12, pp. 308-407.
- HOWLEY, G.S., 1907: Geological map of Newfoundland, 1:108,800 (reprinted 1915, 1925).
- HUGHES, C.J., 1973: Spilites, keratophyres and the igneous spectrum: Geol. Mag., v. 109 (6), pp. 513-527.
- JONES, J.G., 1969: Pillow lavas as depth indicators: Am. J. Sci., v. 267, pp. 181-195.
- \_\_\_\_\_ and NELSON, P.H.H., 1970: The flow of basaltic lava from air into water - its structural expression and stratigraphic significance: Geol. Mag., v. 107 (1), pp. 13-19.
- JUKES, J.B., 1843: General report of the Geological Survey of Newfoundland during the years 1839 and 1840: London, Murray (pub.), 160 p.
- KARVINEN, W.O., 1980: Geology and evolution of gold deposits, Timmins area, Ontario: In Genesis of Archean Volcanic-Hosted Gold Deposits, Symp. Ont. Geol. Surv. (#5293), Roberts, R.G. (ed.).
- KAY, M., 1970: Flysch and bouldery mudstone in northeast Newfoundland: Geol. Assoc. Can., Spec. Paper 7, pp. 155-164.
- \_\_\_\_\_, 1972: Dunnage Mélange and lower Palaeozoic deformation in northeastern Newfoundland: 24th Int. Geol. Congr., Proc., Sect. 3, pp. 122-132.
- \_\_\_\_\_, 1976: Dunnage Mélange and subduction of the Protoacadian Ocean, northeast Newfoundland: Geol. Soc. Am., Spec. Paper 175, 49 p.
- \_\_\_\_\_ and WILLIAMS, H., 1963: Ordovician-Silurian relationships on New World Island, Notre Dame Bay, northeast Newfoundland: Geol. Soc. Am. Bull., v. 74, p. 807.
- KEAN, B.F. and STRONG, D.F., 1975: Geochemical evolution of an Ordovician Island arc of the central Newfoundland Appalachians: Am. J. Sci., v. 275, pp. 97-118.



- KENNEDY, G.C. and HOLSTER, W.T., 1966: Pressure-volume-temperature and phase relations of water and CO<sub>2</sub>: In Handbook of Physical Constants, Clark, S.P. (ed.), Geol. Soc. Am. Mem., v. 97, pp. 371-383.
- KERRICH, R. and FRYER, B.J., 1979: Archean precious metal hydrothermal systems, Dome Mine, Abitibi Greenstone Belt. II - REE and oxygen isotope relations: Can. J. Earth Sci., v. 16, pp. 440-458.
- \_\_\_\_\_, FYFE, W.S. and ALLISON, I., 1977: Iron reduction around gold quartz veins, Yellowknife District, Northwest Territories, Canada: Econ. Geol., v. 72, pp. 657-663.
- KONNERUP-MADSEN, J., 1981: Fluid inclusions in quartz from deep-seated granitic inclusions of south Norway: Lithos, v. 12, pp. 13-23.
- KRETSCHMAR, U. and SCOTT, S.D., 1976: Phase relations involving arsenopyrite in the system Fe-As-S and their application: Can. Mineral., v. 14, pp. 364-386.
- KRAUSKOPF, K.B., 1951: The solubility of gold: Econ. Geol., v. 46, pp. 858-870.
- \_\_\_\_\_, 1971: The source of ore metals: Geochim. Cosmochim. Acta, v. 35, pp. 643-659.
- KRUPKA, K.M., OHMOTO, H. and WICKMAN, F.E., 1977: A new technique in neutron activation analysis of Na/K ratios of fluid inclusions and its application to the gold-quartz veins at O'Brien Mine, Quebec, Canada: Can. J. Earth Sci., v. 14, pp. 2760-2770.
- KUNO, H., 1960: High Alumina Basalt: J. Pet., v. 1, pp. 121-145.
- LOWRY, H.H. and ERICKSON, W.R., 1927: The densities of coexisting liquid and gaseous carbon dioxide and the solubility of water in liquid CO<sub>2</sub>: J. Am. Chem. Soc., v. 49, pp. 2929-2934.
- McBIRNEY, A.R., 1963: Factors governing the nature of submarine volcanism: Bull. Volcanol., v. 26, pp. 455-469.
- MIYASHIRO, A., 1973: Metamorphism and Metamorphic Belts: George Allen and Unwin Ltd., London (pp. 442).
- MOORE, C.R., 1979: Geology and mineralization of the former Broken Hills gold mine, Hikurangi, Coromandel, New Zealand: N.Z. J. Geol. Geophys., v. 22, pp. 339-351.
- MOORE, J.G., 1970: Water content of basalt erupted on the ocean floor: Contr. Mineral. Petrol., v. 28, pp. 272-279.

- \_\_\_\_\_ and PECK, D.L., 1962: Accretionary lapilli in volcanic rocks of the Western Continental United States: J. Geol., v. 70, pp. 183-193.
- \_\_\_\_\_, PHILLIPS, P.L., GRIGG, R.W., PETERSON, D.W., and SWANSON, D.A., 1973: Flow of lava into the sea, 1969-1971 Kilauea Volcano, Hawaii: Geol. Soc. Am. Bull., v. 84, pp. 537-546.
- MURRAY, A. and HOWLEY, J.P., 1881: Geological Survey of Newfoundland from 1864 to 1880: Geol. Surv. Nfld. Pub., 536 p.
- NEALE, E.R.W., 1958: Baie Verte, Newfoundland: Geol. Surv. Can., Map 10 - 1958.
- PARTHE, E. and CROCKET, J.H., 1972: Platinum metals: In Handbook of Geochemistry, Wedepohl, K.H. (ed.), Springer-Verlag, pp. 78A1-78A4.
- PAYNE, J.G. and STRONG, D.F., 1978: Origin of the Twillingate trondhjemite, North Central Newfoundland - partial melting in the roots of an island arc: In Trondhjemites, Dacites and Related Rocks, Barker, F. (ed.), Elsevier, pp. 489-516.
- PEARCE, J.A. and CANN, J.R., 1973: Tectonic setting of basic volcanic rocks determined using trace element analyses: Earth Planet. Sci. Lett., v. 19, pp. 290-300.
- PHILLIPS, W.J., 1974: Mechanical effects of retrograde boiling and its probable importance in formation of some porphyry ore deposits: Trans. Inst. Min. Metall. Lond., v. 83 (B), pp. 42-43.
- PIRANJO, F., 1979: Geology, geochemistry and mineralization of the Endeavour Inlet Antimony-gold Prospect, Marlborough Sands, New Zealand: N.Z. J. Geol. Geophys., v. 22, pp. 227-237.
- POTTER, R.W., 1977: Pressure corrections for fluid inclusion homogenization temperature based on the volumetric properties of the system NaCl-H<sub>2</sub>O: U.S. Geol. Surv. Res., v. 5, pp. 603-608.
- RADTKE, A.S. and SCHEINER, B.J., 1970: Studies of hydrothermal gold deposition - (1) Carlin Gold Deposit, Nevada - the role of carbonaceous material in gold deposition: Econ. Geol. v. 65, pp. 87-102.
- RANKIN, A.H., 1978: Macrofluid inclusions in fluorite from the North Pennine Ore field, Current research on fluid inclusions: Geol. Soc. Lond. J., v. 134, pp. 393.
- ROEDDER, E., 1965: Liquid CO<sub>2</sub> inclusions in olivine-bearing nodules and phenocrysts from basalts: Am. Mineral., v. 50, pp. 1746-1782.
- \_\_\_\_\_, 1972: Composition of fluid inclusions: U.S. Geol. Surv. Prof. Paper 440-JJ, 164 p.

- \_\_\_\_\_, 1976: Fluid inclusion evidence on the genesis of ores in sedimentary and volcanic rocks: In Handbook of Strata-bound and Stratiform Ore Deposits, Wolf, K.H. (ed.), v. 2, pp. 67-110. Elsevier.
- \_\_\_\_\_ and BODNAR, R.J., 1980: Geologic pressure determinations from fluid inclusion studies: Ann. Rev. of Earth Planet. Sci., v. 8, pp.
- ROSASCO, G.J., ROEDDER, E. and SIMMONS, J.H., 1975: Laser-excited Raman spectroscopy for non-destructive partial analysis of individual phases in fluid inclusions in minerals: Science, v. 190, pp. 557-560.
- RUST, B.R., 1979: Facies Models 2 - Coarse alluvial deposits: In Facies Models, Geosci. Can. Repr. Series, 1, Walker, R.G. (ed.), Geol. Assoc. Can.
- SAMPSON, E., 1923: Ferruginous chert formations of Notre Dame Bay: J. Geol., v. 31, pp. 571-598.
- SAWKINS, F.J., O'NEIL, J.R., and THOMPSON, J.M., 1979: Fluid inclusion and geochemical studies of vein gold deposits, Baguio District, Philippines: Econ. Geol., v. 74, pp. 1420-1434.
- SCOTT, S.D., 1973: Experimental calibration of the sphalerite geobarometer: Econ. Geol., v. 68, pp. 466-474.
- SCOTT, S.D. and BARNES, H.L., 1971: Sphalerite geothermometry and geobarometry: Econ. Geol., v. 66, pp. 653-669.
- SEWARD, T.M., 1973: Thiocomplexes of gold and the transport of gold in hydrothermal ore solutions: Geochim. Cosmochim. Acta, v. 37, pp. 379-399.
- SMITHERINGALE, W.G., 1972: Low-potash Lushs Bight tholeiites: Ancient oceanic crust in Newfoundland?: Can. J. Earth Sci., v. 9, pp. 574-588.
- SNELGROVE, A.K., 1928: The geology of the central Mineral belt of Newfoundland: Can. Inst. Min. Metal., Bull. No. 197, pp. 1057-1127.
- \_\_\_\_\_, 1935: Geology of gold deposits of Newfoundland: Geol. Surv. Nfld., Bull. No. 2, 45 p.
- STRONG, D.F., 1972: Sheeted diabases of central Newfoundland - new evidence for Ordovician sea-floor spreading: Nature, v. 235, pp. 102-104.
- \_\_\_\_\_, 1973: Lushs Bight and Roberts Arm Groups of Central Newfoundland - possible juxtaposed oceanic and island arc volcanic suites: Geol. Soc. Am. Bull., v. 84, pp. 3917-3928.
- \_\_\_\_\_, 1974 (Editor): Plate tectonic setting of Newfoundland mineral occurrences - A guidebook for the NATO Advanced Studies Institute on metallogeny and plate tectonics, 171 p.

- \_\_\_\_\_, 1977: Volcanic regimes of the Newfoundland Appalachians: Geol. Assoc. Can., Spec. Paper 16, pp. 61-90.
- \_\_\_\_\_, and PAYNE, J.G., 1973: Early Palaeozoic volcanicsm and metamorphism of the Moreton's Harbour-Twillingate Area, Newfoundland: Can. J. Earth Sci., v. 10, pp. 1364-1379.
- \_\_\_\_\_, and HARRIS, A.H., 1974: The petrology of Mesozoic alkaline intrusives of central Newfoundland: Can. J. Earth Sci., v. 11, pp. 1208-1219.
- SWINDEN, H.S. and STRONG, D.F., 1976: A comparison of plate tectonic models of metallogenesis in the Appalachians, the North American Cordillera, and the East Australian Palaeozoic: In Metallogeny and Plate Tectonics, Strong, D.F. (ed.), Geol. Assoc. Can., Spec. Paper 14, pp. 441-470.
- TAKENOUCHI, S. and KENNEDY, G.C., 1965a: The solubility of carbon dioxide in NaCl-solutions at high temperatures and pressures: Am. J. Sci., v. 263, pp. 445-454.
- \_\_\_\_\_, 1965b: Dissociation pressures of the phase  $\text{CO}_2\text{-}5.75\text{ H}_2\text{O}$ : J. Geol., v. 73, pp. 383-390.
- TILLING, R.I., GOTTFRIED, D. and ROWE, J.J., 1973: Gold abundance in igneous rocks - bearing on gold mineralization: Econ. Geol., v. 68, pp. 168-186.
- TISCHENDORF, G., 1977: Geochemical and petrographic characteristics of silicic magmatic rocks associated with rare-element mineralization: In Metallization associated with Acid Magmatism, Stempok, M., Burnol, L. and Tischendorf, G. (eds.), Ustr. Ust. Geol., Praha, v. 2, pp. 41-46.
- TODHEIDE, K. and FRANCK, E.V., 1963: Das Zweiphasengebeit und die Kritsche Kurve in system Kohlendioxid-Wasser bis zv Drucken von 3500 bars: Z. Phys. Chem. Neuefolge, v. 37, pp. 388-401.
- TOURET, J., 1977: The significance of fluid inclusions in metamorphic rocks: In Thermodynamics in Geology, Fraser, D.G. (ed.). D. Reidel Publ. Co., Amst., pp. 203-227.
- TUCKER, C.M., 1976: Quarternary studies in Newfoundland - a short review: Maritime Sed., v. 12 (2), pp. 61-73.
- TUGARINOV, A.I. and NAUMOV, V.B., 1972: Physico-chemical parameters of hydrothermal mineral formation: Geochem. Intn., v. 9, pp. 161-167.
- TUREKIAN, K.K. and WEDEPOHL, K.H., 1961: Distribution of the elements in some major units of the Earth's Crust: Geol. Soc. Am. Bull., v. 72, pp. 175-192.

- TWENHOFEL, W.H. and SHROCK, R.R., 1937: Silurian strata of Notre Dame Bay and Exploits Valley, Newfoundland: Geol. Soc. Am. Bull., v. 48, pp. 1743-1772.
- UPADHYAY, H.D., 1973: The Betts Cove Ophiolite and related rocks of the Snooks Arm Group, Newfoundland: Ph.D. Thesis, Memorial Univ. of Nfld., 224 p.
- WADSWORTH, M.E., 1884: Notes on the rocks and ore deposits in the vicinity of Notre Dame Bay, Newfoundland: Am. J. Sci., v. 28, pp. 94-104.
- WALKER, R.G., 1979: Facies and facies models - 1. General Introduction: In Facies Models, Geosci. Can. Repr. Series 1, Walker, R.G. (ed.), Geol. Assoc. Can. (pp. 1-8).
- WEISBROD, A. and POTY, B., 1975: Thermodynamics and geochemistry of the hydrothermal evolution of the Mayres pegmatite: southeastern Massif - Central France (Part 1): Petrol. (Paris), v. 1, pp. 1-16.
- WEISSBERG, B.G., 1969: Gold-silver ore grade precipitates from New Zealand Hydrothermal waters: Econ. Geol., v. 64, pp. 95-108.
- \_\_\_\_\_, 1970: Solubility of gold in hydrothermal alkaline sulphide solutions: Econ. Geol., v. 65, pp. 551-556.
- WENTWORTH, C.K. and WILLIAMS, H., 1932: The classification and terminology of the pyroclastic rocks: Report of Sedimentation, 1930-1932, pp. 19-53.
- WHITE, D.E., 1974: Diverse origins of hydrothermal ore fluids: In Stable isotopes as Applied to Problems of Ore Deposits: Econ. Geol., v. 69, pp. 954-973.
- WILLIAMS, H., 1963a: Twillingate Map Area, Newfoundland: Geol. Surv. Can., Paper 63-36.
- \_\_\_\_\_, 1963b: Botwood Map Area, Newfoundland: Geol. Surv. Can., Map 60-1963.
- \_\_\_\_\_, 1963c: Relationships between base metal mineralization and volcanic rocks in northeastern Newfoundland: Can. Min. J., v. 84, pp. 39-42.
- \_\_\_\_\_, 1979: Appalachian Orogen in Canada: Can. J. Earth Sci., v. 16, pp. 792-807.
- \_\_\_\_\_ and MALPAS, J., 1972: Sheeted dikes and brecciated dike rocks within transported igneous complexes, Bay of Islands, W. Newfoundland: Can. J. Earth Sci., v. 9, pp. 1216-1229.



- \_\_\_\_\_ and PAYNE, J.G., 1975: The Twillingate granite and nearby volcanic groups - an island arc complex in northeastern Newfoundland: Can. J. Earth Sci., v. 12, pp. 982-995.
- \_\_\_\_\_, DALLMEYER, R.D. and WANLESS, R.K., 1976: Geochronology of the Twillingate Granite and Herring Neck Group, Notre Dame Bay, Newfoundland: Can. J. Earth Sci., v. 13, pp. 1591-1601.
- WINCHESTER, J.A. and FLOYD, P.A., 1977: Geochemical discrimination of different magma series and their differentiation products: Chem. Geol., v. 20, pp. 325-343.
- WINKLER, H.G.F., 1976: Petrogenesis of Metamorphic Rocks: 4th Edition, Springer-Verlag, N.Y., 334 p.
- WRIGHT, J.V., SMITH, A.L., and SELF, S., 1980: A working terminology of pyroclastic deposits: J. Volcanol. Geotherm. Res., v. 8, pp. 315-336.
- YMPA, P.J.M., 1963: Rejuvenation of ore deposits as exemplified by Belle-donne metalliferous province: Thesis, Univ. of Leiden, 212 p.

## APPENDIX 1

### ANALYTICAL TECHNIQUES

#### A.1.1. X-Ray Fluorescence Spectrometry

The elements As, Zn, Pb, Ni, Y, Zr, Ga, Th, U and Rb were determined using a Philips 1450, fully automated X-ray fluorescence spectrometer, equipped with spectrometer/detector, X-ray generator, HP mini-computer, teletype input/output, and a self-feeding sample tray. Pressed-pellet discs were made by mixing approximately 10 g powdered rock sample thoroughly with 1-1.5 g of binding agent (Union Carbide Phenolic Resin, material TR-16933) in a Spex-Mill shaker. The mixture was then pressed into a disc in a Herzog hydraulic press at a pressure of 300 tons psi, for 60 sec. The disc was then baked at 200°C for 10 minutes. The sample discs must be clearly labelled and stored in a moisture-controlled cabinet. Several sulphide-rich samples blistered on baking and so, could not be analysed. Calibration for As was made by D. Press, using U.S.G.S. standard samples:

|          |       |       |        |      |       |     |
|----------|-------|-------|--------|------|-------|-----|
| Sample   | SY-2  | SY-3  | MG-R,1 | SU-1 | MP-1  | W-1 |
| As (ppm) | 17    | 20    | 1.0    | 418  | 7900  | 1.9 |
| Sample   | PCC-1 | AgV-1 | BCR-1  | G-2  | GSP-1 |     |
| As (ppm) | 0.05  | 0.8   | 0.7    | 0.25 | 0.09  |     |

and analysed using K $\alpha$  1, 2, LiF 200 crystal, and the fine collimator scintillometer counter.

A similar calibration was attempted for Sb, using weighed amounts of powdered stibnite, mixed with various proportions of standard powdered quartzite, but the results were highly erratic and the Sb-calibration was unsuccessful.

The precision and accuracy of other elements were determined by analysing standard rock samples.

TABLE A.1.i  
Precision and Accuracy of Trace Element Analyses: XRF

|     | Ni | Zn | Ga | Rb  | Sr  | Y  | Zr  | Nb  | Pb | As   |
|-----|----|----|----|-----|-----|----|-----|-----|----|------|
| W-1 | 70 | 85 | 20 | 22  | 189 | 24 | 98  | 8   | 7  | 1.9  |
| S   | 3  | 2  | 2  | 2   | 6   | 2  | 2   | 1   | 3  | -    |
| N   | 13 | 13 | 13 | 13  | 13  | 13 | 13  | 13  | 13 | -    |
| P   | 78 | 86 | 16 | 21  | 190 | 25 | 105 | 9.5 | 8  | -    |
| G-2 | 2  | 85 | 24 | 166 | 477 | 11 | 292 | 10  | 27 | 0.25 |
| S   | 2  | 2  | 1  | 2   | 7   | 2  | 3   | 1   | 2  | -    |
| N   | 10 | 10 | 10 | 10  | 10  | 11 | 10  | 10  | 10 | -    |
| P   | 6  | 85 | 23 | 170 | 480 | 12 | 300 | 14  | 29 | -    |

S=standard deviation

N=number of deviations

P=published values (Flanagan, 1973)

Very high values of Zn, Pb, As in ore samples are less precise, as the calibration is strictly for trace abundances. At percentage levels of Pb, subsidiary Pb peaks interfere with Ga and give erroneously high values for that element.

#### A.1.2. Atomic Absorption Spectrophotometry: Flame Technique for Major and Minor Elements

The major and minor elements were determined using the Perkin-Elmer model 370 atomic absorption spectrophotometer with digital readout using the flame technique (Analyst: Mrs. G. Andrews). The samples were

prepared using the established procedures (Langmhyr and Paus, 1968). The precision of this method was determined by using a granitic rock standard (G-1) analysed four times, as shown in Table A.1.ii.

TABLE A.1.ii

| Precision of AAS analysis (n=4) |                  |           |      |       |       |
|---------------------------------|------------------|-----------|------|-------|-------|
| Element                         | Published Value* | $\bar{X}$ | S    | Range |       |
|                                 |                  |           |      | low   | high  |
| SiO <sub>2</sub>                | 69.11            | 69.70     | 0.57 | 68.2  | 69.96 |
| Al <sub>2</sub> O <sub>3</sub>  | 15.40            | 15.10     | 0.24 | 14.75 | 15.60 |
| Fe <sub>2</sub> O <sub>3</sub>  | 2.65             | 2.60      | 0.02 | 2.64  | 2.74  |
| MgO                             | 0.76             | 0.80      | 0.05 | 0.75  | 0.82  |
| CaO                             | 1.94             | 2.00      | 0.10 | 1.92  | 2.14  |
| Na <sub>2</sub> O               | 4.07             | 4.30      | 0.02 | 4.07  | 4.21  |
| K <sub>2</sub> O                | 4.51             | 4.56      | 0.02 | 4.50  | 4.57  |
| TiO <sub>2</sub>                | 0.50             | 0.50      | 0.01 | 0.47  | 0.51  |
| MnO                             | 0.03             | 0.03      | 0.0  | -     | -     |

S=standard deviation

$\bar{X}$ = mean

\*Flanagan, 1970

#### A.1.3. Wet-Chemical and Flameless Atomic Absorption Method: Precious Metals

Precious metal (Au, Ag, Pd) concentrations were determined using the wet chemical-flameless atomic absorption spectrophotometry technique of Fryer and Kerrich (1978). The samples were prepared for analysis as follows:

### Sample Preparation

1. Rock samples are powdered to 20  $\mu\text{m}$  grain size using a tungsten-carbide mill (or, if sulphide-rich, a porcelaine mill). Care must be taken to prevent contamination.
2. 5 g of rock powder are weighed accurately into 250 ml Pyrex beakers ("Blanks" are prepared for control).
3. Add 70 ml of aqua regia<sup>1</sup>.
4. Cover and digest for 1 hour on a hotplate; agitate and swirl powder + solution periodically. Care must be taken not to have the plate too hot, otherwise over-boiling and spitting occur, causing loss of sample and contamination.
5. Evaporate the solution to dryness (this may take 5 to 12 hours).
6. Add 40 ml aqua regia and digest on the hot plate for 30 mins.
7. Decant the solution into 50 ml centrifuge tubes; centrifuge.
8. Transfer the clear supernatant solution to a Teflon beaker.
9. Repeat the aqua regia attack on the powder residue, centrifuge and transfer solution to the Teflon beaker.
10. Transfer the rest of the residue to the centrifuging tube with aqua regia washings and re-centrifuge.
11. Reject all residue, after adding solution to Teflon beaker.
12. To the solution (in the Teflon beaker) add 10 ml HF.
13. Evaporate to dryness.
14. Add 1 g  $\text{NH}_4\text{Cl}$  and 10 ml  $\text{HCl}$ .
15. Cover and evaporate to dryness.
16. Repeat addition of  $\text{HCl}$  and evaporation.
17. Add 10 ml  $\text{HCl}$  to take precipitate to solution.
18. Add 30 ml  $\text{H}_2\text{O}$  and digest on a hot plate.

---

<sup>1</sup>Aqua regia - 5 parts conc.  $\text{HCl}$  + 2 parts conc.  $\text{HNO}_3$



19. Transfer solution to a 250 ml Pyrex beaker.
20. Dilute to 75 ml with 8% HCl (v/v). The solution should be clear.
21. Pipette 5 ml tellurium solution<sup>2</sup> (to complex with any precious metals present) and heat the solution to near boiling temperature.
22. Add SnCl<sub>2</sub> solution<sup>3</sup> (using a burette) until the colour of ferric iron (yellow) is bleached (reduced) and Te (with any precious metals) commences to precipitate (black).
23. Add an additional 5 ml SnCl<sub>2</sub> solution (so there is excess present).
24. Heat for 30 min. to coagulate the precipitate; vigorous boiling is required in some cases.
25. Filter the solution using double, fast filter paper and wash thoroughly with 8% HCl v/v at 60°C.
26. Discard filtrate.
27. Dissolve the precipitate off the paper by slowly washing with 50 ml cold aqua regia, collecting filtrate in a 100 ml Pyrex beaker.
28. Wash finally with 10% HCl (v/v) at 60°C.
29. Evaporate the solution to near dryness.
30. Transfer the solution to a 10 ml volumetric flask and take to volume with aqua regia (see below).
31. Transfer analyte to a polyethylene vial and store for analysis.

The samples so prepared were analysed using the HGA graphite furnace assembly (Burner-Nebulizer, number 040-0146) connected to the Perkin-Elmer model 370 atomic absorption spectrophotometer under the conditions outlined in Table A.1.iii.

---

<sup>2</sup>Tellurium solution - 1000 g cm<sup>-3</sup> in 10% HCl; prepared by dissolving Te-metal (99.999% purity) in aqua regia and removing nitrate by two successive evaporations with HCl.

<sup>3</sup>Stannous chloride solution - 20 g fresh SnCl<sub>2</sub>·2H<sub>2</sub>O in 17 ml reagent grade conc. HCl. Dilute to 100 ml with deionized H<sub>2</sub>O.

TABLE A.1.iii  
Instrumental Conditions for the Graphite Furnace Assembly

| Element | nm    | SBW nm | Char. Temp. | Optimum<br>Absorption<br>temp. °C | Sensitivity |
|---------|-------|--------|-------------|-----------------------------------|-------------|
| Ag      | 328.1 | 0.7    | 400         | 2700                              | Ar 8        |
| Au      | 242.8 | 0.7    | 800         | 2700                              | Ar 25       |
| Pd      | 247.6 | 0.2    | 1100        | 2800                              | Ar 160      |

According to Kerrich and Fryer, the analyte should be brought to volume using aqua regia (step 30), but in this study it was found that the concentrated, oxidizing acid severely corroded the graphite furnace such that the results were irreproducible and erratic. With more diluted (i.e. with water) analytes results were better. The analyte was introduced to the graphite boat in aliquots of 20 and 50  $\mu$ l. Between each sample run, standard solutions were analysed for calibration. These solutions were made by dissolving exact weights of pure metal (99.999% purity) in aqua regia and diluting with 10% v/v HCl to various amounts. Successive calibration curves were plotted for each set of sample analyses (e.g. Fig. A.1.i). Higher concentrations of Au and Ag were out of the calibration range, so had to be further diluted. This increased error in analysis. Such samples were checked using the same analytes with flame AAS, which compared well with the values from flameless technique (Table A.1.iv).

TABLE A.1.iv  
Comparison of Gold and Silver Analyses by  
Flame and Flameless Atomic Absorption

| Sample | Au (flame) ppm | Au (flameless) ppm |
|--------|----------------|--------------------|
| SM.2   | 0.84           | 1.00               |
| SM.4   | 2.00           | 1.70               |
| MHH.4  | 9.28           | 3.00*              |
| MHH.6  | 9.04           | 2.60*              |
| SM.53  | 0.72           | 0.70               |
| TR.44  | 2.60           | 2.60               |
| FC.7   | 1.12           | 0.80               |
| Sample | Ag (flame) ppm | Au (flameless) ppm |
| SM.5   | 5.68           | 7.65               |
| TR.44  | 2.46           | 5.14               |
| SM.53  | 2.30           | 2.30               |
| TR.17  | 0.34           | 0.38               |
| SM.16  | 0.12           | 0.14               |
| TR.53  | 60.6           | 12.0*              |
| SB.15  | 0.10           | 0.14               |

\*error induced by excessive dilution)

No internal standard was available but replicate analyses show at least internal consistency. Sensitivity determinations for the precious metals may be calculated using:

$$A = \frac{4.4 \times V \times C}{S}$$

where A is the absorbance, V is the volume, C the concentration and S the sensitivity. Values for the standard solutions showed close agreement with the specified values (users' handbook); Table A.1.iv).

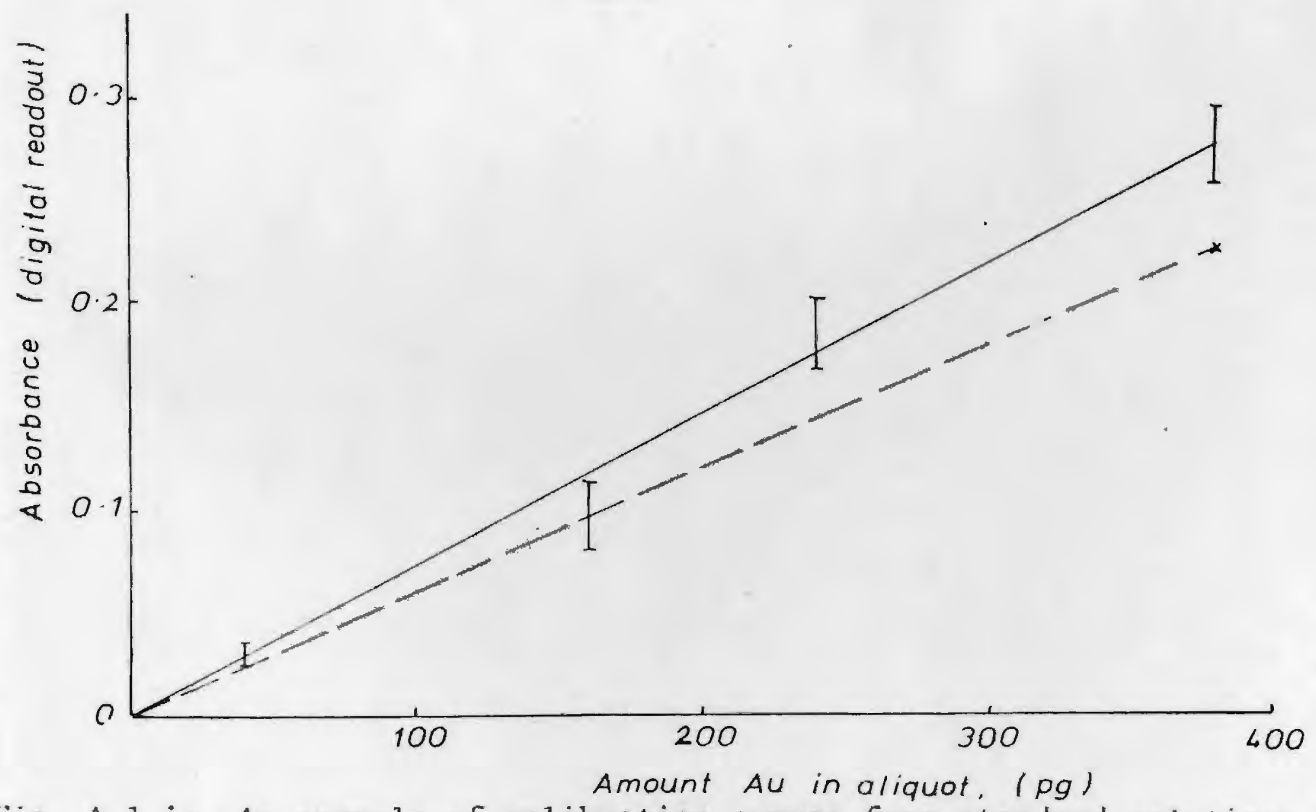
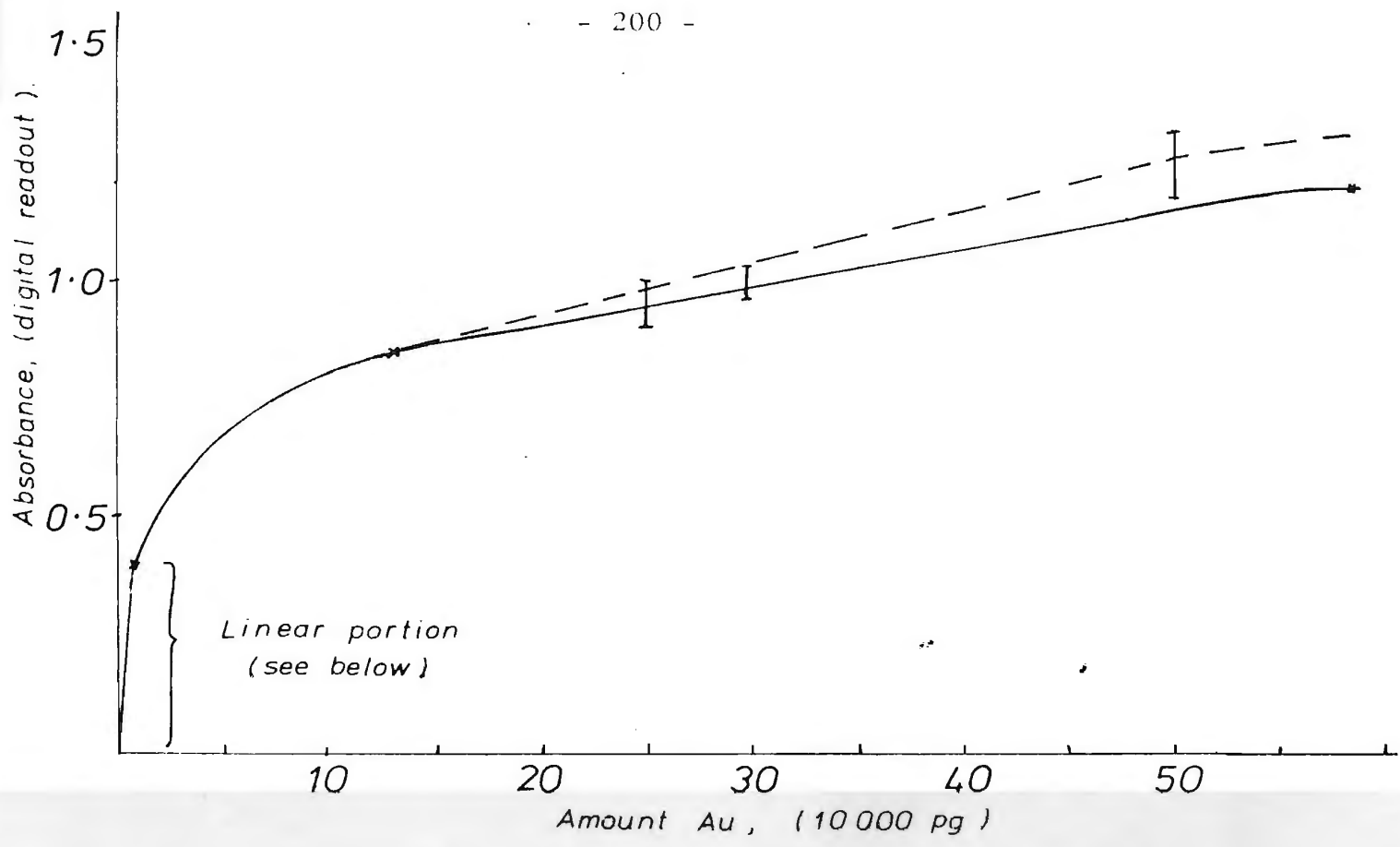


Fig. A.1.i: An example of calibration curves from standard solutions for flameless AAS gold analyses.

Initial calibration curve, solid line; calibration after several analytical runs showing deterioration of the graphite tube, broken line.

Extreme caution is necessary when analysing for low concentrations of precious metals, because of contamination, especially in the wet-chemical digestion (Fryer and Kerrich, 1978). Blank analyses (one in each run of 20) showed values of 1 ppb.

#### A.1.3. Mineral Compositions by Electron Microprobe

Both sulphide and silicate minerals were analysed using an automated electron microprobe; the JEOL JXA-50A electron probe micro-analyzer with Krisel control through PDP-11 computer. Operating conditions include an accelerating voltage of 15 kV, three wavelength-dispersive spectrometers, a beam current of approximately 0.3 microamps, a beam size of approximately 1-2 microns and a counting rate of 30,000 with a default time of 30 seconds. The sulphide major and trace analyses were corrected and calculated by the Krisel Magic program, and the silicate analyses using the Alpha Bence-Albee matrix.

Calibrations were made using various sulphide minerals, pure metals and silicates as appropriate. For each element a background point and counts from five other points were determined. Counting errors in the major elements of the sulphide minerals were mostly <2%.



## APPENDIX 2

### FLUID INCLUSION TECHNIQUES

#### A.2.1. The Chaixmeca Heating/Freezing Stage

The fluid inclusions were examined using an ordinary petrographic microscope stage with high power objectives and high illumination. The thermometric data were derived using the Chaixmeca Heating/Freezing stage comprising an ordinary microscope stage with attached heating and freezing stage, a control unit which monitors the temperature of the stage and commands the heating and cooling of the stage either manually or automatically, and a pressurized liquid N<sub>2</sub>-container which both feeds, and acts as a reservoir for, liquid N<sub>2</sub> through the control unit and then the stage, as illustrated in Figure A.2.i and A.2.ii. The system operates between +600°C and -190°C. Samples are placed at the centre of the top, flat surface of the condenser lens near to the Pt resistance sensor (measuring 100  $\Omega$  at 0°C), and beneath a metallic cover with a polished silica window. The temperature measurements are determined by the Pt sensor which is resolved to  $\pm 0.1^\circ\text{C}$  on the digital readout.

Below 0°C, rapid cooling is induced by the flow of liquid N<sub>2</sub>. A flow of dry N<sub>2</sub> through a plastic sleeve around the objective lens and below the stage prevents excessive ice build-up at low temperatures (modifications by Higgins, 1979). The dry gas is shut off when the temperature is -24°C.

Above 0°C, the plastic tubing and sleeve (for the dry N<sub>2</sub> circulation) must be removed, and a water-cooled jacket is placed around the

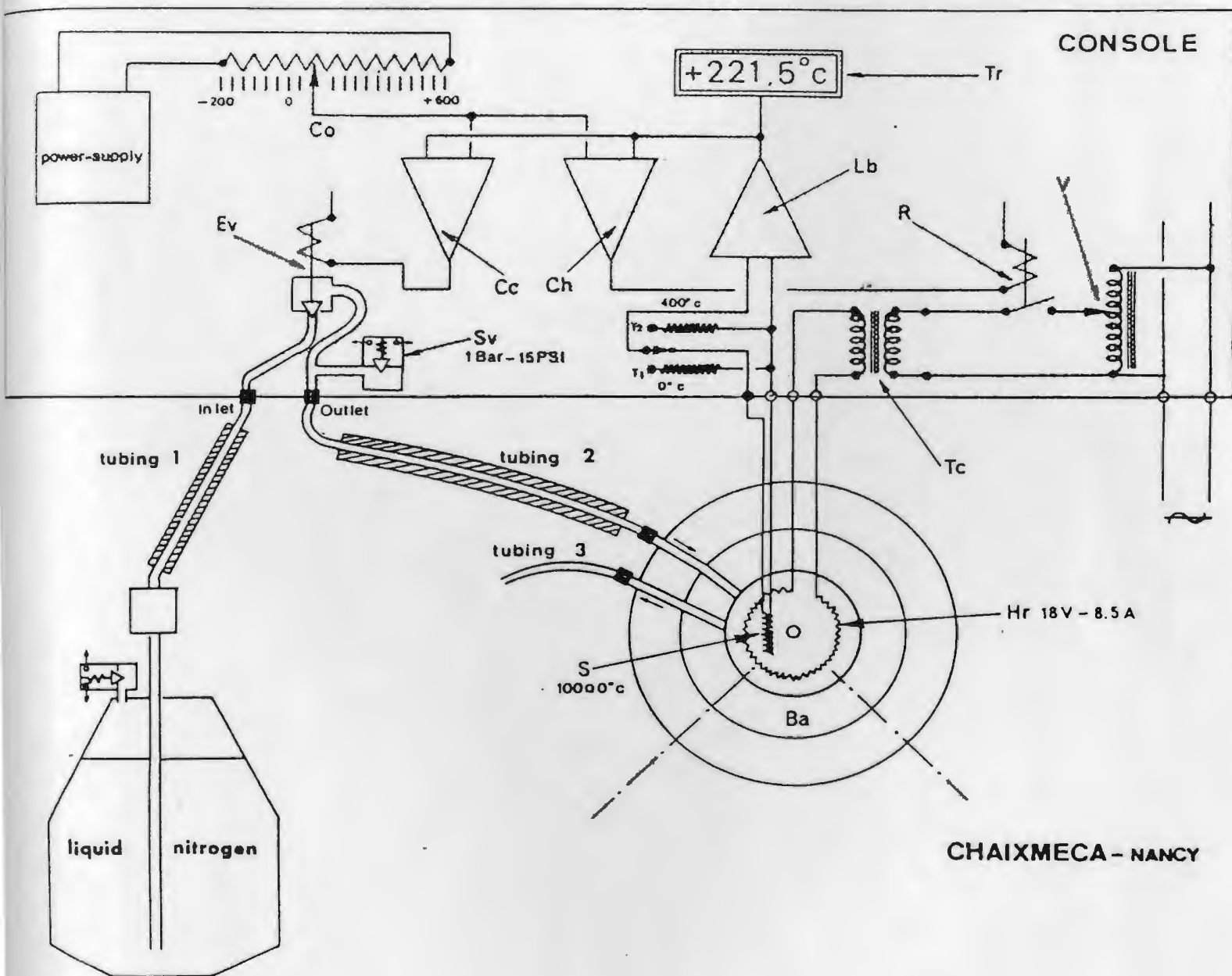
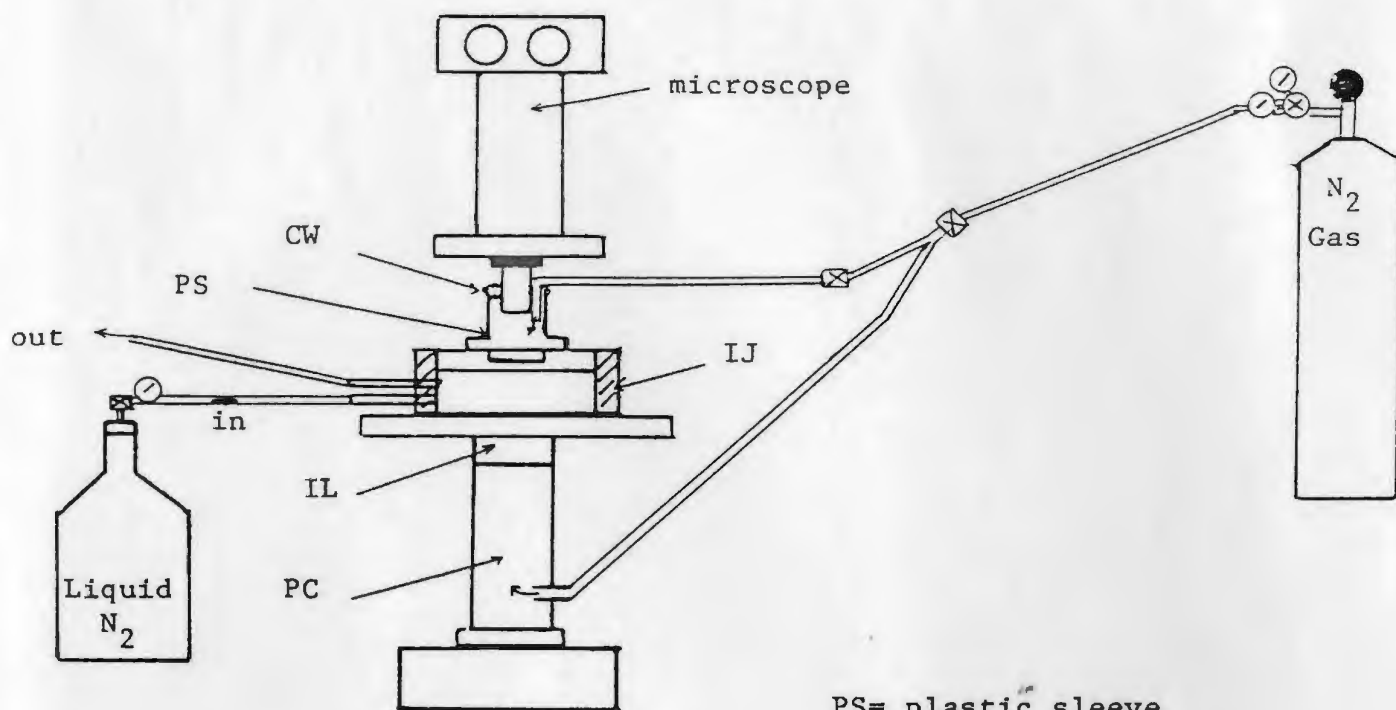


Fig. A.2.i: The Chaixmeca heating/freezing stage, set up for thermometric determinations (from the Chaixmeca users' handbook).

Freezing mode.



PS= plastic sleeve  
 CW= cotton wool  
 IL= infrared lens  
 IJ= Insulating Jacket  
 PC= perspex column  
 CJ= cooling jacket for lens  
 SW= silica window  
 H/F= heating/ freezing stage

Heating mode.

Figures not drawn to scale.

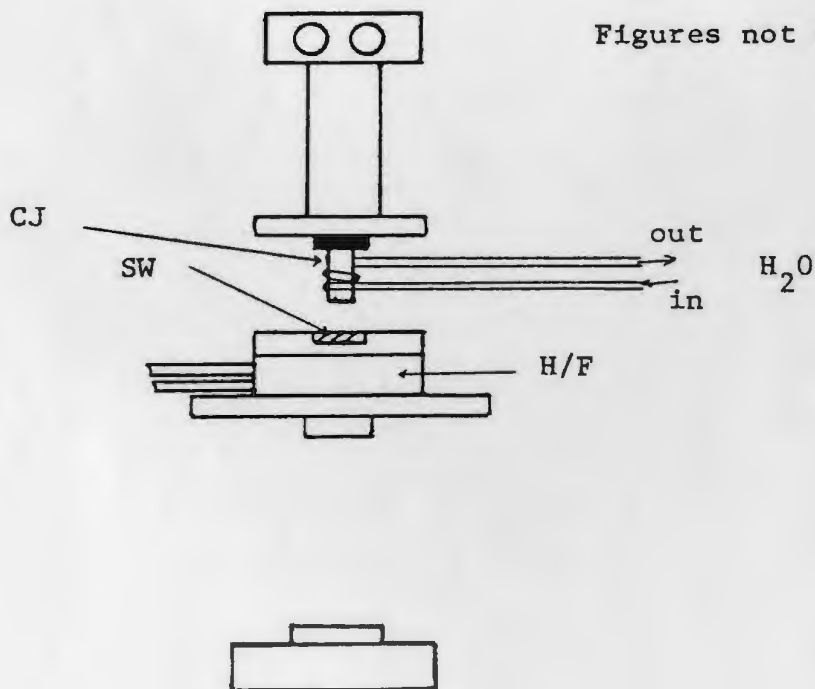


Fig. A.2.ii: The Chaixmeca heating/freezing stage, set up for thermometric determinations (from the Chaixmeca users' handbook; modifications by Higgins, 1980).



objective lens to protect from overheating. A heating rate of  $0.5^{\circ}\text{C min}^{-1}$  is advisable near homogenization temperatures.

The Chaixmeca stage was calibrated (Fig. A.2.iii) by heating a few crystals of chemical standards between several  $1\text{cm}^2$  coverslip glasses to approximate the thickness of a fluid inclusion section ( $600\mu\text{m}$ ), and melting points recorded. Similarly freezing point calibrations are made using chemical standards for freezing of organic liquids. A detailed calibration was made by N. Higgins in 1980, which was found to approximate closely to melting and freezing point values for chemical standards from this study.

Accuracy and precision measurements were made on using chemical standards and representative fluid inclusions. These data indicate that below  $0^{\circ}\text{C}$  measurements are accurate within  $\pm 0.2^{\circ}\text{C}$  ideally. Below  $-40^{\circ}\text{C}$  error is greater, as the Chaixmeca stage does not allow for control at these low temperatures. Observations are variably obscured by condensation in all freezing runs and the formation or disappearance of ice or clathrate are very difficult to see in such small inclusions as in the present study ( $<10\mu\text{m}$ ), which produced further errors in thermometric data below  $0^{\circ}\text{C}$ . All thermometric data are represented in the histogram plots in the text (Chapter 6) using bar widths exceeding the errors of accuracy and measurement.

#### A.2.2. Preparation of Fluid Inclusion Sections

The sections were prepared following the technique of Higgins (1980) as follows:



1. The sample is cut to a block 1 cm x 2 cm x 2.5 cm<sup>2</sup>. Care must be taken not to overheat the sample by friction which may decrepitate inclusions. A thin diamond-edged blade (Felker 5" OL) 5/8) may be used but is so fragile, it is more efficient to use a standard blade at a slow rate.
2. The sample block is slowly ground down 1 mm on a Hillquist coarse vertical grinder to remove any of the sample which may be damaged by frictional heating.
3. The coarsely ground side is ground briefly on the horizontal lap using 220 and 320 grits (carborundum powders) followed by 600 and 800  $\mu$ m abrasive powders on glass.
4. The samples are cleaned and dried thoroughly and the roughly polished side is attached to an ordinary glass thin section plate using a soluble glue (a spray-liquid coverslip\*).

Note: There is a problem with nucleation of air bubbles between the slide and sample which may be decreased by spraying a thick layer of the glass on both the semipolished sample and the slide, and leaving for up to 10 min., periodically stirring, using a botany needle to eliminate the bubbles. The sample may be mounted on the slide when the liquid glass is quite "tacky". Press the sample firmly and allow to dry for 12 to 24 hours. Do not dry by heating.

5. Mounted samples are slowly ground to an approximate thickness of 0.6 to 0.8 mm using the Hillquist coarse vertical grinder. The thickness depends on the translucence of the mineral. The thinner the section, the greater is the risk of loss of fluid inclusions.
6. Grind briefly on the horizontal lap (220 and 320 grits) followed by grinding on glass (600  $\mu$ m and 800  $\mu$ m powders).
7. The sample is then polished by hand on the Unipole polisher using a 1  $\mu$ m alumina powder. Polishing takes  $\geq$  20 minutes per specimen for quartz.
8. The samples for thermometry are removed by dissolving the glass by soaking in Xylene (in a shallow covered tray), for 5 to 12 hours. Clean the sample chip with acetone and dry.
9. Remount the sample (the polished side down) to the glass slide (as step 4).
10. Briefly grind the newly exposed surface on horizontal lap (220 and 320 grits) and on glass (600 and 800  $\mu$ m powders).

---

\*Higgins, 1980, suggests using Trycolac Mk IV distributed by Petrologic Ltd., but this is no longer manufactured and other liquid glass had to be substituted in this study.

11. Polish side (as step 6). Examine inclusions using a petrographic microscope before removing the fragile section from the slide.
12. For thermometry, remove the glass slide by immersion in Xylene. Clean thoroughly with acetone and dry.

The ideal fluid inclusion section will have parallel, optically polished sides and an approximate thickness of 0.5-0.3 mm. Detailed descriptions may be made from carefully cut and ground, unpolished sections using immersion oils and coverslips. These are most suitable for photography and enables morphological and preliminary compositional evaluation of the fluid inclusions, without the time consuming process (steps 6 to 12).

APPENDIX REFERENCES

FLANAGAN, F.J., 1970: Sources of geochemical standards - II - Geochim. Cosmochim. Acta, v. 23, pp. 121-125.

FRYER, B.J. and KERRICH, R., 1978: Determination of precious metals at ppb levels in rocks by a combined wet-chemical flameless AAS technique: Atom. Abs. Newsletter, v. 17 (1), pp. 406-408.

HIGGINS, N.C., 1980: The genesis of the Grey River Tungsten Prospect: a fluid inclusion, geochemical and isotopic study: Unpub. Ph.D. Thesis, M.U.N. Nfld., 404 p.

LANGMHYR, F.J. and PAUS, P.E., 1968: The analysis of inorganic siliceous materials by atomic absorption spectrophotometry and the hydro-fluoric acid decomposition technique, Part I: The analysis of silicate rocks: Anal. Chem. Acta, v. 43, pp. 397-408.





